SPECTROSCOPIC STUDY OF METHANE IN THE $\nu_1 + \nu_4$ BAND BROADENED BY ITSELF, AIR AND HYDROGEN

MD ARIFUZZAMAN
Master of Science, Shah Jalal University of Science and Technology, 2009

A Thesis
Submitted to the School of Graduate Studies
of the University of Lethbridge
in Partial Fulfillment of the
Requirements for the Degree

MASTER OF SCIENCE

Department of Physics and Astronomy
University of Lethbridge
LETHBRIDGE, ALBERTA, CANADA

SPECTROSCOPIC STUDY OF METHANE IN THE $\nu_1 + \nu_4$ BAND BROADENED BY ITSELF, AIR AND HYDROGEN

MD ARIFUZZAMAN

Date of defence: April 27, 2018

Dr. M. Gerken Thesis Supervisor	Professor	Ph.D.
Dr. B. Billinghurst Thesis Examination Committee Member Senior Scientist, Canadian Light Source. Inc. Saskatoon	Adjunct Assistant Professor	Ph.D.
Dr. B. Seyed-Mahmoud Thesis Examination Committee Member	Associate Professor	Ph.D.
Dr. A. Cross Thesis Examination Committee Member	Adjunct Assistant Professor	Ph.D.
Dr. G. Tabisz External Examiner Department of Physics and Astronomy University of Manitoba, Canada	Professor and Senior Scholar	Ph.D.
Dr. D. Naylor Chair, Thesis Examination Committee	Professor	Ph.D.

Dedication

This thesis is dedicated to my beloved parents, my wife and my daughter.

Abstract

This thesis presents the temperature-dependent line-shape studies of methane broadened by itself, air and hydrogen, which is identified as the second most important anthropogenic greenhouse gas in the Earth's atmosphere due to its high global warming potential. A set of 14 laboratory spectra of pure methane and lean mixtures of methane in air were recorded over a range of temperatures from 148.4 to 298.4 K and total sample pressures from 4.5 to 385 Torr using a high-resolution Fourier Transform Spectrometer (FTS) at the Jet Propulsion Laboratory (JPL), California. A coolable absorption gas cell with the optical path length 20.38 cm was used in the recording of methane-air spectra. A non-linear least-squares multi-spectrum fitting program called 'Labfit' was used to determine the Lorentz half-width, pressure-induced shift coefficients along with their temperature dependences, speed-dependence parameters and line-mixing coefficients due to self- and air-broadening of methane in its strongest band $\nu_1 + \nu_4$.

A set of 18 laboratory spectra of methane broadened by itself and hydrogen were also recorded at various temperatures (148.4-298.4 K) and pressures (0.12-385 Torr) using an FTS at JPL. Various line-shape parameters such as line positions, intensities, self- and air-broadened line widths and pressure-induced shifts along with their temperature dependences are reported in the $\nu_1 + \nu_4$ band of methane. A Speed-Dependent Voigt Profile (SDVP) was implemented in the retrieval of line parameters in both cases. The line-mixing coefficients were quantified using the off-diagonal relaxation matrix element formalism. The off-diagonal relaxation-matrix coefficients were determined due to self-, air- and H_2-broadening of methane using Labfit program.

Acknowledgements

All praises is due to almighty God for whom I am here in this world to do these types of research works and I pray Him to accept this as the good deed.

First and foremost, I am deeply thankful to my supervisor, Dr. Michael Gerken, Professor, Department of Chemistry and Biochemistry for his continuous supports and important guidelines throughout my M.Sc. program. I found him very cordial, prompt and helpful. He is an enthusiastic leader in the field of research, from whom I had the privilege of learning not only research work but also the way to be responsible in everyday life. His motivation and guidance helped me to continue and accomplish my thesis works.

I would like to pay special thanks to my previous supervisor, Dr. Adriana Predoi-Cross, who accepted me as a graduate student in her research group. I gained useful knowledge from her about fitting and analyzing spectroscopic data using 'Labfit'.

I would like to express my gratitude to all of my committee members, Dr. Behnam Seyed Mahmoud, Dr. Albert Cross and Dr. Brant Billinghurst for their important guidelines and suggestions to make an executable research plan during my graduate studies.

I am thankful to Dr. Chad Povery, instructor, Physics and Astronomy at University of Lethbridge, who is also an alumnus as a Ph.D. student in our research group. I discussed many research questions with him and I found him very knowledgeable and helpful.

I am grateful to Dr. Keeyoon Sung, scientist at Jet Propulsion Laboratory (JPL), Caltech, who provided me the experimental data for the analysis. I also communicated with him about the fitting procedures and he responded to me very quickly. I am also thankful

to Dr. Malathy Devi, Reseacrh Professor at the College of William and Mary, who provided me useful guidelines about fitting procedures using ‘Labfit’ especially for line-mixing calculations.

Dr. Chris Benner at the College of William and Mary is thanked for allowing me to use his multi-spectrum fitting software “Labfit”. The contribution of Dr. Arlan Mantz from Department of Physics, Geophysics and Astronomy, Connecticut College is highly acknowledged for designing the cryogenic type gas cell, which was used in the recording of my spectra at JPL.

I am very thankful to all of my colleagues and fellows in the Department of Physics and Astronomy, especially to Hoimonti Rozario, Ph.D. student, Robab Hashemi, Ph.D student, Md Kamruzzaman, Ph.D. student, Abdullah Al Mashwood and Nazrul Islam, alumni in our research group.

Last but not least, I would like to pay special thanks to my parents, my beloved daughter Rubaba Afsheen and my wife Rabeya Parvin, because of their unconditional supports along with patience towards the completion of my graduate studies.

Finally, I am grateful to the center of excellence in research of School of Graduate Studies at University of Lethbridge supported by Natural Sciences and Engineering Research Council of Canada (NSERC) and the NSERC-supported AMETHYST program.

Table of Contents

List of Figures

List of Tables

List of Abbreviations

FTS	Fourier Transform Spectrometer
JPL	Jet Propulsion Laboratory
IR	Infrared
EM	Electro Magnetic
FTIR	Fourier Transform Infrared
GWP	Global Warming Potential
HITRAN	High Resolution Transmission Molecular Absorption Database
GEISA	Gestion et Etude des Informations Spectroscopiques Atmosphériques
SDVP	Speed Dependent Voigt Profile
ZPD	Zero Path Difference
SNR	Signal-to-Noise Ratio
ORME	Off-diagonal Relaxation Matrix Elements
EPG	Exponential Power Gap Law

CHAPTER 1: INTRODUCTION

1.1 Overview

Molecular spectroscopy is one of the important techniques by which the molecular structure and different physical and chemical properties of atmospheric gas molecules can be accurately determined. The light-matter interaction is the basis of spectroscopy, and depending on the light used, different kinds of useful information can be obtained about the molecules of interest. Infrared (IR) spectroscopy studies the interaction of molecules with infrared radiation, primarily the absorption of light by molecules. Infrared light can be categorized into three types: near- (13000-4000 cm^{-1}), mid- (4000-400 cm^{-1}) and far-infrared (400-33 cm^{-1}), which are used in the vibrational and rotational spectroscopy of molecules. Infrared spectroscopy is one of the most common techniques for identifying the rotational-vibrational modes of molecules, which are observed usually in gas phase. The chemists also use infrared spectroscopy to determine the functional groups in the complex molecules and it has now widely used in the analysis and classification of human tissues and fluids. Therefore, both theoretical and experimental spectroscopic studies are needed for the identification and characterization of complex molecules in the gas phase.

The global temperature of the Earth's atmosphere increases day by day due to different human activities including the burning of fossil fuels, which increases the concentration of greenhouse gases. The global community is increasingly concerned about this rapid environmental change of our Earth's atmosphere, which necessitates the accurate line-shape studies of different gas molecules. The study of spectral line-shapes in gas-phase spectra is also becoming more important as it produces a better understanding of the radiative properties of the Earth's atmosphere as well remote sensing of terrestrial and

planetary atmospheres, e.g., monitoring temperature profiles of the atmospheres and greenhouse gases from outer planets. Accurate line-shape parameters are also essential in the design of Earth climate models.

Spectral line-shape studies are influenced by the type of molecules, atmospheric conditions of the samples and also the presence of other surrounding gases. Many different gas molecules exist in the atmospheres of Earth and other planets and, therefore, the right choice of gas molecules as perturbers is important in spectroscopic studies of model systems. In addition, atmospheric conditions are not homogeneous, so the spectroscopic line-shape studies of target molecules need to be performed at varying pressures and temperatures relevant to natural environments.

1.2 General information of methane

The present study is focused on the spectroscopic line-shape studies of methane (CH_4) broadened by itself, air, and hydrogen in the spectral range of (4100-4300 cm^{-1}). Methane is a colorless, odorless and highly flammable, non-toxic gas, which is present in the Earth atmosphere as a trace gas. Methane is also found as the main constituent of natural gas. It has a tetrahedral molecular geometry where one central carbon is bounded to four hydrogen atoms via four single bonds with H-C-H angles of 109.5º. Methane is lighter than N_2, major components of air but heavier than H_2 with a melting point of -183º C and a boiling point of -164º C.

1.3 Methane as a greenhouse gas

Methane is chosen as the primary molecule of interest in the present study because it is recognized as the second most important short-lived anthropogenic greenhouse gas, whose emissions must be reduced immediately as recommended by the Kyoto Protocol [1].

One of the important properties of greenhouse gases is that they can easily absorb solar radiation. A term called 'Global-warming potential (GWP)' is used in the computation of the amount of radiation absorbed in the Earth atmosphere. The GWP is calculated by the ratio of heat trapped by any specific gas to the corresponding heat trapped by a CO_2 molecule. The concentration of methane has increased gradually in recent years which amounts to 1,800 ppb and its global warming potential (GWP_{20}- on the basis of a 20-year period) is very high, which is 84-87 times larger than that of CO_2 [2]. Methane gas has a life time of 12.4 years in the atmosphere during which it disappears from the atmosphere through chemical reactions and biological processes. The short lifetime combined with the higher absorption energy of methane results in its higher global warming potential relative to CO_2. This higher energy absorption by CH_4 in the atmosphere increases the global warming (GW) at a very high rate, which compels the spectroscopists to study its line-shape parameters in various absorption bands.

1.4 Methane contribution to carbon cycle

Methane also influences the carbon cycle, in which carbon can be interchanged among the land surface, Earth atmosphere and oceans. Two major greenhouse gases, CO_2 and CH_4 are the main contributors to the carbon cycle, which play a vital role in the Earth's climate system by controlling their levels of concentration in the atmosphere. The amount of carbon contained in different reservoirs such as Earth's atmosphere, ocean, the Earth crust and the terrestrial ecosystem is calculated in a unit of Petagram of Carbon (Pgc). Among which, the Earth's atmosphere holds almost 750 Pgc, in which Co_2 and methane are found as important because their concentrations are linked to the change in temperatures of the atmosphere, i.e., climate change. The methane concentration in the atmosphere has shown a continuous growth [3] in recent years, so it is important to know its spectral parameters

for understanding the atmospheric trend. Therefore, more studies on methane are required to predict the future trend of atmospheric methane well.

1.5 Methane as a constituent of exoplanetary atmosphere

Methane is also considered as one of the "building blocks" in the atmosphere of other Giant solar planets such as Jupiter, Saturn, Uranus and Neptune [4] as well as in exoplanetary atmospheres [5-7]. Methane's presence in Titan's atmosphere plays a vital role like that of water in the Earth's atmosphere at lower temperatures, because it is the source of hydrocarbon hazes which is used to maintain the Titan's thick nitrogen atmosphere. Methane is identified as the primary absorber of the infrared radiation [8], therefore, a detailed knowledge of its infrared spectroscopy plays a substantial role in the remote sensing of Titan's atmosphere. Moreover, the opacity of several brown dwarfs[a] is attributed to the infrared absorption spectroscopy of methane [9], because one of the sources of opacity in a Stellar atmosphere involve the absorption by bound-bound (line) transition.

1.6 Motivation of methane line-shape studies

Accurate measurements of self- and air-broadened half-widths and shift coefficients of methane along with their temperature dependencies in the octad range (~2.3 μm) are very important to quantify the abundance of CH_4 as well as to interpret the infrared spectra of other molecules (HF, CO,…), whose transitions sometimes overlap with various methane bands. These types of laboratory spectroscopic studies of methane in the infrared

[a]Brown dwarfs are astronomical objects that have a size between 15 times and 75 times the mass of Jupiter [adapted from NASA website]

region are still in great demand for providing precise spectroscopic data in support of different ground- and space-based satellite instruments such as **ASCENDS** [Active Sensing of CO_2 Emissions over Nights, Days and Seasons], **MOPITT** [Measurements of Pollution in the Troposphere], **SCIAMACHY** [Scanning Imaging absorption Spectrometer for Atmospheric Chartography] and **GOSAT** [Greenhouse gases Observing SATellite], for most of which the uncertainty in methane concentration is desired to be less than 1% [10].

Though the spectroscopic database HITRAN2012 [11] contains the latest laboratory measurements [12], the temperature- and speed-dependence of broadening and shift coefficients along with line-mixing coefficients of methane in the 'octad' region have not been included. However, the HITRAN2012 database entries were expanded by inserting the improved position and intensity results with less uncertainty from the global study of $^{12}CH_4$ in the wavenumber range (0-4800 cm^{-1}) conducted by Albert et al. [13]. The position and intensity of rotational-vibrational methane transitions in the spectral band (4600-4887 cm^{-1}) were revised also by Daumont et al. [14]. Hence, the temperature-dependent analysis of methane in the $\nu_1 + \nu_4$ band is important to support the above mentioned remote sensing applications and for updating the spectroscopic databases. H_2 is one of the dominant constituents in the atmospheres of Jovian exoplanets and brown dwarfs [15-17]. The line parameters of methane broadened by H_2 have not been included in the public spectroscopic databases, e.g., HITRAN and GEISA. Recently, the necessity of H_2-broadened methane spectroscopic studies have been recognized by HITRAN (Rothman et al.[11] and Wilzewski et al.[18]). Varanasi [19] mentioned the necessity of studies of methane broadened by air and H_2 in support of terrestrial and Jovian atmospheres. The spectroscopic line-shape studies of methane broadened by H_2 in the cold temperature range (148.5-298.4 K) will be helpful in the estimation of hydrogen abundance in the Jovian atmosphere. The

$\nu_1 + \nu_4$ band is one of the strongest interacting bands of methane, whose study is required to interpret the complicated rotational and vibrational IR spectra of methane. The second project of the present work is thus studied with the retrieval of spectroscopic parameters of methane broadened by H_2.

1.7 Summary of previous methane line-shape studies

The previous line-shape studies of methane were mostly performed at room temperature. The first experimental room-temperature study of air-broadened methane in the retrieval of both self- and air-broadened widths and shift coefficients in the spectral range (4138-4600 cm^{-1}) was published by Devi et al. [20] in 1993, and a total of 270 transitions were analyzed for three prominent interacting bands. They analysed a total of five room-temperature recorded absorption spectra with a resolution of 0.01 cm^{-1} using the McMath Fourier transform spectrometer. Smaller broadening coefficients for *E*-species were found compared to *A*- and *F*-transitions were found and most of the retrieved shift coefficients were negative ranging from -0.0179 to +0.0011 $cm^{-1}atm^{-1}$. In the following year, the same authors [21] investigated 29 laboratory spectra and reported the temperature-dependent (212.15-297.15 K) Lorentz half widths and shift coefficients for 740 transitions of air-broadened methane in the spectral range from 4118 to 4615 cm^{-1}. They analyzed 29 spectra using a multi-spectrum non-linear least-squares fitting technique and the line parameters were presented as a function of tetrahedral symmetry species and rotational quantum numbers. They retrieved air-broadened widths and shifts along with their temperature dependences, which were found to be transition dependent. The majority of pressure-induced shift coefficients were negative but about 85% of temperature-dependence shift coefficients were found to be positive.

Pine and Gabard [22] published the collisional line-shape parameters using a first-order approximation for the Q branch transitions in the ν_3 band of methane recorded at pressures ranging from 0.014 to 66.66 kPa. They pointed out that the line-mixing is significant at pressures close to atmospheric. Different buffer gases (H_2, He, N_2, O_2, Ar, CH_4) were used for broadening of methane bands. Uniformly negative values of pressure-induced shift coefficients were obtained for all perturbers except for He.

Comprehensive room-temperature laboratory measurements for retrieving the self- and air-broadening coefficients along with the vibrational dependency of methane bands in the spectral range of 4100-4635 cm^{-1} were performed by Predoi-Cross et al. [23, 24] with the employment of a multi-spectrum non-linear least-square fitting algorithm. They analyzed 10 high-resolution laboratory recorded spectra using the McMath FTS located at National Observatory on Kitt Peak, Arizona and reported self- and air-broadened widths and shift coefficients. According to their observations of self-broadening of methane, the pressure-shift coefficients varied from -0.020 to -0.005 cm^{-1} atm^{-1} and half-width coefficients varied from 0.045 to almost 0.090 cm^{-1} atm^{-1} for 1423 transitions. They reported a total of 1011 transitions for air-broadening of methane as a function of tetrahedral symmetry species and rotational quantum numbers and systemic patterns in variations of their retrieved pressure broadening and pressure-shift coefficients. The vibrational dependency on the half-width and pressure-induced shift coefficients was also reported.

The first room-temperature line-mixing analysis of methane in the wavenumber range of 4410-4629 cm^{-1} for the $\nu_2 + \nu_3$ band was reported by Predoi-Cross et al. [25]. The off-diagonal relaxation matrix elements represents the line mixing coefficients, which were reported for 18 strongest pairs of transitions. The coefficients were shown to vary from 0.0019 to 0.0390 $cm^{-1}atm^{-1}$ and 0.0005 to 0.0205 $cm^{-1}atm^{-1}$ for self- and air-broadening of

methane, respectively. Other theoretical and experimental results for different bands of methane were published in reference [26-34].

Recently, Devi et al. [35] and Hashemi et al. [36] published their findings on temperature-dependent self- and air-broadened methane transitions in the bands $\nu_2 + \nu_3$ and $\nu_3 + \nu_4$, respectively. The necessity of the multi-spectrum analysis of methane in its other strongest band, $\nu_1 + \nu_4$, was pointed out in their publications. The $\nu_1 + \nu_4$ band is one of the most intense bands of methane located at 4020 cm^{-1}, whose line shape parameters are essential to understand the vibration-rotation coupling and Coriolis effects in the fine structure of methane in the combination band. Fourteen high-resolution methane, broadened by itself and air were analysed by Devi et al. [35] using the multi-spectrum non-linear least-squares fitting method. They found slightly higher values in temperature-dependence exponents of air-broadened half widths compared to the self-broadened half widths of methane and the temperature dependences of pressure-induced shift coefficients were larger for self-shift compared to air-shift. As reported in [36], the retrieved half-width coefficients due to self-broadening of methane were higher than for air-broadening of methane. More negative values in self-shift coefficients were obtained than in air-shift coefficients. The trend in their temperature-dependence half-widths and shift coefficients due to self- and air-broadening was similar to the above mentioned studies [35].

Though the line-mixing effects were reflected in previous analyses, one of the most important parameters arising from line-mixing called ‘speed dependency’ are rarely reported. The first project of the present thesis is focused on the retrievals of self- and air-broadened half-width and shifts coefficients along with their temperature dependencies in the $\nu_1 + \nu_4$ band of methane using a multi-spectrum non-linear fitting program.

Previously, a very limited study was carried out in the retrieval of spectroscopic line-shape parameters of methane broadened by H_2. Varanasi [19] studied the collisional broadened half widths of methane in its ν_3 and $2\nu_3$ bands broadened by different perturbers including H_2 in 1971. He showed that the self-broadening of methane depends more strongly on the rotational quantum number compared to foreign broadening of methane by other gas molecules like H_2, He, N_2, O_2 and air. In 1989, Varanasi and Chudamani [37] used the tunable diode laser spectroscopy to study the temperature-dependences of width and shift coefficients for ν_4 band of methane at low temperatures (161–295 K) broadened by He, Ne, Ar, H_2, N_2, O_2 and air. For H_2-broadening of methane, the half widths parameters and temperature exponents varied from 0.0479 to 0.0878 $cm^{-1}atm^{-1}$ and 0.35 to 0.52, respectively. They found all H_2-shift coefficient values as negative ranging from -0.0059 to 0.000 $cm^{-1}atm^{-1}$.

Margolis [38] investigated the combination bands $\nu_1 + \nu_4$ and $\nu_3 + \nu_4$ of CH_4 broadened by H_2 at room-temperature. He recorded spectra using FTS at Kitt peak having unapodized resolution 0.011 cm^{-1} at room-temperature over a range of methane pressures (8.15-15.10 Torr) and hydrogen pressures (297-407 Torr). A gas cell of 80 cm length was used in the recording of spectra. He retrieved more than 200 transitions and ignored many transitions to report in the paper because they were either overlapped with other transitions or too weak or combination of both. All of the shift parameter values he found as negative with larger uncertainties compared to the half-width coefficients. The half-width coefficients were found to be dependent on tetrahedral symmetry species (*A, E, F*). A clear trend of variation in width coefficients for *E* species was observed and the values of the widths for *E* species were found to be smaller than those of *A* and *F* species.

In 1993, Margolis again published the results of H_2-broadening coefficients [39] in the ν_4 band of methane at room temperature and 200 K. He compared the results of broadening parameters for 257 lines with his previously published values in the $\nu_1 + \nu_4$ and $\nu_3 + \nu_4$ bands and he found the average precision of the broadening coefficients ~ 2.5%.

The line-shape studies of $^{13}CH_4$ broadened by H_2 and He were also performed by Margolis [40] at room temperature. He used 1 m FTS at Kitt peak with the resolution of 0.0065 cm^{-1} and two gas cells with path lengths of 25 and 150 cm were used in the recording of spectra. He reported broadening and shift parameters for 266 transitions for *J* values up to 16. He found lower values of H_2-broadened half-width coefficients for E-type transitions compared to other two types (*A*, *F*) transitions. The shift parameters due to H_2-shift were found negative and no discernible pattern of variations in shift coefficients was observed.

1.8 Goal and objectives of my present research

The goal of the present research is to study the temperature-dependent line-shape parameters of methane broadened by itself, air and H_2 in the spectral range of 4100-4300 cm^{-1}.

For the analysis of methane broadened by itself and air, a total of 14 laboratory spectra with high signal-to-noise ratio (≥2000) over a range of pressures (4.5-385 Torr) and temperatures (148.4-298.4 K) were recorded using a Fourier Transform Spectrometer (FTS) at Jet Propulsion Laboratory, California. The Lorentz half-width coefficients and pressure-induced shift coefficients along with their temperature dependences are reported as a function of rotational quantum index $|m|$, where $|m|$ takes lower state *J* values for *P*, *Q*-branch transitions but upper state *J* values for *R*-branch transitions. Line-mixing

coefficients and the speed- dependence parameters are also presented as a function of $|m|$ by using the multi-spectrum fitted software 'Labfit' with the implementation of speed-dependent Voigt profile (SDVP). The results are then compared with the available line-shape parameters in the spectroscopic databases and relevant literature.

In the second project, I investigate the temperature-dependent line-shape studies of methane broadened by itself and hydrogen in the combination band $\nu_1 + \nu_4$ of methane. The Lorentz half-width coefficients along with temperature dependences, pressure-shift coefficients with temperature dependences, speed-dependence parameters and line-mixing coefficients are reported for both self- and H_2-broadening of methane. A multi-spectrum fitted software 'Labfit' was used in the fitting of spectra. Line-mixing parameters in both projects were determined using 'Labfit' through off-diagonal relaxation matrix formalism.

CHAPTER 2: THEORETICAL CONCEPTS

To study the line-shape parameters of methane, it is essential to understand rotational and vibrational spectroscopy. The present study is focused on the analysis of absorption spectroscopy of the methane in its $\nu_1 + \nu_4$ band resulting from the interaction with Infrared (IR) Radiation as the light source. This chapter covers the basic understanding of quantum mechanics of absorption spectra of diatomic molecules and extending the discussion further to spherical top polyatomic molecules. Since methane is a complex polyatomic molecule, the symmetry and band structures of this molecule are also discussed. The different line-shape profiles including the Speed Dependence Voigt Profile (SDVP) are introduced, which are considered as vital to interpret the experimental absorption features of the studied molecule. Another important term "line mixing" is outlined in the end of the chapter. This chapter has been written based on the concepts described in the books of 'Modern Spectroscopy, 4th edition by J. Michael Hollas' [41] and 'Spectra of Atoms of Molecules, 2nd edition by Peter F. Bernath' [42].

2.1 Quantum mechanical aspects of energy

2.1.1 History of quantum mechanics

During the end of nineteenth century, classical mechanics was replaced by quantum mechanics for the better understanding of molecular spectroscopy at the atomic scale. Studying hydrogen as the simplest atom, calculation of its emission spectra was performed by Balmer, which opened the window for spectroscopy of other molecules. For the hydrogen atom, the discrete nature of energy for Balmer series can be given by the following equation:

$$\nu = R_H \left(\frac{1}{2^2} - \frac{1}{n'^2}\right) \quad (2.1)$$

where ν is the frequency of light in unit of Hz, which can be calculated from the ratio of velocity of light and wavelength of the emitted light (c/λ) of the H atom. R_H is the Rydberg constant (1.097×10^7 m^{-1}) for the H atom and n' defines the energy level, whose values are 3, 4, 5, …..

In 1900, Einstein and Planck described the quantization of light and deduced the relationship between energy and wavenumber expressed by:

$$E = nh\nu = nhc\tilde{\nu} \quad (2.2)$$

where n is an integer (0, 1, 2, 3, 4,…), h is Planck's constant, $\tilde{\nu}$ is the wavenumber, which is the reciprocal of wavelength of light and defines the number of waves per unit wavelength in cm.

The present study is based on the infrared spectroscopy of methane. The transitions occur due to both vibration and rotation of the molecules. Therefore, rotational and vibrational spectroscopy are discussed separately.

2.1.2 Rotational energy of a simple diatomic molecule

The rotation of any diatomic molecule can be approximated by the rigid rotor model, in which the molecule can rotate with respect to the center of gravity and the line joining the nuclei is assumed as a rigid and weightless rod (Fig. 2.1). The solution of the Schrödinger equation for a rigid rotor model of diatomic molecule gives the rotational energy,

$$E_r = \frac{h^2}{8\pi^2 I} J(J+1) \quad (2.3)$$

which is quantized, where $I = \mu r^2$ is the moment of inertia of the molecule, $\mu = \frac{m_1 m_2}{m_1 + m_2}$ is the reduced mass of a two-particle system of masses m_1 and m_2, and r is the inter-nuclear distance. J is defined as the rotational quantum number (neglecting the orbital and spin angular momentum assuming rigit-rotor model), whose values are integers: J = 0, 1, 2,…..

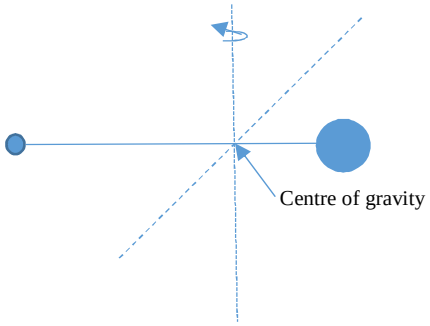

Fig 2.1: Simplified example of the rotation of a heteronuclear diatomic molecule.

2.1.3 The expression of vibrational energy of a simple diatomic molecule

The vibrational energy of a diatomic molecule can be calculated assuming the simple ball-and-spring model, which demonstrates the vibration of the nuclei in the form of stretching and compression of the inter-nuclear bond obeying Hooke's law:

$$F = -kx \tag{2.4}$$

where F is the restoring force, x is the displacement from the equilibrium position due to stretching or compressing, and k is the spring force constant. The Hamiltonian of a diatomic molecule assuming the simple harmonic oscillator can be written as:

$$H = -\frac{h^2}{8\pi^2 \mu}\frac{d^2}{dx^2} + \frac{1}{2}kx^2 \tag{2.5}$$

The time-independent one-dimensional Schrödinger equation takes the following form:

$$\frac{d^2\psi_v(x)}{dx^2} + \left(\frac{8\pi^2 \mu E_v}{h^2} - \frac{4\pi^2 \mu k x^2}{h^2}\right)\psi_v(x) = E\psi_v(x) \tag{2.6}$$

where ψ_v indicates the vibrational wave function. The solution of Eq. (2.6) gives the expression for vibrational energy:

$$E_v = h\nu(v + 1/2) \tag{2.7}$$

in which v is the vibrational quantum number whose values are the integers 0, 1, 2, 3…. The classical vibration frequency, ν relates to the spring constant (k) and the reduced mass (μ) by the following expression:

$$\nu = \frac{1}{2\pi}\sqrt{\frac{k}{\mu}} \tag{2.8}$$

According to Eq. (2.7), the energy for the $v = 0$ gives the zero-point energy of $(h\nu/2)$ and the vibrational energy levels are equally spaced. The vibrational energy in terms of wavenumber $\tilde{\nu}$ can be written as,

$$E_v = hc\tilde{\nu}(v + 1/2) \tag{2.9}$$

The vibrational energy levels are, therefore, equally spaced and separated by $hc\tilde{\nu}$. The potential energy curve for a diatomic molecule using the harmonic oscillator approximation with equally spaced energy level is shown in Fig. 2.2.

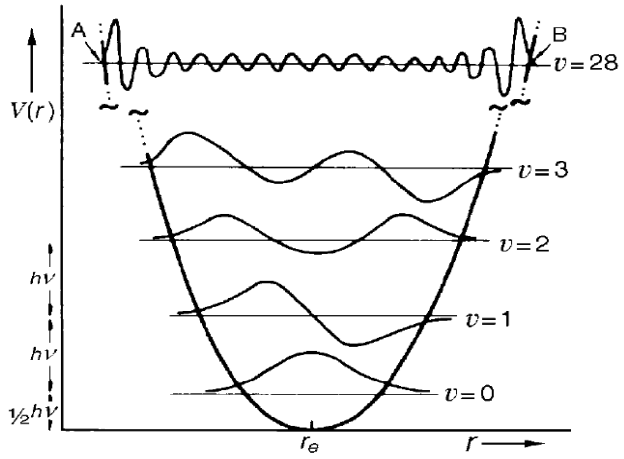

Fig 2.2: The potential energy curve for the harmonic oscillator model, where r_e is the equilibrium position at the bottom of the curve and the vibrational levels are equally spaced. (Source: Page 24, Chapter 1, Modern Spectroscopy, 4th edition, by Michael Hollas [41]).

2.1.4 Interaction of electromagnetic radiation with matter

The interaction of light with molecules is the main focus of molecular spectroscopy. Light is electromagnetic (EM) radiation which is composed of two vector components, electric field $\left(\vec{E}\right)$ and magnetic field $\left(\vec{H}\right)$. They are perpendicular to each other and behave as the oscillating field of strengths $\left|\vec{E}\right|$ and $\left|\vec{H}\right|$, respectively. Fig 2.3 displays the picture of an EM radiation travelling in the x direction, in which both the fields oscillate with the frequency of $2\pi\nu$. The y and z components of $\vec{E}$ and $\vec{H}$ for the depicted EM wave can be written in the following forms:

$$E_y = E_{0y}cos(2\pi\nu t - kx) \tag{2.10}$$

$$H_z = H_{0z}cos(2\pi\nu t - kx) \tag{2.11}$$

where k is known as the wave vector, E_{0y} and H_{0z} are the maximum strength of E_y and H_z.

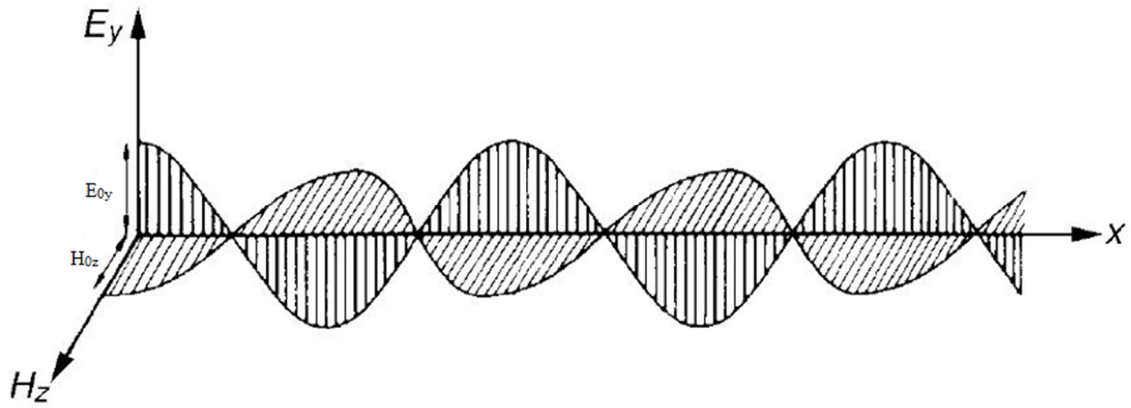

Fig 2.3: The movement of electromagnetic radiation along horizontal direction with having the electric and magnetic components along y and z direction, respectively. (Source: Page 27, Chapter 2, Modern Spectroscopy, 4th edition, by Michael Hollas [41]).

When *EM* radiation is applied to a two-level transition system containing the upper state (n') and lower state (n''), the transition is only possible when the change in energy between two states is equal to the energy of the incident radiation.

$$\Delta E = h\nu = hc\tilde{\nu} \tag{2.12}$$

in which ν and $\tilde{\nu}$ represent the frequency of the radiation in *Hz* and line position in cm^{-1}, respectively, *c* is the speed of light and *h* is Planck's constant with 6.626×10^{-34} m^2 *kg/s*.

The *EM* spectrum covers a wide range of frequencies from radio waves to gamma rays among which infrared (IR) radiation has the wavenumber range from 33-13,000 cm^{-1}. The IR region encompasses three spectral regions; far-, mid- and near-infrared corresponding to (400-33 cm^{-1}), (4000-400 cm^{-1}) and (13000-4000 cm^{-1}), respectively. The fundamental vibrations of most molecules occur in the mid-infrared region, whereas the overtone vibrational transitions and some electronic transitions are observed in the near-IR spectral range. The transition process can be of the following three types (Fig. 2.4):

i) Induced absorption: If the molecular species M absorbs the incident radiation of energy $hc\tilde{\nu}$ which excites the molecule from the lower state, n'' to the upper state n', the transition process is called induced absorption, which is described by the following equation:

$$M + hc\tilde{\nu} \longrightarrow M^* \tag{2.13}$$

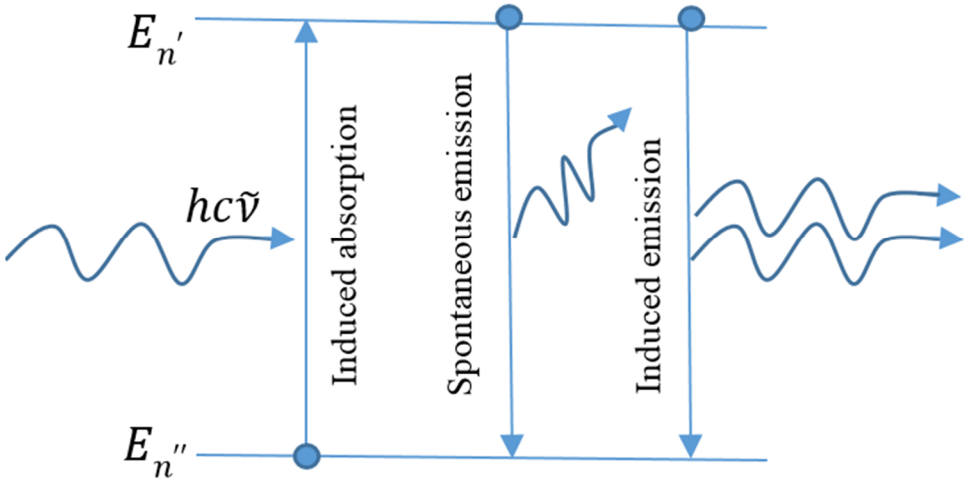

Fig 2.4: Three types of possible transition phenomena occurred due to the interaction of EM radiation with material. (Source: Page 28, Chapter 2, Modern Spectroscopy, 4th edition, by Michael Hollas [41]).

ii) Spontaneous emission: This is the spontaneous process of transition in which the excited molecular state M^* can be de-excited to its original state M by giving up a photon of same energy $hc\tilde{\nu}$ that is necessary for the corresponding excitation. The spontaneous emission can be illustrated by the following equation:

$$M^* - hc\tilde{\nu} \longrightarrow M \tag{2.14}$$

iii) Stimulated emission: The excited molecular state M^* sitting in the upper state n' receives one more quanta of $hc\tilde{\nu}$, which results in the transfer of

electron from higher state to lower state. This transition process can be explained by the equation:

$$M^* + hc\tilde{\nu} \longrightarrow M + 2hc\tilde{\nu} \tag{2.15}$$

2.2 Rotation-vibration spectroscopy

The present study is based on infrared spectroscopy of the methane molecule. The transitions occurs due to both vibration and rotation of the molecule, therefore, rotation-vibration coupling needs to be discussed. Rotational and vibrational spectroscopy are discussed separately. The selection rules for ro-vibration transitions are also discussed briefly in this section.

The intensity is proportional to the square of the transition moment, which is defined by

$$\boldsymbol{R}^{n'n''} = \int \psi^*_{n'} \boldsymbol{\mu} \psi_{n''} d\tau \tag{2.16}$$

where $\psi_{n'}$ and $\psi_{n''}$ are the wave functions associated with states n' and n'', $\boldsymbol{\mu}$ is the electric dipole moment vector, $d\tau$ is used to specify the integral over all coordinates. The transition is either 'forbidden' or 'allowed' depending on the value of $\left|\boldsymbol{R}^{n'n''}\right|^2$,which follows selection rules: $\left|\boldsymbol{R}^{n'n''}\right|^2 = 0$ for forbidden and $\left|\boldsymbol{R}^{n'n''}\right|^2 \neq 0$ for allowed transition.

2.2.1 Pure rotation

The concept of the rotational energy can be understood from the classical concept of energy of a particle rotating around an axis. The energy of a rotating particle around any axis is given by $E = \frac{1}{2} I\omega^2$, where ω is the angular velocity of the particle in unit of *rad/s*, I is the moment of inertia of the particle defined by $I = mr^2$, *m* is the mass of the particle

and r is the perpendicular distance of the particle from the axis of rotation. Classically, the total energy of any arbitrary rotating particle can be expressed by the following equation:

$$E = \frac{1}{2} I_A {\omega_A}^2 + \frac{1}{2} I_B {\omega_B}^2 + \frac{1}{2} I_C {\omega_C}^2 \quad (2.17)$$

A, B, C in the above equation are known as the principal axes of rotation. The total energy due to the rotation of the molecule can be written as:

$$E = \frac{1}{2} \frac{{J_A}^2}{I_A} + \frac{1}{2} \frac{{J_B}^2}{I_B} + \frac{1}{2} \frac{{J_C}^2}{I_C} \quad (2.18)$$

where, I_A, I_B and I_C are the moment of inertia along three principal axes which are equal ($I_A = I_B = I_C$) for methane and J_A, J_B and J_C are the rotational angular momenta along three principal axes A, B and C. The symmetry of methane as a tetrahedral molecule consists of 4 C_3 axes, 3 C_2 axes and 6 vertical plane of reflections (σ_v) and no inversion center, where C_3 and C_2 are the 3-fold and 2-fold axes of rotation, σ_v is the vertical plane of reflection as the symmetry elements.

2.2.2 Rotational spectra

The rotational energy of the spherical top molecule ($I_A = I_B = I_C$), e.g., methane, is given by:

$$E_r = \frac{{J_A}^2 + {J_B}^2 + {J_C}^2}{2I} = \frac{J^2}{2I} \quad (2.19)$$

The quantum mechanical expression of the rotational energy can be derived by taking the operator of $\boldsymbol{J^2}$ on the wavefuncion ψ, i.e., $\boldsymbol{J^2}\psi = \left(h^2/4\pi^2\right) J(J+1)\psi$:

$$E_r = \frac{h^2}{8\pi^2 I} J(J+1) \quad (2.20)$$

which is exactly same as Eq. (2.3) and *J* is known as the rotational quantum number in quantum mechanics and *I* is the moment of inertia.

In IR spectroscopy, the rotational energy term values *F(J)* in cm^{-1} can be calculated by $E_r/(hc)$, which are expressed by:

$$F(J)[cm^{-1}] = BJ(J+1) \tag{2.21}$$

The constant *B* shown in the above equation is known as a rotational constant, whose values are expressed in terms of the wavenumbers dimension by:

$$B[cm^{-1}] = \frac{h}{8\pi^2 cI} \tag{2.22}$$

where *I* is the moment of inertia, the property of a particle to resist the angular acceleration and it is determined as the mass times the square of its perpendicular distance from the axis of rotation.

The transition moment of a two-level rotational transition system can be written as:

$$\boldsymbol{R}_r = \int \psi_r^{'*} \boldsymbol{\mu} \psi_r^{''} d\tau \tag{2.23}$$

where *r* is used to specify the rotational transition, $\boldsymbol{\mu}$ is the dipole moment vector defined as $\boldsymbol{\mu} = q\boldsymbol{d}$, where q is the electric charge and $\boldsymbol{d}$ is the displacement vector directing from negative charge to positive charge. The single and double primes denote the upper state and lower state of the transition system, respectively.

The transition intensity is proportional to the square of the transition moment, and for the transition to be allowed, it must satisfy following selection rules:

i. The dipole moment of the molecule must be non-zero; $\boldsymbol{\mu} \neq 0$.

ii. The change in rotational quantum number between two states must be $\Delta J = \pm 1$.

In absorption spectroscopy, $\Delta J = J' - J''$, where J' corresponds to the quantum number of the upper state and J'' stands for the lower state of the rotational transition. The line positions of the rotational spectra in terms of the wavenumber [cm^{-1}] are given by:

$$\tilde{\nu}_{J' \leftarrow J''}[cm^{-1}] = F\left(J'\right) - F\left(J''\right) = F(J+1) - F(J) = 2B(J+1) \qquad (2.24)$$

The value of J (0, 1, 2…….) in Eq. (2.24) takes the lower rotational quantum state of the vibrational ground state and two consecutive allowed rotational transitions are always separated by a constant spacing of 2B. The value of rotational constant, B can be determined by rotational spectroscopy, from which the moment of inertia of the molecule can be estimated and the bond lengths in the molecule can be confirmed.

2.2.3 Transition intensity

The intensity of the transition depends on the distribution of population in the two different quantum states; the difference in population between ground and excited states of the transition is one of the ways to measure the intensity. The population of any quantum state is defined as the average number of molecules residing in it at any given time. The transition intensity of the molecules is therefore dictated by the population difference and at room temperature (T=25°C) the majority of molecules are in the ground vibrational energy level. The population in the excited J^{th} state of the transition, N_J is related to the population in the ground state, N_0 by the Boltzmann distribution law:

$$\frac{N_J}{N_0} = (2J+1)e^{-\frac{E_r}{kT}} \qquad (2.25)$$

where $(2J + 1)$ represents the degeneracy of the J^{th} level arising due to the symmetry of methane and T is the absolute temperature. The level of population becomes a maximum (J=J_{max}) corresponding to the condition $\frac{d}{dJ}\left(\frac{N_J}{N_0}\right) = 0$.

Therefore, $J_{max} = \sqrt{\left(\frac{kT}{2hcB}\right)} - \frac{1}{2}$ (2.26)

which gives the J for the level with maximum population.

2.2.4 Centrifugal distortion

Since methane as a spherical top molecule has no permanent dipole moment, it should not show any pure rotational spectra, but it exhibits some weak rotational spectra due to centrifugal distortion. The centrifugal distortion of methane molecules induces a dipole moment due to the vibration-rotational coupling for which the atoms are pulled away from each other with high rotational speeds causing the breakdown of its molecular symmetry.

Taking into account the centrifugal distortion term, the equations for the rotational energy term (Eq. (2.21)) and the line positions in cm^{-1} (Eq. (2.24)) can be written in the following way

$$F(J)[cm^{-1}] = BJ(J + 1) - DJ^2(J + 1)^2 \quad (2.27)$$

and $$\tilde{\nu}[cm^{-1}] = F(J + 1) - F(J) = 2B(J + 1) - 4D(J + 1)^3 \quad (2.28)$$

where D is known as the centrifugal distortion constant, which has a negligible effect for lower state J values.

When we consider the rotation of the methane molecule with respect to any of the C_3 rotational axes (any of four *C-H* bond axes), the rest of the *H* atoms are displaced from the axis of rotation slightly which is known as 'centrifugal distortion'. Therefore the spherical rotor molecule transforms into a symmetric rotor system, which provides a very weak rotational spectra.

The vibrational dependency of rotational constant B_v and centrifugal distortion constant D_v are related to the vibration-rotation coupling constants α and β by the following expressions:

$$B_v = B_e - \sum_i \alpha_i \left(v_i + \frac{d_i}{2}\right) \tag{2.29}$$

$$D_v = D_e - \sum_i \beta_i \left(v_i + \frac{d_i}{2}\right) \tag{2.30}$$

where the rotational constants B_e and D_e correspond to the equilibrium state of the potential energy of the molecule, d_i denotes the degeneracy of the vibrational level (where $d_i = 1$ represents the non-degenerate level). The ro-vibrational coupling constants α_i and β_i are very small compared to the rotational constants B_e and D_e at equilibrium. Since there is slight vibrational dependency of both rotational and distortion constants *B* and *D*, so Eq. (2.27) and (2.28) can be written in the modified form given by:

$$F_v(J) = B_v J(J+1) - D_v J^2 (J+1)^2 \tag{2.31}$$

$$\tilde{\nu}[cm^{-1}] = 2B_v(J+1) - 4D_v(J+1)^3 \tag{2.32}$$

2.3 Vibrational spectroscopy

The vibration of the molecule can be approximated as a spring ball system considering the simple harmonic system for a diatomic molecule. For calculating the

vibrational energy of polyatomic molecules like methane, there will be a violation of harmonic approximation and anharmonicity terms will be required to explain the vibrational energy. For any molecule containing *N* number of atoms, 3*N* degrees of freedom describe the motion of the atoms in a molecule. Of these 3*N* degrees of freedom, 3 are associated with the translation of the entire molecule and 3 (for non-linear) / 2 (for linear molecules) are associated with the rotation of the molecule. This means that for polyatomic molecules, 3*N*-5 (lineal molecules) and 3*N*-6 (nonlinear molecules) degrees of freedom are essential to describe their vibrations. Since there are 5 atoms in methane, therefore, 3*N*-6=9 fundamental modes of vibration are required to describe its vibrational motion.

2.3.1 Vibrational energy of a diatomic molecule

The equation for calculating the vibrational energy of a diatomic molecule was given in Eq. (2.7). Similar to rotational term, the vibrational energy levels of a polyatomic molecule can be represented by the following vibrational term values:

$$G(v) = \frac{E_v}{hc} = \tilde{\nu}(v + \frac{1}{2}) \tag{2.33}$$

where $\tilde{\nu}$ is known as the frequency of vibration in cm^{-1} and v is the vibrational quantum number.

2.3.2 Infrared spectra of a diatomic molecule

One of the conditions in IR spectroscopy, the molecule must shows a non-zero change in dipole moment $(d\mu/dr \neq 0)$ with respect to the nuclear coordinate *r*, the internuclear distance. The vibrational analogues of the transition moment of a two level quantum mechanical system can be rewritten in the following way:

$$\boldsymbol{R}_v = \int \psi_v^{'*} \boldsymbol{\mu} \psi_v^{''} dx \tag{2.34}$$

where $\psi_v^{''}$ and $\psi_v^{'*}$ represent the wave functions associated with the lower vibrational states and the upper excited vibrational states of the quantum system, respectively. The superscript $*$ is used to specify the complex conjugate of the lower state, *x* is the separation distance between the nuclear coordinate and the equilibrium position at the bottom of potential energy curve, i.e., $x = (r - r_e)$. For any homo-nuclear diatomic molecule (like O_2), $\boldsymbol{R}_v = 0$ but, $\boldsymbol{R}_v \neq 0$ for any heteronuclear diatomic molecule (like HCl). Thus the change in transition moment can be expanded through a Taylor series as expressed by:

$$\boldsymbol{\mu} = \boldsymbol{\mu}_e + \left(\frac{d\boldsymbol{\mu}}{dx}\right)_e x + \frac{1}{2!}\left(\frac{d^2\boldsymbol{\mu}}{dx^2}\right)_e x^2 + \cdots \tag{2.35}$$

By putting the value of $\boldsymbol{\mu}$ and neglecting higher terms, Eq. (2.34) can be rewritten as:

$$\boldsymbol{R}_v = \boldsymbol{\mu}_e \int \psi_v^{'*} \psi_v^{''} dx + \left(\frac{d\boldsymbol{\mu}}{dx}\right)_e \int \psi_v^{'*} x \psi_v^{''} dx + \cdots \tag{2.36}$$

where the subscript *e* is used to specify the equilibrium. The first term in Eq. (2.36) would be zero because of the orthogonality condition, i.e., for $\psi_v^{'*}$ and $\psi_v^{''}$, if $v' \neq v''$, they are orthogonal and $\int \psi_v^{'*} \psi_v^{''} dx = 0$. Therefore, the vibrational transition moment depends on the change of dipole moment with respect to *x*,

$$\boldsymbol{R}_v = \left(\frac{d\boldsymbol{\mu}}{dx}\right)_e \int \psi_v^{'*} x \psi_v^{''} dx + \cdots \tag{2.37}$$

The transition is either allowed or forbidden depending on the vibrational selection rule ($\Delta v = \pm 1$), where Δv is the change in vibrational states between upper state $v^{'}$ and lower state $v^{''}$. The transition intensity of the molecule due to the vibration of the molecule can thus be determined from the square of the change in the transition moment $(d\boldsymbol{\mu}/dx)_e^2$ and

is also dictated by the population difference between the excited and ground vibrational states and the corresponding equation is modified as:

$$\frac{N_v}{N_0} = e^{-\frac{E_v}{kT}} \tag{2.38}$$

The band in the absorption spectrum is defined by the vibrational transition of the molecule in its gas phase and the transition between two rotational states of the two different vibrational states is referred to as 'line', which is used to determine the fine structure of the molecular band. The 'spectral line' is the results of light-matter interaction, which is a combination of continuous dark or bright lines appeared due to the emission or absorption of light in a narrow wavenumber range. An important feature of spectroscopy is that the selection rules only tell us about the probability of a transition occurring.

The harmonic oscillator approximation will no longer be valid at much larger values of *r* compared to the equilibrium position r_e at the bottom of potential energy curve. The comparative potential energy curves both for the harmonic and anharmonic oscillators models are shown in Fig. 2.5, where the dashed line represent the curve for the harmonic oscillator approximation and the rigid line is for the potential energy curve due to anharmonicty, D_e is the dissociation energy due to the dissociation of nuclei from its equilibrium position at larger distance.

The constant called dissociation energy 'D_e' can be expresses by:

$$D_e \cong \frac{\tilde{\nu}_e{}^2}{4\tilde{\nu}_e x_e} \tag{2.39}$$

where $\tilde{\nu}_e$ represents the vibration wavenumber and $\tilde{\nu}_e x_e$ is the first order anharmonic terms.

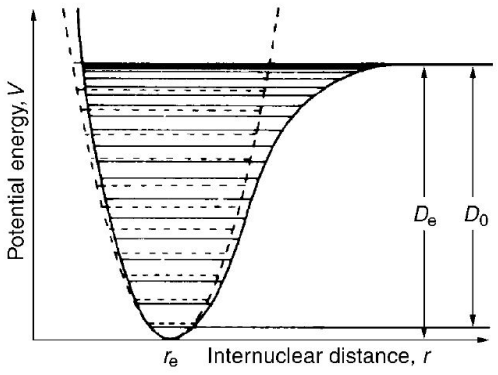

Fig 2.5: The potential energy curves for hetero-nuclear diatomic molecule considering both harmonic and anharmonic approximations. (Source: Page 143, Chapter 6, Modern Spectroscopy, 4th edition, by Michael Hollas [41]).

Thus the deviation from the harmonicity of the molecule also relaxes the vibrational selection rule from $\Delta v = \pm 1$ to $\Delta v = \pm 1, \pm 2, \pm 3, \ldots$ which introduces the concept of overtone bands ($\Delta v = \pm 2, \pm 3, \ldots$). The overtone transitions are usually weaker than those of fundamental bands.

Therefore, with the inclusion of mechanical anharmonicity effects, the vibrational terms (Eq. (2.33)) are modified into the form:

$$G(v) = \tilde{\nu}_e \left(v + \frac{1}{2}\right) - \tilde{\nu}_e x_e \left(v + \frac{1}{2}\right)^2 + \tilde{\nu}_e y_e \left(v + \frac{1}{2}\right)^3 + \cdots \qquad (2.40)$$

where $\tilde{\nu}_e$ represents the vibration wavenumber for the classical oscillator and $\tilde{\nu}_e x_e$ and $\tilde{\nu}_e y_e$ are due to the first and second order anharmonic terms, the higher order terms are neglected.

Unlike the harmonic oscillator problem, the wavenumbers of the transitions for anharmonic models due to vibration of molecules can be deduced to the following expression:

$$\Delta G_{v+1/2} = G(v+1) - G(v) = \tilde{\nu}_e - \tilde{\nu}_e x_e (2v+2) + \tilde{\nu}_e y_e \left(3v^2 + 6v + \frac{13}{4}\right) \qquad (2.41)$$

Thus the wavenumber representation due to the vibration of heteronuclear diatomic molecules considering the anharmonicity effects for fundamental vibration ($\Delta v = \pm 1$) is given by:

$$\Delta G_{v+1/2} = \tilde{\nu}_e - 2\tilde{\nu}_e x_e (v + 1) \tag{2.42}$$

And the transition wavenumbers for the overtone absorption bands due to weak transitions (such as 2←0, 3←0) can be determined by:

$$\Delta G_{v+1/2} = G(v + 2) - G(v) = 2\tilde{\nu}_e - 2(2v + 3)\tilde{\nu}_e x_e \tag{2.43}$$

where $\Delta G_{v+1/2}$ is used to denote the transition wavenumber.

The expression of the zero point energy for the anharmonic approximation is presented by:

$$G(0) = \frac{1}{2}\tilde{\nu}_e - \frac{1}{4}\tilde{\nu}_e x_e + \frac{1}{8}\tilde{\nu}_e y_e \tag{2.44}$$

where all anharmonic higher terms have been neglected except first order terms $\tilde{\nu}_e x_e$ and $\tilde{\nu}_e y_e$.

2.3.3 Vibrational energy of a non-linear polyatomic molecule

Based upon the above discussion for the energy structure of a hetero-nuclear diatomic molecule, the energy expression can be extended further for polyatomic molecules like methane by considering the vibration of the nuclear motion as the product of (*3N-6*) normal modes (Q_N) of vibration and the associated wavefunction for any non-linear molecule can be written in the following fashion:

$$\psi = \psi_1(Q_1).\psi_2(Q_2) \ldots \psi_{3N-6}(Q_{3N-6}) \tag{2.45}$$

Now the total energy of the non-linear polyatomic system can be determined as the summation of the energy for each normal modes of vibration. Therefore, the vibrational energy of a non-linear polyatomic molecule assuming the harmonic approximation can be written as:

$$G(v_1, v_2 \dots v_{3N-6}) = \sum_{i=1}^{3N-6} \tilde{\nu}_i \left(v_i + \frac{d_i}{2}\right) \quad (2.46)$$

In the above equation, d_i denotes the degeneracy of the i^{th} vibrational mode.

The molecule of interest in the present study is methane, which is a complex molecule and it does not follow the complete harmonic approximation. It deviates from the harmonicity and taking into account the anharmonic terms in the calculation, the vibrational energy levels can be written by the following equation:

$$G(v_1, v_2 \dots v_{3N-6}) = \sum_{i=1}^{3N-6} \tilde{\nu}_i \left(v_i + \frac{d_i}{2}\right) + \tilde{\nu}_i \sum_i \sum_{k \geq i} x_{ik}(v_i) \left(v_i + \frac{d_i}{2}\right)\left(v_k + \frac{d_k}{2}\right) \quad (2.47)$$

The terms x_{ik} in the above expression are known as the anharmonicity constants, which arise due to i^{th} and k^{th} modes of vibration and these are accountable for the combination bands. These types of combination bands are usually very weak but still detectable, resulting due to the simultaneous excitation of multiple vibrational modes at a time.

2.4 Rotation-vibration spectroscopy

As per discussion above, it is evident that a pure vibration follows the selection rule $\Delta v = v' - v'' = \pm 1$, v' are the excited vibrational states and v'' are the ground vibrational states. In rotation-vibration spectroscopy, the vibrational and rotational transitions occur simultaneously and each vibrational state contains the rotational transitions with different $J'$and J'' values, J' denote the excited rotational states and J'' specify the ground state

rotational states. In IR absorption spectroscopy, this transition is also known as "ro-vibrational transition".

The ro-vibrational term value is denoted by *S*, which can be written as the summation of both rotational $F_v(J)$ and vibrational $G(v)$ values using equations (2.31) and (2.40):

$$S(v,J) = G(v) + F_v(J) = \tilde{\nu}_e\left(v+\frac{1}{2}\right) - \tilde{\nu}_e x_e\left(v+\frac{1}{2}\right)^2 + \cdots + B_v J(J+1) - D_v J^2(J+1)^2 \tag{2.48}$$

By neglecting the centrifugal distortion and anharmonicity terms, Eq. (2.48) reduces to:

$$S(v,J) = \tilde{\nu}_e\left(v+\frac{1}{2}\right) + B_v J(J+1) \tag{2.49}$$

In ro-vibrational infrared spectroscopy, the transition occurs between $v+1 \leftarrow v$ and is governed by the selection rules $\Delta v = \pm 1$ and $\Delta J = 0, \pm 1$. The ro-vibration transitions in methane cover three complete branches *P*, *Q* and *R* belonging to parallel and perpendicular bands. The band is defined as either parallel or perpendicular depending on the change of the direction of dipole moment with respect to the molecular axis. The branch of transitions for $\Delta J = 0$ is known as Q branch, whereas the branches of transitions for $\Delta J = 1$ and $\Delta J = -1$ are known as P branch and R branch, respectively. Though Q branch is usually known as a 'forbidden', it is also used as an allowed branch of transitions for other molecules like methane.

Taking into account both rotational $\left(\vec{R}\right)$ and vibrational angular momentum $\left(\vec{l}\right)$, the rotational term values can be represented as:

$$F_v(J,l) = B_v\left[J(J+1) - l^2\right] - D_v\left[J(J+1) - l^2\right]^2 \tag{2.50}$$

where the total angular momentum of the molecule $\vec{J} = \vec{R} + \vec{l}$ and hence the total energy of the non-linear ro-vibration system is expressed by:

$$T = \sum_{i=1}^{3N-6} \tilde{\nu}_i \left(v_i + \frac{d_i}{2}\right) + \tilde{\nu}_i \sum_i \sum_{k \geq i} x_{ik}(v_i) \left(v_i + \frac{d_i}{2}\right)\left(v_k + \frac{d_k}{2}\right) +$$

$$\sum_t g_{tt}{}^2 l_t{}^2 + B_v J(J+1) - D_v[J(J+1)]^2 \qquad (2.51)$$

In the above equation, d_i is the degeneracy of the i^{th} energy level. $\tilde{\nu}_i$ represent the wavenumber in cm^{-1} and $g_{tt} = 0$, $l_t = 0$ for nondegenerate level the subscript '*t*' represents the degeneracy modes along with vibrational angular momentum l_t.

2.4.1 Infrared spectra of methane

A methane molecule has five atoms and therefore it has 9 fundamental modes of vibration to describe its vibrational motion, which are known as normal modes of vibration. Four of these normal modes are stretching and five are bending modes. Based on the irreducible presentations of the T_d point group, these fundamentals modes of methane can be assigned to four symmetry species *A*, *E*, F_1 and F_2, where one single vibration (symmetric stretch-ν_1) is the representation of the A_1 species due to four *C-H* bonds stretching, one doubly-degenerate vibration (symmetric bending-ν_2) belongs to the *E* class and two triply-degenerate vibrations (asymmetric *C-H* stretching mode -ν_3 and asymmetric bending mode- ν_4) are representations of the F_2 species. The vibrational modes are defined either as infrared active or not, depending on the ability of producing infrared spectra due to the change in the electric dipole moment. Therefore, the IR active vibrational modes of the methane molecule are asymmetric modes ν_3 and ν_4, which are triply degenerate. The two other low intensity bands ν_1 and ν_2 bands are not IR active. The normal modes of vibration for methane are shown in Fig. 2.6.

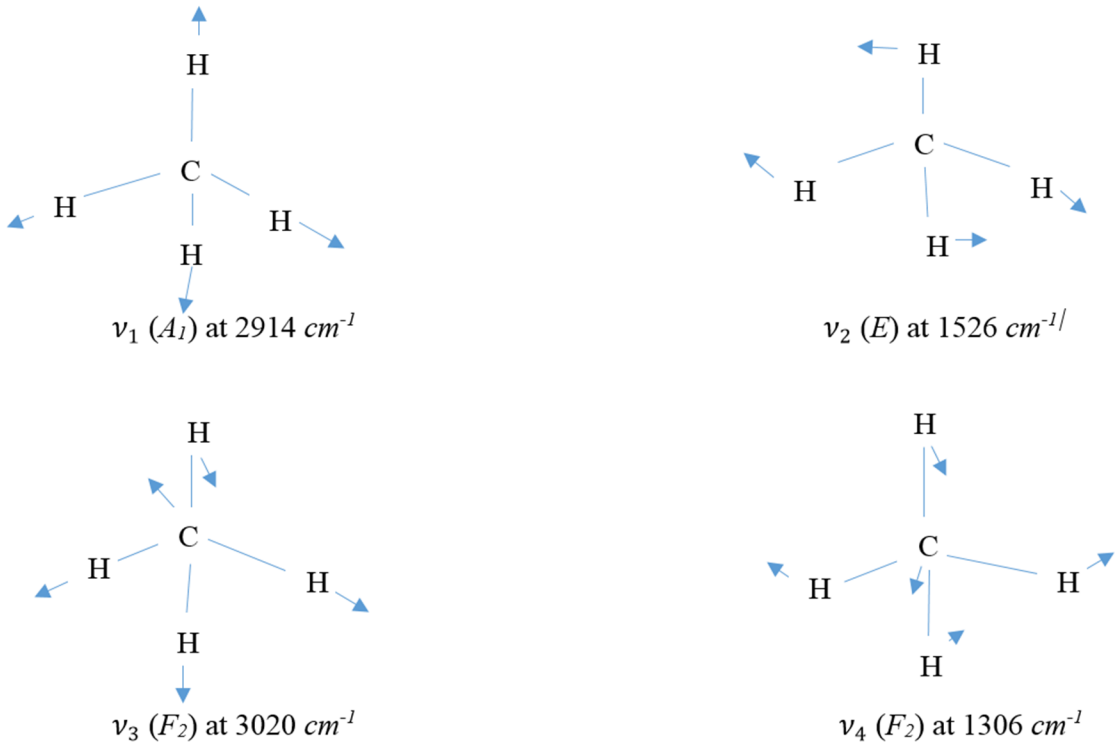

Fig 2.6: The fundamental modes of vibration for methane molecule in which ν_2 is double degenerate, ν_3 and ν_4 are triply degenerate modes.

The present study looks at the combination band $\nu_1 + \nu_4$ of methane in its octad band, i.e., eight interacting bands ($3\nu_4, \nu_2 + 2\nu_4, \nu_1 + \nu_4, \nu_3 + \nu_4, 2\nu_2 + \nu_4, \nu_1 + \nu_2, \nu_2 + \nu_3$, and $2\nu_2$) in the spectral range of 3500 to 4700 cm^{-1}. The quantum states in the rotation vibration transitions of methane are denoted by the rotational quantum number *J*, the rotational symmetry $C(A_1, A_2, E, F_1, F_2)$ and the state *n*, where the single and double prime are used to denote the energy state either as upper or lower.

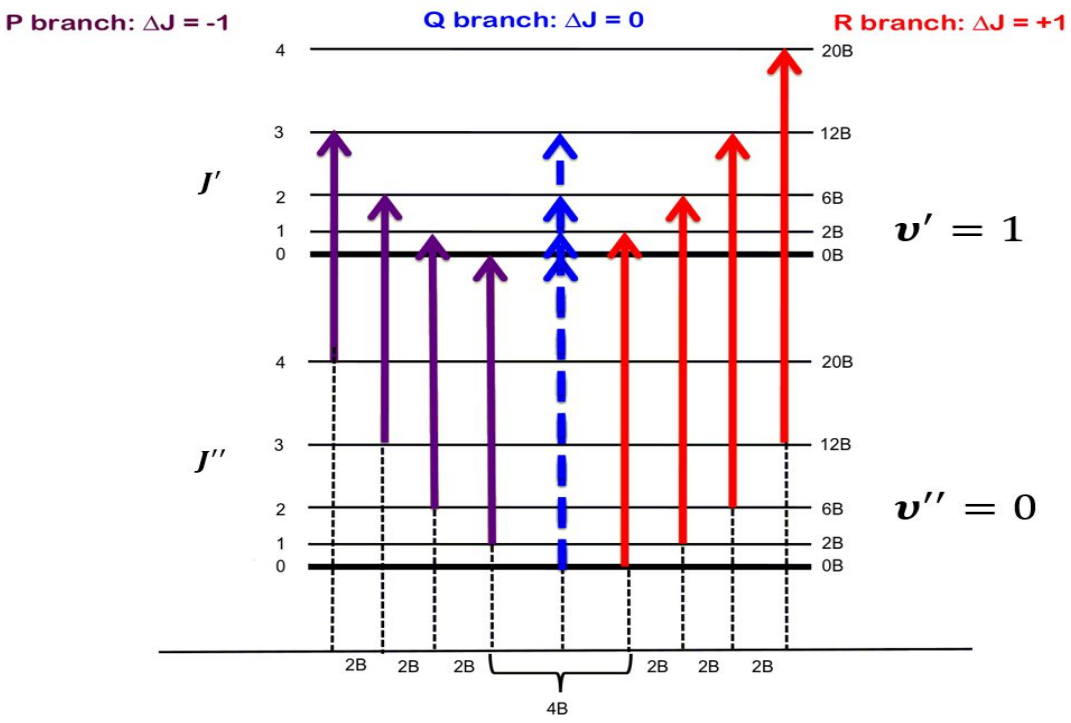

Fig 2.7: Representation of the ro-vibration fundamental transitions describing three complete branches of transition.
[Source:https://chem.libretexts.org/Core/Physical_and_Theoretical_Chemistry/Spectroscopy/Rotational_Spectroscopy/Rovibrational_Spectroscopy]

If the direction of the change in dipole moment is parallel to the molecular axis, the band is known as parallel band which has *P* and *R*- type branches of transition. If the dipole moment changes perpendicular to the molecular axis then it belongs to perpendicular band composed of *P*, *Q* and *R*- branches of transition. *P*, *Q* and *R*- transitions follow the selection rules: $\Delta J = 0, \pm 1$. A typical illustration of the ro-vibration transitions covering all three branches is shown in Fig. 2.7, where *J* represents the rotational energy levels and v denotes the vibrational energy levels, double ($''$) and single primes ($'$) are the representation for lower and upper states, respectively. The index m is defined as *–J*, *J* and *J+1* for *P*, *Q* and *R*- branch of transitions and *J* takes the lower rotational state values.

The transition wavenumbers $\tilde{\nu}_P$, $\tilde{\nu}_Q$ and $\tilde{\nu}_R$ for *P*, *Q* and *R*- branch transitions can be expressed by:

$$\tilde{\nu}_P(J) = S(v+1, J-1) - S(v, J) = \tilde{\nu} - 2BJ \tag{2.52}$$

$$\tilde{\nu}_Q(J) = S(v+1, J) - S(v, J) = \tilde{\nu} \tag{2.53}$$

$$\tilde{\nu}_R(J) = S(v+1, J+1) - S(v, J) = \tilde{\nu} + 2BJ \tag{2.54}$$

where *B* is the rotational constant and *J* takes the lower state values of rotational energy level.

2.5 Theory of line-shapes

In absorption spectroscopy, the 'Beer-Lambert law' is used for the absorption of light. Let us consider the infrared radiation of initial intensity I_0 passing through the homogenous gas medium having a defined path length of an IR gas cell. The final intensity of the radiation is being reduced after the light-gas molecule interaction inside the cell; the light is absorbed by the mixtures of gas in the gas cell, which causes the transition different ro-vibrational states. If the reduced intensity of the radiation is denoted by *I*, then according to Beer-Lambert's principle, it can be written as:

$$I(\nu) = I_0(\nu) e^{-K(\nu)L} \tag{2.55}$$

the ratio of $I(\nu)/I_0(\nu)$ provides the transmittance due to the absorption of the gas sample. The parameter $K(\nu)$ is known as the spectral absorption coefficient, which is related to the line-shape function $g(\nu - \nu_0)$ by the following expression:

$$K(\nu) = p\chi S(T) g(\nu - \nu_0) \tag{2.56}$$

where p is the pressure in atmosphere and χ is the volume mixing ratio between partial to total gas samples, $S(T)$ is the strength of the spectral line as a function of temperature in unit of $cm^{-2}atm^{-1}$, ν_0 is the center frequency of the transition and $g(\nu - \nu_0)$ represents the line shape function.

The spectral line-shape is characterized by its broadening and shift of the line from its center and the broadening of the line is characterized by its full width at half maximum (FWHM). There are basically three broadening processes involved in absorption spectroscopy, namely, natural broadening, Doppler broadening and pressure broadening.

2.5.1 Natural line broadening-Lorentzian line-shape

The frequency at which the transition occurs is called the natural line center and the frequency of various transition gives the concept of line width which covers a wide range of frequencies. Natural line broadening is the intrinsic broadening of the spectral line due to spontaneous transition from excited higher state to lower state. During the absorption of a photon, the electron usually jumps from lower state to higher state and the electron sits in the excited state for a very short time and it spontaneously returns to the ground state with emission of a photon. The number of photons emitted follow the exponential decay law as a function of time, which gives the frequency shift using the Fourier transform relation between frequency and time. The half-life of the excited state can be estimated from Heisenberg's uncertainty relation ($\Delta E \Delta t \geq h/2\pi$), which measures the uncertainty in the measured line position as a consequence of natural line broadening. The transition period of the excited state is related to the Einstein coefficient by the equation;

$$\tau = A_{10}t \tag{2.57}$$

where the Einstein coefficient A_{10} defines the probability of the light being absorbed or emitted by the atom or molecule. The larger the Einstein coefficient *A*, the stronger the transition which means the decay is more rapid. The life time of the population in the excited state is inversely proportional to the decay constant γ.

$$\tau_{sp} = \frac{1}{\gamma} = \frac{1}{A_{n'n''}} \tag{2.58}$$

where $A_{n'n''}$ is the coefficient for transition from higher $n^{'}$ to lower $n^{''}$ state due to spontaneous emission.

The larger $A_{n'n''}$ values gives rise to a wider frequency domain, which ultimately corresponds to a steeper time-domain profile resulting in the characteristics of a Lorentz profile. A Lorentz profile is the result of collisional broadening observed usually at high pressures. Since $A_{n'n''}$ defines the transition probability, which arises from the oscillating dipole moment as a function of cosine, the decaying cosine function gives the finite width of $g(\nu - \nu_{10})$ and the Lorentzian line-shape function is thus represented by:

$$g(\nu - \nu_{10}) = \frac{\gamma}{(\gamma/2)^2 + (2\pi)^2(\nu - \nu_{01})^2} \tag{2.59}$$

where γ is the Lorentz half-width which can be written as a function of pressure and temperature by the following expression:

$$\gamma(T) = \frac{P}{P_0}\gamma_0 \left(\frac{T_0}{T}\right)^n \tag{2.60}$$

In above equation, γ_0 is known as the Lorentz half-width coefficient in unit of $atm^{-1}cm^{-1}$ at standard atmospheric pressure P_0 (1 atm) and room-temperature T_0 (298 K). The normalized Lorentzian profile is illustrated in Fig. 2.8:

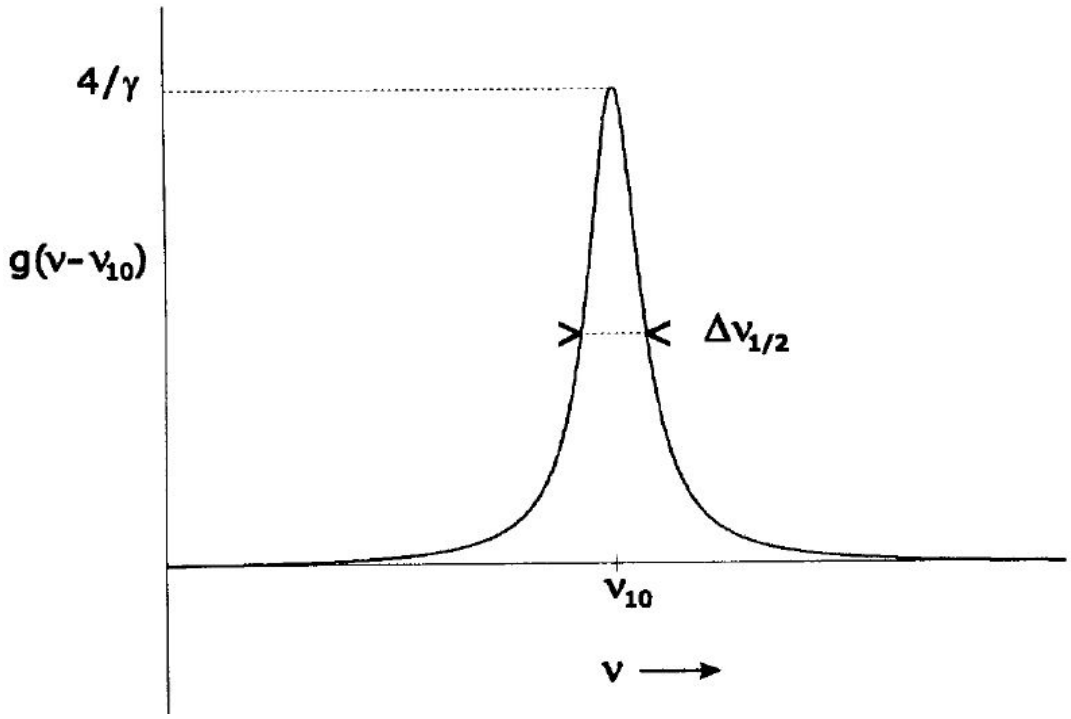

Fig 2.8: Illustration of the normalized Lorentzian line-shape function.

(Source: Page 26, Chapter 1, Spectra of Atoms and Molecules, 2nd edition, by Peter F. Bernath [42]).

At the peak intensity, $\nu = \nu_{10}$ and $g(\nu - \nu_{10})$ gives the value of $4/\gamma$ and the function drops to half value when

$$(2\pi)^2(\nu - \nu_{10})^2 = \frac{\gamma}{4\pi} \tag{2.61}$$

Therefore, the frequency for full width at half maximum of the transition peak is given by;

$$\Delta\nu_{1/2} = \frac{\gamma}{2\pi} = \frac{1}{2\pi\tau_{sp}} \tag{2.62}$$

The Lorentzian profile is thus expressed in terms of $\Delta\nu_{1/2}$ by:

$$g(\nu - \nu_{10}) = \frac{\Delta\nu_{1/2}/2\pi}{(\Delta\nu_{1/2}/2)^2 + (\nu - \nu_{10})^2} \tag{2.63}$$

The effect of natural broadening is usually neglected in the line shape studies of methane.

2.5.2 Doppler broadening-Gaussian line-shape

In case of Doppler broadening, we need to consider a cluster of molecules moving with different velocities in different directions. Molecules moving away or towards an observer give rise to a Doppler shift of the emitted radiation. The frequency of the absorbed or emitted photons, therefore, depends on the velocity distribution of the molecules as illustrated by Maxwell-Boltzmann, which results in different Doppler shifts. The frequency shift for the photons is dictated by the average value of the velocity distributions as a function of thermal energy of the molecular system with respect to the position of the detector. If the molecules move with a velocity v_a approaching the detector, then the observed frequency ν_a of the transition is related to the actual transition frequency ν by the expression:

$$\nu_a = \nu\left(1 - \frac{v_a}{c}\right)^{-1} \tag{2.64}$$

In above equation, c is the speed of light.

Since the Doppler broadening is based on the inhomogeneous behavior of the molecules taking into account the Maxwell-Boltzmann velocity distribution of molecules, it follows the Gaussian shaped function given by:

$$g_D(\nu - \nu_0) = \frac{1}{\nu_0}\left(\sqrt{\frac{mc^2}{2\pi kT}}\right) e^{-mc^2(\nu-\nu_0)^2/(2kT{\nu_0}^2)} \tag{2.65}$$

The corresponding half width due to Doppler broadening is given by equation:

$$\Delta\nu_D = 2\nu_0\sqrt{\frac{2kTln2}{mc^2}} \tag{2.66}$$

where T is the temperature (K) of the gas, k is the Boltzmann constant and m is the molecular mass and ν_0 is the frequency of transition.

The Gaussian profile is usually dominant at lower pressures. Comparing both profiles, the Lorentzian shape has long wings while the Gaussian shape is steeper near the center frequency and sometimes it is called a bell curve. The comparison between Lorentzian and Gaussian line-shape functions is shown in Fig. 2.9.

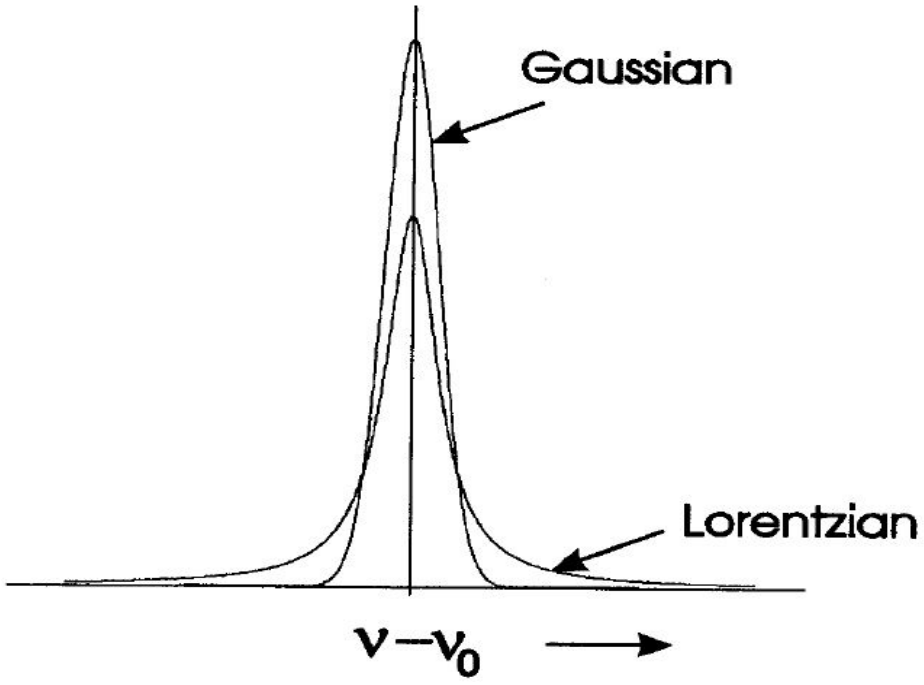

Fig 2.9: Illustration of the normalized Lorentzian line-shape function. (Source: Page 31, Chapter 1, Spectra of Atoms and Molecules, 2nd edition, by Peter F. Bernath [42]).

2.5.3 The Voigt line-shape

Another important line-shape profile called 'Voigt profile' is used in ro-vibrational spectroscopic studies, which is the convolution of Doppler and Lorentzian profiles at intermediate pressures (Lévy et al., 1992). The Doppler profile is usually effective at lower pressures and Lorentz profile is due to the collisional broadening at higher pressures, whereas the Voigt profile can act as either Doppler or Lorentzian depending on the pressure

limits. Since the Doppler line-shape is due to inhomogeneous broadening and Lorentzian line-shape is the results of homogeneous broadening, the Voigt line-shape profile can be written as the convolution of both line-shape functions given by:

$$g(\nu - \nu_0) = \int_{-\infty}^{\infty} g_I(\nu_0' - \nu_0) g_H(\nu - \nu_0')\, d\nu_0' \tag{2.67}$$

with the substitution of $x = \nu_0' - \nu_0$, the above expression can be reduced to

$$g(\nu - \nu_0) = \int_{-\infty}^{\infty} g_I(x) g_H(\nu - \nu_0)\, dx \tag{2.68}$$

where g_I represents the homogeneous Lorentzian function and g_H denotes the Doppler inhomogeneous function and the Voigt shape function $g(\nu - \nu_0)$ as a convolution of both, which is shown in Fig. 2.10.

One important thing to note is that the Voigt profile assumes the spectral lines are collisionally isolated due to inelastic collision, and it works under condition that the intensity due to collisions does not transfer from one part of the spectrum to another. The Voigt shape line profile can also be represented by:

$$g^{voigt}(\nu, \nu_0) = \left(\frac{1}{\gamma_D}\right)\left(\sqrt{\frac{ln2}{\pi}}\right) Re[err(\nu, x, y)] \tag{2.69}$$

where err represents the complex error function and γ_D is the Doppler half-width.

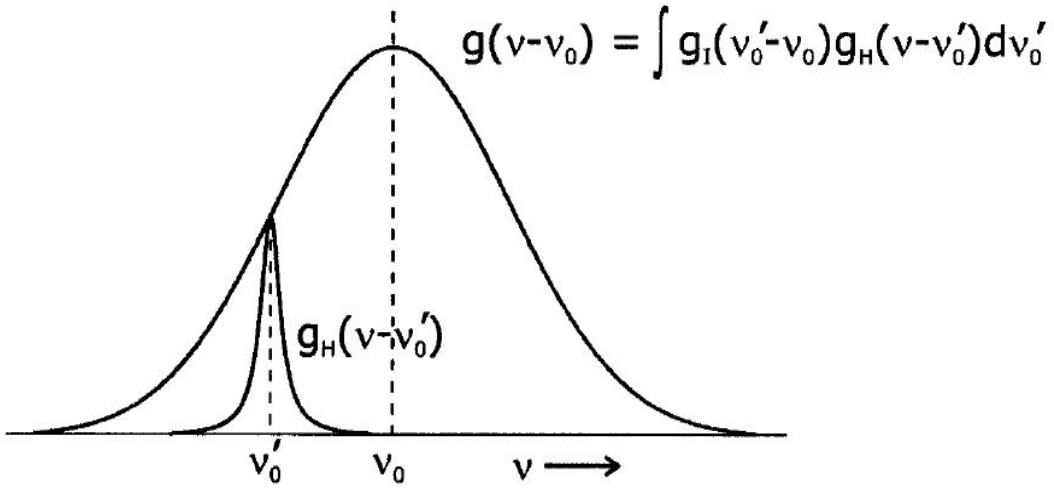

Fig 2.10: Illustration of the Voigt line-shape profile as convolving both Lorentzian and Gaussian functions. (Source: Page 29, Chapter 1, Spectra of Atoms and Molecules, 2nd edition, by Peter F. Bernath[42]).

The parameters *x, y* are dimensionless parameters, which are defined as:

$$x = \left(\sqrt{(ln2)}\right)\frac{(\nu-\nu_0-p\delta^0)}{\gamma_D}, \text{and } y = \left(\sqrt{(ln2)}\right)\frac{\gamma_L}{\gamma_D} \tag{2.70}$$

where δ^0 represents the pressure-induced shift, the suffixes *L* and *D* stands for Lorentzian and Doppler broadening.

2.5.4 The speed-dependent Voigt line-shape

In the Voigt profile, the gas molecules are considered to be moving with the most probable average speed under the influence of Maxwell-Boltzmann distribution of velocities, but in practice all molecules are not moving with the same speed during the perturbation of light molecules by heavier molecules. Even the absorbing molecule will experience its own homogeneous broadening due to its association with different velocity groups [43] and also the collisional width and shift parameters depend on the active speed of the molecules. Therefore, to explain the velocity dependence of line broadening and the

shifts of the lines due to the perturbation of gas molecule by others, an alternative asymmetric line-shape model called 'Speed Dependent Voigt Profile (SDVP)' is needed to be introduced. The expression for the SDVP was first expressed by Berman [44] in the following way:

$$g(\nu - \nu_0) = \frac{\gamma}{\pi}\int \frac{f(\vec{v})d^3v}{\gamma^2+\left(\nu-\nu_0-\vec{k}.\vec{v}\right)^2} = \frac{1}{2\pi}\int \frac{f(\vec{v})d^3v}{\gamma+i\left(\nu-\nu_0-\vec{k}.\vec{v}\right)}+\text{c.c} \tag{2.71}$$

In Eq. (2.71), ν defines the line position, ν_0 corresponds to the center of the line and c.c represents the complex conjugate parts. The function $f(\vec{v})$ is known as Maxwellian velocity distribution function, which is defined by:

$$f(\vec{v}) = (\pi u^2)^{-3/2} e^{-v^2/u^2} \tag{2.72}$$

The symbol u is used to refer the most probable speed of the active molecules and the absorption process occurs in the direction of light propagation vector $\vec{k}$ in parallel with the velocity of collisional molecules. The molecules in the collisional process thus follow the Maxwell distribution and by omitting the factor $\vec{k}.\vec{v}$, Eq. (2.71) turns into a weighted sum of Lorentz shape functions.

The Lorentz half-width and pressure-induced shift coefficients under the assumption of SDVP then can be expressed and modeled as a function of speed in the following way as described in [45]:

$$\gamma_{L_i}(v) = \gamma_{L_i}(v_m)\left(1 + a_{\gamma_{L_i}}\left(V^2 - c\right)\right) \tag{2.73}$$

$$\delta_i^0(v) = \delta_i^0(v_m)\left(1 + a_{\delta_i^0}\left(V^2 - c\right)\right) \tag{2.74}$$

where v_m is the average speed of the molecules during collision, c is the dimensionless parameter whose value is set as 1.5, V is the ratio of the speed of absorbing molecule to the mean speed of the molecules, $a_{\gamma_{L_i}}$ and $a_{\delta_i^0}$ are the speed-dependence Lorentz half-width and pressure-induced shift parameters for the i^{th} line.

2.5.5 Temperature-dependence of line-shape parameters

Since the molecules are considered in their gas phase in the current study, temperature plays an important role in the change of absorbed line position. As a result, the broadening and pressure-induced shift parameters need to be modeled with respect to temperature. The kinetic energy of the gas molecules depend on the temperature and it is assumed that the frequency of the molecules due to collision is linearly dependent on both the density and velocity distribution of molecules. According to this assumption, the temperature-dependence of the half-width can be expressed by following equation:

$$\frac{\gamma(T_1)}{\gamma(T_2)} = \left(\frac{T_1}{T_2}\right)^{-n} \tag{2.75}$$

In the above equation, γ is the pressure broadening coefficient shown as an example, T is the temperature and n is the temperature-dependence exponent. This semi-classical approach is usually valid for higher temperatures and therefore for retrieving the temperature-dependence exponents of both broadening and shift parameters, the spectra of the gas of interest needs to be recorded for a wider range of temperatures.

2.5.6 Line mixing

According to previously described line-shape models, the transitions are usually considered as isolated from each other during the collisional broadening of molecules. Collisional effects are more observable at high pressures (>200 Torr at room temperature) due to the

overlapping of two neighboring spectral lines. This occurs due to the perturbation of both initial and final ro-vibrational states of the transition as a result of the collapse of a sequence of spectral lines with the absorption of a single photon. Consider two adjacent spectral lines having the individual transition frequencies ν_1 and ν_2, which are isolated. The perturbation of the rotational states of two adjacent transitions results in the collapse of those lines with the same transition frequency ν due to the absorption of a single photon through inelastic collision and the process is illustrated in Fig. 2.11.

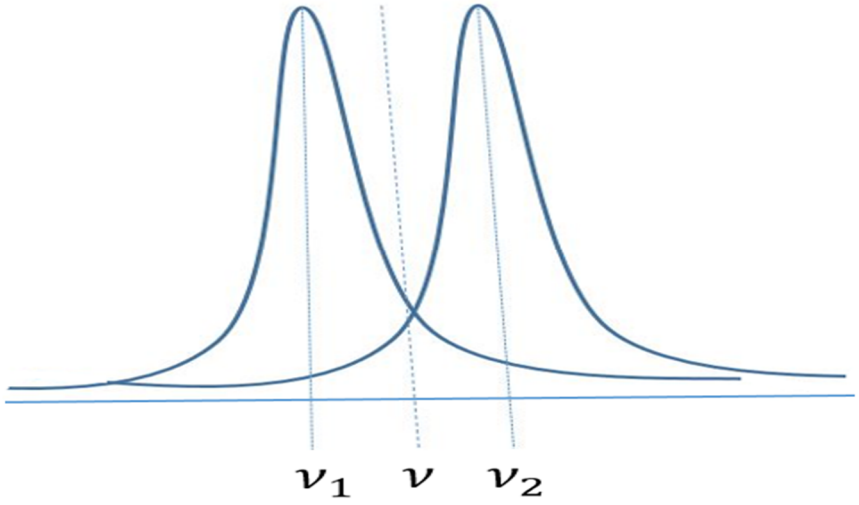

Fig 2.11: Illustration of overlapping the two adjacent spectral lines due to line-mixing effect.

During the interference effect of two adjacent spectral lines in line mixing, the populations can transfer from one rotational state to another state within the same vibrational level through inelastic collision. As a result, ultimately the intensity is transferred effectively form one part to another parts of the spectrum, which is referred to as line-mixing [46]. Certain conditions must be fulfilled during line-mixing as described by Lévy et al. [47], one of which states that the thermal energy of the molecules $(k_B T)$ must be greater than the change

in energy between two rotational states of the specific vibrational energy state during the transition due to inelastic collision. Another condition is that the spectral lines need to be broadened enough to overlap. The electric dipole transitions in the line-mixing measurements of methane among three different rotational symmetries follow the selection rules: $A_1 \leftrightarrow A_2$ and $F_1 \leftrightarrow F_2$ and $E \leftrightarrow E$. Lévy et al. [47] expressed the equation to determine the absorption cross-section incorporating the line-mixing effects as given by:

$$k(\nu) = \frac{1}{\pi}\sum_i S_i^{eff}\left(\frac{\gamma_{L_i}}{\left(\nu-\nu_i^{eff}-P\delta_i^0\right)+{\gamma_{L_i}}^2}\right) + \frac{Y_i\left(\nu-\nu_i^{eff}-P\delta_i^0\right)^2}{\left(\nu-\nu_i^{eff}-P\delta_i^0\right)+{\gamma_{L_i}}^2} \tag{2.76}$$

In Eq. (2.86), Y_i is known as the line-mixing parameters, S_i^{eff} represents the effective line intensity and ν_i^{eff} is termed as the effective line position of the spectrum.

2.5.7 Exponential Power Gap Law (EPG) for line mixing calculation

The line-mixing contributions can be ascertained by a relaxation matrix W [25], in which coupling between sets of transitions is recognized as the off-diagonal matrix elements. The line-shape factor $I(\nu)$ due to collisional effects can be represented in a matrix form [48]:

$$I(\nu) = \boldsymbol{X}^T(\nu\boldsymbol{I} - \boldsymbol{\nu_0} - i\boldsymbol{W})^{-1}\rho\boldsymbol{X} \tag{2.77}$$

Here, $\boldsymbol{I}$ denotes the $N \times N$ identity matrix; $\boldsymbol{\nu_0}$ is a $N \times N$ diagonal matrix for which the diagonal elements are the zero pressure line positions; ρ also represents a $N \times N$ diagonal matrix having the number density of the lower states of each transition diagonally; $\boldsymbol{W}$ stands for the relaxation matrix. $\boldsymbol{X}^T$ denotes the transpose of matrix $\boldsymbol{X}$, which is a $1 \times N$ matrix.

The elements of $\boldsymbol{X}$ are related to the intensity S_j and number density in the lower state ρ_j of j^{th} spectral line by the following equation:

$$X_j = \sqrt{S_j / \rho_j} \tag{2.78}$$

The approach described by Lévy et al. [47] has been adopted in the calculation of line-mixing coefficients.

The approximation called Exponential Power Gap Law (EPG) is used in the present thesis, which describes the relaxation matrix (W) due to the transfer of collisional rates. If the molecules undergo a transition from ground rotational state (k) to any of the higher excited rotational state (j) of the same vibrational state, then the collisional rate of transfer between these two states can be defined by:

$$\kappa_{jk} = a\left[\frac{|\Delta E_{jk}|}{B_0}\right]^{-b} exp\left(\frac{-c|\Delta E_{jk}|}{k_B T}\right) \tag{2.79}$$

Here ΔE_{jk} is the measure of energy difference due to the transition between j^{th} and k^{th} rotational energy levels, B_0 is the rotational constant and, the parameters a, b and c are all fitting parameters used in the non-linear least-square fitting routine.

The transition between two states j and k follow the detailed balanced condition ($\rho_k \kappa_{jk} = \rho_j \kappa_{kj}$), where ρ_k and ρ_j are the population densities at two different rotational energy states of k and j, respectively.

Thus, the off-diagonal elements (W_{jk}) of the relaxation matrix satisfying the detailed balanced condition at constant pressure and temperature can be given by:

$$W_{jk} = W_{kj}\frac{\rho_j}{\rho_k} \tag{2.80}$$

where ρ_j and ρ_k are the density of populations in j^{th} and k^{th} rotational states.

The diagonal elements (W_{kk}) of the relaxation matrix are related to the collisional transfer rate (κ_{jk}) by the following relation:

$$W_{kk} = \frac{1}{2}\left[\sum_j \kappa_{jk}\right]_{upper} + \frac{1}{2}\left[\sum_k \kappa_{jk}\right]_{lower} \tag{2.81}$$

The notations upper and lower in Eq. (2.81) are the representation of two vibrational states of the molecule. The off-diagonal elements (W_{jk}) of the matrix can be determined from the following equation:

$$W_{jk} = -\beta\kappa_{jk} \tag{2.82}$$

in which β is a constant whose value is different for different molecule.

The physical state of the molecule at any time is determined by the relaxation matrix elements and the real and imaginary parts of the diagonal elements of W symbolise the Lorentz widths (γ_{Lk}) and pressure shifts δ_k of the j^{th} spectral line, respectively:

$$W_{kk} = \gamma_{Lk} + i\delta_k \tag{2.83}$$

The line-mixing coefficients due to weaker transitions are thus calculated from the off-diagonal relaxation matrix elements related to the dipole matrix elements $\left(\mu_j, \mu_k\right)$ by the expression below:

$$Y_k(T) = 2\sum_{j\neq k}\frac{\mu_j}{\mu_k}\left(\frac{W_{jk}}{\nu_k - \nu_j}\right) \tag{2.84}$$

The line-mixing coefficients can thus fit for by incorporating Eq. (2.84) into our desired line-shapes.

2.6 Conclusion

To summarize, the Voigt line-shape profile is not sufficient to describe the line-shape studies of any complex molecule like methane. It is evident from previous studies that taking into account the speed dependence of the collisional width and shift improve the residual of the analyzed spectra. Therefore, it is important to include the speed dependence in the spectral analysis for molecules like CO_2, O_2, CH_4, because the mass ratios of these molecules in a buffer gas like air are 1.5, 1.06 and 0.55, respectively, and the effect of the speed of the molecules cannot be ignored. Line-mixing effects are incorporated in the calculation of absorption coefficient of methane molecule. The consequences of the results implementing different line-shape profiles will be observed in the results and discussion chapter.

CHAPTER 3: EXPERIMENTAL AND ANALYSIS TECHNIQUES

The experimental spectra were recorded by Dr. Keeyoon Sung at Jet Propulsion Laboratory (JPL), California with a high-resolution Bruker IFS-125HR Fourier transform spectrometer (FTS). A cryogenic type absorption gas cell was installed in the instrumental setup to control the temperature during recording of the spectra. Multi-spectrum fitting software 'Labfit' developed by Dr. Chris Benner [49] was used in the analysis of methane broadened by itself, air and H_2 spectra. This chapter describes the working principle of the Michelson interferometer employed in the FTS, the recording process of spectra using the FTS at JPL and the analysis methodology of the spectra. The description in this chapter is based on the book 'Fundamentals of Fourier Transform Infrared Spectroscopy', 2nd edition, written by Brian C. Smith [50] and other literature.

3.1 Fourier transform spectroscopy

3.1.1 Michelson Interferometer

One of the major optical components of a FTS is known as the Michelson Interferometer, which was designed by the renowned scientist A. A. Michelson in 1885. As shown in Fig. 3.1, the interferometer consists of two mirrors that are perpendicular to each other, one of which is a fixed mirror and the other is movable. The collimator mirror is used to make the light beams parallel to each other and a beam splitter is used to split the incident radiation into two components, half of the beam is reflected by the beam splitter and travels towards the fixed mirror and another half portion can pass through the splitter towards the movable mirror. The beams will be reflected back from both mirrors and they recombine

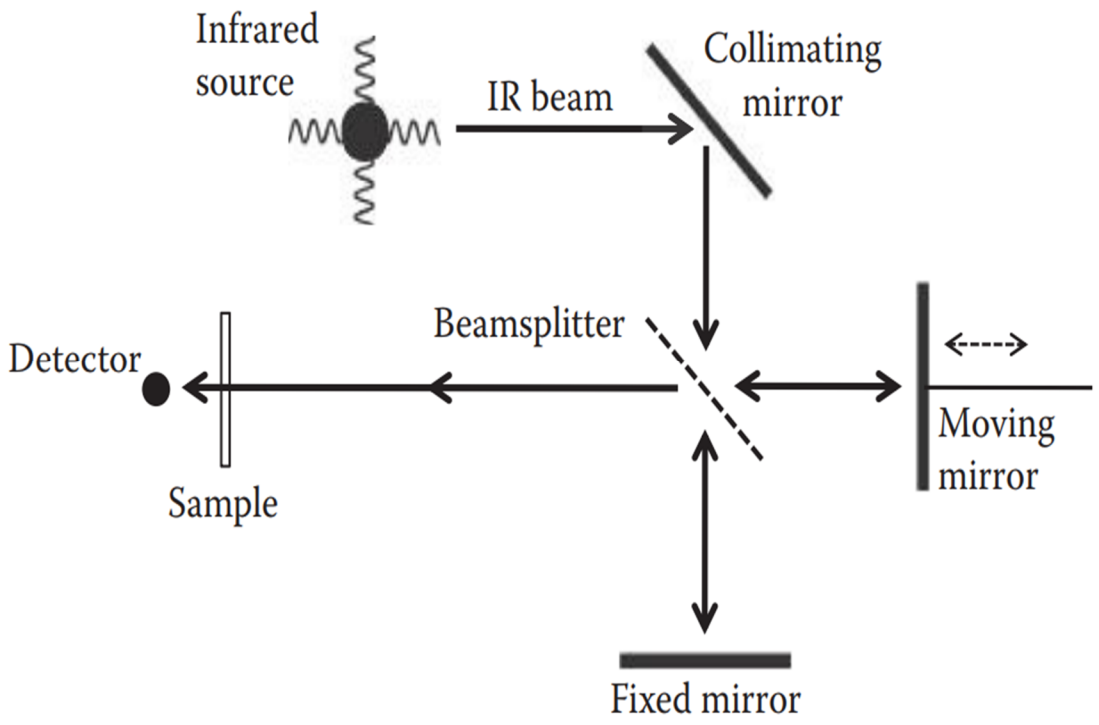

Fig 3.1: Schematic diagram of a Michelson Interferometer. (Source: Page 22, Chapter 2, Fundamentals of Fourier Transform Infrared Spectroscopy, 2nd edition, by Brian C. Smith [50]).

at the beam splitter as a single beam which interacts with the sample. The interference phenomena is due to the difference in optical paths which is modulated by the movement of the moving mirror. The path difference between two light waves (δ) is related to the mirror displacement (Δ) by the following relation:

$$\delta = 2\Delta \tag{3.1}$$

If the two light beams travel an equal optical path length, then there will be no path difference, for which $\delta = 0$, i.e., Zero Path Difference (ZPD). It is mentionable that the value of δ is twice the magnitude of mirror displacement (Δ), because the light waves travel twice the distance while the moving mirror move back and forth with the same distance as shown in Fig. 3.2. The interference become constructive or destructive depending on the

relation between the path difference and the wavelength of the light used. The interference patterns follow the following conditions:

$$\delta = n\lambda \qquad \text{(constructive)} \qquad (3.2)$$

and $$\delta = \left(n + \frac{1}{2}\right)\lambda \qquad \text{(destructive)} \qquad (3.3)$$

where λ is the wavelength of the infrared radiation, n is an integer whose values are 0, 1, 2,3 ……

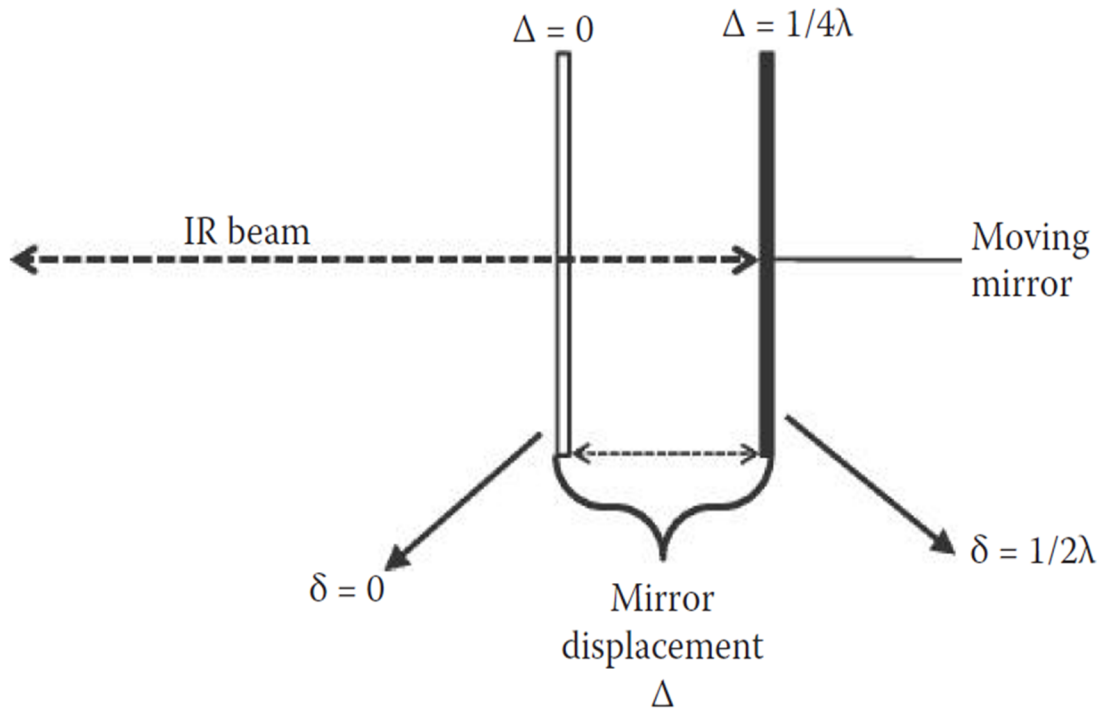

Fig 3.2: Schematic diagram of a Michelson Interferometer. (Source: Page 22, Chapter 2, Fundamentals of Fourier Transform Infrared Spectroscopy, 2nd edition, by Brian C. Smith [50])

The moving mirror can move back and forth along its axis of radiation, which gives rise to a pattern of alternating bright and dark interference fringes forming of the interferogram. The interferogram can then be transformed into a spectrum by applying a Fourier transformation.

3.1.2 Mathematical formulation of Fourier transform

Let us consider the incident radiation used in the Michelson interferometer as a plane wave given by:

$$\psi = A_0 e^{i(\omega t - \boldsymbol{k} \cdot \boldsymbol{x})} \tag{3.4}$$

In above equation, A_0 is the amplitude of the incident wave, ω is the angular frequency of the wave, t is the time, $\boldsymbol{x}$ is the position vector of the wave and $\boldsymbol{k}$ is known as the wave vector, which is given by:

$$\boldsymbol{k} = \frac{2\pi}{\lambda}\hat{k} = 2\pi\tilde{\nu}\hat{k} \tag{3.5}$$

where $\tilde{\nu}$ denotes the wavenumber in cm^{-1} and $\hat{k}$ is the unit vector which is in the direction of the propagation of the wave. If the reflected and transmitted parts of the wave are denoted by ψ_r and ψ_t, then the total wave function $(\psi_{tot} = \psi_r + \psi_t)$ can be written as the combination of both parts of the radiation and the intensity of the radiation reaching the detector can be written in the following way:

$$I(\delta) = \psi_{tot}\psi_{tot}^{*} = \frac{A_0^2}{2}\left[1 + cos\left(\frac{2\pi}{\lambda}\delta\right)\right] = \frac{I_0}{2}[1 + cos(2\pi\tilde{\nu}\delta)] \tag{3.6}$$

Here, I_0 is the intensity of the incident monochromatic wave, which is proportional to the square of the amplitude and δ is the optical path difference. The integrated interferogram of the polychromatic light wave reaching the detector can be written in terms of spectral intensity as given by:

$$I(\delta) = \int_{-\infty}^{+\infty} S(\tilde{\nu}) cos(2\pi\tilde{\nu}\delta)\, d\tilde{\nu} \tag{3.7}$$

The spectrum can then be derived by applying a Fourier transform of the interferogram as shown in the following way:

$$S(\tilde{v}) = \int_{-\infty}^{+\infty} I(\delta) cos(2\pi\tilde{v}\delta)\, d\,\delta \quad (3.8)$$

where $S(\tilde{v})$ represents the corresponding spectrum as a function of spectral line position. When a gas sample is used in infrared spectroscopy. The transmittance of the sample can be determined from the ratio of the reduced intensity to the initial intensity of the IR radiation. The quality of the spectra is very important, which can be improved by taking more scans when recording of spectra. The signal-to-noise ratio (SNR) is determined by taking the inverse of the standard deviation of the peak-to-peak values of the noise level of any spectrum where no absorption lines appear. Then the RMS value of SNR is calculated by computing of all the data points, which results in a better value of SNR(RMS). Thus, the SNR is also linearly related to the square root of the number of scans *N*, i.e. $SNR(N) = \sqrt{N}\, SNR(1)$.

3.1.3 Advantages of Fourier transform spectroscopy

The Fourier Transform spectroscopy technique has several advantages over dispersive techniques, namely the Jacquinot, the Fellget, the Connes and the Michelson advantages [51]. One of the most important advantages of FTS is known as Jacquinot or throughput advantage. Compared with conventional dispersive instruments, more of the incident radiation can be detected in FTS. Therefore, a higher SNR is achievable within a shorter time compared to a dispersive spectrometer.

The second most important advantage of FTS is called the Fellgett or multiplex advantage, by which the SNR of a spectrum can be improved by detecting all wavenumbers of infrared

radiation together rather than successively acquiring individual wavenumber ranges. It also saves time of recording spectra as well as reduces the noise level because the noise at any specific wavenumber is directly proportional to square root of the time spent for observing individual wavenumber ranges.

Another essential improvement of FTS is that the calibration for its interferometer can be done more accurately with long term stability, which is known as the Connes advantage. This can be achieved easily because well-known HeNe lasers and are used in FTS for which the wavenumber is known.

The last advantage of FTS is known as the Michelson or resolving power advantage. An interferometer possesses the simplest and most intrinsic optical design, which provides the best resolution of the instrument and remains constant throughout the data collection process. This is possible because of the use of a Jacquinot stop aperture size in the interferometer, which remains constant during the whole scanning process. Since no change of gratings or slits are needed in FTS, the signals can be recorded continuously without any disturbance.

3.2 Description 125 HR Fourier transform spectroscopy at JPL

A Bruker IFS 125HR Fourier transform spectrometer (FTS) available at the Laboratory of Molecular Spectroscopy located in the Jet Propulsion Laboratory (JPL), Pasadena, California was used by Dr. Keeyoon Sung to record 14 high-resolution laboratory spectra of pure methane ($^{12}CH_4$) and with the mixture of dilute air and 18 spectra with mixture of H_2 gas for two different projects. A cryogenic absorption gas cell [52] was installed into the sample compartment of the FTS for recording absorption spectra.

3.2.1 Infrared source of radiation used in FTS at JPL

Two main sources of radiation are used in FTIR spectroscopy, an air-cooled source and water-cooled source. The second one also known as a 'Globar' source of radiation, was used in the FTS experimental set up at JPL. A Globar light source usually consists of a silicon carbide rod, which can be heated to temperatures up to 1200 K [53]. Compared to air-cooled systems, a Globar source offers greater throughput and less noise during the recording of spectra. The illumination ability of a Globar light source extends up to 100 μm [54] and the aperture diameter of the FTS at JPL was set as 1 mm.

3.2.2 Beam splitters used in FTS at JPL

A beam splitter is an optical device which is used to split the incident radiation into two parts, one of them gets reflected by the moving mirror and another part by the fixed mirror. The choice of beam splitters depend on the radiation used. Calcium fluoride (CaF_2) was used in the splitting of near-IR radiation used in the current experimental set up at JPL. The CaF_2 material as a beam splitter offers the utmost quality in terms of purity and consistency and caused very low absorption, which covers the spectral range of near-IR from 2 to 8 microns. Compared to other IR materials, CaF_2 offers high transmission of usually more than 90%.

3.2.3 Detector used in FTS at JPL

The infrared intensity is finally transformed into an amplified signal, which is collected as an interferogram. InSb detector being a quantum-type detector was used in the FTS set up at JPL, which possesses the photoconductive property with covering a wide spectral range from 0.6 to 5.5 μm [55]. It provides high SNR and can detect the signal very

quickly with higher performance [56]. The operating temperature for InSb photodetectors can go beyond 77 K without losing their quantum efficiency up to 160 K [55, 56].

3.2.4 Absorption gas cells used in FTS at JPL

Two cryogenic absorption gas cells were designed at Connecticut College and installed with the empty cell placed into the sample compartment of Bruker IFS-125HR FTS at JPL. Two cryogenic gas cells known as the 'single pass gas cell' with optical path length of 20.38 cm and a 'multi-pass Herriot gas cell' with absorption path length of 20.94 cm, were used in the recording of methane broadened by air and H_2 spectra. The cell body of the cells were made of oxygen-free copper, which offered the excellent conductive performance of 4.01-5.57 W/(cm K) with operating temperatures between 80 and 300 K [57] with a stability factor of ±0.01 K. The indium made seal was used to attach the cell body to the ZnSe window of 50 mm diameter to prevent it from optical fringing. The gas cells were surrounded by a vacuum box in order to achieve the better temperature stability and the complete absorption gas cells were finally placed into the sample compartment of the FTS. A He-refrigerator cooling system and a heater of 50 ohm were used to achieve the constant temperature. A temperature controller and two temperature sensors made of Si diodes were used to control the temperature with a stability factor of ≤ 0.01 K. The details of the gas cells can be found in [52, 58] and pictures are shown in Fig. 3.3.

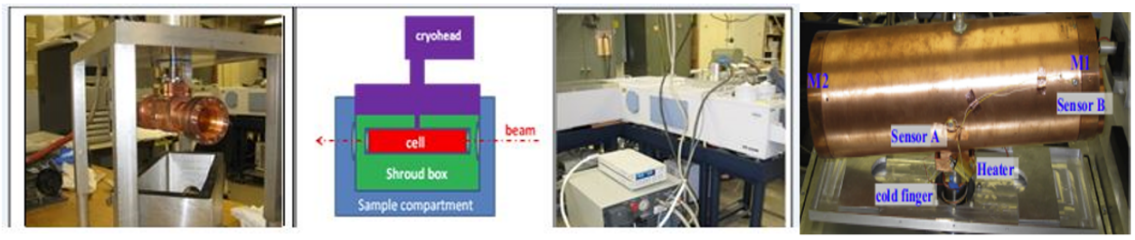

(a) (b) (c) (d)

Fig 3.3: Schematic diagram of the experimental set-up at JPL [52]. (a) Assembly of the absorption gas cell with vacuum shroud box, (b) the gas cell set up placed in the sample compartment, (c) FTS set up attached to the electrical machine, (d) the Herriot cell.

3.3 Recording and analysis methodology of laboratory spectra

3.3.1 Methane-air spectra

A total of 14 methane-air spectra were recorded over the range of temperatures from 148.4 K to room-temperature (298.4 K) and at pressures varying between 4.5 and 385 Torr. The resolution of the instruments was maintained at 0.005 cm^{-1} and the maximum optical path difference was about 90 cm. Among 14 spectra, 8 of them were recorded of pure (99.9% isotopically ^{12}C enriched) $^{12}CH_4$. Dry air was used to get 6 air-mixed CH_4 spectra with a volume mixing ratio of methane in the mixtures from 0.043 to 0.096. After loading samples in the gas cell, approximately 20 minutes were allowed for getting the correctly recorded spectra under stable atmospheric conditions. The interferograms were collected around every 10 min and then individually Fourier Transformed to check for problems before being included in the final averaged spectrum. Approximately 5-7 hours were spent to record a single spectrum and a phase correction using the Mertz method [59, 60] was applied in the process of Fourier transformation. All spectra were recorded without interval to maintain a constant calibration factor and a high signal-to-noise ratio of more than 2000 was achieved in the recording of each spectrum. The calibration was done with reference to the ν_3 transitions of water vapor. An average calibration factor was determined for each

spectrum and the wavenumber scales of the individual spectrum were multiplied by the calibration factor. Temperature sensors and a properly calibrated Baratron gauge were used to record the temperature and pressure of the recorded spectra. The experimental conditions for methane-air spectra having the same path length of 20.38 cm are outlined in Table 3.1

Table 3.1: Experimental conditions for the methane-air spectra recorded at JPL.

Spectra no.	Gas sample	VMR[a]	P (Torr)[b]	T (K)[c]
bk2534	$^{12}CH_4$	1.00	385.0	298.4
bk2557	$^{12}CH_4$	1.00	22.2	250.0
bk2556	$^{12}CH_4$	1.00	121.5	250.0
bk2551	$^{12}CH_4$	1.00	9.90	200.0
bk2550	$^{12}CH_4$	1.00	43.95	200.0
bk2549	$^{12}CH_4$	1.00	169.0	200.0
bk2540	$^{12}CH_4$	1.00	4.5	148.4
bk2537	$^{12}CH_4$	1.00	149.0	148.5
bk2544	$^{12}CH_4$+Air	0.043	225.3	148.4
bk2560	$^{12}CH_4$+Air	0.055	112.6	250.0
bk2559	$^{12}CH_4$+Air	0.057	254.6	250.0
bk2554	$^{12}CH_4$+Air	0.073	148.5	200.0
bk2553	$^{12}CH_4$+Air	0.074	299.9	200.0
bk254	$^{12}CH_4$+Air	0.096	95.0	148.4

VMR[a]=Volume mixing ratio, P[b] is the total sample pressure and T[c] is the temperature of the recorded spectra.

3.3.2 Methane-H_2 spectra

The experimental conditions for the methane-H_2 spectra with varying path lengths are listed in Table 3.2.

Table 3. 2: Experimental conditions for the methane-H_2 spectra recorded at JPL.

Spectra no.	Gas sample	Path length (cm)	VMR[a]	P (Torr)[b]	T (K)[c]
bk2534	$^{12}CH_4$	20.38	1.00	385.0	298.4
bk2557	$^{12}CH_4$	20.38	1.00	22.2	250.0
bk2556	$^{12}CH_4$	20.38	1.00	121.5	250.0
bk2551	$^{12}CH_4$	20.38	1.00	9.90	200.0
bk2550	$^{12}CH_4$	20.38	1.00	43.95	200.0
bk2549	$^{12}CH_4$	20.38	1.00	169.0	200.0
bk2540	$^{12}CH_4$	20.38	1.00	4.5	148.4
bk2537	$^{12}CH_4$	20.38	1.00	149.0	148.5
kp4731	$^{12}CH_4$	20.94	1.00	0.12	220.2
Kp4740	$^{12}CH_4$+H_2	20.94	0.00033	198.09	148.5
Bk4735	$^{12}CH_4$+H_2	20.94	0.00037	168.47	160.3
kp4738	$^{12}CH_4$+ H_2	20.94	0.00088	197.83	160.3
kp4724	$^{12}CH_4$+ H_2	20.94	0.0022	96.92	200.3
kp4723	$^{12}CH_4$+ H_2	20.94	0.0022	235.6	200.3
kp4702	$^{12}CH_4$+ H_2	17.65	0.00373	294.92	293.8
kp4703	$^{12}CH_4$+ H_2	17.65	0.00374	100.25	293.8
kp4727	$^{12}CH_4$+ H_2	20.94	0.0121	263.67	220.2
kp4728	$^{12}CH_4$+ H_2	20.94	0.0122	150.16	220.2

VMR[a]=Volume mixing ratio, P[b] is the total sample pressure and T[c] is the temperature of the recorded spectra.

3.3.3 Analysis methodology

The multi-spectrum non-linear least-square fitting software 'Labfit' developed by Chris Benner at the College of William and Mary [48, 49] was used to perform the analysis of methane broadened by air and H_2 in the $(\nu_1 + \nu_4)$ band over the spectral range from 4100-4300 cm^{-1}. The software deconvolved the absorption lines from the experimental spectra by considering the fact that the instrumental line-shape as a sinc function was modified to account for the finite size of the aperture. The Labfit program has the ability of fitting the desired parameters for individual spectra and then subsequently adding all spectra in the entire spectral band. Among different built-in line-shape models, the Speed-Dependent Voigt Profile (SDVP) was implemented in the line-shape calculations and the off-diagonal relaxation matrix formalism was used in the quantification of the line-mixing calculations. The initial values of line parameters used in the least-squares fittings were

taken from the HITRAN2012 [11] database. Different parameters (line position, intensity, width, shift, etc.) were floated and a maximum of 3 iterations was used during the fitting of spectra. One of the main objectives of the fitting was to minimize the difference between experimental and simulated spectra i.e. to improve the residuals of the multi-spectrum fitting. All pure methane spectra were added first, then all air-mixed and H_2-mixed spectra were subsequently added by multi-spectrum fitting technique. An algorithm called Lavenberg-Marquardt [61, 62] was used in the minimization of the residuals and the details of the algorithm are available in [49]. Examples of simultaneously fitted multi-spectrum residuals of methane broadened by air and H_2 are shown in Fig. 3.4 (a) and (b).

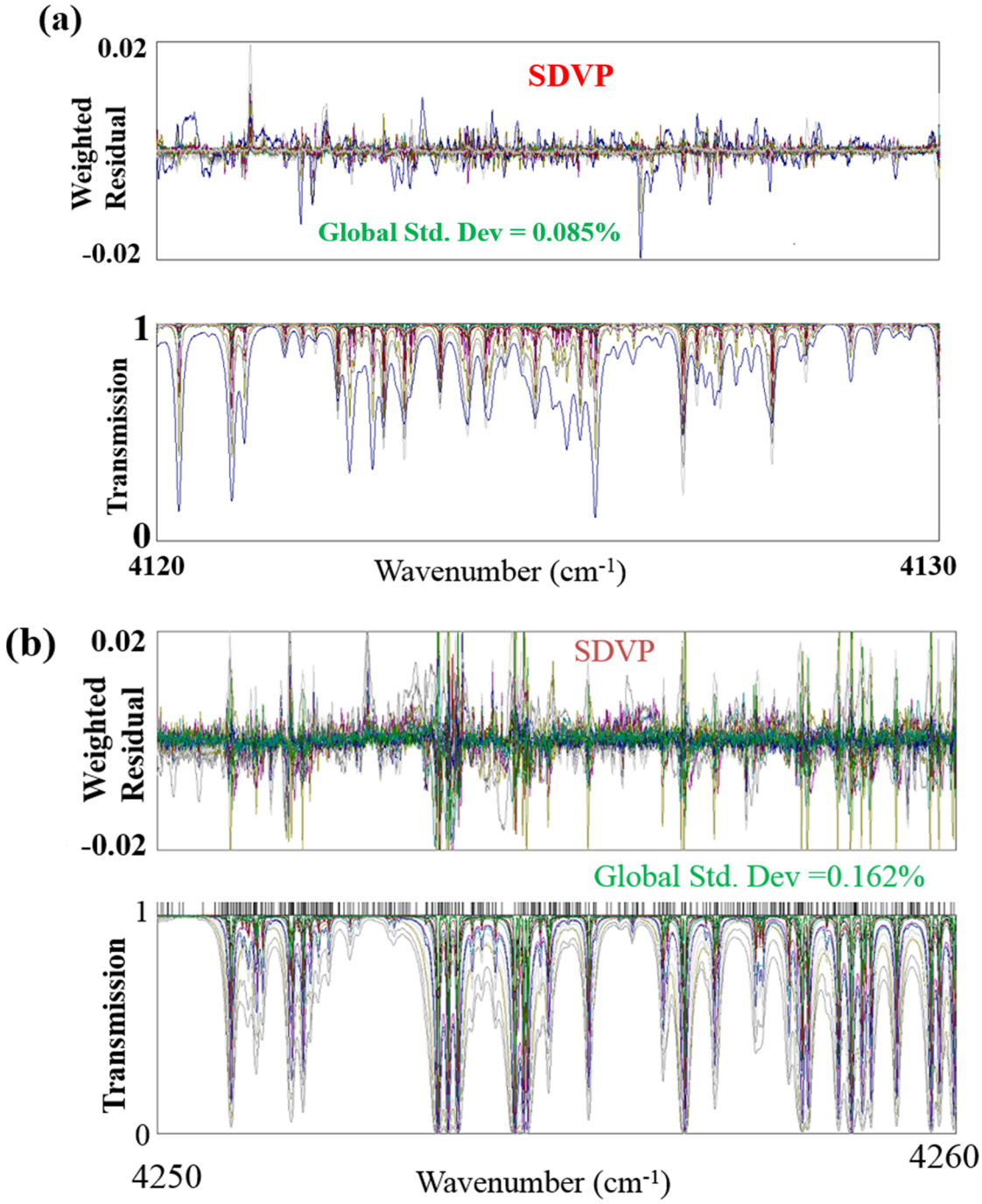

Fig 3.4: A typical multi-spectrum fitted residual of the $\nu_1 + \nu_4$ band of (a) methane-air and (b) methane-H_2 implementing SDVP.

CHAPTER 4: LINE-SHAPE STUDY OF METHANE BROADENED BY ITSELF AND AIR

4.1 Introduction

The different line-shape parameters of self- and air-broadened methane in the $\nu_1 + \nu_4$ band are retrieved in the current thesis. The laboratory spectra were recorded using a high-resolution Fourier Transform Spectrometer (FTS) at the Jet Propulsion Laboratory. The analysis has been performed for methane broadened by air using a multi-spectrum fitting technique called 'Labfit' which was developed by Benner et al. [49]. This global fitting routine finds the local minimum by adjusting the parameters related to each spectrum (e,g., background polynomial, residual phase error, channel spectra) and up to 15 parameters (e.g., line position, intensity, lower state energy and different line-shape coefficients and their temperature dependences) can be floated for multi spectra fitting. The individual spectrum was given specific weight in the fitting depending on the SNR and maximum weight factor up to 1.0 was provided for most of the spectra having highest SNR. The spectra were fitted with different line-shape models (Voigt, SDVP and SDVP with line mixing) to get the better residuals.

Among various retrieved parameters, Lorentz half-width $\gamma_L(p,T)$, line position $\nu(p)$ and pressure induced-shift coefficient $\delta^0(T)$ are determined by the following three equations:

$$\gamma_L(p,T) = p\left[\gamma_L^0(foreign)(p_0,T_0)(1-\chi)[T_0/T]^{n_1}\right] + \left[\gamma_L^0(self)(p_0,T_0)\chi[T_0/T]^{n_2}\right], \quad (4.1)$$

$$\nu(p) = \nu_0 + p[\delta^0(foreign)(1-\chi) + \delta^0(self)\chi], \quad (4.2)$$

$$\delta^0(T) = \delta^0(T_0) + \delta'(T - T_0). \quad (4.3)$$

where $\gamma_L^0(p_0, T_0)$ and $\delta^0(T)$ stand for pressure broadening and pressure-induced shift coefficients, respectively in units of $(\mathrm{cm}^{-1}\mathrm{atm}^{-1})$ at atmospheric pressure p_0 (1 atm) and standard temperature T_0 (25^0 C). $\gamma_L(p, T)$ represents the Lorentz half-width of the spectral line in cm^{-1} at pressure p and temperature T, χ is the volume mixing ratio of methane in the sample mixtures, n_1 and n_2 are the temperature-dependence exponents for air- and self-broadening, respectively. Eq. (4.2) gives the pressure-induced shift in position from its line center ν_0 both in cm^{-1} and δ' denotes the temperature dependence of pressure-shift coefficients. The term 'foreign' appearing in Eqs. (4.1-4.2) represents the air or H_2 gas that were used as the broadener during the experiments. As observed in Eq. (4.1), the Lorentz half-width depends on both gas sample temperatures and pressures. Therefore, analysis of laboratory spectra over a wide range of sample gas pressures and temperatures are crucial for accurate remote sensing of different planetary atmospheres.

The speed dependence of the Lorentz broadening is expressed by:

$$\gamma_L^0 = \gamma_L^0(v_m)\left(1 + S\left[\left(v/v_p\right)^2 - c\right]\right) \quad (4.4)$$

In above equation, v, v_m and v_p symbolise the speed, thermal mean speed and most probable speed of the molecules for line broadening, respectively. The parameter S is the speed-dependent parameter (unitless) and the constant value of c is set as 1.5 regardless of molecule, which is part of the speed-dependence model arising from the ratio of thermal mean speed to the most probable speed.

The line-mixing coefficients are retrieved through off-diagonal relaxation matrix formalism represented by the following equation:

$$W_{jj} = \gamma_{Lj} + i\delta_j \tag{4.5}$$

In Eq. (4.5), the real and imaginary parts of the diagonal elements of the relaxation matrix W represent the Lorentz widths $\left(\gamma_{Lj}\right)$ and pressure shifts δ_j of the j^{th} spectral line, respectively.

4.2 Description of retrieved parameters for methane broadened by air

A total of 14 spectra are analyzed in this project among which 8 are due to the self-broadening of methane and the other 6 spectra are recorded for air-broadening of methane. In total 208 transitions were determined and reported for the complete three bands (*P, Q, R)* of methane in the spectral range of 4100-4300 cm^{-1}. The number of transitions for individual line-shape parameters is outlined in Table 4.1 and the detail list of retrieved line parameters can be found in Appendix A and B. Data points for a few individual parameters which could not be accurately determined are omitted because of the low intensity of the transition and/or overlap with neighboring transitions. The parameters of those undetermined transitions have been kept the same as those recorded in HITRAN 2012 database. All retrieved parameters have been presented in terms of the rotational quantum number $|m|$, where m values are defined as $-J$, J and $J + 1$ for *P*, *Q* and *R*- branch transitions, respectively. The positions and intensities are calculated theoretically to compare with the measured data, which will be presented later in this section. All retrieved parameters of the present study have been presented graphically for transitions

corresponding to the three different symmetry species types *A*, *E* and *F* as indicated by rectangular, upper triangle and lower triangle symbols, respectively.

Table 4.1: Number of retrieved line parameters due to self- and air-broadening of methane.

Self/Air	Position	Intensity	Lorentz width	Pressure shift	n^a	$\delta'^{,b}$	ORME^c	S^d
Self	208	205	200	179	158	134	94	75
Air			149	110	117	92	46	

n^a stands for temperature-dependence of broadening, $\delta'^{,b}$ is used for temperature dependency in pressure-induced shift coefficient, ORME^c represents for off-diagonal relaxation matrix elements and S^d is used for speed-dependence parameters.

4.2.1 Self- and air-broadening coefficients and their temperature dependences

Selected results of for both air- and self-broadening parameters for P, Q and R transitions along with temperature dependences of methane in its $\nu_1 + \nu_4$ band are listed in Table 4.2. Fig. 4.1 shows the comparison in residual for multi-spectrum fitting of methane spectra broadened by itself and air with 3 different fitting profiles: Voigt, speed dependent Voigt and speed dependent Voigt with line mixing. The residual is the difference between experimental and simulated spectra. The residual was improved mostly by fitting with the speed dependent Voigt profile with line mixing.

Table 4.2: Sample of retrieved self- and air- broadening parameters along with their temperature-dependence exponents obtained by multi-spectrum fitting using SDVP.

Iml	Low State $(J''C''n'')$	Upper State $(J'C'n')$	Position[a] (cm^{-1})	Intensity[a] (cm/mol)	Air-width[a] $(cm^{-1}atm^{-1})$	Self-width[a] $(cm^{-1}atm^{-1})$	$(n_1)^{a,b}$	$(n_2)^{a,b}$
1	2E 1	1E 6	4207.48727(1)	7.920(1)x10^{-22}	0.0620(5)	0.0811(4)	0.93(1)	0.84(1)
1	$1F_1$ 1	$1F_2$ 9	4218.41614(1)	1.299(2)x10^{-21}	0.0596(4)	0.0774(8)	0.84(1)	0.94(3)
1	$0A_1$ 1	$1A_2$ 4	4223.90646(1)	2.231(2)x10^{-21}	0.0523(2)	0.0819(4)	0.76(1)	0.71(1)
2	$1F_1$ 1	$2F_2$ 15	4229.19507(1)	2.095(2)x10^{-21}	0.0574(2)	0.0784(3)	0.90(1)	0.86(1)
3	$3F_2$ 1	$2F_1$ 15	4201.40058(1)	1.681(2)x10^{-21}	0.0636(3)	0.0838(4)	0.91(1)	0.83(1)
3	$3F_1$ 1	$2F_2$ 16	4201.84819(1)	1.685(2)x10^{-21}	0.0640(3)	0.0833(3)	0.92(1)	0.84(1)
3	$3A_2$1	$3A_1$ 7	4218.78453(1)	3.807(4)x10^{-21}	0.0592(3)	0.0825(5)	0.83(1)	0.80(1)
3	2E 1	3E 13	4234.41871(1)	1.817(2)x10^{-21}	0.0533(2)	0.0751(4)	0.87(1)	0.73(1)
4	$3A_2$ 1	$4A_1$ 10	4239.25185(1)	4.851(4)x10^{-21}	0.0581(3)	0.0748(5)	0.74(1)	0.83(1)
4	$4F_2$1	$3F_1$ 23	4194.75695(1)	1.848(2)x10^{-21}	0.0575(3)	0.0792(4)	0.85(1)	0.90(1)
5	5E 1	4E 19	4188.64944(1)	1.292(1)x10^{-21}	0.0547(2)	0.0736(2)	0.85(1)	0.824(5)
5	$5A_1$ 1	$4F_2$ 29	4190.45684(1)	1.950(2)x10^{-21}	0.0602(4)	0.0820(4)	0.87(1)	0.86(1)
5	4E 1	5E 20	4244.43763(1)	1.922(2)x10^{-21}	0.0539(3)	0.0665(4)	0.83(1)	
6	6E 1	6E 26	4214.30919(1)	1.290(1)x10^{-21}	0.0586(4)	0.0772(3)	0.86(1)	0.82(1)
6	$6F_1$ 1	$5F_2$ 34	4181.81703(1)	1.757(1)x10^{-21}	0.0614(2)	0.0791(2)	0.87(1)	0.856(4)
6	$6A_2$ 1	$5A_1$ 10	4183.82934(1)	2.983(2)x10^{-21}	0.0578(2)	0.0793(1)	0.87(1)	0.812(3)
6	6E 1	5E 23	4184.54674(1)	1.229(1)x10^{-21}	0.0574(3)	0.0749(2)	0.86(1)	0.86(1)
7	$7F_1$ 2	$6F_2$ 40	4174.49344(1)	1.488(1)x10^{-21}	0.0594(2)	0.0776(2)	0.85(1)	0.821(4)
7	$7A_2$ 1	$6A_1$ 15	4176.64743(1)	2.517(2)x10^{-21}	0.0566(2)	0.0775(1)	0.82(1)	0.826(3)
7	$7F_1$ 1	$6F_2$ 41	4178.52765(1)	1.593(1)x10^{-21}	0.0575(2)	0.0767(2)	0.83(1)	0.819(4)
7	$6A_1$ 1	$7A_2$ 14	4253.51921(1)	3.647(3)x10^{-21}	0.0550(2)	0.0771(2)	0.86(1)	0.73(1)
7	6E 1	7E 25	4254.63877(1)	1.523(2)x10^{-21}	0.0531(3)	0.0756(6)	0.84(1)	0.69(2)
8	$7F_1$ 2	$8F_2$ 43	4258.53364(1)	1.316(2)x10^{-21}	0.0584(4)	0.0751(4)	0.87(1)	0.84(1)
8	$8F_1$ 1	$7F_2$ 45	4168.48594(1)	1.219(1)x10^{-21}	0.0589(3)	0.0769(2)	0.85(1)	0.808(4)
9	$8A_1$1	$9A_2$ 17	4264.81856(1)	1.953(3)x10^{-21}	0.0472(4)	0.0719(3)	0.74(1)	0.78(1)
9	$9F_1$ 1	$8F_2$ 54	4165.7622(1)	1.094(1)x10^{-21}	0.0504(3)	0.0686(1)	0.72(2)	0.792(4)
9	$9A_2$ 1	$8A_1$ 18	4159.05384(1)	1.613(4)x10^{-21}	0.0560(3)	0.0739(2)	0.78(1)	0.819(3)
9	$9F_2$ 2	$8F_1$ 51	4159.49119(1)	1.005(1)x10^{-21}	0.0610(4)	0.0783(2)	0.79(2)	0.794(4)
9	$9F_1$ 3	$8F_2$ 52	4160.03620(1)	1.015(1)x10^{-21}	0.0610(4)	0.0783(2)	0.79(2)	0.782(5)
9	$8F_2$ 1	$9F_1$ 46	4263.75117(2)	8.17(1)x10^{-22}	0.0576(7)	0.0751(4)	0.78(3)	0.81(1)
10	$10A_2$1	$9A_1$ 19	4156.88723(2)	1.502(3)x10^{-21}	0.0524(7)	0.0710(5)	0.70(3)	0.82(1)
10	$10A_1$1	$9A_2$ 21	4152.61348(1)	1.652(1)x10^{-21}	0.0554(3)	0.0745(2)	0.76(1)	0.784(4)
10	$10A_2$1	$10A_1$20	4206.07311(2)	8.250(1)x10^{-22}	0.0503(9)	0.0682(4)	0.71(5)	0.77(1)
10	$9A_1$ 1	$10A_2$16	4267.13466(1)	1.584(2)x10^{-21}	0.0532(5)	0.0728(3)	0.81(2)	0.79(1)
10	$9F_2$ 1	$10F_1$ 48	4268.97289(2)	9.390(1)x10^{-22}	0.0500(7)	0.0702(3)	0.76(3)	0.73(1)
11	$10F_2$2	$11F_1$ 53	4272.1593(5)	6.010(3)x10^{-22}	0.051(18)	0.0689(8)	0.67(10)	0.77(2)

[a] Statistical uncertainties are given in parentheses.

[b] n_1 and n_2 are temperature-dependence exponents of air- and self-broadened half-width coefficients, respectively.

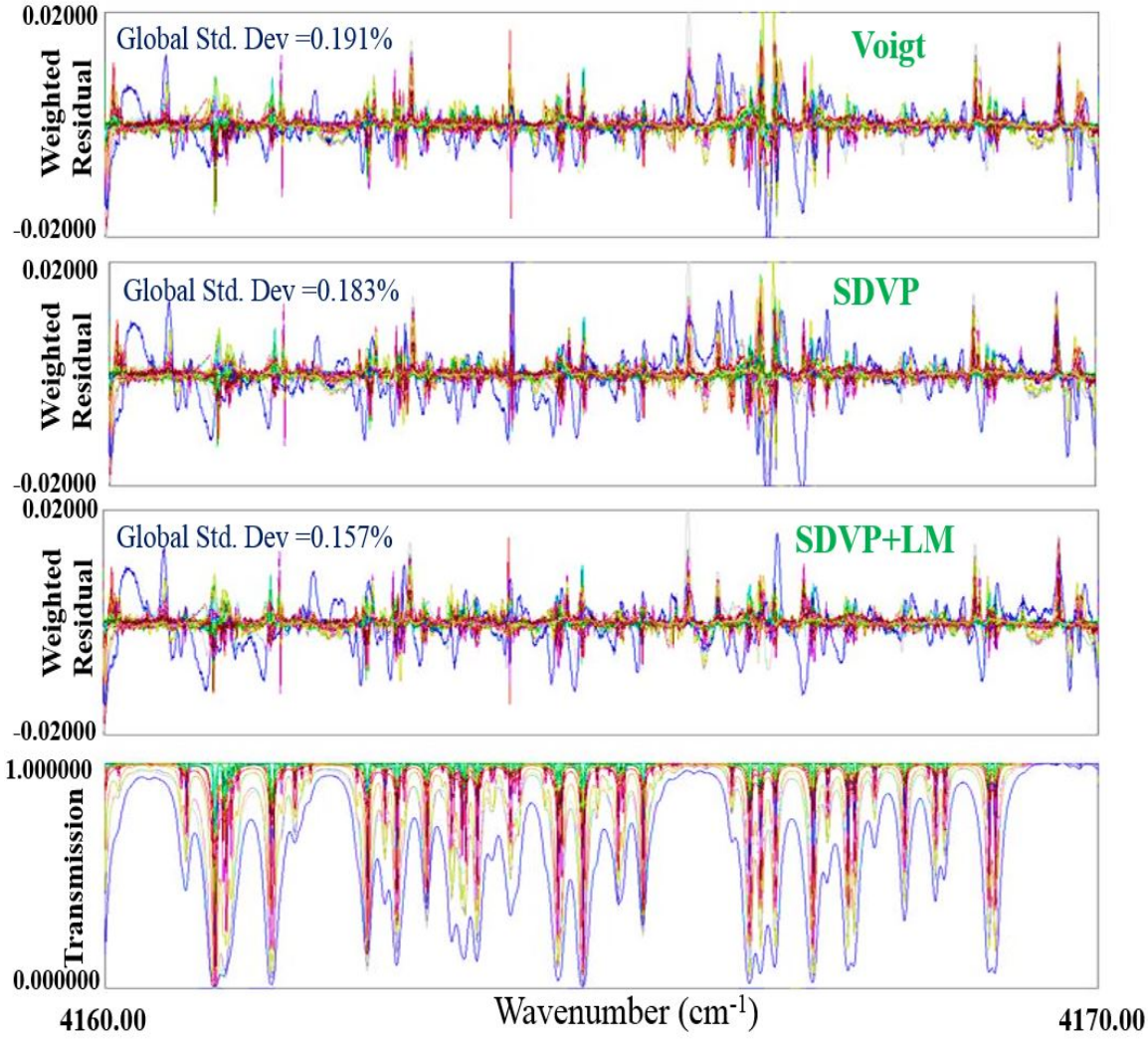

Fig 4.1: Residuals of multi-spectrum fitting of methane broadened by itself and air spectra in the $\nu_1 + \nu_4$ band. The green colors in the transmission panel represent the pure spectra, whereas other colors represent the mixed spectra.

The symbols A_1, A_2, E, F_1 and F_2 correspond to the tetrahedral symmetry species of the rotational quantum number J. The upper and lower state quantum numbers (J, C, n) are distinguishable by single and double prime, respectively. All retrieved pressure-broadening half-width coefficients along with temperature dependences are plotted in terms of the rotational symmetry species (A, E, F) as a function of $|m|$ values (Fig. 4.2-4.6). As shown in Figs. 4.2(a) and 4.3(a), the air-broadening and self-broadening half-width coefficients vary from 0.0381(5)-0.0696(7) $cm^{-1}atm^{-1}$ and 0.0534(16)-0.0905(7) $cm^{-1}atm^{-1}$ at 296 K, respectively. The broadening coefficients in both cases show higher values for the F-symmetry transitions than those of A and E symmetry transitions with E-type transitions displaying the lowest values.

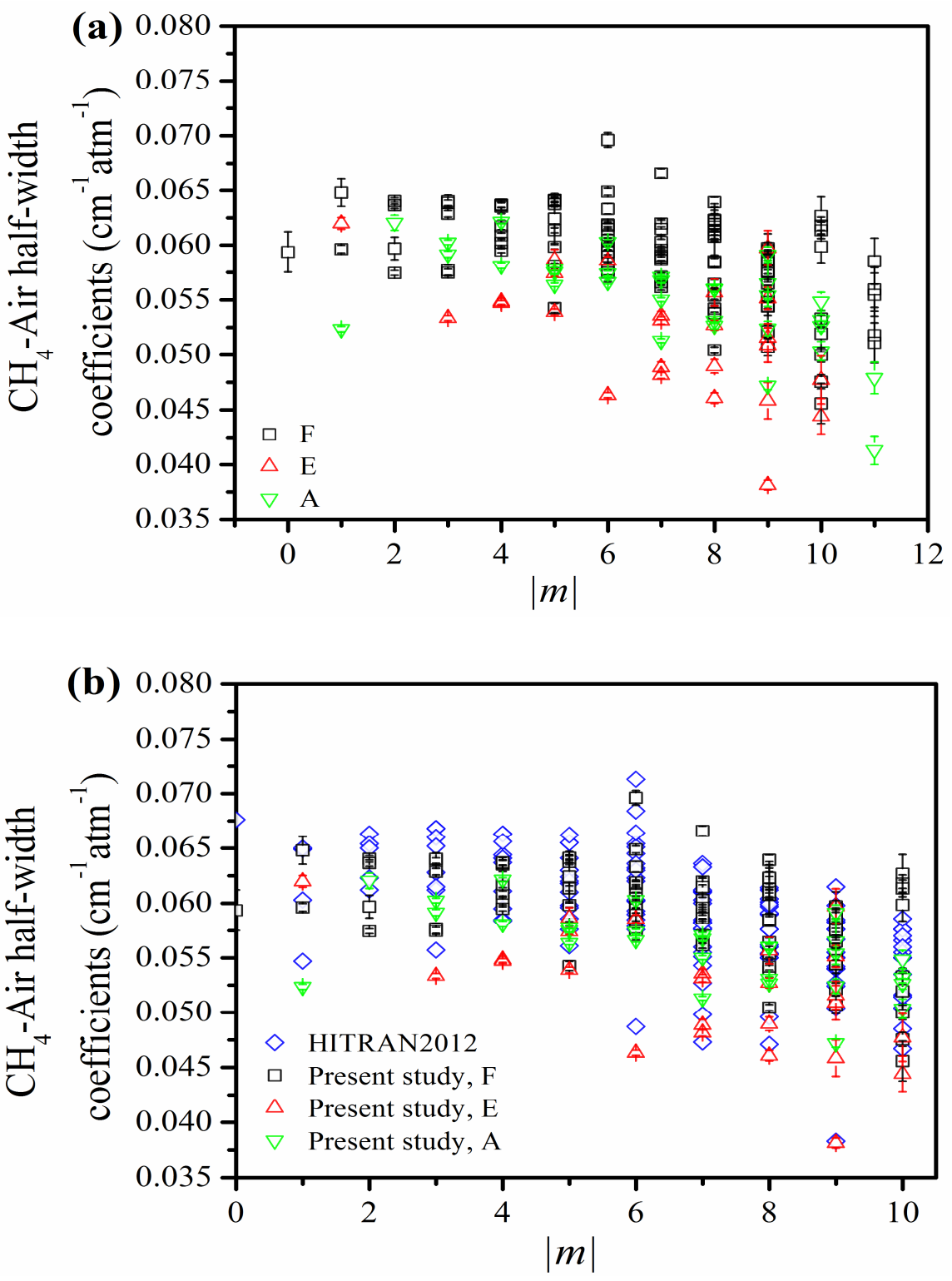

Fig 4.2: (a) Variation of CH_4-air half-width coefficients corresponding to A, E and F transitions, (b) comparison of air-width coefficients with HITRAN2012 database as a function of |m| in the $\nu_1 + \nu_4$ band of methane.

As shown in Figs. 4.2b and 4.3b, the measured broadening (both self- and air-) coefficients agree well with the HITRAN2012 [11] entries and also comply fairly with the GEISA2015 [63] database values within the average difference of 2.44% (air-b) and 3.7% (self-b). As shown in Fig. 4.4, the self-broadening parameters show higher values than the air-broadening parameters and which is similar to previous findings for different ro-vibrational bands of methane [23, 24, 35, 36] . The overall trend of change in air- and self-broadening parameters of CH_4 are also comparable to those literature.

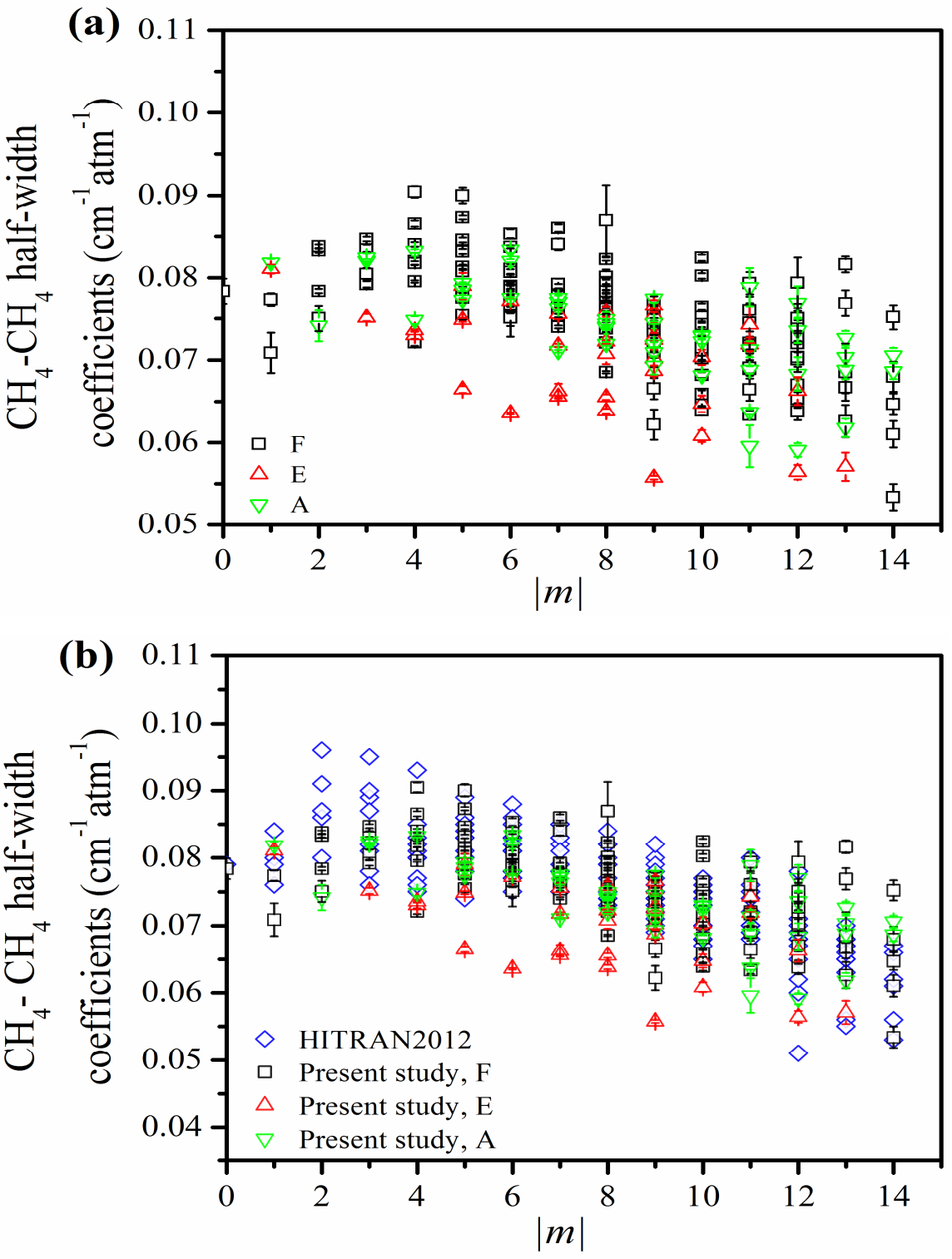

Fig 4.3: (a) Variation of CH_4- CH_4 half-width coefficients corresponding to A, E and F transitions as a function of |m| in the $\nu_1 + \nu_4$ band of methane, (b) comparison of self-width coefficients with HITRAN2012 database entries. The error bars which cannot be seen, are smaller than the size of the symbols used.

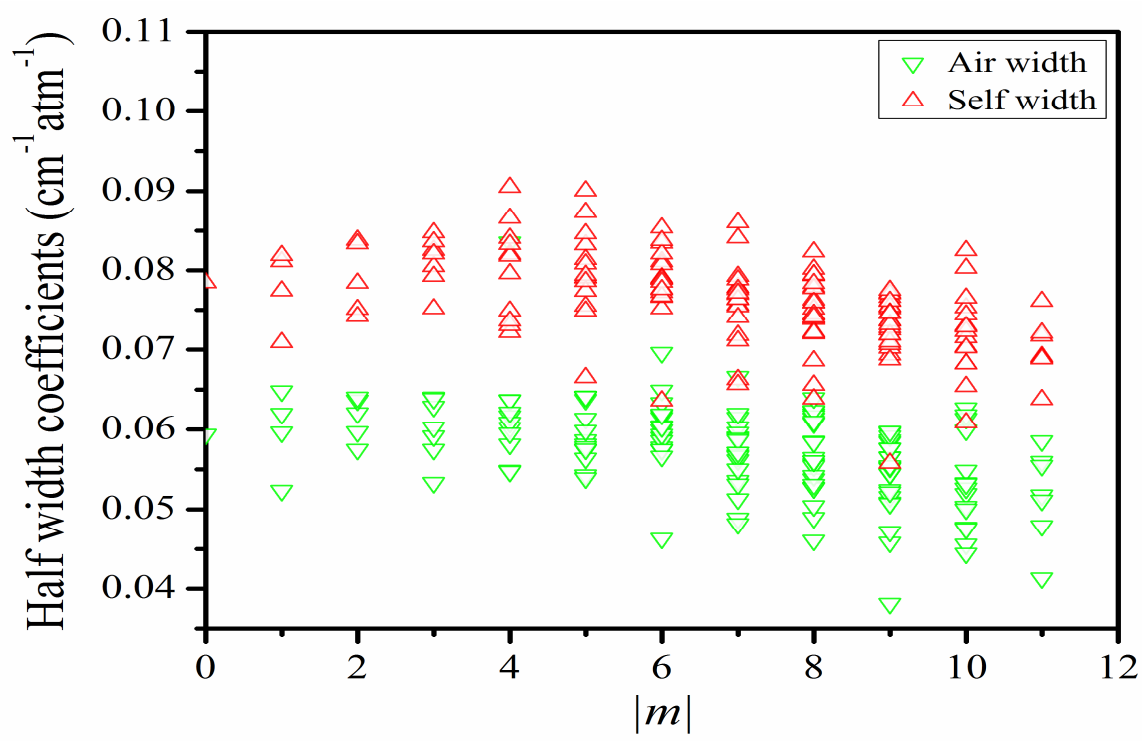

Fig 4.4: Comparison of CH_4-H_2 and CH_4-CH_4 half-width coefficients corresponding to A, E and F transitions in the $\nu_1 + \nu_4$ band of methane.

The temperature-dependence exponents of both air- and self-broadening parameters were retrieved by using the power law Eq. (4.1), and the results are presented in Figs. 4.5(a,b). As illustrated in Figs. 4.5a and 4.5b, the values for the temperature exponents of air-broadening (n_1) and self-broadening (n_2) of methane vary from 0.69(2) and 0.62(3), respectively, up to 0.97(4) and 0.99(3). The present study shows discrepancies with the earlier measured values [21], because that study was carried out for a small range of temperatures. The temperature-dependence exponents, n_1 and n_2 have been compared with respect to tetrahedral symmetry species types (*A*, *E*, *F*), which show higher values for the *F* symmetry transitions compared to *A* and *E*-type transitions in both cases.

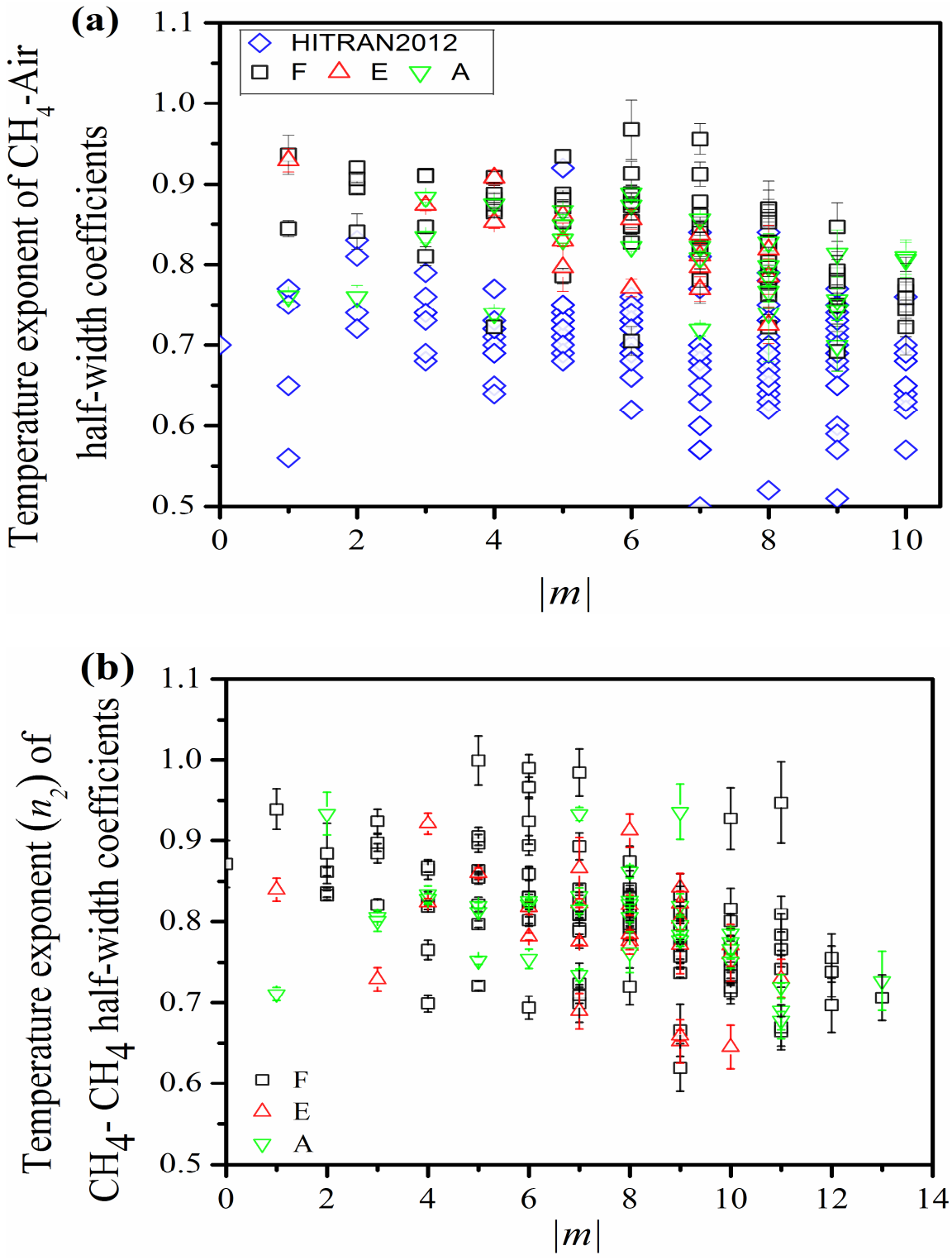

Fig 4.5: Variation in temperature-dependence exponents of (a) CH_4-air and (b) CH_4-CH_4 half-width coefficients corresponding to A, E and F transitions in the $\nu_1 + \nu_4$ band of methane. The error bars which cannot be seen, are smaller than the size of the symbols used.

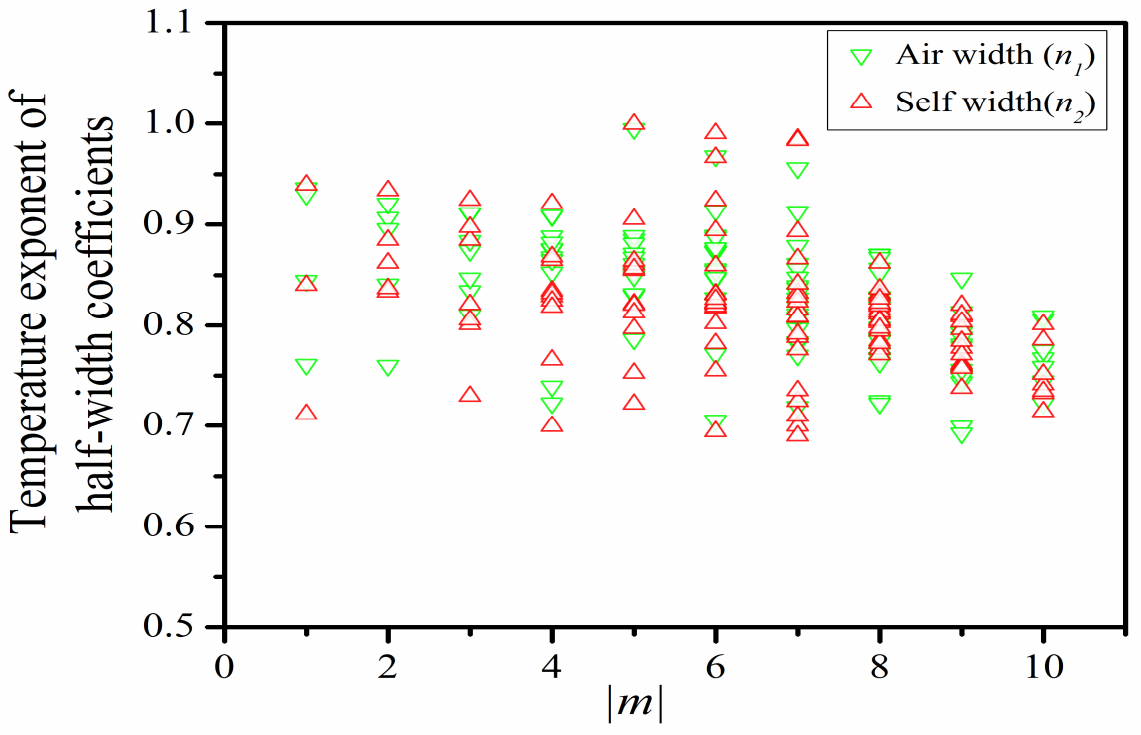

Fig 4.6: Comparison between temperature exponents of CH_4-air and CH_4-CH_4 half-width coefficients corresponding to A, E and F transitions in the $\nu_1 + \nu_4$ band of methane.

As shown in Fig. 4.5(a), the temperature-dependence exponents of the air-half-width coefficient have larger values than those of HITRAN2012 entries. I believe that this discrepancy is due to the fact that the values stored in Ref. [11] are from an older study that is less accurate in temperature measurements and also covers a different temperature range than the present study (room temperature to 148.42 K). As shown in Fig. 4.6, the variation in temperature-dependence exponents of self- and air-broadening coefficients are very similar for most of the transitions but show slightly higher values for air-broadening case, which agrees well with the literature [33, 35, 36].

4.2.2 Self- and air-shift coefficients along with temperature dependences

Recently reported [35, 36] pressure-induced self- and air-shift coefficients of methane in the octad region displayed negative values, which are also reflected in the present investigation as illustrated in Figs. (4.7-4.9) and Table 4.3.

Table 4.3: Sample of retrieved self- and air-induced shift parameters along with their temperature-dependence exponents and speed-dependence parameters.

lml	Lower state $(J''C''n'')$	Upper state $(J'C'n')$	Air-shift[a] $(cm^{-1}atm^{-1})$	Self-shift $(cm^{-1}atm^{-1})$	TD[a] Air-shift $(cm^{-1}atm^{-1}K^{-1})$	TD[a] Self-shift $(cm^{-1}atm^{-1}K^{-1})$	S[b]
1	$0A_1$ 1	$1A_2$ 4	-0.00070(4)	-0.0107(7)	0.000094(4)	0.000102(9)	0.04(1)
1	$0A_1$ 1	$1A_2$ 4	-0.0052(3)	-0.0123(5)	0.000107(2)	0.000079(6)	0.05(1)
2	2E 1	1E 6	-0.0070(8)	-0.0104(5)	0.000063(7)	0.000093(6)	0.06(1)
2	$1F_1$ 1	$2F_2$ 15	-0.0064(3)	-0.0106(3)	0.000043(3)	0.000032(3)	0.01(1)
3	$3A_2$ 1	$3A_1$ 7	-0.0074(3)	-0.0066(7)	0.000046(2)	0.000135(9)	0.02(1)
3	2E 1	3 E 13	-0.0056(3)	-0.0105(5)	0.000071(3)	0.000077(6)	0.03(1)
4	$4F_2$ 1	$3F_1$ 23	-0.0062(4)	-0.0138(3)	0.000062(4)	0.00004(3)	0.04(1)
4	$3A_2$ 1	$4A_1$ 10	-0.0066(2)	-0.0115(4)	0.000051(2)	-0.000028(5)	0.06(1)
5	4E 1	5E 20	-0.0066(3)	-0.0126(4)	0.00006(2)	0.000050(5)	0.12(1)
6	6E 1	6E 26	-0.0062(5)	-0.0105(3)	0.000056(5)	0.000066(3)	0.05(1)
6	6E 1	5E 23	-0.0056(4)	-0.0116(2)	0.000064(4)	0.000067(2)	0.06(1)
7	$7A_2$ 1	$7A_1$ 15	-0.0071(3)	-0.0112(3)	0.000059(3)	0.000082(4)	0.08(1)
7	$7A_2$ 1	$6A_1$ 15	-0.0072(2)	-0.0129(1)	0.00006(2)	0.000072(1)	0.064(4)
8	$8F_1$ 2	$7F_2$ 45	-0.0086(4)	-0.0136(1)	0.000070(4)	0.000079(1)	0.03(1)
8	$7F_1$ 2	$8F_2$ 43	-0.0039(5)	-0.0094(3)	0.000034(6)	0.000050(3)	0.04(1)
9	$9F_1$ 1	$8F_2$ 54	-0.0078(4)	-0.0137(1)	0.000063(5)	0.000077(1)	0.04(1)
9	$9F_1$ 1	$8F_2$ 54	-0.0055(2)	-0.0087(4)	0.000035(2)	0.000050(4)	0.01(1)
10	$10A_2$1	$9A_1$ 19	-0.0095(7)	0.0133(5)	0.000024(9)	0.000047(5)	0.11(1)
10	$9F_2$ 1	$10F_1$ 48	-0.0078(9)	-0.0133(3)	0.00007(10)	0.000067(3)	0.04(1)

TD[a] is used as temperature-dependence and S^b stands for speed dependence parameters.

From Fig. 4.7a, it can be seen that the measured CH_4-air shift coefficients lie between -0.0171(10) and -0.0026(3) $cm^{-1}atm^{-1}$. When compared in Fig. 4.7b, the measured CH_4-air shift coefficients agree well with HITRAN2012 database results. They also agree well with GEISA2015 [63] entries with the variation from 0.01 to 0.07. The overall variation in shift

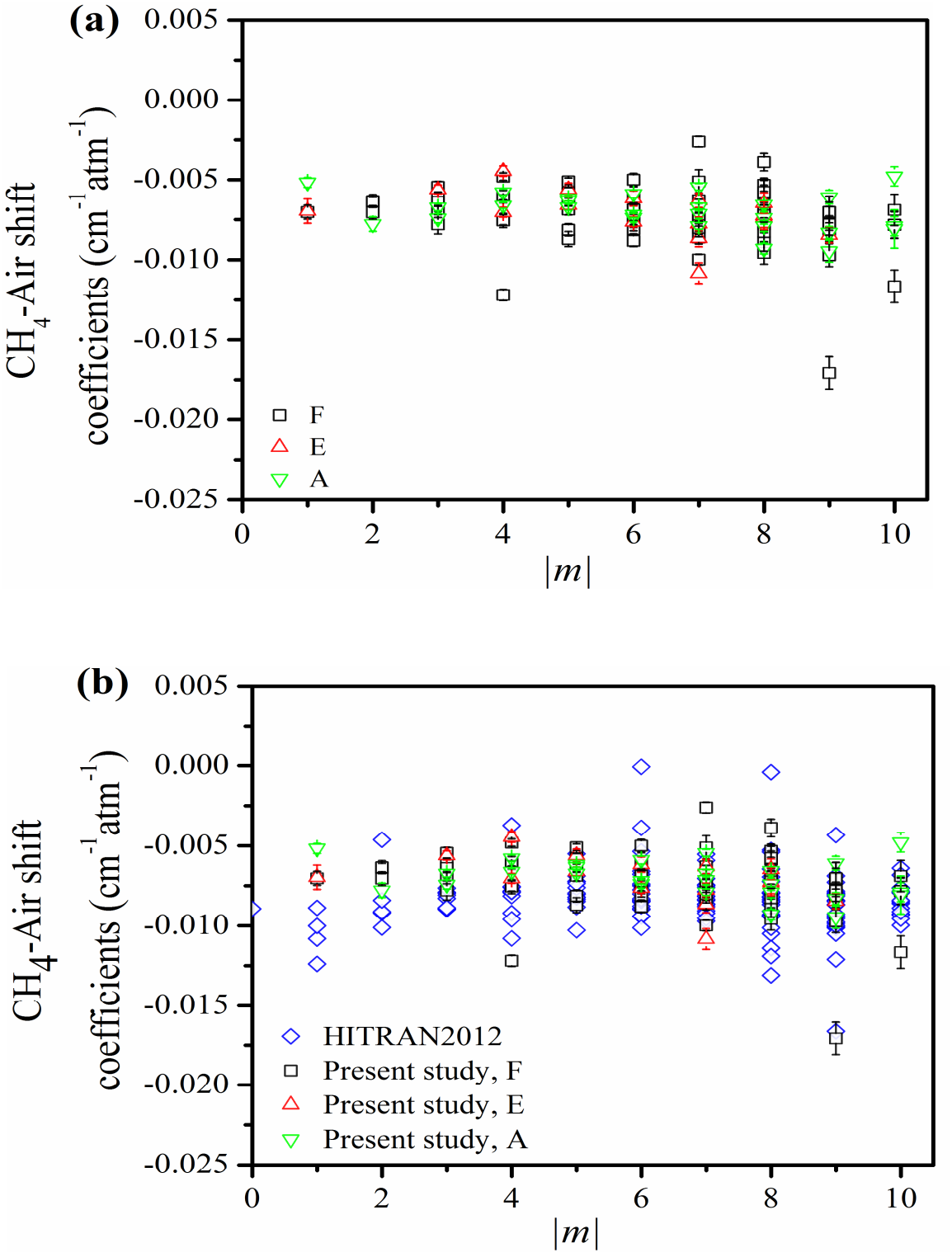

Fig 4.7: (a) Variation of CH_4-air pressure-shift coefficients corresponding to A, E and F transitions, (b) comparison of CH_4-air pressure-shift coefficients with HITRAN2012 database entries as a function of |m| in the $\nu_1 + \nu_4$ band of methane. The error bars which cannot be seen, are smaller than the size of the symbols used. The CH_4-air shift coefficients are measured at 296 K.

coefficients does not follow any symmetric pattern compared to width coefficients, possibly attributable to the line-mixing contributions [23].

Fig. 4.8 shows the variation of self-shift coefficients as a function of $|m|$, which change from -0.0243(6) to -0.0033(15) $cm^{-1}atm^{-1}$. Since HITRAN2012 and GEISA2015 have not included the results for self-shift coefficient, they are compared among different rotational symmetry species which show higher values in overall for *F* transitions than those of *A* and *E* transitions (Fig. 4.8). The self-shift parameters are compared to those from the ν_4 band study [31, 32, 64] displaying a somewhat wider range of deviation for each $|m|$. The air- and self-pressure shift coefficients are compared (Fig. 4.9) for the same transitions as a function of $|m|$, and display more negative values of self-shift compared to CH_4-air shift coefficients, which is similar to references [21, 23, 24, 35, 36].

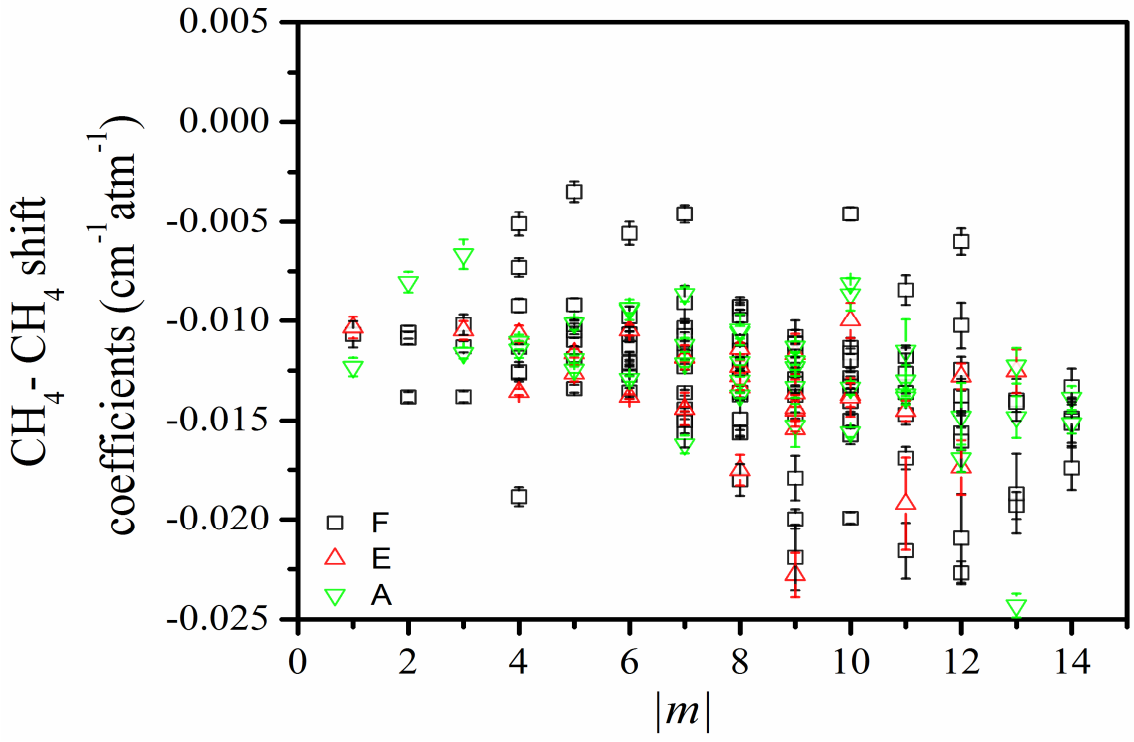

Fig 4.8: Variation of CH4-air pressure-shift coefficients corresponding to A, E and F transitions as a function of |m| in the $\nu_1 + \nu_4$ band of methane. The error bars which cannot be seen, are smaller than the size of the symbols used.

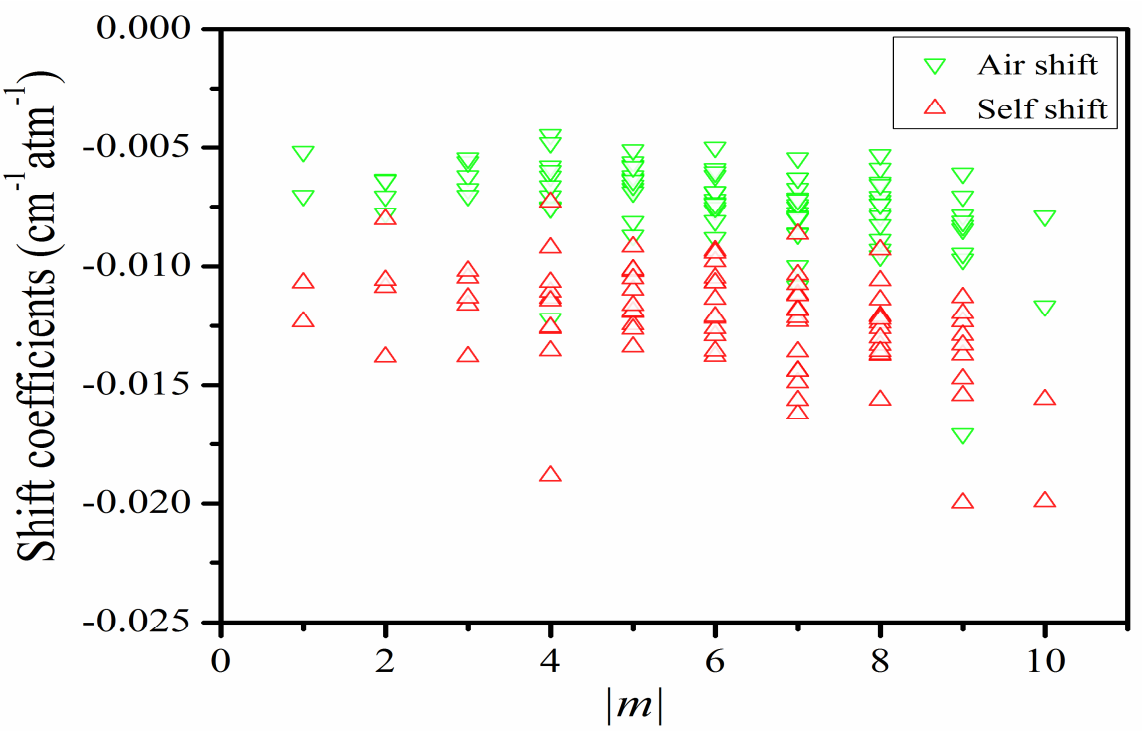

Fig 4.9: Comparison of CH_4-air and CH_4-CH_4 shift coefficients corresponding to A, E and F transitions in the $\nu_1 + \nu_4$ band of methane.

The temperature-dependence of pressure-shift coefficients of methane transitions is important and should be included in the latest spectroscopic databases. Temperature-dependence of CH_4-air and CH_4-CH_4 pressure-shift coefficients were measured by employing a linear model (Eq. 4.3) and the results are presented in Fig. 4.10(a-b) and Table 4.3. As per our measurements, temperature-dependence of CH_4-air shift parameters vary from 0.000033(2) to 0.00014(4) $cm^{-1}atm^{-1}K^{-1}$ and the self-shift parameters range from 0.000028(4) to 0.000141(12) $cm^{-1}atm^{-1}K^{-1}$. The temperature dependences due to self- and air-shift are compared and presented in Fig. 4.11. As seen from Fig. 4.11, no clear different trend is visible between the temperature-dependence of air-shift and self-shift coefficients in the present work. Due to the lack of available data, it was not possible to compare these parameters with those from databases.

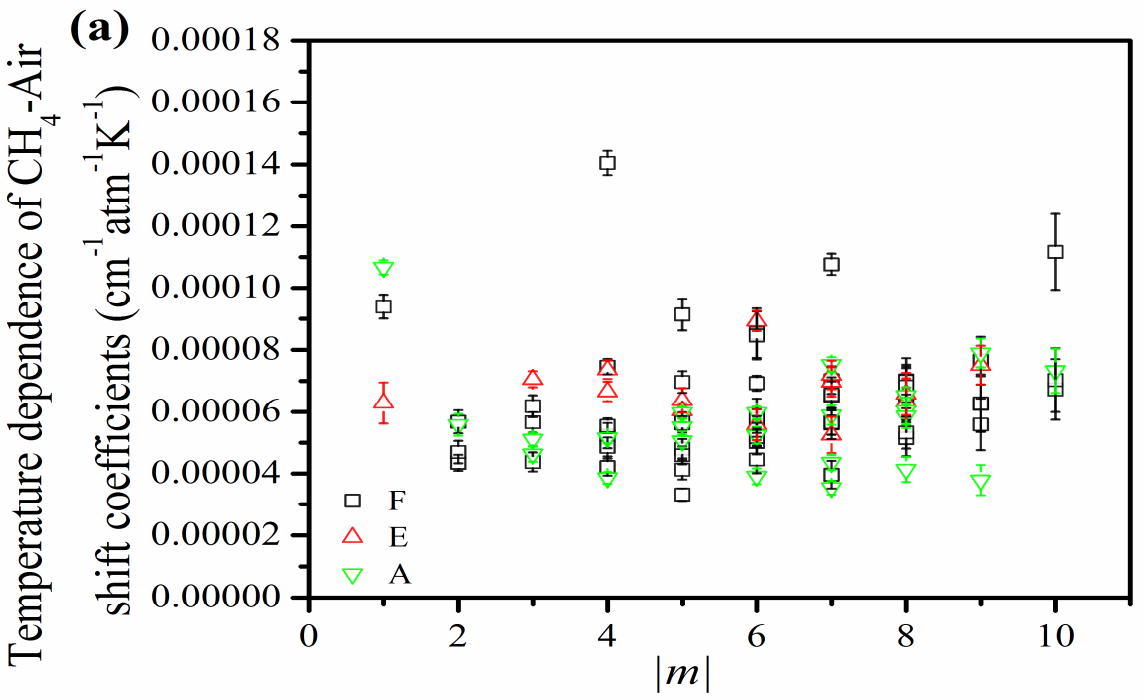
(a)
Temperature dependence of CH4-Air shift coefficients (cm-1atm-1K-1)
0.00018
0.00016
0.00014
0.00012
0.00010
0.00008
0.00006
0.00004
0.00002
0.00000
F
E
A
0
2
4
6
8
10
|m|

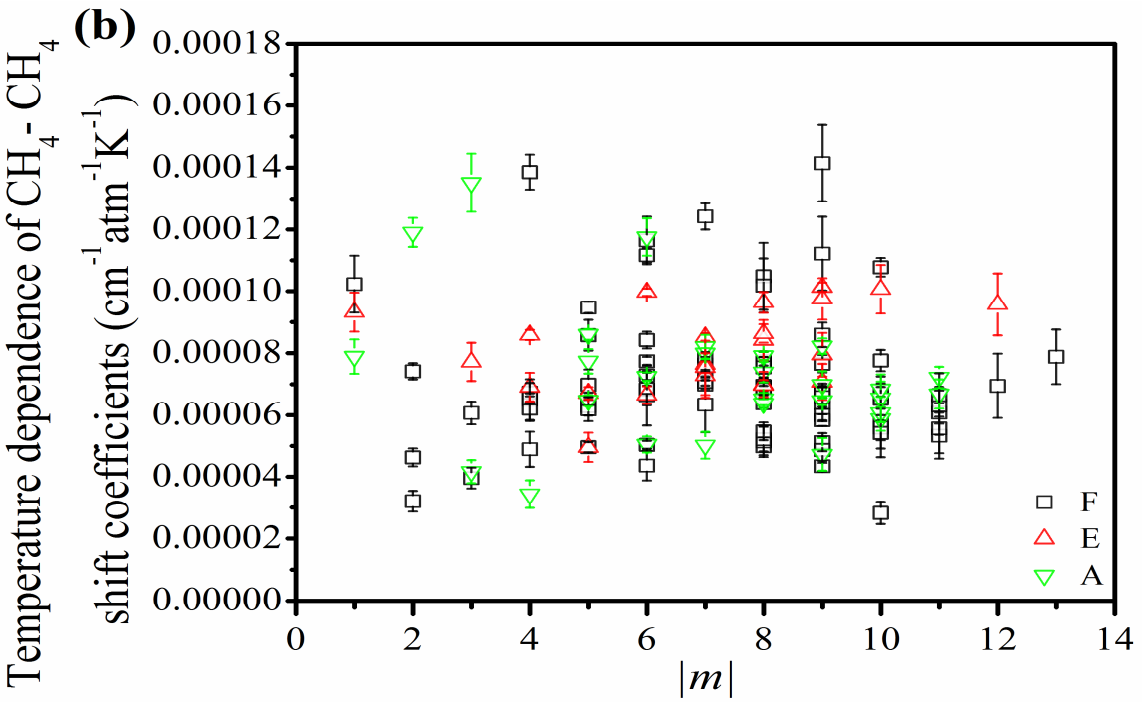

Fig 4.10: Temperature-dependence of (a) CH_4-air and (b) CH_4-CH_4 shift coefficients as a function of |m| in the $\nu_1 + \nu_4$ band of methane with inter-symmetry comparisons. The error bars which cannot be seen, are smaller than the size of the symbols used.

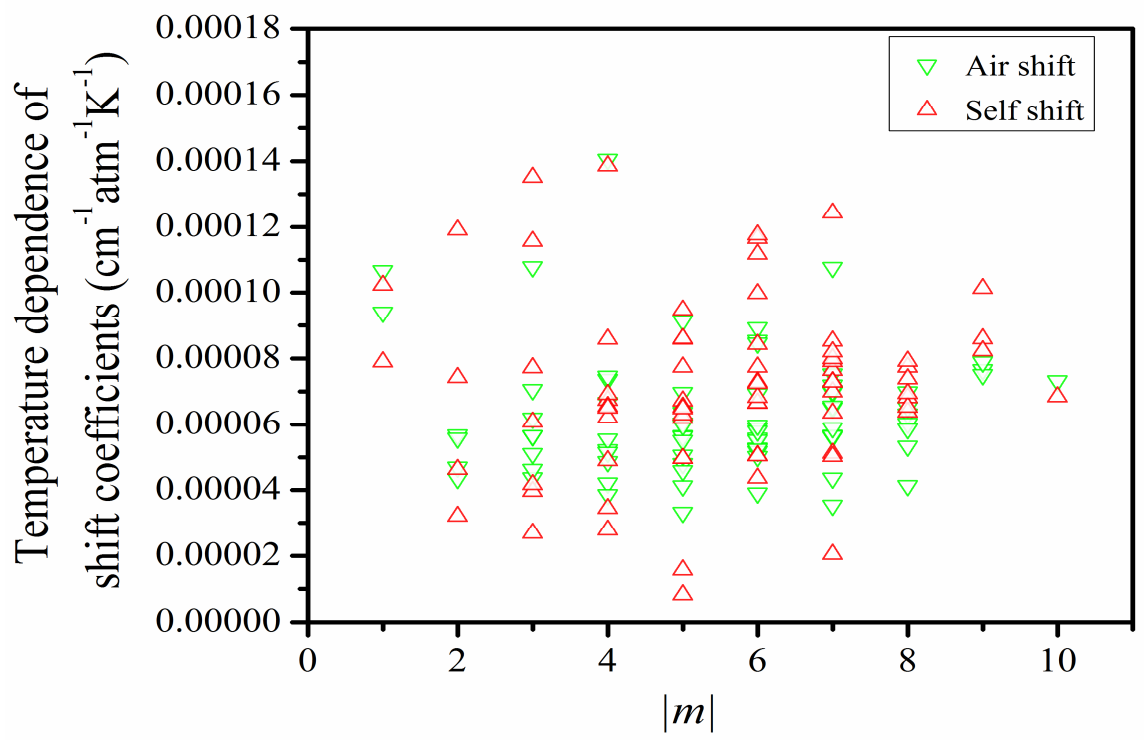

Fig 4.11: Comparison of temperature dependences of CH_4-air and CH_4-CH_4 shift coefficients corresponding to A, E and F transitions in the $\nu_1 + \nu_4$ band of methane.

4.2.3 Speed-dependence parameters

Since the SDVP was implemented in the fitting procedure, I was able to measure speed-dependence (*S*) parameters which are important in molecular dynamics. I have compared my results among transitions of different degeneracies of rotational symmetry species (*A*, *E* and *F*) of the vibrational band $\nu_1 + \nu_4$. It is apparent from Fig. 4.12 that, the measured speed- dependence parameters vary from 0.04(1) to 0.19(1) and the range of values is close to previous studies [35, 36]. The speed-dependence parameters show the dependency on the rotational symmetry species and was shown to increase with |*m*| values. The average value of speed dependence parameter due to air-broadening of methane is 0.091, which is smaller than the calculated value of 0.013 performed by Kochanov [65].

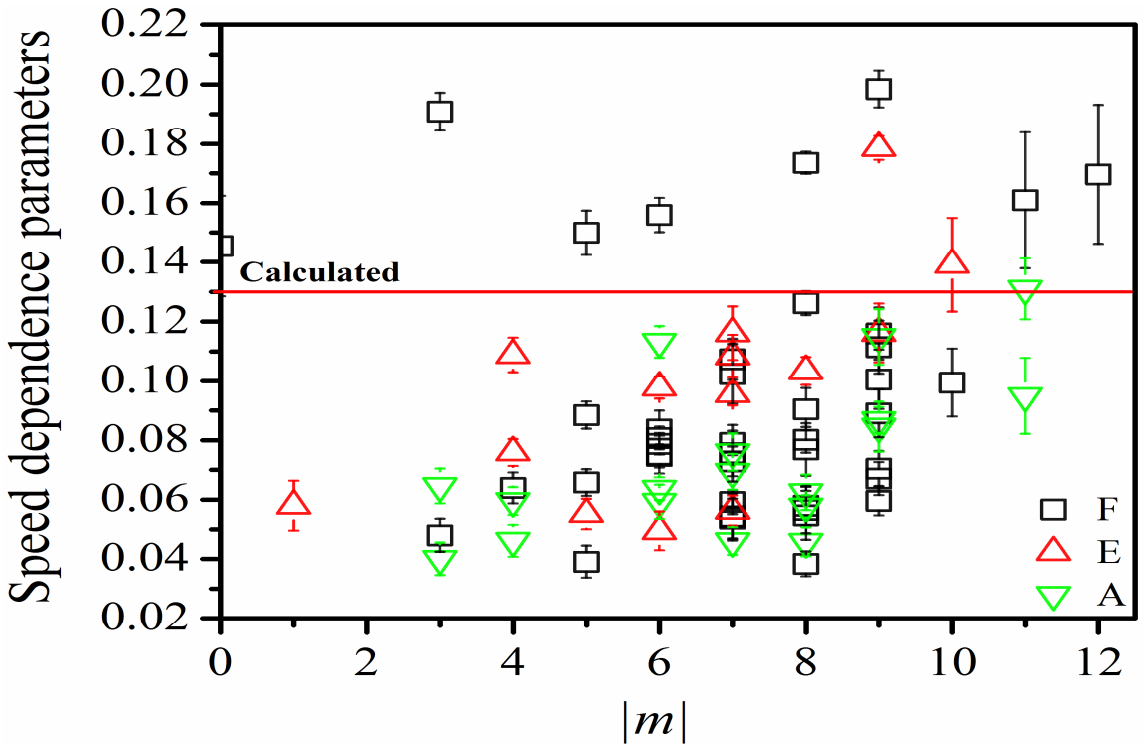

Fig 4.12: Variation in speed dependence parameters of methane broadened by air in the $\nu_1 + \nu_4$ band as a function of |m|. The error bars which cannot be seen, are smaller than the size of the symbols used.

4.2.4 Off-diagonal relaxation matrix elements

Previously [22, 25, 35, 36, 66] two main methods were used for line-mixing analyses: the first-order approximation and the off-diagonal relaxation matrix element formalism. The off-diagonal relaxation matrix element mechanism has been used in the present line-mixing analysis for 94 self-broadened and 46 air-broadened transitions, which are listed in Table 4.4.

Table 4.4: List of retrieved line-mixing coefficients due to self- and air-broadening of methane in the band $\nu_1 + \nu_4$.

			Off diagonal relaxation matrix elements	
Position (cm^{-1})	**|m|**	**Line-mixing Pairs**	**CH_4-Air broadening[a] ($cm^{-1}atm^{-1}$)**	**CH_4-CH_4 broadening[a] ($cm^{-1}atm^{-1}$)**
4118.91542	6	$6F_1$ 1 ⟶ $5F_2$ 27		0.0244(17)
4119.12945	6	$6F_2$ 2 ⟶ $5F_1$ 28		
4119.419111	12	$12F_1$ 3 ⟶ $11F_2$ 66		0.0172(21)
4119.700352	12	$12F_2$ 3 ⟶ $11F_1$ 69		
4122.444509	12	$12F_1$ 2 ⟶ $11F_2$ 67	0.0029(5)	
4122.736709	12	$12F_2$ 1 ⟶ $11F_1$ 71		
4136.167128	11	$11F_1$ 3 ⟶ $10F_2$ 63	0.0253(6)	0.0237(4)
4136.817899	11	$11F_2$ 3 ⟶ $10F_1$ 63		
4153.651517	10	$10F_1$ 1 ⟶ $9F_2$ 59		0.0058(3)
4154.102169	10	$10F_2$ 2 ⟶ $9F_1$ 59		
4159.491305	9	$9F_2$ 2 ⟶ $8F_1$ 51	0.0147(12)	0.0236(4)
4160.035843	9	$9F_1$ 3 ⟶ $8F_2$ 52		
4165.578642	9	$9F_2$ 1 ⟶ $8F_1$ 52		0.0033(1)
4165.762113	9	$9F_1$ 1 ⟶ $8F_2$ 54		
4167.1577	8	$8F_2$ 2 ⟶ $7F_1$ 47	0.0164(18)	0.0281(7)
4168.48589	8	$8F_1$ 2 ⟶ $7F_2$ 45		
4172.8268	9	$9A_2$ 1 ⟶ $8A_1$ 19	0.0277(25)	0.0145(8)
4173.95807	9	$9A_1$ 1 ⟶ $8A_2$ 18		
4173.009946	9	$9F_2$ 2 ⟶ $8F_1$ 53	0.0079(9)	0.0155(3)
4173.231512	9	$9F_1$ 3 ⟶ $8F_2$ 55		
4177.713984	9	$9F_1$ 1 ⟶ $8F_2$ 58		0.0021(3)
4177.781651	9	$9F_2$ 1 ⟶ $8F_1$ 55		
4178.252415	7	$7F_2$ 1 ⟶ $6F_1$ 40		0.0018(1)
4178.527636	7	$7F_1$ 1 ⟶ $6F_2$ 41		
4181.817074	6	$6F_1$ 1 ⟶ $5F_2$ 34	0.0105(10)	0.0131(4)
4182.336902	6	$6F_2$ 2 ⟶ $5F_1$ 34		

4189.89872	5	$5F_2$ 1 ⟶ $4F_1$ 27	0.024(32)	0.0274(23)
4190.45562	5	$5F_1$ 1 ⟶ $4F_2$ 29		
4201.400581	3	$3F_2$ 1 ⟶ $2F_1$ 15		0.0069(2)
4201.848098	3	$3F_1$ 1 ⟶ $2F_2$ 16		
4203.36652	11	$11F_1$ 1 ⟶ $11F_2$ 59		0.0039(3)
4203.37226	11	$11F_2$ 1 ⟶ $11F_1$ 61		
4206.648252	7	$7F_1$ 2 ⟶ $6F_2$ 42	0.0528(39)	0.0195(31)
4207.17361	6	$6F_2$ 1 ⟶ $6F_1$ 36		
4209.871337	7	$7F_1$ 1 ⟶ $6F_2$ 43		0.003(5)
4209.980328	7	$7F_2$ 1 ⟶ $6F_1$ 43		
4212.67804	7	$7F_1$ 1 ⟶ $7F_2$ 41		0.0037(6)
4212.99085	7	$7F_2$ 1 ⟶ $7F_1$ 43		
4213.072723	10	$10F_2$ 2 ⟶ $10F_1$ 56		0.0102(17)
4213.600841	10	$10F_1$ 1 ⟶ $10F_2$ 57		
4217.5507	3	$3F_1$ 1 ⟶ $3F_2$ 20		0.0063(9)
4218.075313	3	$3F_2$ 1 ⟶ $3F_1$ 22		
4219.653719	8	$8F_2$ 2 ⟶ $8F_1$ 48		0.003(5)
4219.785966	8	$8F_2$ 2 ⟶ $8F_1$ 49		
4222.07045	9	$9F_2$ 2 ⟶ $9F_1$ 54		0.0219(18)
4222.57608	9	$9F_1$ 3 ⟶ $9F_2$ 54		
4223.54765	9	$9F_2$ 2 ⟶ $8F_1$ 67		
4223.87868	9	$9F_1$ 3 ⟶ $8F_2$ 69		
4223.61303	6	$6F_1$ 1 ⟶ $5F_2$ 35	0.0118(5)	0.0114(4)
4223.81497	6	$6F_2$ 2 ⟶ $5F_1$ 36		
4228.60199	8	$8F_1$ 1 ⟶ $7F_2$ 55		0.0278(45)
4229.99949	8	$8F_2$ 1 ⟶ $7F_1$ 57		
4233.810945	7	$7F_2$ 1 ⟶ $6F_1$ 45		
4234.297037	7	$7F_1$ 1 ⟶ $6F_2$ 46		
4239.428901	4	$3F_2$ 1 ⟶ $4F_1$ 25	0.0118(5)	0.0114(4)
4239.577754	4	$3F_1$ 1 ⟶ $4F_2$ 26		
4238.46631	13	$13F_1$ 1 ⟶ $13F_2$ 80		0.0278(45)
4239.55487	12	$12F_1$ 3 ⟶ $12F_2$ 73		
4242.181681	5	$5F_2$ 1 ⟶ $4F_1$ 28		0.0006(1)
4242.2068	5	$5F_1$ 1 ⟶ $4F_2$ 31		
4245.85675	5	$5F_1$ 1 ⟶ $4F_2$ 32		0.0076(3)
4246.15194	5	$5F_2$ 1 ⟶ $4F_1$ 29		
4249.14676	6	$5F_1$ 1 ⟶ $6F_2$ 34	0.0059(4)	0.0133(3)
4249.439323	6	$5F_2$ 1 ⟶ $6F_1$ 32		
4251.6621	6	$6F_1$ 1 ⟶ $5F_2$ 40		0.0419(24)
4251.66864	6	$6F_2$ 2 ⟶ $5F_1$ 42		
4253.645665	7	$6F_1$ 1 ⟶ $7F_2$ 37	0.0133(3)	0.0127(3)
4253.768118	7	$6F_2$ 2 ⟶ $7F_1$ 38		
4253.51925	7	$6A_1$ 1 ⟶ $7A_2$ 14	0.0182(12)	0.0231(7)

4254.48124	7	$6A_2$ 2 ⟶ $7A_1$ 13		
4257.549435	10	$10F_1$ 1 ⟶ $10F_2$ 67		0.0207(13)
4257.58786	10	$10F_2$ 2 ⟶ $10F_1$ 66		
4258.533596	8	$7F_1$ 2 ⟶ $8F_2$ 43	0.0096(11)	0.003(5)
4258.831764	8	$7F_2$ 2 ⟶ $8F_1$ 42		
4259.691916	8	$7F_1$ 1 ⟶ $8F_2$ 44	0.0032(6)	0.003(5)
4259.976554	8	$7F_2$ 1 ⟶ $8F_1$ 43		
4263.51064	9	8E 2 ⟶ 9E 30		
4264.59887	9	8E 1 ⟶ 9E 31		
4261.67571	9	$8F_2$ 2 ⟶ $9F_1$ 45		0.0138(22)
4262.94334	9	$8F_1$ 2 ⟶ $9F_2$ 45		
4266.496434	10	$9A_2$ 1 ⟶ $10A_1$ 17	0.0364(18)	0.035(7)
4267.134589	10	$9A_1$ 1 ⟶ $10A_2$ 16		
4266.606323	10	$9F_2$ 2 ⟶ $10F_1$ 47	0.0235(7)	0.0238(3)
4266.75511	10	$9F_1$ 3 ⟶ $10F_2$ 48		
4268.909019	10	$9F_1$ 1 ⟶ $10F_2$ 50	0.0025(5)	0.0038(3)
4268.972843	10	$9F_2$ 1 ⟶ $10F_1$ 48		
4280.951177	13	$12F_1$ 2 ⟶ $13F_2$ 61		0.0029(3)
4281.093062	13	$12F_2$ 1 ⟶ $13F_1$ 63		
4282.12807	7	$7F_2$ 2 ⟶ $7F_1$ 52		0.0256(23)
4282.541148	7	$7F_1$ 2 ⟶ $7F_2$ 50		
4284.513121	3	$3F_1$ 1 ⟶ $2F_2$ 18	0.0031(7)	0.0049(4)
4284.574479	3	$3F_2$ 1 ⟶ $2F_1$ 18		
4287.785453	6	$6F_2$ 2 ⟶ $6F_1$ 44	0.0314(27)	0.0139(9)
4287.953274	6	$6F_1$ 1 ⟶ $6F_2$ 44		
4288.660556	5	5E 1 ⟶ 4E 27	0.0109(16)	0.0063(10)
4288.801408	5	$5F_1$ 1 ⟶ 5F2 36		
4288.846124	5	5E 1 ⟶ 5E 24	0.0109(18)	0.0063(11)
4288.898266	5	$5F_2$ 1 ⟶ $5F_1$ 37		
4294.556414	4	$4F_1$ 1 ⟶ $4F_2$ 31		0.0424(29)
4294.592776	4	$4F_2$ 1 ⟶ $3F_1$ 32		
4298.206083	4	$4F_1$ 1 ⟶ $4F_2$ 32		0.0025(4)
4298.499938	4	$4F_2$ 1 ⟶ $4F_1$ 29		

[a] Statistical uncertainties are given in parentheses. The blank spaces in table is appeared because the line mixing coefficients were not possible to be determined correctly for those transitions.

The off-diagonal relaxation matrix coefficients for both self- and air-broadening were retrieved using 'Labfit'. The possible transitions for line-mixing among tetrahedral symmetry species follow rules: $A_1 \leftrightarrow A_2$, $F_1 \leftrightarrow F_2$ and $E \leftrightarrow E$. Fig. 4.13a and Fig. 4.14a

show the variations in line mixing coefficients as a function of |*m*| for air- and self-broadening of methane, respectively. As shown in Fig. 4.13a and Fig. 4.14a, the off-diagonal relaxation matrix elements for air-broadening vary from 0.0025(5) to 0.0528(39) $cm^{-1}atm^{-1}$ for maximum value of |m|=11, whereas for self-broadening the coefficients vary from 0.0006(10) to 0.0419(24) $cm^{-1}atm^{-1}$ for |m| values up to 12. The results are compared with references [25, 31, 33, 35, 64, 67, 68], which show a fair agreement as shown in Figs. 4.13b and 4.14b. Temperature-dependence of line-mixing coefficients was not possible to determine in this study. More theoretical efforts are needed for the temperature-dependence exponents of line-mixing coefficients. Besides the group of Tran (broadened by N_2, air, He and H_2 [68, 69]), semi-classical calculations for line-mixing of nitrogen-broadened methane at room-temperature were performed successfully by Gabard and Boudon [70]; however, more experimental and theoretical line-mixing measurements in this complex "Octad" band of methane are needed to confirm their vibrational dependences.

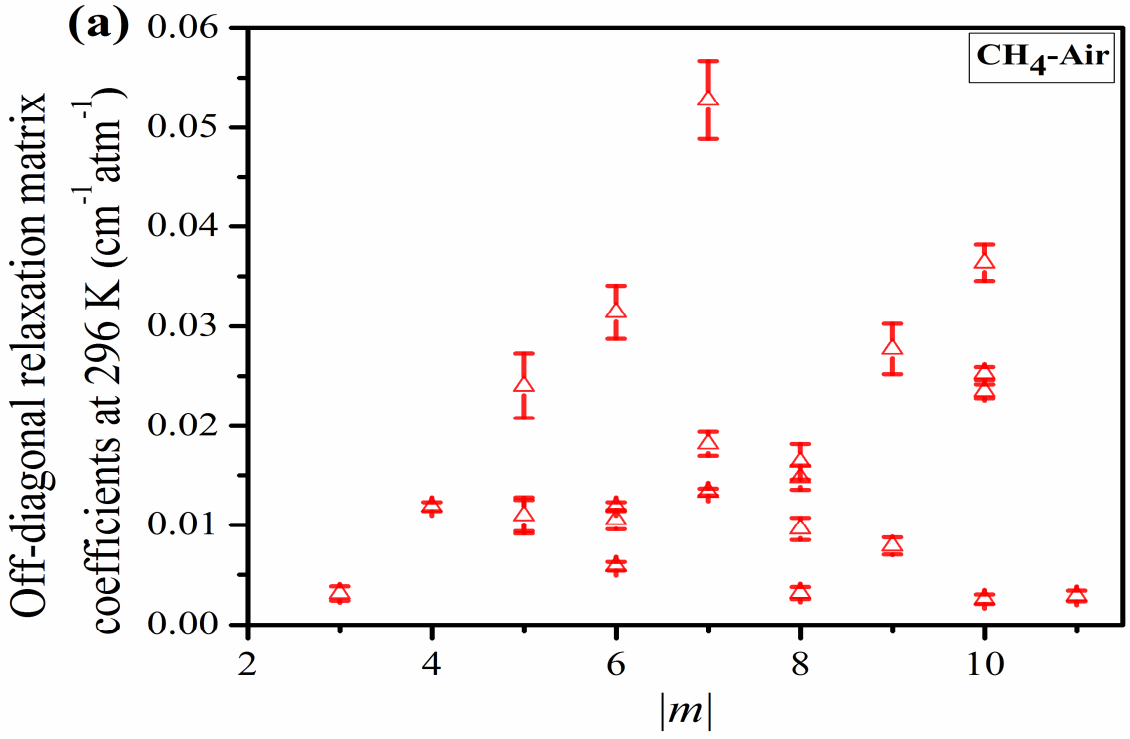

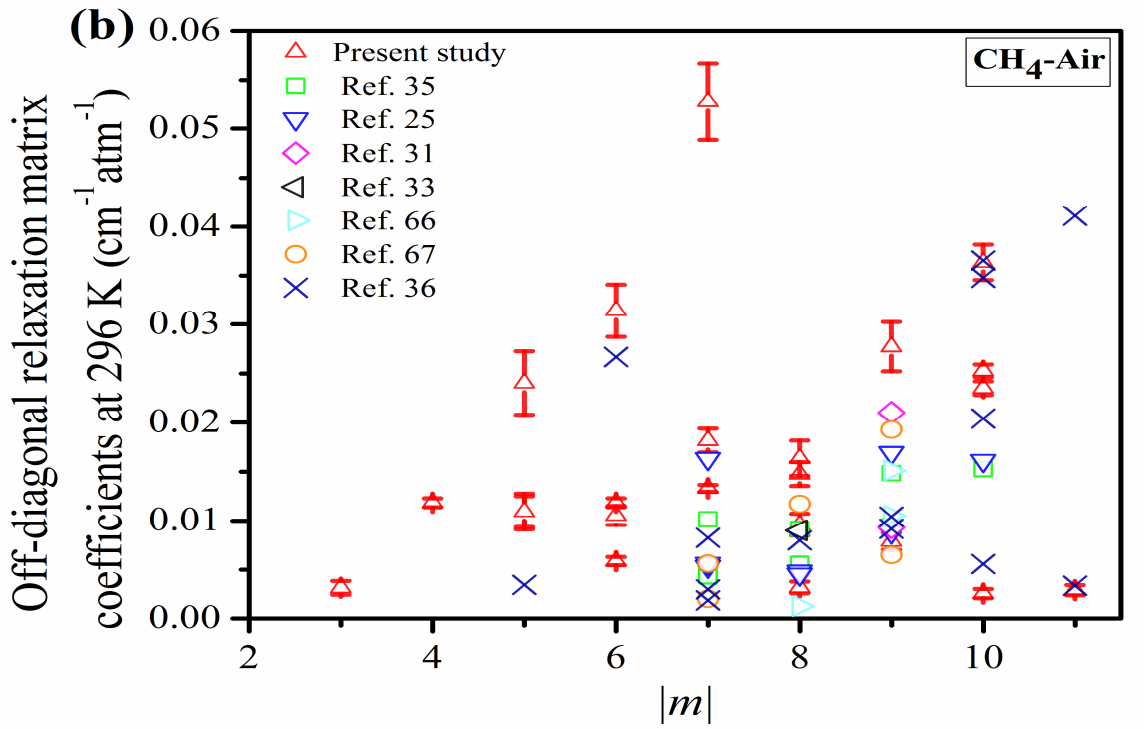

Fig 4.13: Off-diagonal relaxation matrix element coefficients of air-broadening in the $\nu_1 + \nu_4$ band of methane as a function of |m| compared to Refs [25, 31, 33, 35, 36, 66, 67]. The error bars which cannot be seen, are smaller than the size of the symbols used.

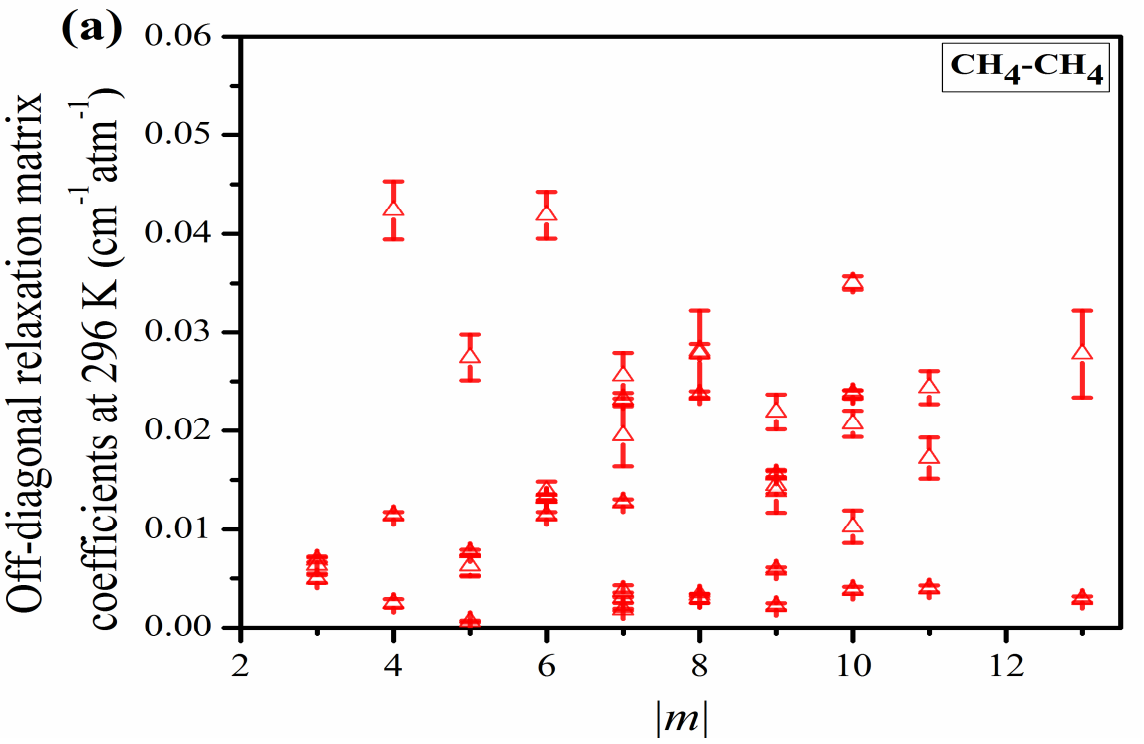

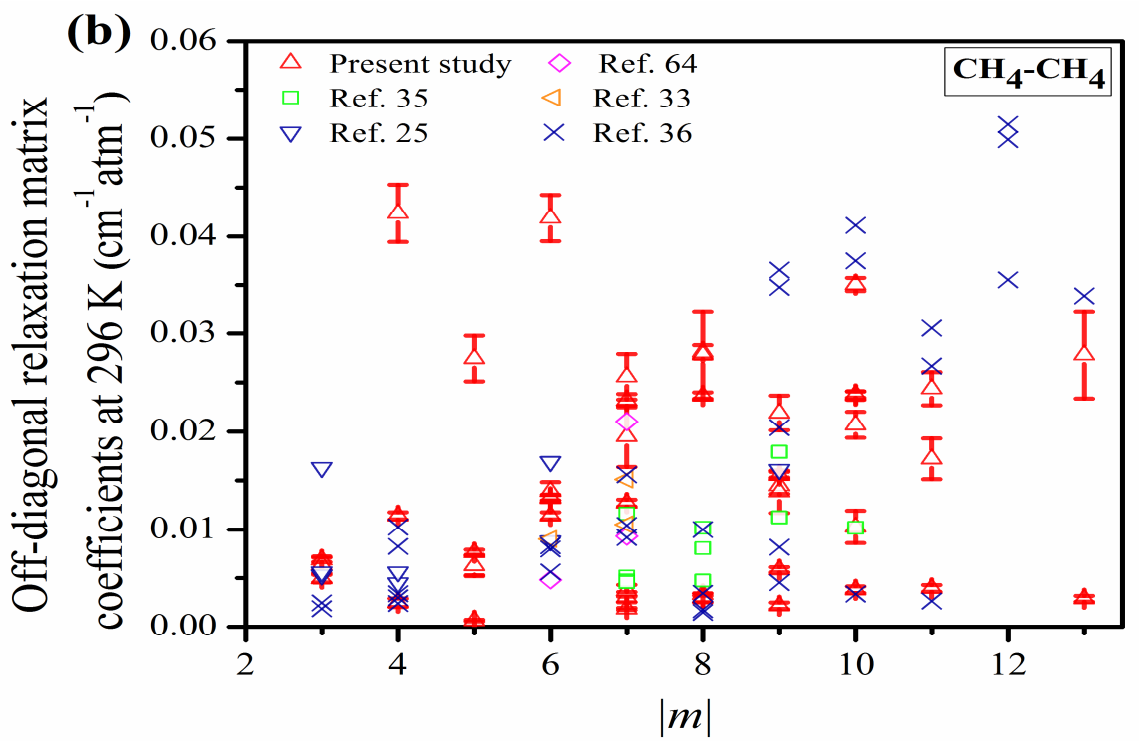

Fig 4.14: Off-diagonal relaxation matrix element coefficients due to self-broadening of methane in the $\nu_1 + \nu_4$ band as a function of |m| compared to Refs [25, 33, 35, 36, 64]. The error bars which cannot be seen, are smaller than the size of the symbols used.

4.2.5 Comparisons of line positions and intensities

Selected measured line position and intensity values with respect to absolute values of *m* are given in Table 4.5 and 4.6 along with the calculated values and database records for the same set of transitions. The line positions and intensities were calculated by Tyuterev et al. [71] using a mixed approach combining ab initio potential energy and dipole moment surfaces with empirical optimization of line positions. Initial ab initio calculations were described by Nikitin et al. [72, 73]. The details about the empirical optimizations of effective Hamiltonians derived by contact transformation method [74] can be found in [75]. Fig. 4.15 presents the difference of the retrieved line positions through spectral simulation compared to the calculated, HITRAN2012 [11] and GEISA2015 [63] results as a function of $|m|$ and the difference was calculated just by subtracting our retrieved position from

those values (e.g. retrieved-HITRAN2012). The average difference in line position of the present study with calculated, HITRAN2012 and GEISA2015 database are 0.000530, 0.00217 and 0.00081 cm^{-1}, respectively and the overall agreement in position is in the order of magnitude 10^{-3} cm^{-1}.

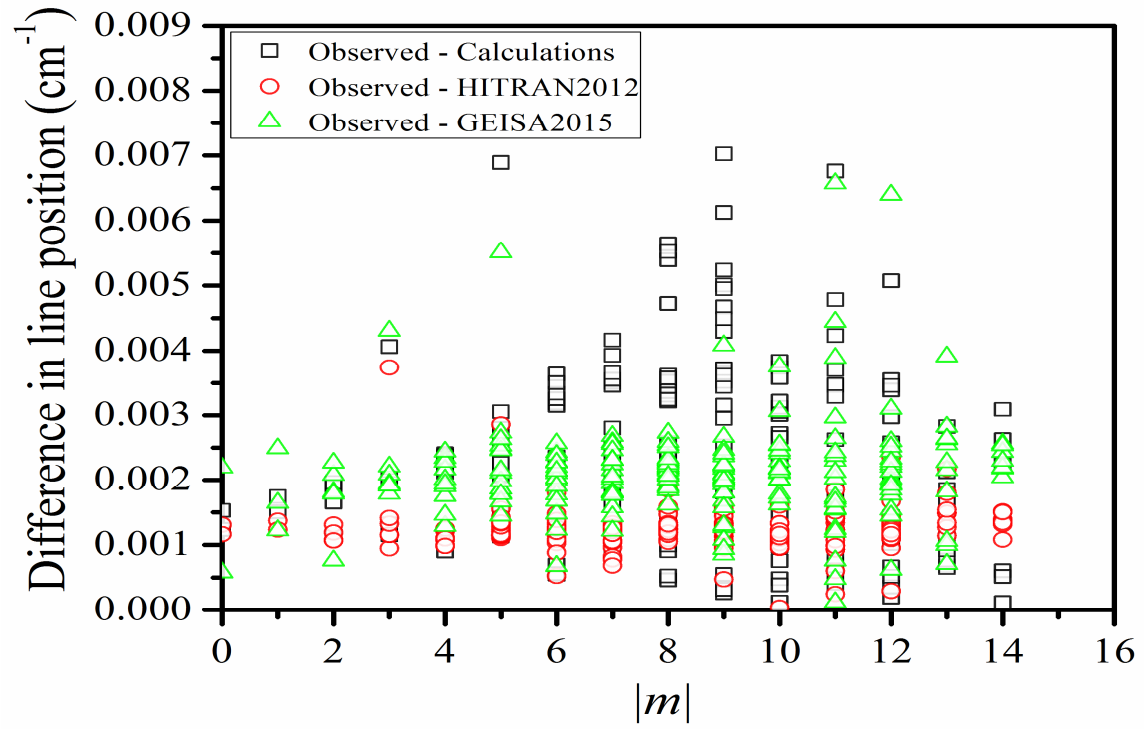

Fig 4.15: Comparison in line positions of methane $\nu_1 + \nu_4$ band as a function of |m|.

The percentage differences in line intensities compared to calculated, HITRAN2012 and GEISA2015 are illustrated in Fig. 4.16 as a funtion of $|m|$. The comparison in intensities provides a fair agreement with both calculated and spectroscopic database entries. From Fig. 4.16, it can be seen that the percentage differences in intensities are less than 15% in all three cases and the observed intensities are more comparable with GEISA2015 database entries.

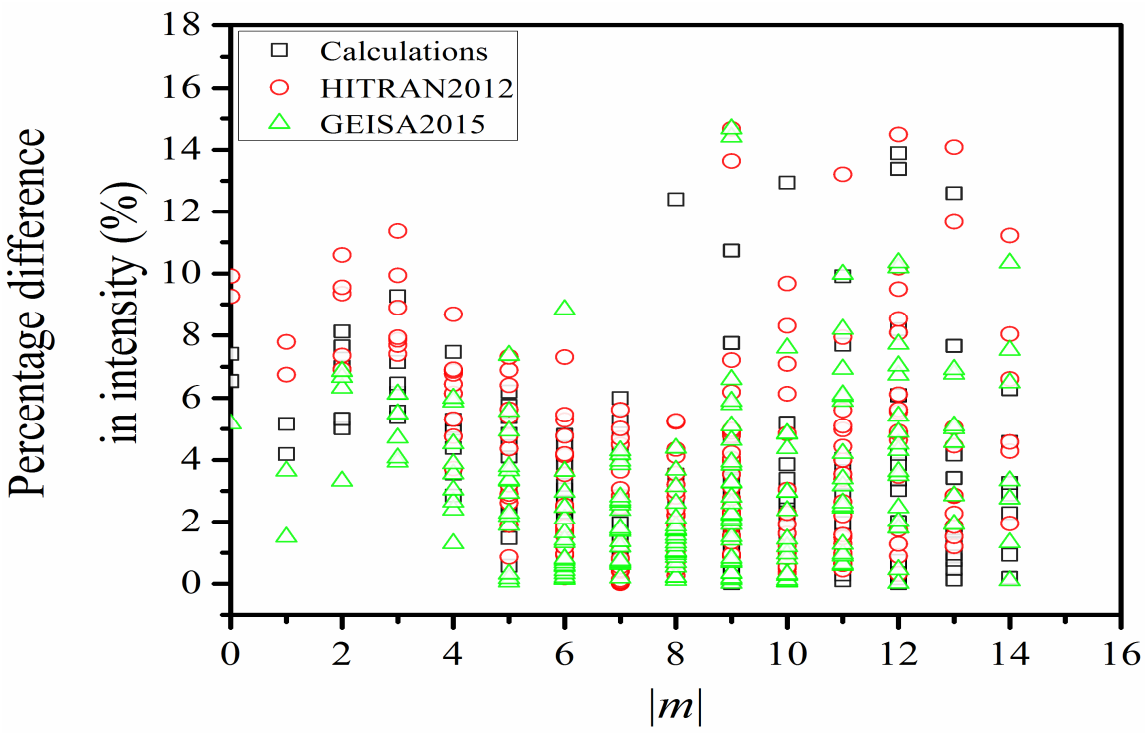

Fig 4.16: Comparison in line intensities of methane $\nu_1 + \nu_4$ band with calculated, HITRAN2012 and GEISA2015 entries as a function of |m|.

Table 4.5: Sample data for comparing observed position with calculated, HITRAN2012 and GEISA2015 results.

Transition		Position (cm^{-1})			
I*m*I	*J'C'n'*←*J''C''n''*	Observed	Calculated	HITRAN	GEISA
2	1E 6←2E 1	4207.48727 (1)	4207.485	4207.486	4207.486
2	$2F_1$ 14←$2F_2$ 1	4218.33559 (2)	4218.334	4218.335	4218.076
3	$2A_1$ 6←$3A_2$ 1	4200.82101 (2)	4200.819	4200.819	4200.819
4	$3F_2$ 21←$4F_1$ 1	4195.97055 (1)	4195.968	4195.969	4195.969
4	$3A_2$ 8←$4A_1$ 1	4196.39505 (1)	4196.393	4196.393	4196.394
5	4E 19←5E 1	4188.64944 (1)	4188.647	4188.647	4188.648
5	$4F_1$ 29←$5F_1$ 1	4190.45691 (1)	4190.455	4190.456	4190.456
6	$5A_2$ 12←$6A_1$ 1	4181.35520 (1)	4181.353	4181.353	4181.354
6	$5F_1$ 34←$6F_2$ 2	4182.33700 (1)	4182.335	4182.334	4182.336
7	6 F_1 39←$7F_2$ 2	4175.67469 (1)	4175.672	4175.673	4175.672
7	$7F_2$ 41←$7F_1$ 1	4212.67806 (1)	4212.674	4212.676	4212.677
8	$7F_1$ 47←$8F_2$ 2	4167.15765 (1)	4167.156	4167.155	4167.156
8	8E 30←8E 1	4210.05412 (7)	4210.052	4210.052	4210.052
8	$8A_2$ 15←$8A_1$ 1	4210.63473 (1)	4210.631	4210.632	4210.633
9	$9F_1$ 45←$8F_2$ 2	4261.67572 (3)	4261.680	4261.673	4261.674
9	$9A_2$ 17←$8A_1$ 1	4264.81856 (1)	4264.816	4264.816	4264.817
10	$10F_1$ 47←$9F_2$ 2	4266.60628 (2)	4266.605	4266.604	4266.605
10	10E 32←9E 1	4267.55016 (5)	4267.551	4267.548	4267.550
11	$11A_2$ 18←$10A_1$ 1	4271.57012 (7)	4271.569	4271.569	4271.569
11	$11A_1$ 17←$10A_2$ 1	4273.53677 (10)	4273.535	4273.535	4273.518
12	12E 38←11E 2	4275.13837 (9)	4275.136	4275.136	4275.137
12	$12F_2$ 58←$11F_1$ 1	4278.24434(7)	4278.244	4278.242	4278.243
13	$13F_1$ 63←$12F_2$ 1	4281.09334(6)	4281.092	4281.092	4272.092
13	$13A_2$ 22←$12A_1$ 1	4282.77640(6)	4282.777	4282.775	4272.775

Table 4.6: Sample data for comparing observed position with calculated, HITRAN2012 and GEISA2015 results.

	Transition	Intensity(cm/mol)			
l*m*l	$J'C'n' \leftarrow J''C''n''$	Observed	Calculated	HITRAN	GEISA
2	1E 6←2E 1	7.924 (1) x10^{-21}	8.270x10^{-22}	8.497x10^{-22}	8.223x10^{-22}
2	$2F_1$ 14←$2F_2$ 1	1.907 (5) x10^{-21}	2.050x10^{-22}	1.108x10^{-21}	1.466x10^{-21}
3	$2A_1$ 6←$3A_2$ 1	2.706 (5) x10^{-21}	2.930x10^{-21}	2.985x10^{-21}	2.905x10^{-21}
4	$3F_2$ 21←$4F_1$ 1	1.908 (3) x10^{-21}	2.040x10^{-21}	2.071x10^{-21}	1.989x10^{-21}
4	$3A_2$ 8←$4A_1$ 1	3.200 (2) x10^{-21}	3.410x10^{-21}	3.476x10^{-21}	3.358x10^{-21}
5	4E 19←5E 1	1.292 (1) x10^{-21}	1.330x10^{-21}	1.342x10^{-21}	1.310x10^{-21}
5	$4F_1$ 29←$5F_1$ 1	1.968 (2) x10^{-21}	2.050x10^{-21}	2.078x10^{-21}	2.029x10^{-21}
6	$5A_2$ 12←$6A_1$ 1	2.868 (2) x10^{-21}	3.000x10^{-21}	2.999x10^{-21}	2.935x10^{-21}
6	$5F_1$ 34←$6F_2$ 2	1.763 (1) x10^{-21}	1.810x10^{-21}	1.814x10^{-21}	1.762x10^{-21}
7	$7F_2$ 41←$7F_1$ 1	1.521 (2) x10^{-21}	1.560x10^{-21}	1.540x10^{-21}	1.562x10^{-21}
7	6 F_1 39←$7F_2$ 2	1.495 (1) x10^{-21}	1.530x10^{-21}	1.523x10^{-21}	1.516x10^{-21}
8	$7F_1$ 47←$8F_2$ 2	1.206 (1) x10^{-21}	1.230x10^{-21}	1.207x10^{-21}	1.192x10^{-21}
8	8E 30←8E 1	2.541 (2) x10^{-22}	2.530x10^{-22}	2.415x10^{-22}	2.511x10^{-22}
8	$8A_2$ 15←$8A_1$ 1	1.872 (2) x10^{-21}	1.910x10^{-21}	1.853x10^{-21}	1.891x10^{-21}
9	$9F_1$ 45←$8F_2$ 2	1.146 (3) x10^{-21}	1.190x10^{-21}	1.135x10^{-21}	1.162x10^{-21}
9	$9A_2$ 17←$8A_1$ 1	1.953 (3) x10^{-21}	2.050x10^{-21}	2.033x10^{-21}	2.019x10^{-21}
10	$10F_1$ 47←$9F_2$ 2	1.004 (1) x10^{-21}	9.79x10^{-22}	9.266x10^{-22}	9.573x10^{-22}
10	10E 32←9E 1	5.537 (5) x10^{-22}	6.360x10^{-22}	6.130x10^{-22}	5.992x10^{-22}
11	$11A_2$ 18←$10A_1$ 1	1.047 (7) x10^{-21}	1.047x10^{-21}	9.972x10^{-22}	1.057x10^{-21}
11	$11A_1$ 17←$10A_2$ 1	9.410 (9) x10^{-22}	9.420x10^{-22}	9.561x10^{-22}	8.556x10^{-22}
12	12E 38←11E 2	2.716 (2) x10^{-22}	2.560x10^{-22}	2.372x10^{-22}	2.461x10^{-22}
12	$12F_2$ 58←$11F_1$ 1	3.730 (2) x10^{-22}	3.720x10^{-22}	3.683x10^{-22}	3.556x10^{-22}
13	$13F_1$ 63←$12F_2$ 1	2.170 (1) x10^{-22}	2.160x10^{-22}	2.066x10^{-22}	2.065x10^{-22}
13	$13A_2$ 22←$12A_1$ 1	3.672 (2) x10^{-22}	3.720x10^{-22}	3.683x10^{-22}	3.556x10^{-22}

CHAPTER 5: LINE-SHAPE STUDY OF METHANE BROADENED BY ITSELF AND HYDROGEN

5.1 Introduction

In this study, a total of 18 spectra were analyzed due to the self- and H_2-broadening of methane, which were recorded at various temperatures (148.4 – 298.4 K) and pressures (0.12 – 385 Torr). A total of 198 transitions were analyzed with respect to self- and H_2-broadening of methane in the spectral range of 4100-4300 cm^{-1}. The multi-spectrum fitting program 'Labfit' was used to determine the self- and H_2-broadened half-width coefficients, pressure-induced shift coefficients along with temperature dependences, speed–dependence parameters of line broadening and the line-mixing coefficients. The same fitting procedures are used here as described in section 4.1 of methane-air project in the previous chapter.

The number of transitions that were used to obtain line parameters are listed in Table 5.1. The detail list of retrieved line parameters can be found in Appendix C and D. The parameters for few transitions are not reported in the thesis, they were not possible to be determined correctly due to very weak transitions and/or overlap with neighboring transitions. The absorption lines of water vapor were used as calibration standards in the recording of methane broadened by itself and H_2.

Table 5.1: Number of retrieved line parameters due to self- and H_2 broadening of methane.

Self/Air	Position	Intensity	Lorentz width	Pressure shift	n^a	$\delta'^{,b}$	ORME^c	S^d
Self	198	198	198	181	176	169	80	110
H_2			198	187	129	79	60	

n^a stands for temperature-dependence of broadening, $\delta'^{,b}$ is used for temperature dependency in pressure-induced shift coefficient, ORME^c represents for off-diagonal relaxation matrix elements and S^d is used for speed-dependence parameters.

The residuals of multi-spectrum fits of methane broadened by itself and H_2 in the spectral range 4180-4190 cm^{-1} using three fitting models (Voigt, Speed dependent Voigt and speed dependent Voigt with line mixing) are shown in Fig. 5.1.

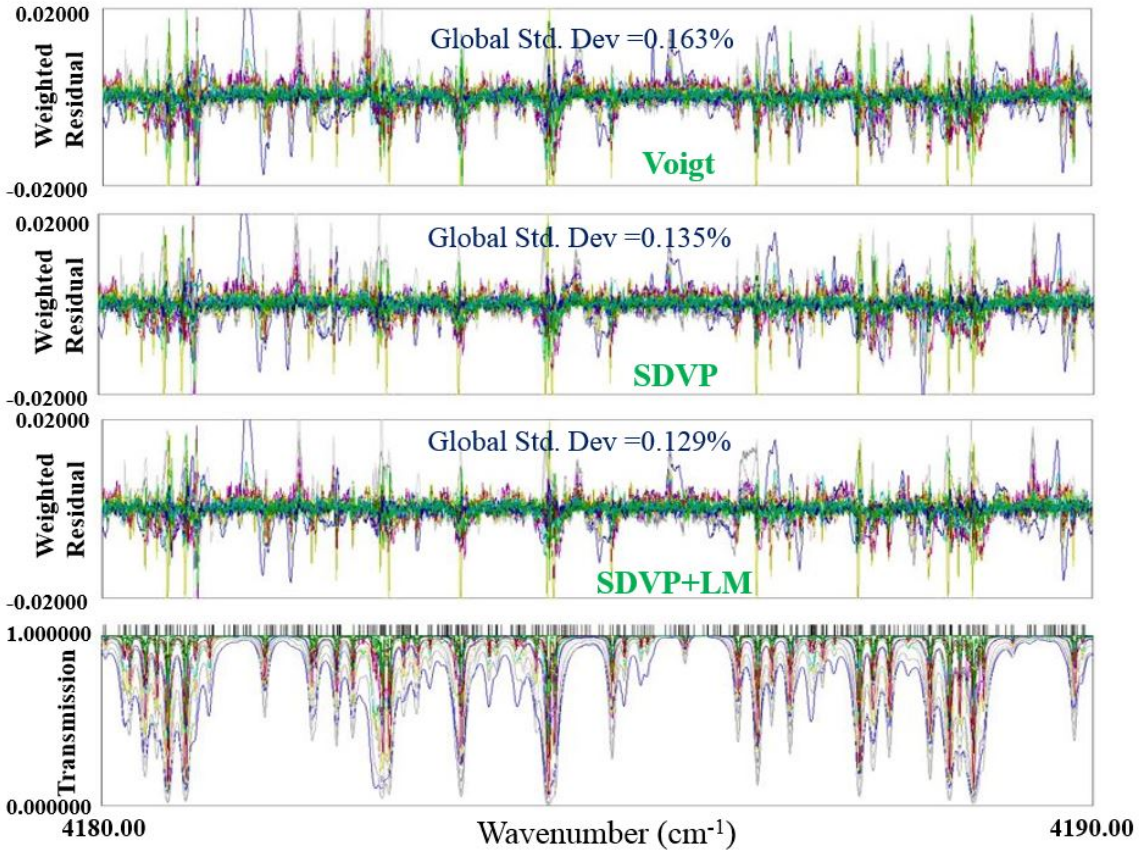

Fig 5.1: Residuals of multi-spectrum fitting of methane broadened by itself and hydrogen spectra in the $\nu_1 + \nu_4$ band.

5.2 Self- and H_2-broadened half-width coefficients and temperature dependences

The self- and H_2-broadened half-width coefficients along with their temperature dependences of methane in the $\nu_1 + \nu_4$ band are determined on a line-by-line basis using Eq. (4.1) and selected values are listed with their uncertainties in Table 5.2. The results are discussed with respect to the tetrahedral symmetry species (A_1, A_2, E, F_1 and F_2) of methane and as a function of the rotational quantum index $|m|$.

Table 5.2: Sample of retrieved self- and air- broadening parameters along with their temperature-dependence exponents obtained by multi-spectrum fitting using SDVP.

lml	Lower State $(J''C''n'')$	Upper State $(J'C'n')$	Position[a] (cm^{-1})	Intensity[a] (cm^{-1}/mol)	Air-width[a] $(cm^{-1}atm^{-1})$	Self-width[a] $(cm^{-1}atm^{-1})$	$(n_1)^{a,b}$	$(n_2)^{a,b}$
1	$1F_1$ 1	$1F_2$ 9	4218.416115(1)	$1.317(1)x10^{-21}$	0.0654(4)	0.0762(6)	0.48(1)	0.95(2)
2	$1F_1$ 1	$2F_2$ 15	4229.195067(1)	$2.204(2)x10^{-21}$	0.0651(2)	0.0790(2)	0.50(1)	0.81(1)
2	2E 1	1E 6	4207.487244(1)	$8.053(1)x10^{-22}$	0.0658(4)	0.0818(4)	0.47(1)	0.81(1)
2	2E 1	2E 11	4218.07734(1)	$1.121(4)x10^{-21}$	0.0697(4)	0.0887(5)	0.32(1)	0.67(1)
3	$2F_2$ 1	$3F_1$ 21	4234.35149(1)	$2.728(4)x10^{-21}$	0.0711(4)	0.0790(5)	0.45(1)	0.89(1)
3	$3A_21$	$2A_1$ 6	4200.821017(1)	$2.828(3)x10^{-21}$	0.0651(3)	0.0779(3)	0.53(1)	0.83(1)
3	$3F_21$	$2F_1$ 15	4201.400550(1)	$1.708(2)x10^{-21}$	0.0668(2)	0.0812(2)	0.48(1)	0.86(1)
4	3 F_21	4 F_1 25	4239.428865(1)	$3.052(4)x10^{-21}$	0.0687(3)	0.0820(3)	0.49(1)	0.84(1)
4	4E 1	3E 14	4195.649714(1)	$1.316(1)x10^{-21}$	0.0564(1)	0.0749(2)	0.46(1)	0.79(1)
4	$4A_1$ 1	$4A_2$ 9	4216.474061(1)	$4.043(5)x10^{-21}$	0.0669(2)	0.0812(2)	0.48(1)	0.82(1)
5	5E 1	4E 19	4188.649414(1)	$1.304(1)x10^{-21}$	0.0630(1)	0.0749(2)	0.86(1)	0.86(1)
5	4E 1	5E 20	4244.437574(1)	$1.922(2)x10^{-21}$	0.0579(2)	0.0730(2)	0.50(1)	0.82(1)
6	$6F_2$ 1	$5F_1$ 35	4184.387552(1)	$1.838(1)x10^{-21}$	0.0618(2)	0.0798(2)	0.56(1)	0.80(1)
7	$6F_2$ 2	$7F_1$ 38	4253.768243(1)	$2.291(2)x10^{-21}$	0.0649(3)	0.0797(4)	0.54(1)	0.79(1)
7	6E 1	7E 25	4254.638687(1)	$1.544(2)x10^{-21}$	0.0597(4)	0.0726(6)	0.55(1)	0.73(2)
7	$7F_2$ 1	$7F_1$ 43	4212.990834(1)	$1.521(3)x10^{-21}$	0.0636(5)	0.0799(5)	0.68(2)	0.77(2)
7	$7A_2$ 1	$7A_1$ 15	4216.675194(1)	$2.603(2)x10^{-21}$	0.0632(5)	0.0763(3)	0.54(1)	0.85(1)
8	$7A_2$ 1	$8A_1$ 15	4258.695654(1)	$2.975(3)x10^{-21}$	0.0623(2)	0.0735(2)	0.51(1)	0.84(1)
8	7E 1	8E 29	4258.941223(1)	$7.780(1)x10^{-22}$	0.0496(3)	0.0638(3)	0.45(2)	0.76(1)
8	$8A_1$ 1	$8A_2$ 15	4210.634690(1)	$1.875(1)x10^{-21}$	0.0587(2)	0.0718(2)	0.53(1)	0.80(1)
8	8E 1	8E 31	4211.351872(2)	$5.010(1)x10^{-22}$	0.0627(7)	0.0762(6)	0.49(3)	0.81(1)
8	$8F_2$ 1	$8F_1$ 46	4215.381817(1)	$1.009(1)x10^{-21}$	0.0613(3)	0.0757(3)	0.55(2)	0.82(1)
9	$9A_21$	$8A_1$ 18	4159.053776(1)	$1.619(2)x10^{-21}$	0.0598(1)	0.0736(2)	0.44(1)	0.81(1)
9	$9F_1$ 1	$8F_2$ 52	4160.036111(1)	$9.897(1)x10^{-22}$	0.060(1)	0.0762(2)	0.54(1)	0.80(1)
9	$9F_11$	$9F_2$ 50	4208.447501(2)	$7.510(1)x10^{-22}$	0.0575(4)	0.0699(3)	0.57(2)	0.83(1)
9	9E 1	9E 35	4214.451581(1)	$5.151(1)x10^{-22}$	0.0603(7)	0.0722(8)	0.65(4)	0.79(3)
10	$10A_11$	$9A_2$ 21	4252.613689(1)	$1.578(3)x10^{-21}$	0.0631(2)	0.0754(2)	0.43(1)	0.76(1)
10	10E 2	10E 38	4217.773981(3)	$3.302(1)x10^{-22}$	0.0459(6)	0.0602(6)	0.47(4)	0.65(2)
11	$10F_1$ 2	$11F_2$ 52	4272.010898(3)	$5.473(3)x10^{-22}$	0.0670(8)	0.0807(7)	0.65(3)	0.76(1)
11	$11A_2$ 1	$11A_1$ 21	4211.256385(2)	$4.845(1)x10^{-22}$	0.0574(5)	0.0685(4)	0.57(3)	0.71(1)
12	11E 2	12E 38	4275.138151(4)	$1.719(1)x10^{-22}$	0.0437(5)	0.0557(4)	0.44(4)	0.67(2)
13	$12F_1$ 3	$13F_2$ 60	4279.255197(6)	$2.458(1)x10^{-22}$	0.0634(9)	0.0772(7)	0.52(5)	0.88(2)
13	$12A_1$ 2	$13A_2$ 21	4279.171847(4)	$3.830(1)x10^{-22}$	0.0574(6)	0.0702(4)		0.80(2)

[a]Statistical uncertainties are given in parentheses.
[b]n_1 and n_2 are temperature-dependence exponents of air- and self-broadened half-width coefficients, respectively.

Figs. 5.2(a,b) show the variation in H_2-broadening and self-broadening Lorentz half-width coefficients as a function of $|m|$ corresponding to rotational symmetry species types (*A, E, F*) of methane. As shown in Fig. 5.2(a), H_2-broadened half-width coefficients vary from 0.0422(18) to 0.0718(5) $cm^{-1}atm^{-1}$, whereas self-broadened half-width coefficients range from 0.0548(2) to 0.0887(5) $cm^{-1}atm^{-1}$ as displayed in Fig. 5.2(b), both measured at 296 K for $|m|$ values up to 14. The range of my measured H_2-broadened half-width coefficients are close to the previously obtained H_2-broadened values (0.0479-0.0878 $cm^{-1}atm^{-1}$) in the ν_4 fundamental band study of methane [37] at temperatures ranging from 161-295 K. The half-width coefficients in this study follow the same trend of variation as found in the air-broadened methane study described in chapter 4. The half-width coefficients due to self- and H_2-broadening show higher values for *F* symmetric transitions compared to those of the species *A*, *E* , which is same as the finding of the air-broadening analysis (see Figs. 4.2a, 4.3a in chapter 4). In most cases, the half-width coefficients show the usual trend of variation with giving lower values for *E*-type transitions, which is similar to previous CH_4-H_2 ν_4 band studies [37, 38] and (ν_2, ν_4) band studies of methane [30].

The comparison between self- and H_2-broadened half-width coefficients is shown in Fig. 5.3. As shown in Fig. 5.3, it is clearly seen that the values of self-broadening half-width coefficients are larger compared to the H_2-broadening widths.

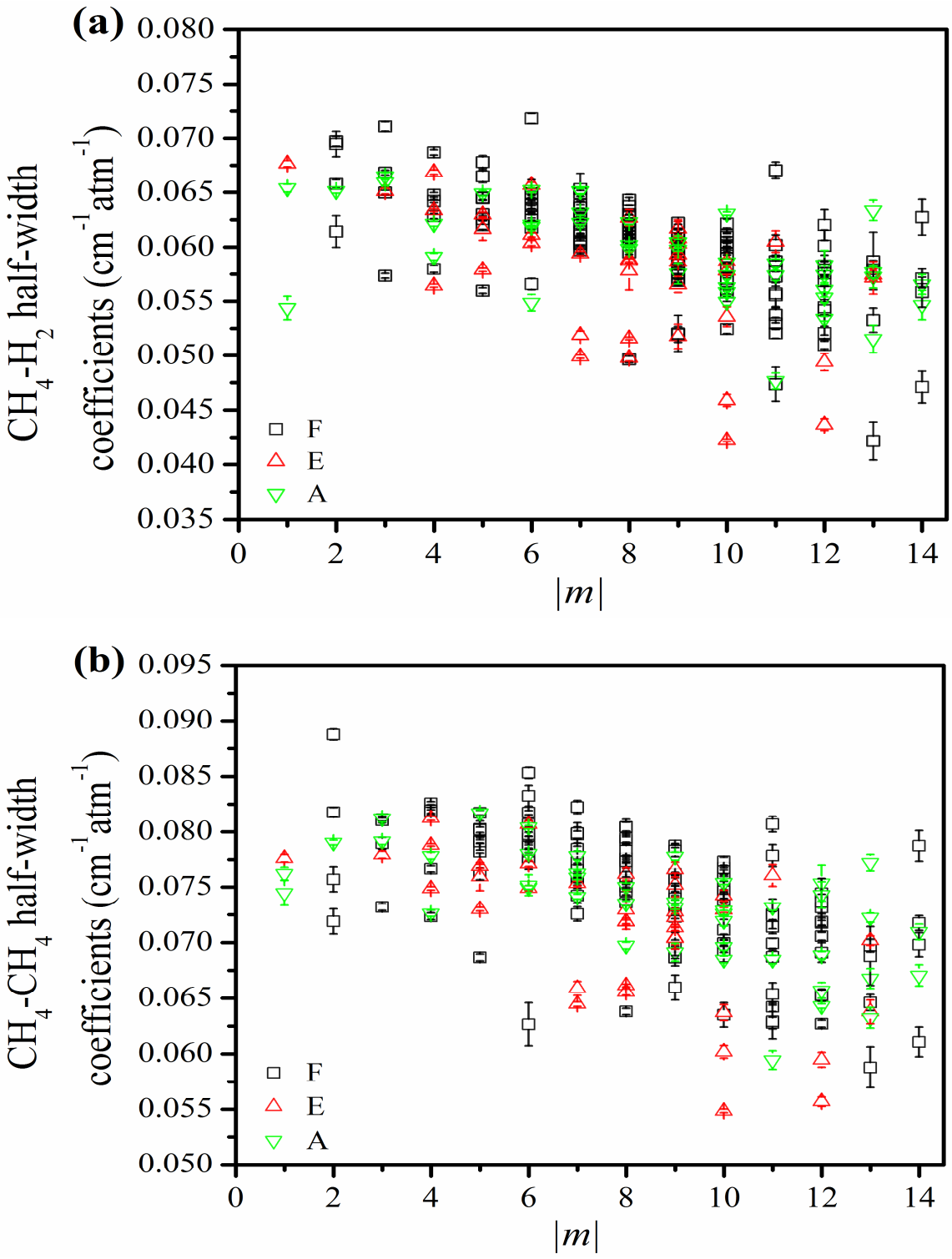

Fig 5.2: Variation of (a) CH_4-H_2 and (b) CH_4-CH_4 half-width coefficients corresponding to A, E and F transitions in the $\nu_1 + \nu_4$ band of methane. The error bars which cannot be seen, are smaller than the size of the symbols used.

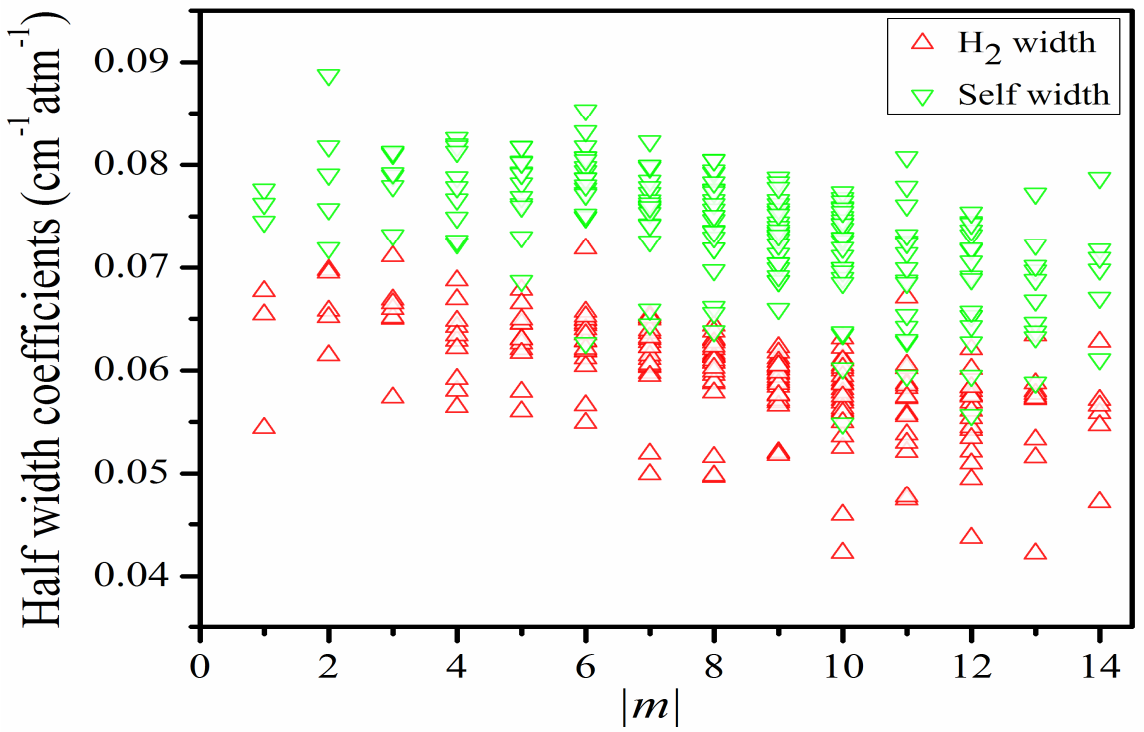

Fig 5.3: Comparison of CH_4-H_2 and CH_4-CH_4 half-width coefficients corresponding to A, E and F transitions in the $\nu_1 + \nu_4$ band of methane.

The temperature-dependence exponents n_1 due to H_2-broadening and n_2 due to self-broadening of methane are plotted as a function of $|m|$ in Fig. 5.4(a,b). As mentioned in Table 5.1, the number of n_1 measurements due to self-broadening (176) were higher than n_2 measurements due to H_2-broadening (129) and both of them show relatively high measurement uncertainties at higher $|m|$ values possibly due to weaker transitions. As shown in Fig. 5.4(a,b), the values of n_1 vary between 0.32(1) and 0.68(2) and n_2 ranges from 0.64(3) to 1.06(2). Varshani and Chudamani [37] published their temperature-dependence of H_2-broadened half-width coefficients (0.35-0.52) which are close to the present results (0.32-0.68). Though a pattern of variation is observed in the retrieval of n_1 values, which provide lower values due to *E*-symmetry transitions with some exceptions up to $|m|$=10, but no clear pattern of variation is observed in the values of n_2.

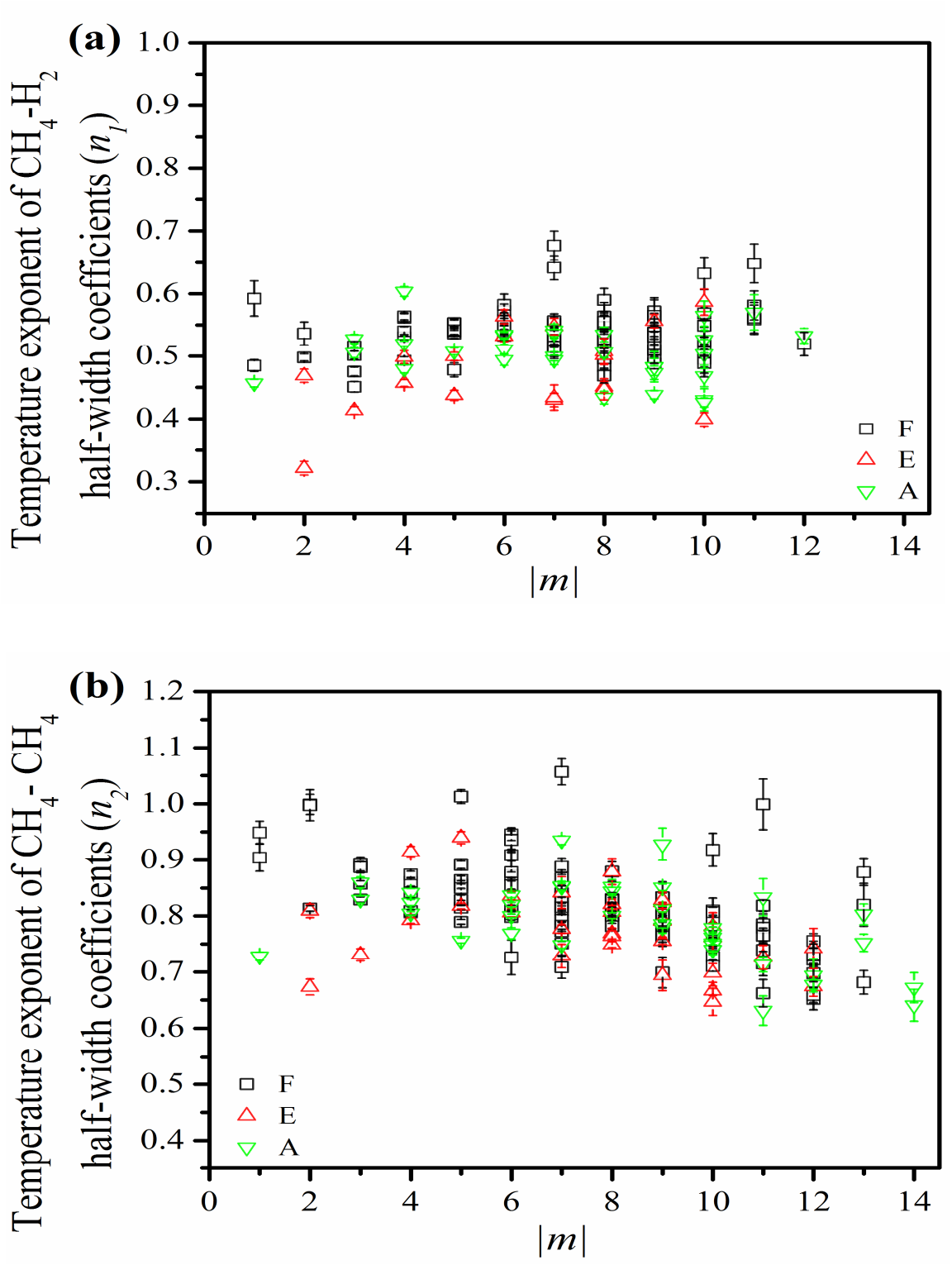

Fig 5.4: Variation in temperature-dependence exponents of (a) CH_4-H_2 and (b) CH_4-CH_4 half-width coefficients corresponding to A, E and F transitions in the $\nu_1 + \nu_4$ band of methane. The error bars which cannot be seen, are smaller than the size of the symbols used.

Fig. 5.5 compares the temperature-exponent values of n_1 and n_2 as a function of $|m|$, which show clearly the larger values due to self-broadening up to $|m| = 10$ and after that it gives some exceptions. Though the temperature dependences on H_2-broadening shows values up to $|m| = 13$, but the in case of self-broadening values up to $|m| = 14$ could be obtained.

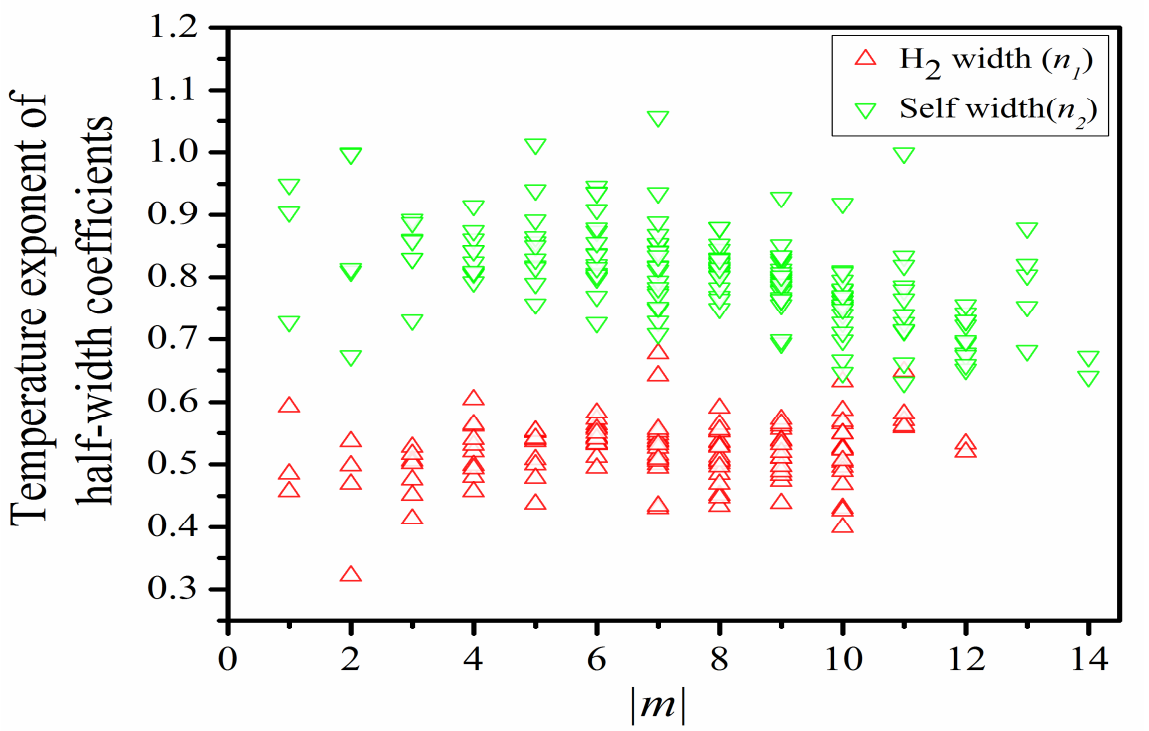

Fig 5.5: Comparison between temperature exponents of CH_4-H_2 and CH_4-CH_4 half-width coefficients corresponding to A, E and F transitions in the $\nu_1 + \nu_4$ band of methane.

5.3 H_2- and self-shift coefficients along with temperature dependences

The pressure-induced self- and H_2-shift coefficients and their temperature dependences of methane in the $\nu_1 + \nu_4$ band were determined using Eqs. (4.2-4.3) as a function of $|m|$. The measured values are tabulated in Table 5.3.

Table 5.3: Selection of retrieved self- and H_2-induced shift parameters along with their temperature-dependence exponents and speed dependence parameters.

lml	Lower state $(J''C''n'')$	Upper state $(J'C'n')$	Air-shift[a] $(cm^{-1}atm^{-1})$	Self-shift[a] $(cm^{-1}atm^{-1})$	TD[b] Air-shift[a] $(cm^{-1}atm^{-1}K^{-1})$	TD[b] Self-shift[a] $(cm^{-1}atm^{-1}K^{-1})$	S[c]
1	$1F_1$ 1	$1F_2$ 9	-0.0099(3)	-0.0104(5)	0.000045(3)	0.000129(7)	0.05(1)
2	$1F_1$ 1	$2F_2$ 15	-0.0099(2)	-0.0091(3)	0.000016(2)	0.000088(3)	0.05(1)
2	2E 1	1E 6	-0.0101(4)	-0.0098(4)	0.000034(4)	0.000118(5)	0.06(1)
2	2E 1	2E 11	-0.0102(3)		0.000045(3)	0.000228(10)	0.08(1)
3	$2F_2$ 1	$3F_1$ 21	-0.0059(3)		0.000031(2)	0.000142(7)	0.16(1)
3	$3A_2$ 1	$2A_1$ 6	-0.0113(3)	-0.0080(4)	0.000038(2)	0.000137(4)	0.07(1)
3	$3F_2$ 1	$2F_1$ 15	-0.0083(3)	-0.0102(2)	0.000038(3)	0.000065(2)	0.04(1)
4	$4A_1$ 1	$4A_2$ 9	-0.0089(2)	-0.0096(3)	0.000029(2)	-0.000061(4)	0.05(1)
5	4E 1	5E 20	-0.0089(2)	-0.0119(3)	0.000018(2)	0.000068(4)	0.09(1)
7	$6F_2$ 2	$7F_1$ 38	-0.0125(2)	-0.0118(3)	0.000055(2)	0.000146(4)	0.06(1)
7	6E 1	7E 25	-0.0096(4)	-0.0132(5)	0.000030(4)	0.000078(6)	0.06(1)
7	$7F_2$ 1	$7F_1$ 43	-0.0077(4)	-0.0151(6)			0.07(1)
7	$7A_2$ 1	$7A_1$ 15	-0.0104(2)	-0.0103(3)	0.000038(2)	0.000102(3)	0.05(1)
8	$7A_2$ 1	$8A_1$ 15	-0.0084(2)	-0.0102(3)	0.000024(2)	0.000080(3)	0.05(1)
8	8E 1	8E 31	-0.0091(6)	-0.0117(5)		0.000090(4)	0.07(1)
8	$8F_2$ 1	$8F_1$ 46	-0.0074(3)	-0.0090(3)		0.000092(3)	0.07(1)
9	$9F_1$1	$9F_2$ 50	-0.00930(3)	0.0115(2)		0.000090(3)	0.09(1)
9	9E 1	9E 35	-0.0093(6)	-0.0100(8)		0.000091(11)	0.10(1)
10	$9F_1$ 3	$10F_2$ 48	-0.0143(3)	-0.0160(3)	0.000044(5)	0.000127(1)	
10	$9A_1$1	$10A_2$ 16	-0.0112(2)	-0.0146(2)	0.000032(4)	0.000084(2)	
11	$10F_1$ 2	$11F_2$ 51	-0.0124(3)	-0.0155(3)		0.000069(3)	0.07(1)
11	$10A_1$ 1	$11A_2$ 18	-0.0092(6)	-0.0108(7)		0.000083(9)	0.11(1)
12	11E 1	12E 39	-0.0098(7)	-0.0146(6)		0.000095(10)	0.13(2)
12	$11F_1$ 1	$12F_2$ 58	-0.0082(5)	-0.0136(4)		0.000061(6)	0.15(1)

[a]Statistical uncertainty, TD[b] is used as temperature-dependence and S^c stands for speed dependence parameters which has no unit.

All measured self- and H_2-shift coefficients are found to be negative similar to previous studies [37-40]. No discernible patterns are observed in the variations of shift coefficients as a function of rotational symmetry species, which is similar to the previous studies [37, 38, 40]. As shown in Fig. 5.6a, the measured CH_4-H_2 shift coefficients vary

from -0.0164(7) to -0.0035(3) $cm^{-1}atm^{-1}$, while the self-shift coefficients range from -0.0233(10) to -0.0040 (3) $cm^{-1}atm^{-1}$ as shown in Fig. 5.6b. Chudamani and Varanasi [37] found their H_2-shift coefficients ranging from -0.0055 to 0.0005 $cm^{-1}atm^{-1}$ and Margolis [38] found his shift coefficient values ranging in between -0.01430 and 0.00009 $cm^{-1}atm^{-1}$. The retrieved pressure-shift coefficients in my present study are consistent with those studies in the sense that most of them are negative with few exceptions in their results. My retrieved shift coefficients values are different possibly due to the fact that the present study is carried out over a wide range of pressures and temperatures compared to the previous studies.

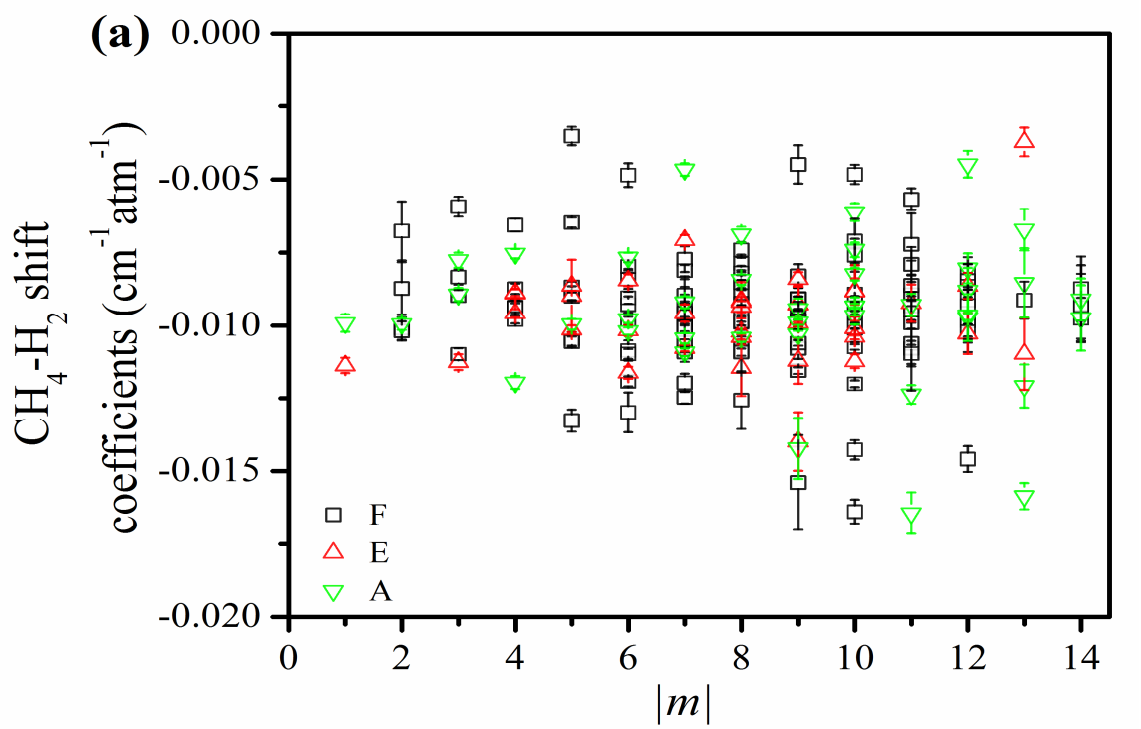

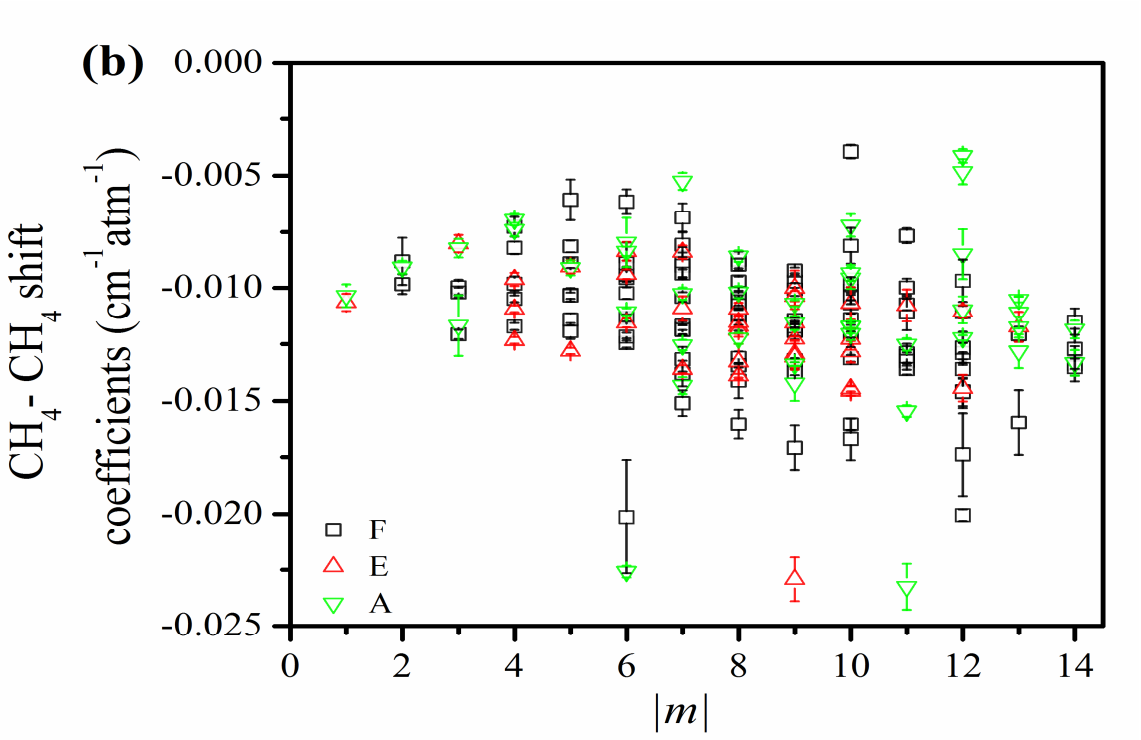

Fig 5.6: Variation of (a) CH_4-H_2 and (b) CH_4-CH_4 shift coefficients corresponding to A, E and F transitions as a function of |m| in the $\nu_1 + \nu_4$ band of methane. The error bars which cannot be seen, are smaller than the size of the symbols used.

Fig. 5.7 shows the comparison in shift values due to H_2- and self-shift coefficients of methane for the same transitions and the errors bar are not included in this comparison. From Fig. 5.7, it is seen that the measured self-shift coefficients are close to the H_2-shift coefficients with showing a slight higher values in H_2-shift. It is also seen that the shift coefficients due to both self- and H_2-shift show larger variations for $|m|$ values from 6 to 13.

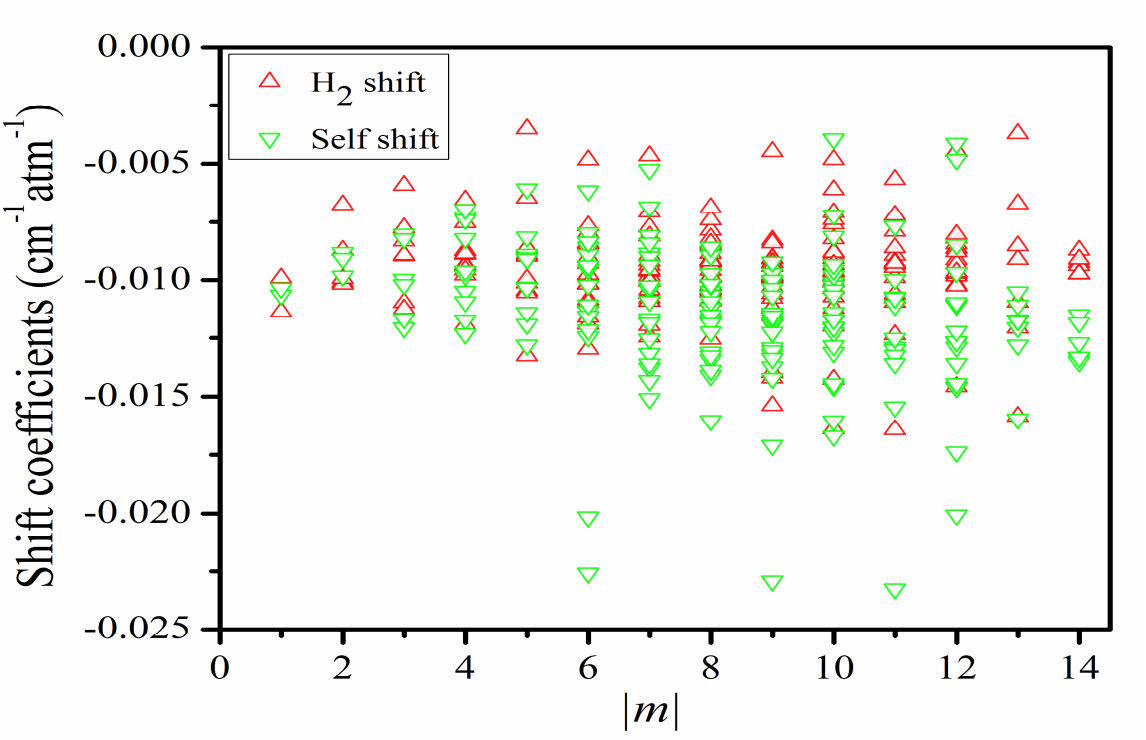

Fig 5.7: Comparison of CH_4-H_2 and CH_4-CH_4 shift coefficients corresponding to A, E and F transitions in the $\nu_1 + \nu_4$ band of methane.

A linear temperature dependence Eq. (4.3) was used to determine the temperature-dependence of H_2- and self-shift coefficients of methane. The measured temperature dependences of CH_4-CH_4 and CH_4-H_2 shift coefficients are plotted in Fig. 5.8(a) and 5.8(b), respectively as a function of $|m|$. As seen from both figures, similar to shift coefficients no systemic pattern of variations is observed in their temperature dependences with respect to (*A, E, F*) symmetry transitions. All temperature-dependence of shift coefficients are found to be positive. As shown in both figures, the temperature dependences of H_2-shift range from 0.000013(1) to 0.000075(5) $cm^{-1}atm^{-1}K^{-1}$ and those for self-shift parameters vary from 0.000033(3) to 0.000228(10) $cm^{-1}atm^{-1}K^{-1}$. No published results are available to compare the present study with.

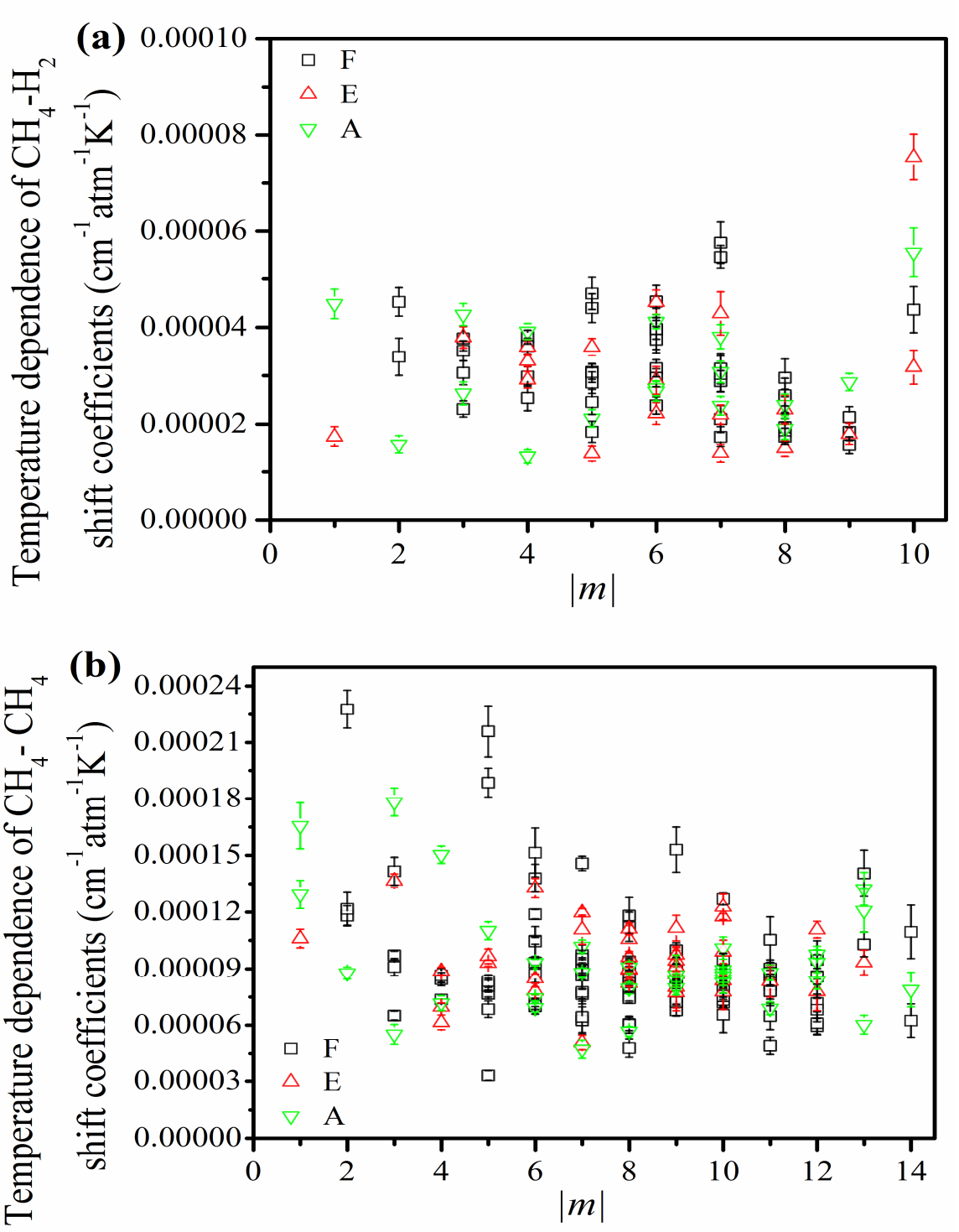

Fig 5.8: Variation in temperature-dependence of (a) CH_4-H_2 and (b) CH_4-CH_4 shift coefficients corresponding to A, E and F transitions as a function of |m| in the $\nu_1 + \nu_4$ band of methane. The error bars which cannot be seen, are smaller than the size of the symbols used.

The temperature dependences due to self- and H_2-shift coefficients are compared and they are shown in Fig. 5.9. From Fig. 5.9, it is seen that the temperature dependences of the H_2-shift show smaller values than self-shift. On the contrary, for methane-air project, the temperature dependences of CH_4-air were higher than those of self-shift, which may be due to the fact of H_2 being lighter than CH_4.

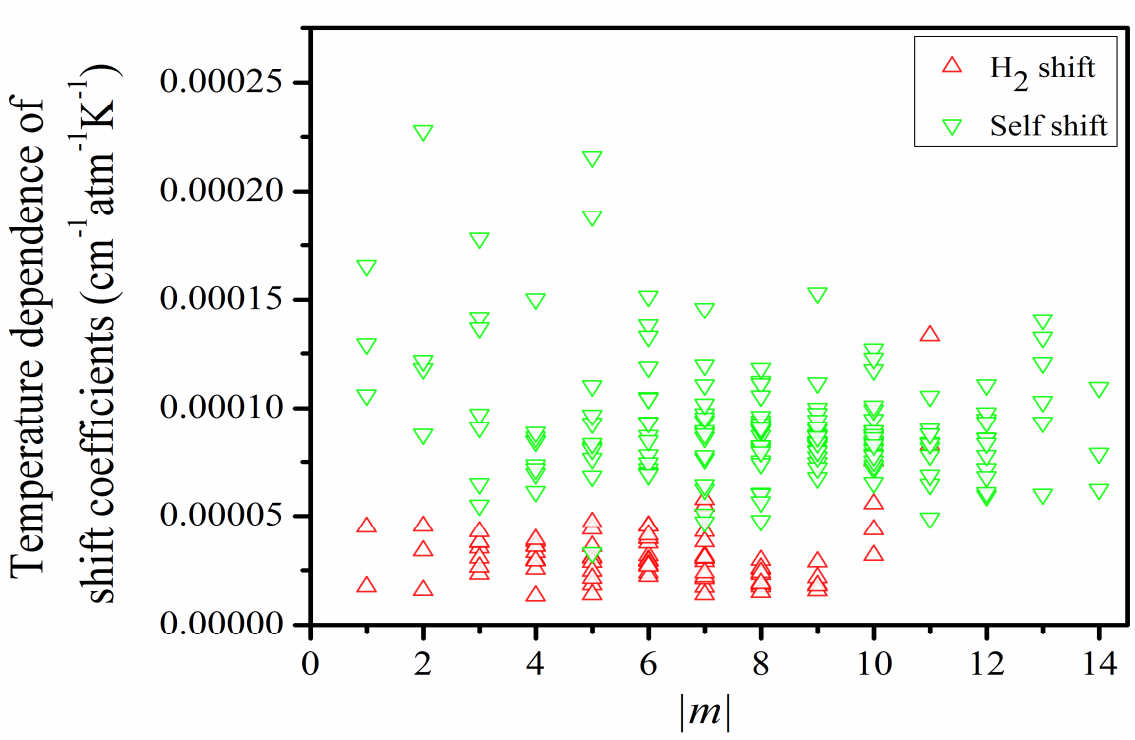

Fig 5.9: Comparison of temperature dependences of CH_4-H_2 and CH_4-CH_4 shift coefficients corresponding to A, E and F transitions in the $\nu_1 + \nu_4$ band of methane.

5.4 Speed-dependence analysis

The speed-dependence parameters are determined for the first time in the analysis of methane broadened by H_2. The speed dependence due to self- and H_2-broadening are presented for three rotational symmetry species (A, E, F) in the vibrational band $\nu_1 + \nu_4$ as function of $|m|$ in Fig. 5.10. The values are found to be positive varying from 0.02(1) to 0.16(1). No other experimental or theoretical speed dependence results are published in this band of methane broadened by H_2 to compare with. The speed-dependence parameters

are found to be dependent on the rotational quantum number and they show gradual increase with |m| values. The average value of the retrieved speed dependence parameters is lower than the calculated value performed by Kochanov [65]. Most of previous studies reported the value of these parameters ranging up to 0.17. More theoretical and laboratory studies are required in other bands of methane broadened by H_2 to comments on the vibrational dependency of these parameters.

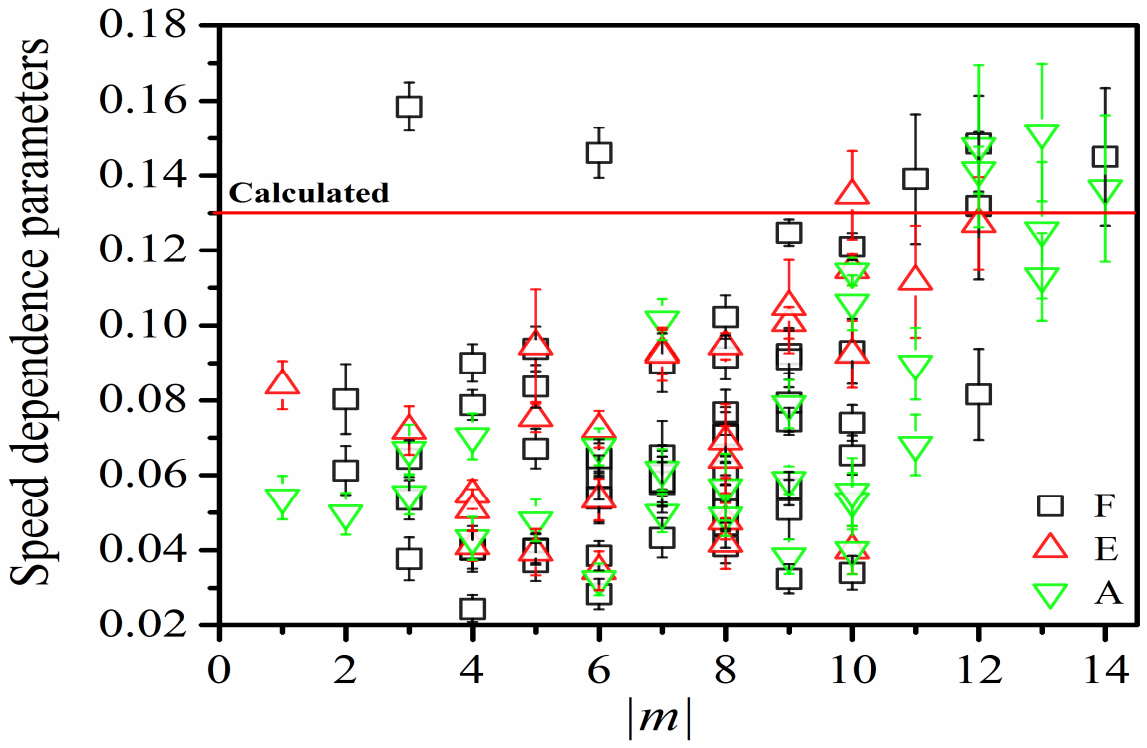

Fig 5.10: Variation in speed dependence parameters of methane broadened by H_2 in the $\nu_1 + \nu_4$ band as a function of |m|. The error bars which cannot be seen, are smaller than the size of the symbols used.

5.5 Off-diagonal relaxation matrix coefficients

The off-diagonal relaxation matrix element mechanism was used in the retrieval of line-mixing coefficients for 40 pairs of transitions due to self-broadening and 33 pairs of transitions for H_2-broadening. The results for line-mixing coefficients are listed in Table 5.4. The line-mixing parameters were determined through the off-diagonal relaxation

formalism by providing extra line-mixing pairs at the end of the input files in Labfit program. The possible transitions for line-mixing among tetrahedral symmetry species follow the rules: $A_1 \leftrightarrow A_2$, $F_1 \leftrightarrow F_2$ and $E \leftrightarrow E$. As seen in Fig. 5.11 (a,b), off-diagonal relaxation matrix coefficients for both H_2-broadening and self-broadening are found positive. The H_2-broadened line-mixing coefficients vary from 0.0106(3) to 0.0482(23) $cm^{-1}atm^{-1}$, while self-broadening line-mixing coefficients vary from 0.0014(3) to 0.0237(4) $cm^{-1}atm^{-1}$.

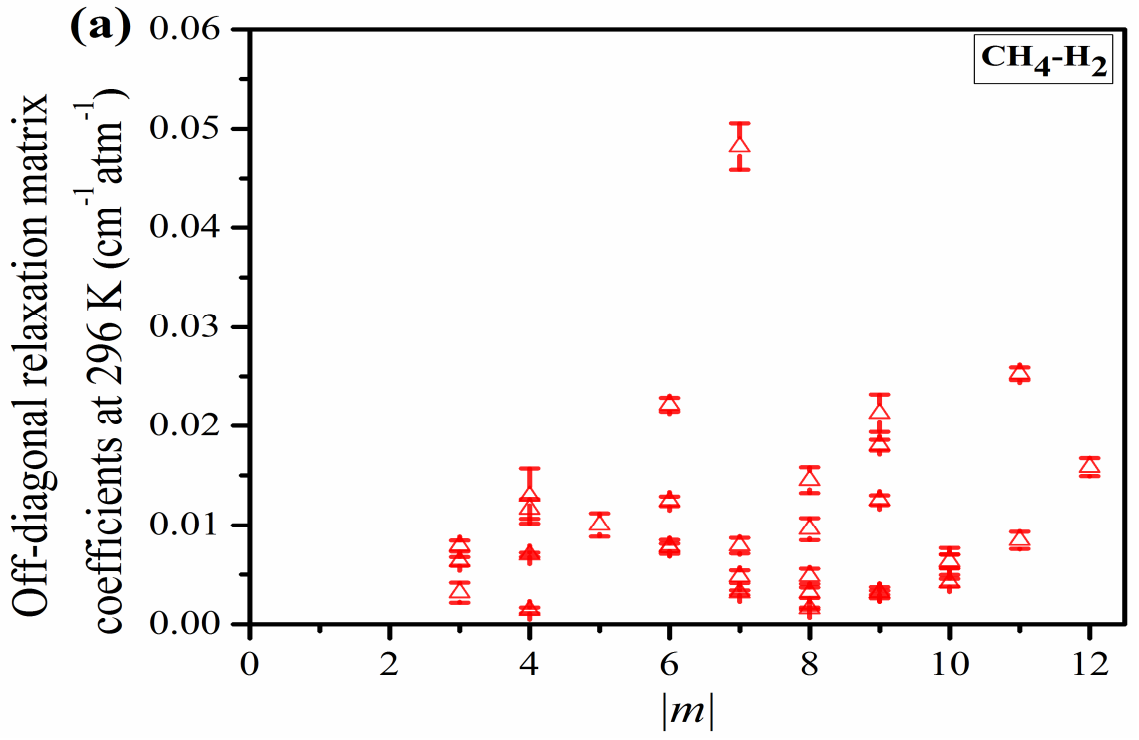

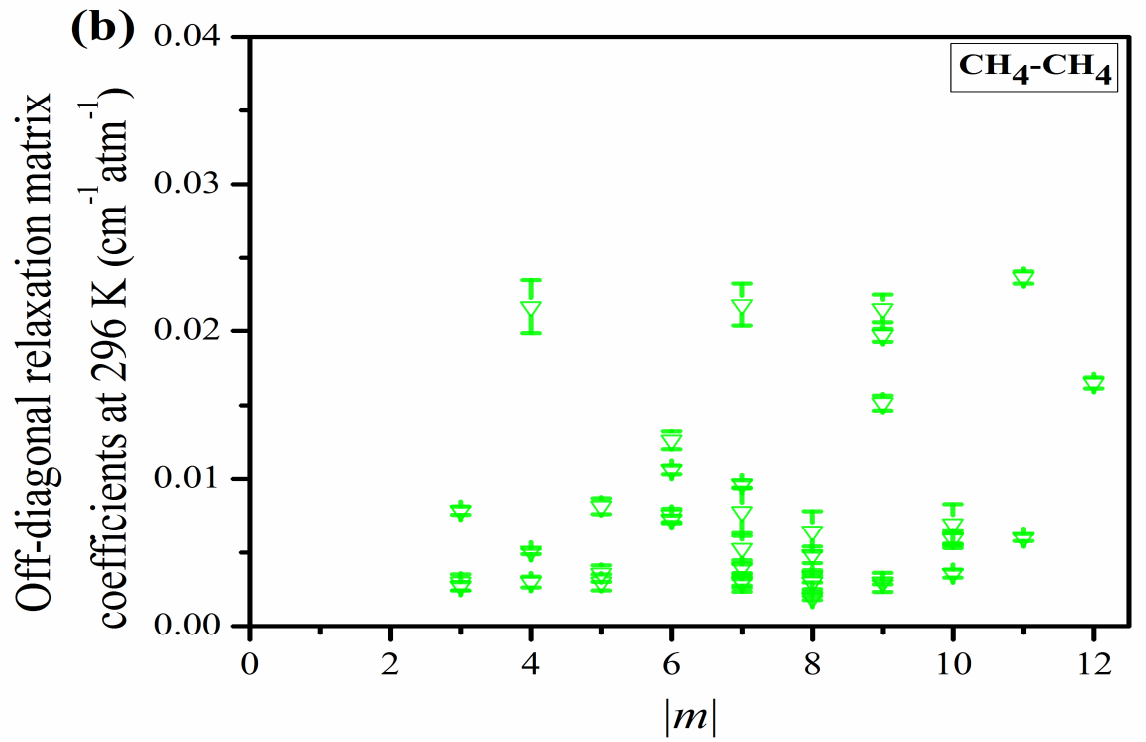

Fig 5.11: Off-diagonal relaxation matrix element coefficients for (a) CH_4-H_2 and (b) CH_4-CH_4 broadening in the $\nu_1 + \nu_4$ band as a function of |m|. The error bars which cannot be seen, are smaller than the size of the symbols used.

Fig. 5.12 shows the comparison in line-mixing coefficients due to H_2- and self-broadening of methane as a function of $|m|$. Though the line-mixing coefficients are close in both cases, the H_2-broadening gives comparatively higher values, which is expected. The temperature-dependence of line-mixing coefficients were not possible to be determined correctly. No H_2-broadened line-mixing results are available in the octad range for comparing with my present line-mixing coefficients. More experimental and theoretical line-mixing measurements in different bands of methane are needed to confirm the vibrational dependences of H_2-broadened line-mixing coefficients.

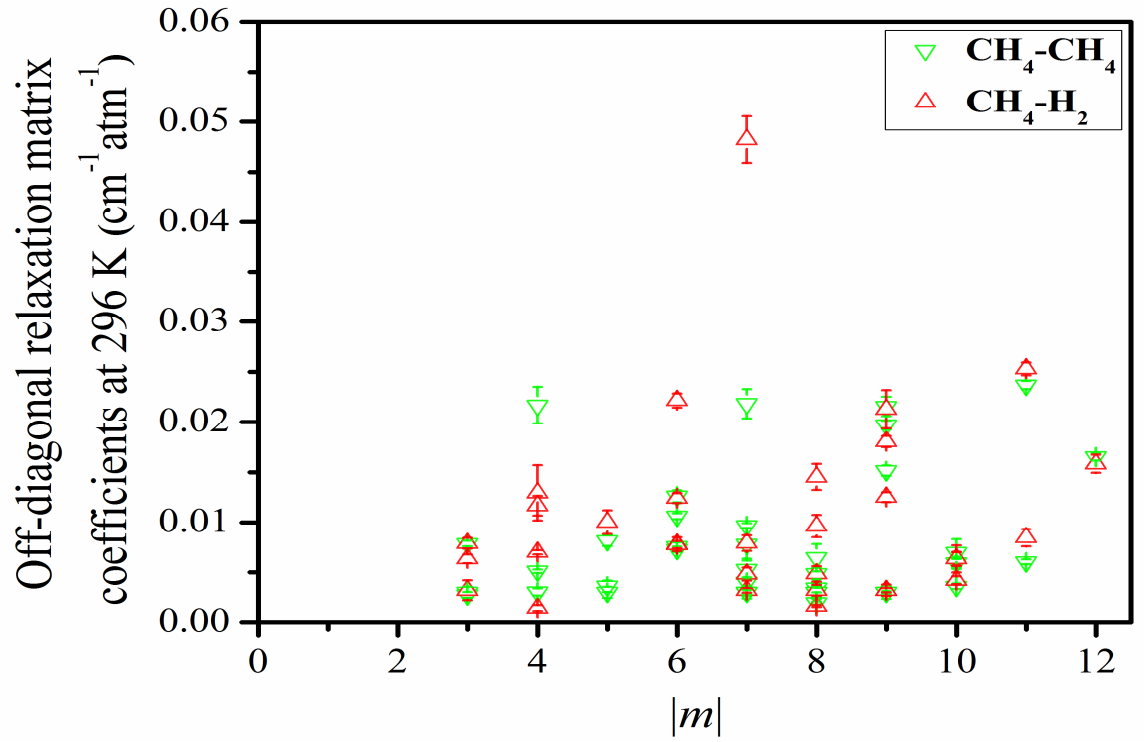

Fig 5.12: Comparison in off-diagonal relaxation matrix element coefficients due to H_2- and self-broadening of methane in the $\nu_1 + \nu_4$ band as a function of |m|. The error bars which cannot be seen, are smaller than the size of the symbols used.

Table 5.4: List of retrieved line-mixing coefficients due to self- and H_2-broadening of methane in the band $\nu_1 + \nu_4$.

			Off diagonal relaxation matrix elements	
Position (cm^{-1})	**$\|m\|$**	**Line-mixing pairs**	**CH_4-H_2 broadening[a] ($cm^{-1}atm^{-1}$)**	**CH_4-CH_4 broadening[a] ($cm^{-1}atm^{-1}$)**
4119.419111	12	$12F_1$ 3 ⟶ $11F_2$ 66	0.0158(9)	0.0165(4)
4119.700352		$12F_2$ 3 ⟶ $11F_1$ 69		
4136.167128	11	$11F_1$ 3 ⟶ $10F_2$ 63	0.0253(6)	0.0237(4)
4136.817899		$11F_2$ 3 ⟶ $10F_1$ 63		
4142.626092	11	$11F_1$ 1 ⟶ $10F_2$ 66	0.0085(9)	0.006(2)
4142.646404		$11F_2$ 1 ⟶ $10F_1$		
4153.651517	10	$10F_1$ 1 ⟶ $9F_2$ 59	0.0042(4)	0.0036(3)
4154.102169		$10F_2$ 2 ⟶ $9F_1$ 59		
4159.491305	9	$9F_2$ 2 ⟶ $8F_1$ 51	0.018(6)	0.0197(4)
4160.035843		$9F_1$ 3 ⟶ $8F_2$ 52		
4165.578642	9	$9F_2$ 1 ⟶ $8F_1$ 52	0.0032(2)	0.003(1)
4165.762113		$9F_1$ 1 ⟶ $8F_2$ 54		
4173.009946	9	$9F_2$ 2 ⟶ $8F_1$ 53	0.0125(5)	0.0151(5)
4173.231512		$9F_1$ 3 ⟶ $8F_2$ 55		
4177.713984	9	$9F_1$ 1 ⟶ $8F_2$ 58	0.0032(6)	0.003(6)
4177.781651		$9F_2$ 1 ⟶ $8F_1$ 55		
4178.252415	7	$7F_2$ 1 ⟶ $6F_1$ 40	0.0032(2)	0.003(2)
4178.527636		$7F_1$ 1 ⟶ $6F_2$ 41		
4181.817074	6	$6F_1$ 1 ⟶ $5F_2$ 34	0.0078(7)	0.0075(4)
4182.336902		$6F_2$ 2 ⟶ $5F_1$ 34		
4189.774267	8	$8F_2$ 2 ⟶ $7F_1$ 49	0.0016(1)	0.0019(1)
4189.8976		8E 2 ⟶ 7E 32		
4190.486393	8	$8F_1$ 2 ⟶ $7F_2$ 47	0.0032(5)	0.0034(4)
4190.809754		$8F_2$ 1 ⟶ $7F_1$ 50		
4194.757044	4	$4F_2$ 1 ⟶ $3F_1$ 23	0.0014(3)	
4195.970544		$4F_1$ 1 ⟶ $3F_2$ 21		
4198.506629	8	$8F_2$ 1 ⟶ $7F_1$ 52	0.0145(13)	0.0064(14)
4198.985272		$8F_1$ 1 ⟶ $7F_2$ 50		
4201.400581	3	$3F_2$ 1 ⟶ $2F_1$ 15	0.0079(5)	0.0079(3)
4201.848098		$3F_1$ 1 ⟶ $2F_2$ 16		
4206.648252	7	$7F_1$ 2 ⟶ $6F_2$ 42		0.0053(11)
4207.196401		$7F_2$ 2 ⟶ $6F_1$ 41		
4207.161599	9	$9F_2$ 1 ⟶ $8F_1$ 58	0.0213(19)	0.0215(10)
4207.395957		$9F_1$ 1 ⟶ $8F_2$ 61		
4209.871337	7	$7F_1$ 1 ⟶ $6F_2$ 43	0.0048(6)	0.003(4)
4209.980328		$7F_2$ 1 ⟶ $6F_1$ 43		
4212.67804	7	$7F_1$ 1 ⟶ $7F_2$ 41	0.0079(8)	0.004(5)

4212.99085		$7F_2$ 1 ⟶ $7F_1$ 43		
4213.072723	10	$10F_2$ 2 ⟶ $10F_1$ 56		0.0069(13)
4213.600841		$10F_1$ 1 ⟶ $10F_2$ 57		
4215.628587	5	$5F_1$ 1 ⟶ $5F_2$ 32		0.003(6)
4216.24412		$5F_2$ 1 ⟶ $5F_1$ 33		
4217.5507	3	$3F_1$ 1 ⟶ $3F_2$ 20	0.0032(10)	0.003(5)
4218.075313		$3F_2$ 1 ⟶ $3F_1$ 22		
4219.653719	8	$8F_2$ 2 ⟶ $8F_1$ 48	0.0048(8)	0.0048(6)
4219.785966		$8F_2$ 2 ⟶ $8F_1$ 49		
4223.612969	6	$6F_1$ 1 ⟶ $5F_2$ 35	0.0077(4)	0.0073(3)
4223.814946		$6F_2$ 2 ⟶ $5F_1$ 36		
4233.810945	7	$7F_2$ 1 ⟶ $6F_1$ 45		0.003(6)
4234.297037		$7F_1$ 1 ⟶ $6F_2$ 46		
4239.428901	4	$3F_2$ 1 ⟶ $4F_1$ 25	0.007(2)	0.0051(2)
4239.577754		$3F_1$ 1 ⟶ $4F_2$ 26		
4240.381603	7	$7F_1$ 1 ⟶ $6F_2$ 49		0.0078(16)
4240.736259		$7F_2$ 1 ⟶ $6F_1$ 48		
4242.181681	5	$5F_2$ 1 ⟶ $4F_1$ 28	0.01(12)	0.0081(5)
4242.2068		$5F_1$ 1 ⟶ $4F_2$ 31		
4249.14676	6	$5F_1$ 1 ⟶ $6F_2$ 34	0.0124(5)	0.0106(3)
4249.439323		$5F_2$ 1 ⟶ $6F_1$ 32		
4253.645665	7	$6F_1$ 1 ⟶ $7F_2$ 37		0.0096(3)
4253.768118		$6F_2$ 2 ⟶ $7F_1$ 38		
4258.533596	8	$7F_1$ 2 ⟶ $8F_2$ 43	0.0096(11)	0.003(7)
4258.831764		$7F_2$ 2 ⟶ $8F_1$ 42		
4259.263863	5	$5F_2$ 1 ⟶ $4F_1$ 30		0.0036(6)
4259.797756		$5F_1$ 1 ⟶ $4F_2$ 33		
4259.691916	8	$7F_1$ 1 ⟶ $8F_2$ 44		0.003(5)
4259.976554		$7F_2$ 1 ⟶ $8F_1$ 43		
4266.496434	10	$9A_2$ 1 ⟶ $10A_1$ 17	0.0063(7)	0.0059(4)
4266.606323		$9F_2$ 2 ⟶ $10F_1$ 47		
4266.75511	10	$9F_1$ 3 ⟶ $10F_2$ 48	0.0063(14)	0.0059(6)
4267.134589		$9A_1$ 1 ⟶ $10A_2$ 16		
4268.909019	10	$9F_1$ 1 ⟶ $10F_2$ 50	0.0063(7)	0.0059(4)
4268.972843		$9F_2$ 1 ⟶ $10F_1$ 48		
4282.12807	7	$7F_2$ 2 ⟶ $7F_1$ 52	0.0482(23)	0.0218(15)
4282.541148		$7F_1$ 2 ⟶ $7F_2$ 50		
4284.513121	3	$3F_1$ 1 ⟶ $2F_2$ 18	0.0063(4)	0.0027(3)
4284.574479		$3F_2$ 1 ⟶ $2F_1$ 18		
4287.785453	6	$6F_2$ 2 ⟶ $6F_1$ 44	0.0221(7)	0.0126(6)
4287.953274		$6F_1$ 1 ⟶ $6F_2$ 44		
4294.556414	4	$4F_1$ 1 ⟶ $4F_2$ 31	0.0129(28)	0.0217(18)
4294.592776		$4F_2$ 1 ⟶ $4F_1$ 32		

4298.206083	4	$4F_1$ 1 $\longrightarrow$ $4F_2$ 32	0.0116(10)	0.003(4)
4298.499938		$4F_2$ 1 $\longrightarrow$ $4F_1$ 29		

[a]Statistical uncertainties. The blank spaces in the table are appeared because the line mixing coefficients were not possible to be determined for those transitions.

CHAPTER 6: CONCLUSION

6.1 Summary of methane broadened by itself and air

In this study, the simultaneous multi-spectrum non-linear least-squares fitting software 'Labfit' was used to measure precise line-shape parameters, such as CH_4-CH_4 and CH_4-air half-widths and pressure-shift coefficients along with their temperature dependences, off-diagonal relaxation matrix element coefficients and speed-dependence parameters of air-broadened methane in the $\nu_1 + \nu_4$ band. Both self-broadening and temperature-dependence exponents of self-broadening coefficients were found to be slightly higher than CH_4-air broadening analogues. In contrast, the CH_4-air shift coefficients were larger than self-shift coefficients (less negative) of methane but the temperature dependencies for self-shift coefficients were higher than those for CH_4-air shift coefficients. The line-mixing parameters were measured through off-diagonal relaxation matrix element formalism, which provided slightly higher values for air-broadening. The speed-dependence parameters have been presented for the first time (for transitions in the $\nu_1 + \nu_4$ band) whose values vary from 0.038 to 0.198 and the values appeared to increase with $|m|$ values. The measured line positions and intensities show good agreement with the calculated values and spectroscopic database results with average difference in line position of 0.00117 cm^{-1} and the maximum variation of line intensity of 15.4%.

6.2 Summary of methane broadened by itself and H_2

The line-shape parameters due to self- and hydrogen-broadening of methane were determined by using SDVP model. The self-width coefficients and their temperature-dependence coefficients were found to be higher than those for H_2-broadening. All shift coefficients were found to be negative but their temperature dependences were found

positive and no systematic patterns of variations were found. Speed-dependence parameters were found positive varying from 0.024 to 0.158. The line-mixing coefficients for both self- and H2-broadening were found positive and the values are very close to each other.

Overall, the present spectroscopic studies of methane is useful towards the better understanding of hydrocarbon cycles in the Earth's atmosphere as well as the cold Jovian atmosphere. The retrieved line shape parameters especially for methane broadened by itself and H_2 can be used to update the spectroscopic databases like HITRAN and GEISA.

6.3 Future directions

Although the line-mixing coefficients were determined at room-temperature due to self-, air- and H_2-broadening of methane, their temperature dependences need to be determined. For the H_2-broadening analysis, I have determined line-shape parameters in the $\nu_1 + \nu_4$ band of methane. The same type of analysis is essential in the two interacting bands, $\nu_2 + \nu_3$ and $\nu_3 + \nu_4$, of methane in its octad region to confirm their vibrational dependencies. The present line-shape study for methane broadened by H_2 is carried out for cold atmospheric applications, the study needs to be extended to room temperature and for exo-atmospheric applications at higher temperatures.

Another important abundant molecule found in exo-planetary atmospheres is He. So it is essential to carry out the line-shape studies of methane broadened by He at different experimental conditions in different bands of methane.

Appendix

Appendix A: Supplementary data of line widths and their temperature dependences for CH_4 broadened by itself and air

lml	Lower state	Upper state	Position[a] (cm^{-1})	Intensity[a] (cm/mol)	Air-width[a] ($cm^{-1}atm^{-1}$)	Self-width[a] ($cm^{-1}atm^{-1}$)	n_1[a,b]	n_2[a,b]
1	1F1 1	0F2 4	4212.98051(2)	4.27E-22(2)	0.0594(19)	0.0784(15)		0.87(3)
1	0A1 1	1A2 4	4223.90646(1)	2.231E-21(2)	0.0523(2)	0.0819(4)	0.76(1)	0.71(1)
1	1F1 1	1F2 9	4218.41614(1)	1.299E-21(2)	0.0596(4)	0.0774(8)	0.84(1)	0.94(3)
2	2F2 1	1F1 10	4207.20565(5)	1.031E-21(12)	0.0648(13)	0.0709(24)	0.94(2)	
2	2E 1	1E 6	4207.48727(1)	7.92E-22(1)	0.062(5)	0.0811(5)	0.93(1)	0.84(1)
2	2F2 1	2F1 14	4218.33559(2)	1.907E-21(5)	0.0597(10)	0.075(16)	0.84(2)	0.88(4)
2	1F1 1	2F2 15	4229.19507(1)	2.095E-21(2)	0.0574(2)	0.0784(3)	0.9(1)	0.86(1)
3	3A2 1	2A1 6	4200.82101(2)	2.706E-21(5)	0.062(7)	0.0741(19)	0.76(1)	0.93(3)
3	3F2 1	2F1 15	4201.40058(1)	1.681E-21(2)	0.0636(3)	0.0838(3)	0.91(1)	0.83(1)
3	3F1 1	2F2 16	4201.84819(1)	1.685E-21(2)	0.064(3)	0.0833(3)	0.92(1)	0.84(1)
3	2E 1	3E 13	4234.41871(1)	1.817E-21(2)	0.0533(2)	0.0751(4)	0.87(1)	0.73(1)
3	3F2 1	3F1 22	4218.07962(3)	8.31E-22(3)	0.0577(5)	0.0846(19)	0.89(3)	
3	2F2 1	3F1 21	4234.35157(1)	2.604E-21(4)	0.064(6)	0.0805(7)	0.81(1)	0.92(2)
3	3A2 1	3A1 7	4218.78453(1)	3.807E-21(4)	0.0592(3)	0.0825(5)	0.83(1)	0.8(1)
3	3F1 1	3F2 20	4217.55071(1)	2.295E-21(2)	0.0639(3)	0.0836(4)	0.91(1)	0.88(1)
4	4A1 1	3A2 8	4196.39505(1)	3.2E-21(3)	0.0602(2)	0.0821(2)	0.88(1)	0.81(1)
4	4F1 1	3F2 21	4195.97055(1)	1.908E-21(2)	0.0629(3)	0.0847(3)	0.91(1)	0.82(1)
4	4F2 1	3F1 23	4194.75695(1)	1.848E-21(2)	0.0575(3)	0.0792(4)	0.85(1)	0.9(1)
4	3F1 1	4F2 26	4239.57744(2)	2.68E-21(12)	0.0835(6)	0.0905(7)	0.72(1)	0.7(1)
4	4F1 1	4F2 27	4216.99381(1)	2.384E-21(2)	0.0636(2)	0.084(3)	0.91(1)	0.87(1)
4	4E 1	4E 18	4217.36149(1)	1.595E-21(2)	0.0549(3)	0.073(5)	0.91(1)	0.92(1)
4	3A2 1	4A1 10	4239.25185(1)	4.851E-21(4)	0.0581(3)	0.0748(5)	0.74(1)	0.83(1)
4	3F2 1	4F1 25	4239.4289(1)	2.992E-21(3)	0.0637(2)	0.0866(4)	0.87(1)	0.77(1)
4	4A1 1	4A2 9	4216.47409(1)	3.959E-21(3)	0.0621(2)	0.0832(2)	0.88(1)	0.83(1)
5	5F1 2	4F2 28	4188.34878(1)	1.912E-21(1)	0.0595(2)	0.0796(2)	0.86(1)	0.818(4)
5	5E 1	4E 19	4188.64944(1)	1.292E-21(1)	0.0547(2)	0.0736(2)	0.85(1)	0.824(5)
5	5F1 1	4F2 29	4190.45691(1)	1.968E-21(2)	0.0609(2)	0.0818(3)	0.88(1)	0.83(1)
5	5F1 1	4F2 29	4190.45684(1)	1.95E-21(2)	0.0602(4)	0.082(4)	0.87(1)	0.86(1)
5	4A1 1	5A2 11	4244.81993(1)	4.849E-21(3)	0.0575(2)	0.0786(2)	0.831(5)	0.75(5)
5	4F2 1	5F1 30	4244.11276(1)	2.881E-21(2)	0.0598(2)	0.0808(2)	0.85(1)	0.80(4)
5	5F2 1	4F1 27	4189.8981(1)	1.888E-21(4)	0.0617(3)	0.0721(4)	0.89(1)	
5	4E 1	5E 20	4244.43763(1)	1.922E-21(2)	0.0539(3)	0.0665(4)	0.83(1)	
5	5F2 1	5F1 33	4216.24415(1)	2.235E-21(2)	0.0638(3)	0.0832(3)	0.89(1)	0.85(1)
5	5E 1	5E 22	4218.35005(2)	1.581E-21(6)	0.0586(10)	0.079(16)	0.8(3)	
5	4F1 1	5F2 28	4244.56818(1)	2.846E-21(2)	0.0641(2)	0.0846(3)	0.88(1)	0.82(1)
5	5F1 1	5F2 32	4215.62878(1)	2.374E-21(2)	0.0581(2)	0.0873(3)	0.93(1)	0.72(1)
5	5F1 2	5F2 33	4218.68791(2)	2.036E-21(4)	0.0543(4)	0.09(10)	0.88(1)	0.99(3)
6	6F2 2	5F1 34	4182.337(1)	1.763E-21(1)	0.0641(2)	0.0813(3)	0.88(1)	0.86(1)

6	5F1 1	6F2 34	4249.14677(1)	1.526E-21(2)	0.0696(7)	0.0853(5)	0.87(2)	0.98(2)
6	6F1 1	5F2 34	4181.81703(1)	1.757E-21(1)	0.0614(2)	0.0791(2)	0.87(1)	0.86(4)
6	6F2 2	6F1 38	4217.89755(1)	1.995E-21(2)	0.0649(3)	0.079(4)	0.85(1)	0.97(1)
6	6A2 1	6A1 14	4215.04378(1)	3.172E-21(3)	0.0603(2)	0.0821(2)	0.87(1)	0.82(0)
6	6E 1	6E 26	4214.30919(1)	1.29E-21(1)	0.0586(4)	0.0772(3)	0.86(1)	0.82(1)
6	5F2 1	6F1 32	4249.43948(1)	2.637E-21(2)	0.0619(2)	0.0837(2)	0.88(1)	0.822(4)
6	6F2 1	6F1 37	4214.5053(1)	1.913E-21(2)	0.0599(4)	0.079(5)	0.89(1)	0.89(1)
6	6A1 1	6A2 13	4219.1589(1)	3.283E-21(3)	0.0574(2)	0.0834(4)	0.89(1)	0.75(1)
6	6F1 1	6F2 39	4218.54437(1)	1.992E-21(3)	0.0615(5)	0.0766(9)	0.88(1)	0.92(3)
6	5F1 1	6F2 35	4250.93073(1)	8.85E-22(2)	0.0633(5)	0.0807(4)	0.91(1)	0.86(1)
6	5F1 2	6F2 33	4248.78721(2)	2.753E-21(9)	0.059(6)	0.0811(6)	0.7(2)	0.69(1)
6	5F1 2	6F2 34	4249.13218(3)	6.66E-22(2)	0.0578(11)	0.0751(10)	0.97(4)	0.83(4)
6	5F1 1	6F2 33	4248.7991(17)	2.65E-22(8)				
6	6E 1	5E 23	4184.54674(1)	1.229E-21(1)	0.0574(3)	0.0749(2)	0.86(1)	0.86(1)
6	6A1 1	5A2 12	4181.3552(1)	2.868E-21(2)	0.0564(2)	0.0774(2)	0.85(1)	0.82(4)
6	6F2 1	5F1 35	4184.38755(1)	1.803E-21(2)	0.064(3)	0.0755(6)	0.79(1)	0.9(1)
6	6A2 1	5A1 10	4183.82934(1)	2.983E-21(2)	0.0578(2)	0.0793(1)	0.87(1)	0.812(3)
7	7E 1	6E 27	4175.18305(1)	9.89E-22(1)	0.0463(2)	0.0636(1)	0.77(1)	0.782(4)
7	7F2 1	6F1 40	4178.2524(1)	1.585E-21(1)	0.0604(2)	0.0785(1)	0.85(1)	0.83(4)
7	7F1 2	6F2 40	4174.49344(1)	1.488E-21(1)	0.0594(2)	0.0776(2)	0.85(1)	0.821(4)
7	7F1 1	6F2 41	4178.52765(1)	1.593E-21(1)	0.0575(2)	0.0767(2)	0.83(1)	0.819(4)
7	7A2 1	6A1 15	4176.64743(1)	2.517E-21(2)	0.0566(2)	0.0775(1)	0.82(1)	0.826(3)
7	7F2 2	6F1 39	4175.67469(1)	1.495E-21(1)	0.0618(2)	0.0789(2)	0.89(1)	0.823(4)
7	6A2 1	7A1 13	4254.48128(1)	3.756E-21(4)	0.0571(2)	0.0763(3)	0.82(1)	0.98(1)
7	6F1 1	7F2 37	4253.64557(1)	2.313E-21(3)	0.062(3)	0.0788(5)	0.83(1)	0.89(2)
7	7E 1	7E 29	4218.14263(2)	1.059E-21(2)	0.0489(5)	0.0663(9)	0.8(2)	0.87(4)
7	7A2 1	7A1 15	4216.67523(1)	2.588E-21(3)	0.0568(3)	0.0775(3)	0.81(1)	0.83(1)
7	7F1 2	6F2 35	4114.87652(15)	1.16E-22(1)		0.0754(26)		
7	7F2 2	7F1 45	4217.59306(2)	1.571E-21(4)	0.0603(6)	0.0778(9)	0.96(2)	0.98(3)
7	6F2 2	7F1 38	4253.76818(2)	2.217E-21(8)	0.0666(4)	0.086(5)	0.88(1)	0.71(1)
7	7F1 1	7F2 41	4212.67806(1)	1.521E-21(2)	0.0571(3)	0.0763(3)	0.83(1)	0.79(1)
7	6F2 1	7F1 39	4254.59508(1)	2.252E-21(3)	0.0596(3)	0.0841(7)	0.86(1)	0.7(2)
7	7F2 1	7F1 43	4212.99072(2)	1.525E-21(4)	0.0615(9)	0.0792(7)	0.78(3)	0.79(2)
7	6E 1	7E 25	4254.63877(1)	1.523E-21(2)	0.0531(3)	0.0756(6)	0.84(1)	0.69(2)
7	7F1 2	7F2 44	4219.20277(1)	1.574E-21(3)	0.059(4)	0.0778(8)	0.91(1)	0.72(3)
7	6A1 1	7A2 14	4253.51921(1)	3.647E-21(3)	0.055(2)	0.0771(2)	0.86(1)	0.73(1)
8	8E 2	7E 30	4167.52654(1)	8.07E-22(0)	0.0482(3)	0.0656(1)	0.77(2)	0.77(4)
8	8F1 1	7F2 46	4172.24391(1)	1.311E-21(1)	0.0566(3)	0.074(2)	0.78(1)	0.83(5)
8	8F2 2	7F1 47	4167.15765(1)	1.206E-21(1)	0.0586(3)	0.0763(2)	0.84(1)	0.81(4)
8	8F2 1	7F1 48	4169.91906(1)	1.24E-21(2)	0.0562(3)	0.0754(2)	0.82(1)	0.84(4)
8	7F1 1	8F2 44	4259.69199(1)	1.758E-21(2)	0.0554(4)	0.0759(3)	0.82(1)	0.82(1)
8	7E 1	8E 29	4258.94129(1)	7.76E-22(1)	0.0461(5)	0.0638(3)	0.79(2)	0.77(1)
8	8F2 1	8F1 46	4215.38185(1)	1.013E-21(1)	0.0585(6)	0.0762(3)	0.77(2)	0.81(1)

8	7A2 1	8A1 15	4258.69571(1)	2.942E-21(3)	0.0531(2)	0.0744(2)	0.8(1)	0.86(1)
8	8A1 1	8A2 15	4210.63473(1)	1.872E-21(2)	0.0527(3)	0.072(2)	0.77(1)	0.81(1)
8	8E 1	7E 31	4172.11767(1)	8.73E-22(1)	0.0536(4)	0.0718(2)	0.81(2)	0.82(1)
8	7F2 2	8F1 41	4256.98437(2)	5.61E-22(1)	0.0622(10)	0.0794(4)	0.87(3)	0.83(1)
8	8F1 1	8F2 47	4210.94457(2)	1.055E-21(1)	0.0538(6)	0.0738(4)	0.87(2)	0.82(1)
8	7F2 1	8F1 43	4259.97661(1)	1.238E-21(2)	0.0608(5)	0.0777(4)	0.85(2)	0.83(1)
8	7F2 2	8F1 42	4258.83183(1)	1.136E-21(1)	0.0623(5)	0.0794(5)	0.86(2)	0.81(1)
8	8F2 2	8F1 48	4219.65375(2)	7.69E-22(1)	0.0617(7)	0.0779(3)	0.83(3)	0.8(1)
8	8E 2	8E 33	4219.34894(2)	7.04E-22(1)	0.049(6)	0.0655(3)	0.82(3)	0.78(1)
8	8E 1	8E 31	4211.35189(3)	5.04E-22(1)	0.0557(12)	0.0759(7)		0.82(1)
8	7F1 2	8F2 43	4258.53364(1)	1.316E-21(2)	0.0584(4)	0.0751(4)	0.87(1)	0.84(1)
8	7F2 1	8F1 42	4258.8699(3)	3.83E-22(1)	0.0619(15)	0.0801(9)		0.84(2)
8	8E 1	8E 30	4210.05412(7)	2.54E-22(2)		0.0708(12)		0.91(2)
8	7F2 1	8F1 41	4257.02245(5)	2.22E-22(1)	0.0614(24)	0.0793(8)		0.87(2)
8	8A1 1	7A2 16	4172.44434(1)	2.176E-21(2)	0.0513(2)	0.0711(2)	0.72(1)	0.82(1)
8	8F1 2	7F2 45	4168.48594(1)	1.219E-21(1)	0.0589(3)	0.0769(2)	0.85(1)	0.81(4)
9	9F1 3	8F2 52	4160.0362(1)	1.015E-21(1)	0.0639(4)	0.0823(2)	0.8(2)	0.78(5)
9	9F2 2	8F1 51	4159.49119(1)	1.005E-21(1)	0.061(4)	0.0783(2)	0.79(2)	0.79(4)
9	9E 1	8E 36	4163.00358(1)	7.03E-22(1)	0.0527(5)	0.0722(2)	0.72(2)	0.78(5)
9	9F2 1	8F1 52	4165.57858(1)	1.124E-21(1)	0.0542(3)	0.0721(2)	0.76(2)	0.80(4)
9	9F1 1	9F2 50	4208.44754(2)	7.56E-22(1)	0.0507(8)	0.0706(4)		0.83(1)
9	9A1 1	8A2 17	4161.05395(1)	1.706E-21(1)	0.056(2)	0.0741(2)	0.83(1)	0.83(5)
9	9A1 1	9A2 19	4216.07149(2)	1.198E-21(2)	0.0591(7)	0.0775(5)	0.81(3)	0.8(1)
9	9F2 1	9F1 51	4208.56282(2)	7.79E-22(2)	0.0544(9)	0.0736(4)		0.76(1)
9	8F2 1	9F1 46	4263.75117(2)	8.17E-22(1)	0.0576(7)	0.0751(4)	0.78(3)	0.81(1)
9	9E 1	9E 35	4214.4516(3)	5.14E-22(2)	0.0509(16)	0.0725(12)		0.77(4)
9	9F1 2	9F2 51	4214.74553(2)	7.66E-22(1)	0.0584(10)	0.0761(5)		0.79(1)
9	8A1 1	9A2 17	4264.81856(1)	1.953E-21(3)	0.0472(4)	0.0719(3)	0.74(1)	0.78(1)
9	8F1 1	9F2 46	4264.56617(2)	1.118E-21(2)	0.0521(6)	0.0736(4)	0.79(2)	0.76(1)
9	8F1 2	9F2 45	4262.94329(2)	9.49E-22(2)	0.0553(11)	0.0736(6)	0.85(3)	0.81(1)
9	8F2 2	9F1 45	4261.67572(3)	1.146E-21(3)	0.0576(10)	0.0772(6)	0.79(4)	0.76(2)
9	9F1 3	9F2 53	4217.16519(4)	6.23E-22(2)	0.0544(19)	0.0702(10)		0.67(3)
9	9A2 1	9A1 16	4216.90237(5)	6.04E-22(5)	0.0565(21)	0.0693(11)		0.94(3)
9	9F2 2	9F1 52	4217.18084(5)	4.78E-22(3)		0.0622(18)		
9	9A2 1	8A1 18	4159.05384(1)	1.613E-21(4)	0.056(3)	0.0739(2)	0.78(1)	0.819(3)
9	9F1 1	8F2 54	4165.7622(1)	1.094E-21(1)	0.0504(3)	0.0686(1)	0.72(2)	0.792(4)
9	9F1 2	8F2 53	4162.68965(2)	1.028E-21(3)	0.0564(4)	0.0743(2)	0.77(2)	0.821(5)
9	8E 1	9E 31	4264.59898(3)	4.83E-22(1)	0.0516(13)	0.0687(6)		0.84(2)
9	8E 1	9E 30	4263.59643(3)	3.98E-22(1)	0.0597(16)	0.0766(8)		0.82(2)
9	8E 2	9E 29	4261.69096(4)	7.17E-22(3)	0.0458(17)	0.0754(10)		0.65(3)
9	8F1 1	9F2 45	4263.0144(8)	1.25E-22(1)		0.0666(13)		0.83(3)
9	8E 2	9E 30	4263.51062(8)	1.57E-22(1)		0.0702(21)		
9	9F1 3	8F2 52	4160.03676(26)			0.087(43)		0.72(2)

10	10E 2	9E 38	4150.54943(1)	6.4E-22(1)	0.0381(5)	0.0558(2)		0.66(1)
10	10F2 3	9F1 58	4150.05814(2)	9.24E-22(3)	0.0565(6)	0.0754(3)	0.78(3)	0.74(1)
10	10A1 1	9A2 21	4152.61348(1)	1.652E-21(1)	0.0554(3)	0.0745(2)	0.76(1)	0.784(4)
10	10A2 1	9A1 19	4156.88723(2)	1.502E-21(3)	0.0524(7)	0.071(5)	0.7(3)	0.82(1)
10	10F2 2	9F1 59	4154.10224(1)	9.5E-22(1)	0.0553(5)	0.0731(2)	0.69(2)	0.76(1)
10	10F1 1	9F2 59	4153.6515(1)	9.42E-22(1)	0.0576(5)	0.0746(2)	0.75(2)	0.77(1)
10	10F1 2	9F2 58	4151.01679(1)	9.48E-22(1)	0.0597(5)	0.0761(2)	0.75(2)	0.8(1)
10	10E 1	9E 39	4156.92255(2)	5.05E-22(1)	0.0551(10)	0.0728(5)		0.8(1)
10	10F2 1	9F1 60	4156.8746(5)	6.54E-22(4)	0.0595(15)	0.0718(9)		0.62(3)
10	10F2 2	10F1 56	4213.07282(12)	5.14E-22(13)	0.0519(17)	0.0715(15)		0.76(2)
10	9E 1	10E 32	4267.55016(5)	5.54E-22(5)	0.0477(22)	0.0703(9)		0.77(3)
10	10F2 3	9F1 58	4150.05767(4)	1.037E-21(6)	0.0586(9)	0.077(2)		0.8(1)
10	9F2 2	10F1 47	4266.60628(2)	1.004E-21(1)	0.0613(8)	0.0824(4)	0.74(3)	0.73(1)
10	9F1 3	10F2 48	4266.75528(2)	9.93E-22(1)	0.0618(8)	0.0802(3)	0.77(3)	0.8(1)
10	10E 2	10E 38	4217.77403(4)	3.33E-22(1)	0.0444(16)	0.0608(7)		0.65(3)
10	10F1 1	10F2 57	4213.60096(3)	5.04E-22(1)	0.0599(15)	0.0765(4)		0.77(1)
10	9A1 1	10A2 16	4267.13466(1)	1.584E-21(2)	0.0532(5)	0.0728(3)	0.81(2)	0.79(1)
10	10A2 1	10A1 20	4206.07311(2)	8.25E-22(1)	0.0503(9)	0.0682(4)		0.77(1)
10	9A2 1	10A1 17	4266.49645(1)	1.555E-21(2)	0.0526(5)	0.0723(3)	0.81(2)	0.75(1)
10	9F2 1	10F1 48	4268.97289(2)	9.39E-22(1)	0.05(7)	0.0702(3)	0.76(3)	0.73(1)
10	9F1 1	10F2 50	4268.90908(2)	8.91E-22(1)	0.0475(6)	0.0682(3)	0.72(3)	0.74(1)
10	9F1 2	10F2 49	4267.48632(2)	9.33E-22(1)	0.0533(7)	0.0743(4)	0.77(3)	0.71(1)
10	10F2 1	10F1 54	4206.0107(5)	5.08E-22(5)	0.0456(18)	0.0654(10)		0.93(4)
10	10F1 2	10F2 58	4217.26503(3)	4.91E-22(2)	0.0627(17)	0.0753(8)		0.82(3)
10	10A1 1	10A2 19	4215.96665(3)	8.58E-22(2)	0.0548(9)	0.073(5)		0.77(1)
10	10E 1	10E 37	4205.98668(7)	3.14E-22(3)		0.0647(10)		0.76(3)
11	11F2 1	10F1 72	4155.79352(7)	1.22E-22(0)		0.0659(6)		0.72(2)
11	11F1 1	10F2 73	4155.94847(7)	1.19E-22(1)		0.0639(6)		0.75(2)
11	11A2 1	11A1 21	4211.25643(3)	4.88E-22(1)	0.0479(14)	0.0688(5)		0.72(2)
11	11F1 2	11F2 61	4215.4239(6)	3.14E-22(2)		0.0794(14)		
11	10F1 1	11F2 52	4272.01066(7)	5.78E-22(5)	0.0585(21)	0.0761(9)		0.74(2)
11	11E 1	11E 41	4211.82193(7)	2.04E-22(1)		0.0719(8)		0.73(2)
11	10A1 1	11A2 18	4271.57012(7)	1.047E-21(7)		0.0789(23)		
11	11F2 1	11F1 61	4203.37035(14)	4.17E-22(10)		0.0665(13)		0.95(5)
11	10F1 2	11F2 51	4271.12833(5)	6.13E-22(2)	0.0555(20)	0.0721(8)		0.81(2)
11	10F2 3	11F1 52	4270.85482(5)	6.21E-22(3)	0.056(20)	0.0717(9)		0.78(3)
11	10E 2	11E 34	4270.99282(19)	3.78E-22(10)				
11	10F2 2	11F1 53	4272.1593(5)	6.01E-22(3)	0.0511(18)	0.0689(8)		0.77(2)
11	10A2 1	11A1 17	4273.53677(10)	9.41E-22(9)		0.0596(26)		
11	11F2 2	11F1 63	4211.6042(6)	2.98E-22(2)	0.0518(25)	0.0691(7)		0.67(3)
11	11F2 3	11F1 64	4217.2007(7)	3.13E-22(2)		0.0717(17)		
11	11E 2	11E 42	4218.24804(8)	3E-22(2)		0.0743(22)		
11	11F1 3	11F2 62	4218.57467(9)	3.13E-22(3)		0.0745(32)		

11	11F1 1	11F2 59	4203.36517(42)				
12	12F1 1	12F2 66	4200.85115(21)	1.91E-22(4)			
12	12F1 1	11F2 79	4148.90173(5)	1.34E-22(1)		0.0634(6)	0.66(2)
12	12A1 1	11A2 27	4149.00754(3)	2.26E-22(0)	0.0413(13)	0.0637(3)	0.68(1)
12	12F2 1	12F1 65	4209.46141(12)	1.7E-22(2)		0.0741(18)	
12	11E 2	12E 38	4275.13837(9)	2.72E-22(2)		0.0564(9)	
12	12A1 2	12A2 22	4218.94838(8)	2.99E-22(2)		0.077(20)	
12	12F2 2	12F1 67	4214.87965(11)	1.78E-22(2)		0.0751(18)	
12	11A2 1	12A1 20	4276.71785(8)	6.31E-22(4)		0.0683(20)	
12	11F1 1	12F2 58	4278.24434(7)	3.73E-22(2)		0.0638(11)	
12	12F2 3	12F1 68	4217.95006(12)	1.93E-22(2)		0.0794(31)	
12	12A2 1	12A1 23	4216.59435(8)	3.12E-22(2)		0.0736(15)	
12	12F1 3	12F2 69	4218.52577(21)	2.04E-22(4)			
12	11F2 1	12F1 57	4278.22145(7)	3.69E-22(2)		0.0653(11)	
12	11F2 3	12F1 55	4275.29453(8)	3.85E-22(1)		0.0727(8)	0.76(3)
12	11F1 2	12F2 57	4275.87984(7)	3.81E-22(2)		0.0701(9)	0.7(3)
12	11F1 3	12F2 56	4275.05715(8)	3.72E-22(2)		0.067(9)	0.74(3)
12	12A1 1	12A2 21	4200.95235(8)	2.42E-22(1)		0.0591(8)	
12	11F2 2	12F1 56	4276.58958(8)	3.79E-22(3)		0.0704(18)	
12	12F1 2	12F2 68	4209.85379(17)	1.66E-22(2)		0.072(28)	
12	11E 1	12E 39	4276.5072(11)	2.55E-22(2)		0.0663(17)	
12	12E 2	12E 46	4214.48913(42)				
13	12A1 1	13A2 22	4282.7764(6)	3.67E-22(2)		0.0618(11)	
13	12F1 1	13F2 62	4282.75272(16)	2.17E-22(4)		0.0686(34)	
13	12F2 1	13F1 63	4281.09334(8)	2.17E-22(1)		0.0667(7)	0.71(3)
13	13F1 4	13F2 74	4218.843(29)	9.8E-23(3)			
13	12A2 1	13A1 20	4279.41413(9)	3.76E-22(2)		0.0726(9)	0.73(4)
13	12F1 3	13F2 60	4279.25543(15)	2.44E-22(2)		0.0769(16)	
13	12F1 2	13F2 61	4280.95108(9)	2.62E-22(1)		0.0816(10)	
13	12A1 2	13A2 21	4279.17205(9)	3.81E-22(2)		0.0704(11)	
13	12E 2	13E 40	4280.23957(22)	1.4E-22(2)		0.0571(17)	
13	12F2 3	13F1 60	4279.10614(20)	1.42E-22(2)		0.0626(20)	
13	12E 1	13E 41	4282.74049(23)	1.45E-22(4)			
13	13A1 1	13A2 26	4207.81607(16)	1.47E-22(1)		0.0688(11)	
14	13A1 1	14A2 21	4285.28036(10)	2E-22(1)		0.0706(9)	
14	13F2 3	14F1 63	4283.31849(18)	1.24E-22(1)		0.0752(15)	
14	13F2 1	14F1 65	4287.15352(16)	1.23E-22(1)		0.061(16)	
14	13A2 1	14A1 22	4283.91571(11)	1.93E-22(1)		0.0687(10)	
14	13F1 2	14F2 66	4285.44726(16)	1.16E-22(1)		0.0647(13)	
14	13F1 1	14F2 67	4287.17862(17)	1.15E-22(2)		0.0534(16)	
14	13F2 2	14F1 64	4284.18755(19)	1.19E-22(2)		0.068(18)	

[a]Statistical uncertainties are given in parentheses. [b]n_1 and n_2 are temperature-dependence exponents of air- and self-broadened half-width coefficients, respectively.

Appendix B: Supplementary data of line shifts along with their temperature dependences and speed dependences parameters for CH_4 broadened by itself and air

lml	Lower state	Upper state	Position[a] (cm^{-1})	Air-shift[a] ($cm^{-1}atm^{-1}$)	Self-shift[a] ($cm^{-1}atm^{-1}$)	TD[b] air-shift[a] ($cm^{-1}atm^{-1}K^{-1}$)	TD[b] self-shift[a] ($cm^{-1}atm^{-1}K^{-1}$)	$S^{a,c}$
1	1F1 1	0F2 4	4212.98051(2)					0.15(2)
1	0A1 1	1A2 4	4223.90646(1)	-0.0052(3)	-0.0123(5)	0.000107(2)	0.000079(6)	
1	1F1 1	1F2 9	4218.41614(1)	-0.007(4)	-0.0107(7)	0.000094(4)	0.000102(9)	
2	2E 1	1E 6	4207.48727(1)	-0.007(8)	-0.0104(5)	0.000063(7)	0.000093(6)	0.06(1)
2	2F2 1	1F1 10	4207.20565(5)			0.00008(10)	0.000121(11)	
2	1F1 1	2F2 15	4229.19507(1)	-0.0064(3)	-0.0106(3)	0.000043(3)	0.000032(3)	
2	2F2 1	2F1 14	4218.33559(2)					
3	3A2 1	2A1 6	4200.82101(2)	-0.0078(5)	-0.0081(5)	0.000056(4)	0.000119(5)	
3	3F2 1	2F1 15	4201.40058(1)	-0.0064(4)	-0.0109(3)	0.000047(4)	0.000046(3)	
3	3F1 1	2F2 16	4201.84819(1)	-0.0071(4)	-0.0138(3)	0.000057(4)	0.000074(3)	
3	2E 1	3E 13	4234.41871(1)	-0.0056(3)	-0.0105(5)	0.000071(3)	0.000077(6)	
3	3F2 1	3F1 22	4218.07962(3)	-0.0078(6)		0.000108(7)		
3	2F2 1	3F1 21	4234.35157(1)	-0.0064(6)		0.000056(5)	0.000116(11)	
3	3A2 1	3A1 7	4218.78453(1)	-0.0074(3)	-0.0066(7)	0.000046(2)	0.000135(9)	
3	3F1 1	3F2 20	4217.55071(1)	-0.0054(3)	-0.0102(5)	0.000044(3)		
4	4A1 1	3A2 8	4196.39505(1)	-0.0067(2)	-0.0116(3)	0.000051(2)	0.000042(4)	0.04(1)
4	4F1 1	3F2 21	4195.97055(1)	-0.007(3)	-0.0113(3)	0.000057(3)	0.000061(4)	
4	4F2 1	3F1 23	4194.75695(1)	-0.0062(4)	-0.0138(3)	0.000062(4)	0.00004(3)	
4	5F1 1	4F2 29	4190.45691(1)	-0.0075(3)	-0.0126(3)	0.000049(3)	0.000067(3)	
4	4E 1	4E 18	4217.36149(1)	-0.0045(3)	-0.0107(4)	0.000067(3)	0.000069(5)	
4	3F1 1	4F2 26	4239.57744(2)	-0.0122(4)	-0.0189(5)	0.000075(2)	0.000065(7)	0.19(1)
4	4F1 1	4F2 27	4216.99381(1)	-0.006(3)	-0.0092(4)	0.000042(3)	0.000062(4)	
4	3A2 1	4A1 10	4239.25185(1)	-0.0066(2)	-0.0115(4)	0.000051(2)		0.06(1)
4	3F2 1	4F1 25	4239.4289(1)	-0.0048(2)	-0.0073(5)			0.05(1)
4	4A1 1	4A2 9	4216.47409(1)	-0.0058(2)	-0.0111(4)	0.000039(2)	0.000034(4)	0.05(1)
5	5F1 2	4F2 28	4188.34878(1)	-0.0062(2)	-0.0113(2)	0.000055(2)	0.000065(2)	
5	5E 1	4E 19	4188.64944(1)	-0.0071(3)	-0.0136(2)	0.000074(3)	0.000086(2)	0.08(0)
5	4E 1	5E 20	4244.43763(1)	-0.0066(3)	-0.0126(4)	0.00006(2)	0.00005(5)	0.11(1)
5	5F1 2	5F2 33	4218.68791(2)	-0.0087(5)		0.000091(5)		
5	4A1 1	5A2 11	4244.81993(1)	-0.0062(2)	-0.0101(3)	0.000055(1)	0.000077(4)	0.059(5)
5	4F2 1	5F1 30	4244.11276(1)	-0.0051(2)	-0.0102(2)	0.000033(2)		0.06(1)
5	5F1 1	4F2 29	4190.45684(1)	-0.0076(4)	-0.0126(5)	0.000052(4)	0.000049(6)	
5	5F2 1	5F1 33	4216.24415(1)	-0.0058(3)	-0.0092(3)	0.000041(3)	0.000062(4)	
5	5E 1	5E 22	4218.35005(2)					
5	4F1 1	5F2 28	4244.56818(1)	-0.0064(2)	-0.0105(4)	0.000056(2)	0.000086(5)	
5	5F1 1	5F2 32	4215.62878(1)	-0.0064(3)	-0.011(3)	0.000046(3)	0.000063(3)	
5	5F2 1	4F1 27	4189.8981(1)	0.0048(4)	-0.0051(6)	0.00014(4)	0.000139(6)	
6	6F2 2	5F1 34	4182.337(1)	-0.0081(4)	-0.0134(2)	0.00007(4)	0.000095(2)	0.088(5)
6	6F1 1	5F2 34	4181.81703(1)	-0.0058(3)	-0.0102(2)	0.000048(3)	0.00005(2)	0.066(5)

6	5F1 1	6F2 34	4249.14677(1)		-0.0056(6)	0.000085(8)	0.000116(8)	0.15(1)
6	6F2 2	6F1 38	4217.89755(1)	-0.005(4)	-0.0107(4)	0.00005(4)	0.000044(5)	0.08(1)
6	6A2 1	6A1 14	4215.04378(1)	-0.0059(2)	-0.0094(3)	0.000039(3)	0.00005(3)	0.06(1)
6	6E 1	6E 26	4214.30919(1)	-0.0062(5)	-0.0105(3)	0.000056(5)	0.000066(3)	0.05(1)
6	5F2 1	6F1 32	4249.43948(1)	-0.0073(2)	-0.0136(2)	0.000069(2)	0.000112(2)	0.04(1)
6	6F2 1	6F1 37	4214.5053(1)	-0.0075(5)	-0.0098(5)	0.000045(4)	0.000068(5)	
6	6A1 1	6A2 13	4219.1589(1)	-0.0074(3)	-0.0094(5)	0.000052(3)	0.000118(6)	
6	6F1 1	6F2 39	4218.54437(1)	-0.006(6)	-0.0114(8)	0.000059(6)	0.000066(10)	
6	5F1 1	6F2 35	4250.93073(1)	-0.0073(9)	-0.0113(3)	0.000085(8)	0.000084(3)	0.06(1)
6	5F1 2	6F2 33	4248.78721(2)				0.000109(7)	
6	5F1 2	6F2 34	4249.13218(3)		-0.0127(12)			
6	5F1 1	6F2 33	4248.7991(17)					
6	6F2 1	5F1 35	4184.38755(1)	-0.0069(3)	-0.0119(2)	0.000057(3)	0.000065(2)	
6	6A2 1	5A1 10	4183.82934(1)	-0.0067(2)	-0.0125(2)	0.00006(2)	0.000086(2)	
7	7E 1	6E 27	4175.18305(1)	-0.0076(3)	-0.0138(1)	0.000089(3)	0.0001(1)	0.098(4)
7	7F2 1	6F1 40	4178.2524(1)	-0.0069(3)	-0.0122(1)	0.000052(3)	0.00005(1)	0.079(4)
7	7F1 2	6F2 40	4174.49344(1)	-0.0069(3)	-0.0107(1)	0.000055(3)	0.000073(1)	0.081(4)
7	7F1 1	6F2 41	4178.52765(1)	-0.0081(3)	-0.0126(1)	0.000058(3)	0.000068(1)	0.075(4)
7	7A2 1	6A1 15	4176.64743(1)	-0.0072(2)	-0.0129(1)	0.00006(2)	0.000072(1)	0.064(4)
7	6F1 1	7F2 37	4253.64557(1)	-0.0026(3)	-0.0046(4)			0.08(1)
7	7E 1	7E 29	4218.14263(2)	-0.0108(6)	-0.0144(8)		0.000076(10)	0.12(1)
7	7A2 1	7A1 15	4216.67523(1)	-0.0071(3)	-0.0112(3)	0.000059(3)	0.000082(4)	0.08(1)
7	7F2 1	7F1 43	4212.99072(2)	-0.0072(10)	-0.015(7)			
7	6E 1	7E 25	4254.63877(1)	-0.0063(4)	-0.0118(6)	0.000072(5)	0.000073(7)	
7	7F1 2	7F2 44	4219.20277(1)	-0.008(6)	-0.0157(7)	0.000065(6)		
7	6A1 1	7A2 14	4253.51921(1)	-0.0055(2)	-0.0087(4)	0.000035(2)	0.00005(4)	
7	7F2 2	6F1 39	4175.67469(1)	-0.0088(4)	-0.0121(1)	0.000053(4)	0.000077(1)	
7	7F1 1	7F2 41	4212.67806(1)	-0.0063(5)	-0.0104(2)	0.000056(5)	0.000076(2)	0.05(1)
7	6F2 1	7F1 39	4254.59508(1)	-0.0072(4)	-0.0108(7)	0.000056(4)	0.000063(9)	
7	7F1 2	6F2 35	4114.87652(15)					
7	7F2 2	7F1 45	4217.59306(2)	-0.0051(7)	-0.0091(8)			0.1(1)
7	6F2 2	7F1 38	4253.76818(2)	-0.01(3)	-0.0149(4)	0.000108(3)	0.000124(4)	0.16(1)
7	6A2 1	7A1 13	4254.48128(1)	-0.0067(2)	-0.0162(5)	0.000075(2)		0.11(1)
8	8E 2	7E 30	4167.52654(1)	-0.0078(4)	-0.0144(1)	0.00007(5)	0.000085(1)	0.096(4)
8	7F1 1	8F2 44	4259.69199(1)	-0.0053(4)	-0.0122(3)	0.00007(4)	0.000069(3)	0.11(1)
8	8F1 1	7F2 46	4172.24391(1)	-0.0074(4)	-0.0118(2)	0.000057(4)	0.000073(2)	0.079(4)
8	8F2 2	7F1 47	4167.15765(1)	-0.008(4)	-0.0112(1)	0.00004(4)	0.000071(1)	0.059(4)
8	8F2 1	7F1 48	4169.91906(1)	-0.0075(4)	-0.0123(1)	0.000066(4)	0.00007(1)	0.07(1)
8	8E 1	7E 31	4172.11767(1)	-0.0087(5)	-0.0119(2)	0.000053(6)	0.000075(2)	0.06(1)
8	8A1 1	7A2 16	4172.44434(1)	-0.0079(2)	-0.0122(2)	0.000044(2)	0.00008(2)	0.046(5)
8	8F1 2	7F2 45	4168.48594(1)	-0.0086(4)	-0.0136(1)	0.00007(4)	0.000079(1)	
8	7E 1	8E 29	4258.94129(1)	-0.0065(6)	-0.0114(3)	0.000066(7)	0.000086(3)	0.11(1)
8	8F2 1	8F1 46	4215.38185(1)	-0.0058(8)	-0.0098(3)	0.000066(9)	0.000075(3)	0.09(1)

8	7A2 1	8A1 15	4258.69571(1)	-0.0066(3)	-0.0106(3)	0.000065(3)	0.000074(3)	0.07(1)
8	8A1 1	8A2 15	4210.63473(1)	-0.0074(4)	-0.013(2)	0.00006(4)	0.000065(2)	0.06(1)
8	7F2 2	8F1 41	4256.98437(2)		-0.0115(4)		0.000052(4)	0.08(1)
8	8F1 1	8F2 47	4210.94457(2)	-0.0096(7)	-0.0121(3)		0.000069(2)	0.06(1)
8	7F2 1	8F1 43	4259.97661(1)	-0.0083(7)	-0.0136(3)	0.000068(7)	0.000077(4)	0.05(1)
8	7F2 2	8F1 42	4258.83183(1)	-0.0058(8)	-0.0093(5)		0.000051(5)	0.05(1)
8	8F2 2	8F1 48	4219.65375(2)		-0.011(3)		0.000055(3)	0.05(1)
8	8E 2	8E 33	4219.34894(2)	-0.0073(9)	-0.0123(3)		0.000096(3)	
8	8E 1	8E 31	4211.35189(3)		-0.0128(5)		0.00007(4)	
8	7F1 2	8F2 43	4258.53364(1)	-0.0039(5)	-0.0094(3)		0.00005(3)	
8	7F2 1	8F1 42	4258.8699(3)		-0.0149(9)		0.000105(11)	
8	8E 1	8E 30	4210.05412(7)		-0.0175(8)		0.000084(6)	
8	7F2 1	8F1 41	4257.02245(5)		-0.018(8)		0.000102(9)	
9	9F1 3	8F2 52	4160.0362(1)	-0.0089(6)	-0.0156(2)	0.00007(7)	0.000069(2)	0.174(4)
9	9F2 2	8F1 51	4159.49119(1)	-0.0059(5)	-0.0093(1)		0.000064(1)	0.126(4)
9	9E 1	8E 36	4163.00358(1)	-0.0074(6)	-0.0133(1)	0.000063(8)	0.00007(2)	0.103(5)
9	9F2 1	8F1 52	4165.57858(1)	-0.0072(4)	-0.0124(1)	0.000053(5)	0.000068(1)	0.08(4)
9	9A1 1	8A2 17	4161.05395(1)	-0.0093(3)	-0.0138(1)	0.000059(4)	0.000079(1)	0.058(4)
9	9A2 1	8A1 18	4159.05384(1)	-0.0079(3)	-0.0121(1)	0.000041(4)	0.000064(1)	0.046(5)
9	9F1 1	8F2 54	4165.7622(1)	-0.0078(4)	-0.0137(1)	0.000063(5)	0.000077(1)	0.04(1)
9	9F1 2	8F2 53	4162.68965(2)	-0.0071(5)	-0.0126(1)	0.000051(6)	0.000069(2)	0.06(1)
9	9A1 1	9A2 19	4216.07149(2)		-0.012(4)		0.00007(4)	0.08(1)
9	9F2 1	9F1 51	4208.56282(2)	-0.0078(11)	-0.0131(3)		0.000049(4)	0.1(1)
9	8F2 1	9F1 46	4263.75117(2)	-0.007(10)	-0.0111(3)		0.000066(3)	0.08(1)
9	9E 1	9E 35	4214.4516(3)		-0.0117(10)			
9	9F1 2	9F2 51	4214.74553(2)		-0.0132(5)		0.000064(6)	
9	8A1 1	9A2 17	4264.81856(1)	-0.0061(4)	-0.0113(3)	0.000079(5)	0.000082(2)	
9	8F1 1	9F2 46	4264.56617(2)	-0.0081(7)	-0.0129(4)	0.000077(8)	0.000086(4)	
9	8F1 2	9F2 45	4262.94329(2)		-0.0108(3)		0.000051(3)	
9	8F2 2	9F1 45	4261.67572(3)				0.000056(8)	
9	9F1 1	9F2 50	4208.44754(2)	-0.0071(11)	-0.0129(3)		0.000067(3)	0.11(1)
9	9F1 3	8F2 52	4160.03676(26)					
9	8E 1	9E 31	4264.59898(3)		-0.0144(7)		0.000097(7)	
9	8E 1	9E 30	4263.59643(3)		-0.0136(7)		0.000079(7)	
9	8E 2	9E 29	4261.69096(4)		-0.0228(11)			
9	8F1 1	9F2 45	4263.0144(8)		-0.0179(11)		0.000141(12)	
9	8E 2	9E 30	4263.51062(8)					
9	9F1 3	9F2 53	4217.16519(4)					
9	9A2 1	9A1 16	4216.90237(5)		-0.0153(11)			
9	9F2 2	9F1 52	4217.18084(5)		-0.0219(16)			
10	10E 2	9E 38	4150.54943(1)	-0.0085(5)	-0.0154(1)	0.000075(6)	0.000101(1)	0.19(1)
10	10F2 3	9F1 58	4150.05814(2)		-0.0115(3)	0.000063(9)	0.000058(2)	0.2(1)
10	10A1 1	9A2 21	4152.61348(1)	-0.0083(4)	-0.0123(1)	0.000038(5)	0.000065(1)	0.087(4)

10	10A2 1	9A1 19	4156.88723(2)	-0.0095(7)	-0.0133(5)		0.000047(5)	0.11(1)
10	10F2 2	9F1 59	4154.10224(1)	-0.0079(6)	-0.0137(1)	0.000056(8)	0.00006(2)	0.07(1)
10	10F1 1	9F2 59	4153.6515(1)	-0.0071(6)	-0.012(1)		0.000043(2)	0.06(5)
10	10F1 2	9F2 58	4151.01679(1)	-0.0097(7)	-0.0147(2)	0.000063(9)	0.000067(2)	0.07(1)
10	10E 1	9E 39	4156.92255(2)		-0.0145(5)		0.000071(6)	0.12(1)
10	10F2 1	9F1 60	4156.8746(5)		-0.0112(12)		0.000112(12)	
10	10F2 3	9F1 58	4150.05767(4)	-0.0171(10)	-0.02(5)		0.000077(3)	
10	9F2 2	10F1 47	4266.60628(2)		-0.0046(3)		0.000028(4)	0.12(1)
10	9F1 3	10F2 48	4266.75528(2)	-0.0117(10)	-0.0199(3)	0.000112(12)	0.000108(3)	0.09(1)
10	10E 2	10E 38	4217.77403(4)		-0.0137(6)		0.000101(8)	0.14(2)
10	10F1 1	10F2 57	4213.60096(3)		-0.0129(3)		0.000056(4)	0.1(1)
10	9A1 1	10A2 16	4267.13466(1)	-0.0079(6)	-0.0156(2)	0.000073(7)	0.000068(2)	
10	10A2 1	10A1 20	4206.07311(2)	-0.0081(12)	-0.0134(3)		0.000059(4)	
10	9A2 1	10A1 17	4266.49645(1)	-0.0048(6)	-0.0081(3)		0.000061(3)	
10	9F2 1	10F1 48	4268.97289(2)	-0.0078(9)	-0.0133(3)	0.00007(10)	0.000067(3)	
10	9F1 1	10F2 50	4268.90908(2)	-0.0078(8)	-0.0131(3)	0.000067(10)	0.000066(3)	
10	9F1 2	10F2 49	4267.48632(2)	-0.0069(10)	-0.0113(3)		0.000078(3)	
10	10F2 1	10F1 54	4206.0107(5)		-0.014(7)			
10	10F1 2	10F2 58	4217.26503(3)		-0.0116(8)			
10	10A1 1	10A2 19	4215.96665(3)		-0.0087(8)		0.000065(8)	
10	10E 1	10E 37	4205.98668(7)		-0.0138(10)			
10	10F2 2	10F1 56	4213.07282(12)		-0.012(6)		0.000054(8)	
10	9E 1	10E 32	4267.55016(5)		-0.01(9)			
11	11F1 1	10F2 73	4155.94847(7)		-0.0157(5)		0.000058(8)	
11	11F2 1	10F1 72	4155.79352(7)		-0.015(4)		0.000065(7)	
11	11A2 1	11A1 21	4211.25643(3)		-0.0138(3)		0.000067(5)	0.09(1)
11	11F1 2	11F2 61	4215.4239(6)		-0.0126(10)			0.16(2)
11	10F1 1	11F2 52	4272.01066(7)		-0.0118(5)		0.000061(7)	
11	11E 1	11E 41	4211.82193(7)		-0.0145(5)			
11	10A1 1	11A2 18	4271.57012(7)		-0.0115(16)			
11	11F2 1	11F1 61	4203.37035(14)		-0.0216(14)			
11	10F1 2	11F2 51	4271.12833(5)		-0.0169(6)		0.000053(7)	
11	10F2 3	11F1 52	4270.85482(5)		-0.0084(8)			
11	10E 2	11E 34	4270.99282(19)					
11	10F2 2	11F1 53	4272.1593(5)		-0.0147(5)		0.000066(7)	
11	10A2 1	11A1 17	4273.53677(10)					
11	11F2 2	11F1 63	4211.6042(6)		-0.0118(4)		0.000056(8)	
11	11F2 3	11F1 64	4217.2007(7)					
11	11E 2	11E 42	4218.24804(8)		-0.0192(23)			
11	11F1 3	11F2 62	4218.57467(9)					
11	11F1 1	11F2 59	4203.36517(42)					
12	12F1 1	12F2 66	4200.85115(21)					
12	12F1 1	11F2 79	4148.90173(5)		-0.0136(3)		0.000063(6)	

12	12A1 1	11A2 27	4149.00754(3)	-0.0137(2)	0.000072(3)	0.13(1)
12	12F2 1	12F1 65	4209.46141(12)	-0.0138(8)		
12	11E 2	12E 38	4275.13837(9)	-0.0128(6)	0.000096(10)	
12	12A1 2	12A2 22	4218.94838(8)			
12	12F2 2	12F1 67	4214.87965(11)	-0.0102(12)		
12	11A2 1	12A1 20	4276.71785(8)			
12	11F1 1	12F2 58	4278.24434(7)	-0.0156(9)		
12	12F2 3	12F1 68	4217.95006(12)			
12	12A2 1	12A1 23	4216.59435(8)	-0.0148(17)		
12	12F1 3	12F2 69	4218.52577(21)			
12	11F2 1	12F1 57	4278.22145(7)	-0.0144(9)		
12	11F2 3	12F1 55	4275.29453(8)	-0.0227(6)		
12	11F1 2	12F2 57	4275.87984(7)	-0.0124(6)		
12	11F1 3	12F2 56	4275.05715(8)	-0.006(7)	0.000069(10)	
12	12A1 1	12A2 21	4200.95235(8)	-0.0169(7)		
12	11F2 2	12F1 56	4276.58958(8)	-0.0161(15)		
12	12F1 2	12F2 68	4209.85379(17)	-0.021(22)		
12	11E 1	12E 39	4276.5072(11)	-0.0174(14)		
12	12E 2	12E 46	4214.48913(42)			
13	12A1 1	13A2 22	4282.7764(6)	-0.0148(11)		
13	12F1 1	13F2 62	4282.75272(16)	-0.0187(20)		
13	12F2 1	13F1 63	4281.09334(8)	-0.0141(5)	0.000079(9)	
13	13F1 4	13F2 74	4218.843(29)			
13	12A2 1	13A1 20	4279.41413(9)	-0.0243(6)		
13	12F1 3	13F2 60	4279.25543(15)	-0.014(10)		
13	12F1 2	13F2 61	4280.95108(9)	-0.0193(7)		
13	12A1 2	13A2 21	4279.17205(9)			
13	12E 2	13E 40	4280.23957(22)	-0.0125(11)		
13	12F2 3	13F1 60	4279.10614(20)			
13	12E 1	13E 41	4282.74049(23)			
13	13A1 1	13A2 26	4207.81607(16)	-0.0123(9)		
14	13A1 1	14A2 21	4285.28036(10)	-0.0151(5)		
14	13F2 3	14F1 63	4283.31849(18)	-0.0133(9)		
14	13F2 1	14F1 65	4287.15352(16)	-0.015(11)		
14	13A2 1	14A1 22	4283.91571(11)	-0.0139(6)		
14	13F1 2	14F2 66	4285.44726(16)	-0.0149(8)		
14	13F1 1	14F2 67	4287.17862(17)	-0.0174(11)		
14	13F2 2	14F1 64	4284.18755(19)	-0.0152(12)		

[a]Statistical uncertainties are given in parentheses. TD[b] stands for temperature dependences and *S*[c] stands for speed-dependence parameters.

Appendix C: Supplementary data of line widths and their temperature dependences for CH_4 broadened by itself and H_2

lml	Lower state	Upper state	Position[a] (cm^{-1})	Intensity[a] (cm/mol)	H_2-width[a] ($cm^{-1}atm^{-1}$)	Self-width[a] ($cm^{-1}atm^{-1}$)	n_1[a,b]	n_2[a,b]
1	0A1 1	1A2 4	4223.906441(1)	2.318E-21(3)	0.0677(3)	0.0776(3)	0.46(1)	0.73(1)
1	1F1 1	1F2 9	4218.416115(1)	1.317E-21(1)	0.0654(4)	0.0762(6)	0.48(1)	0.95(2)
1	1F1 1	0F2 4	4212.980503(2)	4.42E-22(1)	0.0544(11)	0.0745(11)	0.59(3)	0.9(2)
2	1F1 1	2F2 15	4229.195067(1)	2.204E-21(2)	0.0651(2)	0.079(2)	0.5(1)	0.81(1)
2	2E 1	2E 11	4218.077734(1)	2.121E-21(4)	0.0697(4)	0.0887(5)	0.32(1)	0.67(1)
2	2E 1	1E 6	4207.487244(1)	8.05E-22(1)	0.0658(4)	0.0818(4)	0.47(1)	0.81(1)
2	2F2 1	1F1 10	4207.205927(3)	1.174E-21(4)	0.0614(14)	0.0719(11)	0.54(2)	1(2)
2	2F2 1	2F1 14	4218.335579(1)	1.981E-21(4)	0.0695(12)	0.0757(11)		1(3)
3	3F1 1	2F2 16	4201.848149(1)	1.727E-21(1)	0.065(2)	0.081(2)	0.5(1)	0.829(5)
3	2E 1	3E 13	4234.418669(1)	1.861E-21(2)	0.0573(2)	0.0732(3)	0.41(1)	0.73(1)
3	2F2 1	3F1 21	4234.351497(1)	2.728E-21(4)	0.0711(4)	0.079(5)	0.45(1)	0.89(1)
3	3A2 1	2A1 6	4200.821017(1)	2.828E-21(3)	0.0651(3)	0.0779(3)	0.53(1)	0.83(1)
3	3F2 1	2F1 15	4201.40055(1)	1.708E-21(2)	0.0668(2)	0.0812(2)	0.48(1)	0.86(1)
3	3A2 1	3A1 7	4218.784496(1)	3.926E-21(6)	0.0665(3)	0.0792(3)	0.51(1)	0.86(1)
3	3F1 1	3F2 20	4217.55068(1)	2.353E-21(2)	0.0659(3)	0.0812(3)	0.52(1)	0.89(1)
4	3F1 1	4F2 26	4239.577837(1)	3.076E-21(3)	0.0621(2)	0.0778(3)	0.56(1)	0.81(1)
4	3A2 1	4A1 10	4239.251865(1)	4.944E-21(6)	0.0591(3)	0.0726(3)	0.6(1)	0.84(1)
4	3F2 1	4F1 25	4239.428865(1)	3.052E-21(4)	0.0687(3)	0.082(3)	0.49(1)	0.84(1)
4	4E 1	3E 14	4195.649714(1)	1.316E-21(1)	0.0564(1)	0.0749(2)	0.46(1)	0.79(1)
4	4F1 1	3F2 21	4195.970545(5)	1.977E-21(1)	0.0642(1)	0.0826(1)	0.53(5)	0.806(4)
4	4F2 1	3F1 23	4194.757054(1)	1.935E-21(1)	0.0628(2)	0.0767(3)	0.56(1)	0.86(1)
4	4A1 1	3A2 8	4196.395062(4)	3.318E-21(2)	0.0634(1)	0.0788(1)	0.52(4)	0.804(3)
4	4F1 1	4F2 27	4216.993786(1)	2.435E-21(2)	0.0648(2)	0.0818(2)	0.54(1)	0.87(1)
4	4E 1	4E 18	4217.361452(1)	1.613E-21(2)	0.058(3)	0.0723(3)	0.5(1)	0.91(1)
4	4A1 1	4A2 9	4216.474061(1)	4.043E-21(5)	0.0669(2)	0.0812(2)	0.48(1)	0.82(1)
5	4A1 1	5A2 11	4244.819887(1)	4.94E-21(6)	0.063(2)	0.0769(2)	0.51(1)	0.756(5)
5	5E 1	4E 19	4188.649414(1)	1.304E-21(1)	0.0579(2)	0.073(2)	0.5(1)	0.82(1)
5	5F1 2	4F2 28	4188.348757(5)	1.942E-21(1)	0.063(1)	0.0782(1)	0.55(1)	0.815(4)
5	4F1 1	5F2 28	4244.568138(1)	2.93E-21(3)	0.0649(2)	0.0817(3)	0.54(1)	0.83(1)
5	5F1 1	5F2 32	4215.628731(2)	2.203E-21(6)	0.0665(6)	0.0802(3)	0.48(1)	0.89(1)
5	5F1 1	4F2 29	4190.456858(1)	2.003E-21(1)	0.0626(2)	0.0792(3)	0.55(1)	0.86(1)
5	5F2 1	5F1 33	4216.244118(1)	2.269E-21(2)	0.0645(2)	0.0817(2)	0.54(1)	0.86(1)
5	5F2 1	4F1 27	4189.898113(1)	1.959E-21(4)	0.062(4)	0.0762(5)	0.55(1)	1.01(1)
5	5F1 2	5F2 33	4218.684057(3)	2.883E-21(42)	0.0678(6)	0.0803(7)		0.85(2)
5	4E 1	5E 20	4244.437574(1)	1.945E-21(2)	0.056(3)	0.0687(3)	0.44(1)	0.94(1)
5	4F2 1	5F1 30	4244.112724(1)	2.942E-21(3)	0.0645(2)	0.0791(2)	0.54(1)	0.789(4)
5	5E 1	5E 22	4218.350008(2)	1.528E-21(5)	0.0616(10)	0.0759(13)		
6	5E 1	6E 22	4248.792264(11)	1.447E-21(21)	0.0648(13)	0.0627(19)		
6	5F1 2	6F2 34	4249.132117(2)	6.78E-22(2)	0.0549(8)	0.0752(10)		0.88(4)

6	5F2 1	6F1 32	4249.439413(1)	2.696E-21(2)	0.0649(2)	0.0817(2)	0.53(1)	0.803(5)
6	5F1 1	6F2 35	4250.930668(1)	8.85E-22(1)	0.0635(3)	0.0807(3)	0.54(1)	0.85(1)
6	5F1 1	6F2 34	4249.146763(1)	1.539E-21(2)	0.0718(5)	0.0853(5)	0.58(2)	0.94(2)
6	6F1 1	6F2 39	4218.544326(1)	2.007E-21(2)	0.064(5)	0.0773(6)	0.56(1)	0.94(2)
6	5F1 2	6F2 33	4248.786427(4)	2.22E-21(26)	0.0566(5)	0.0832(9)	0.55(2)	0.73(3)
6	6F2 2	5F1 34	4182.336963(1)	1.772E-21(1)	0.0643(2)	0.0794(2)	0.54(1)	0.87(1)
6	6A2 1	5A1 10	4183.829312(5)	3.037E-21(2)	0.0619(1)	0.078(1)	0.53(1)	0.8(3)
6	6A1 1	5A2 12	4181.355176(5)	2.909E-21(2)	0.062(2)	0.075(2)	0.53(1)	0.837(4)
6	6F1 1	5F2 34	4181.81703(1)	1.766E-21(1)	0.0628(2)	0.0786(2)	0.54(1)	0.815(4)
6	6F2 1	5F1 35	4184.387552(1)	1.838E-21(1)	0.0618(2)	0.0798(2)	0.56(1)	0.8(1)
6	6E 1	5E 23	4184.546623(1)	1.211E-21(2)	0.0611(2)	0.0749(2)	0.53(1)	0.84(1)
6	6E 1	6E 26	4214.309149(1)	1.293E-21(1)	0.0604(2)	0.0771(2)	0.56(1)	0.81(1)
6	6A2 1	6A1 14	4215.043748(1)	3.224E-21(3)	0.0652(2)	0.0804(2)	0.51(1)	0.82(4)
6	6A1 1	6A2 13	4219.158856(1)	3.355E-21(4)	0.0657(3)	0.0807(3)	0.49(1)	0.77(1)
6	6F2 1	6F1 37	4214.505278(1)	1.931E-21(2)	0.0628(3)	0.0777(4)	0.57(1)	0.91(1)
6	6F2 2	6F1 38	4217.897509(1)	1.996E-21(3)	0.0646(3)	0.0787(3)	0.54(1)	0.95(1)
7	6A1 1	7A2 14	4253.519163(1)	3.706E-21(4)	0.0594(2)	0.0753(2)	0.54(1)	0.75(1)
7	7A2 1	7A1 15	4216.675194(1)	2.603E-21(2)	0.0632(2)	0.0763(3)	0.54(1)	0.85(1)
7	7F2 1	6F1 40	4178.252417(1)	1.584E-21(1)	0.0611(2)	0.0773(3)	0.52(1)	0.81(1)
7	7E 1	7E 29	4218.142548(1)	1.058E-21(1)	0.0519(4)	0.0659(6)	0.43(2)	0.84(3)
7	6F2 1	7F1 39	4254.59503(1)	2.302E-21(3)	0.0638(4)	0.0822(6)	0.55(1)	0.71(2)
7	6F2 2	7F1 38	4253.768243(1)	2.291E-21(2)	0.0649(3)	0.0797(3)	0.54(1)	0.79(1)
7	6E 1	7E 25	4254.638687(1)	1.544E-21(2)	0.0597(4)	0.0726(6)	0.55(1)	0.73(2)
7	6A2 1	7A1 13	4254.481225(1)	3.803E-21(4)	0.0651(2)	0.0759(2)	0.49(1)	0.94(1)
7	6F1 1	7F2 37	4253.64555(1)	2.311E-21(2)	0.0651(3)	0.0778(4)	0.51(1)	0.89(1)
7	7E 1	6E 27	4175.183036(1)	1.004E-21(1)	0.0499(2)	0.0645(2)	0.43(1)	0.78(1)
7	7F1 1	7F2 41	4212.678024(1)	1.524E-21(1)	0.0604(2)	0.076(2)	0.56(1)	0.78(1)
7	7F2 2	6F1 39	4175.674689(1)	1.501E-21(1)	0.0627(2)	0.0785(2)	0.51(1)	0.82(1)
7	7F1 1	6F2 41	4178.527643(1)	1.597E-21(1)	0.0614(2)	0.0757(2)	0.53(1)	0.82(1)
7	7F1 2	6F2 40	4174.493451(1)	1.489E-21(1)	0.0622(2)	0.076(3)	0.51(1)	0.84(1)
7	7A2 1	6A1 15	4176.647424(1)	2.537E-21(3)	0.0622(2)	0.0741(2)	0.5(1)	0.85(1)
7	7F1 2	7F2 44	4219.202731(1)	1.584E-21(2)	0.0606(4)	0.0765(6)	0.53(2)	0.75(2)
7	7F1 2	6F2 34	4113.092352(5)	5.49E-23(3)	0.0653(14)	0.0799(9)		0.83(2)
7	7F2 2	7F1 45	4217.592981(1)	1.556E-21(3)	0.063(6)	0.0742(7)	0.64(2)	1.06(2)
7	7F1 2	6F2 35	4114.87633(3)	1.161E-22(5)	0.0603(8)	0.0758(6)		0.87(1)
7	7F2 1	7F1 43	4212.990834(1)	1.521E-21(3)	0.0636(5)	0.0799(5)	0.68(2)	0.77(2)
8	7E 1	8E 29	4258.941223(1)	7.78E-22(1)	0.0496(3)	0.0638(3)	0.45(2)	0.76(1)
8	7F1 1	8F2 44	4259.691917(1)	1.76E-21(2)	0.061(3)	0.075(3)	0.55(1)	0.81(1)
8	7A2 1	8A1 15	4258.695654(1)	2.975E-21(3)	0.0623(2)	0.0735(2)	0.51(1)	0.84(1)
8	7F2 1	8F1 43	4259.976549(1)	1.237E-21(1)	0.0607(3)	0.0775(3)	0.55(1)	0.83(1)
8	7F1 2	8F2 43	4258.533574(1)	1.313E-21(2)	0.0602(3)	0.075(3)	0.53(1)	0.83(1)
8	7F2 2	8F1 41	4256.9843(2)	5.6E-22(1)	0.0629(5)	0.0792(3)	0.56(2)	0.82(1)
8	7F2 1	8F1 41	4257.022338(4)	2.2E-22(1)	0.062(10)	0.0783(6)		0.88(2)

8	7F2 2	8F1 42	4258.831772(1)	1.137E-21(1)	0.063(4)	0.0794(4)	0.53(1)	0.81(1)
8	7F2 1	8F1 42	4258.869833(2)	3.83E-22(1)	0.0637(8)	0.0804(7)		0.82(2)
8	7F2 1	8F1 43	4259.977137(5)	1.059E-21(11)	0.0643(5)	0.0805(4)	0.48(2)	0.81(1)
8	8E 2	7E 30	4167.526484(1)	8.078E-22(4)	0.0516(1)	0.0661(1)	0.45(1)	0.75(1)
8	8F2 2	7F1 47	4167.157619(1)	1.206E-21(1)	0.0613(1)	0.0766(1)	0.51(1)	0.802(5)
8	8F1 2	7F2 45	4168.485903(1)	1.218E-21(1)	0.0614(2)	0.0773(2)	0.51(1)	0.782(5)
8	8F2 1	7F1 48	4169.919017(1)	1.239E-21(1)	0.0616(2)	0.075(2)	0.54(1)	0.81(1)
8	8A1 1	8A2 15	4210.63469(1)	1.875E-21(1)	0.0587(2)	0.0718(2)	0.53(1)	0.8(1)
8	8F1 1	8F2 47	4210.944546(1)	1.052E-21(1)	0.0613(4)	0.0746(3)	0.5(2)	0.8(1)
8	8E 1	8E 31	4211.351872(2)	5.01E-22(1)	0.0627(7)	0.0762(6)		0.81(1)
8	8E 1	8E 30	4210.053981(9)	2.49E-22(3)	0.0578(18)	0.0729(18)		0.88(2)
8	8E 2	8E 33	4219.348893(1)	7.04E-22(1)	0.0498(3)	0.0656(3)	0.51(2)	0.77(1)
8	8E 1	7E 31	4172.117678(1)	8.68E-22(1)	0.0589(2)	0.0719(3)	0.5(1)	0.82(1)
8	8F2 1	8F1 46	4215.381817(1)	1.009E-21(1)	0.0613(3)	0.0757(3)	0.55(2)	0.82(1)
8	8A1 1	7A2 16	4172.444341(1)	2.196E-21(4)	0.0599(2)	0.0697(3)	0.43(1)	0.85(1)
8	8F1 1	7F2 46	4172.243915(1)	1.313E-21(1)	0.0595(2)	0.0736(3)	0.47(1)	0.83(1)
8	8F2 2	8F1 48	4219.653706(1)	7.66E-22(1)	0.0607(3)	0.0776(3)	0.59(2)	0.8(1)
9	8F2 1	9F1 46	4263.751122(2)	8.17E-22(1)	0.0611(4)	0.0755(4)	0.51(2)	0.81(1)
9	8F1 1	9F2 46	4264.566102(1)	1.118E-21(2)	0.0571(4)	0.0734(4)	0.52(2)	0.76(1)
9	8F1 2	9F2 45	4262.943221(2)	9.43E-22(2)	0.0576(6)	0.074(5)	0.53(2)	0.8(1)
9	8A1 1	9A2 17	4264.818493(1)	1.956E-21(2)	0.0586(3)	0.0713(3)	0.48(1)	0.79(1)
9	9F1 1	9F2 50	4208.447501(2)	7.51E-22(1)	0.0575(4)	0.0699(3)	0.57(2)	0.83(1)
9	8E 1	9E 31	4264.598911(2)	4.87E-22(1)	0.0565(7)	0.0704(6)		0.82(2)
9	9A1 1	9A2 19	4216.071417(1)	1.189E-21(1)	0.0604(6)	0.0778(4)	0.48(2)	0.78(1)
9	9F2 1	9F1 51	4208.562798(2)	7.76E-22(1)	0.0589(4)	0.0732(3)	0.54(2)	0.77(1)
9	9F1 2	9F2 51	4214.745506(2)	7.63E-22(1)	0.0608(4)	0.0757(4)	0.56(3)	0.79(1)
9	9E 1	9E 35	4214.451581(2)	5.15E-22(1)	0.0603(7)	0.0722(8)		0.79(3)
9	9A2 1	9A1 16	4216.902358(3)	6.02E-22(3)	0.0576(10)	0.0691(8)		0.93(3)
9	9E 1	8E 30	4115.990616(7)	5E-23(0)	0.0608(16)	0.0752(11)		0.79(3)
9	9F1 3	9F2 53	4217.165159(3)	6.22E-22(2)	0.0519(7)	0.0687(8)		0.7(3)
9	8E 1	9E 30	4263.596388(3)	3.97E-22(1)	0.0617(8)	0.0766(7)		0.83(2)
9	8E 2	9E 30	4263.51055(7)	1.57E-22(1)	0.0591(26)	0.073(21)		
9	8F1 1	9F2 45	4263.014328(7)	1.25E-22(1)	0.052(17)	0.066(11)		0.83(3)
9	8F2 2	9F1 45	4261.675688(2)	1.148E-21(3)	0.0601(7)	0.0783(6)		0.76(2)
9	8E 2	9E 29	4261.690861(3)	7.07E-22(3)	0.0518(11)	0.0704(10)		0.69(3)
9	9A1 1	8A2 17	4161.053923(1)	1.692E-21(1)	0.0605(3)	0.0731(2)	0.47(1)	0.85(1)
9	9F1 1	8F2 54	4165.762154(1)	1.095E-21(5)	0.0569(1)	0.0687(1)	0.5(1)	0.79(1)
9	9F2 1	8F1 52	4165.578602(1)	1.104E-21(5)	0.0584(1)	0.0723(1)	0.49(1)	0.78(1)
9	9E 1	8E 36	4163.003536(1)	7.029E-22(5)	0.0593(2)	0.0727(1)	0.56(1)	0.75(1)
9	9F1 2	8F2 53	4162.689677(2)	1.035E-21(3)	0.0596(2)	0.0744(2)	0.51(1)	0.8(1)
9	9A2 1	8A1 18	4159.053776(1)	1.619E-21(2)	0.0598(1)	0.0736(2)	0.44(1)	0.81(1)
9	9F2 2	8F1 51	4159.491209(1)	1.004E-21(1)	0.0622(1)	0.0787(2)	0.56(1)	0.78(1)
9	9F1 3	8F2 52	4160.036111(1)	9.9E-22(1)	0.06(1)	0.0762(2)	0.54(1)	0.8(1)

10	9F1 3	10F2 48	4266.755118(2)	9.7E-22(1)	0.0609(4)	0.0764(3)	0.49(2)	0.81(1)
10	9A1 1	10A2 16	4267.134602(1)	1.583E-21(1)	0.0587(3)	0.0729(2)	0.47(2)	0.78(1)
10	9A2 1	10A1 17	4266.496427(1)	1.553E-21(2)	0.0558(3)	0.0726(3)	0.43(2)	0.74(1)
10	9F1 2	10F2 49	4267.486265(2)	9.3E-22(1)	0.0582(4)	0.0743(3)	0.52(2)	0.71(1)
10	9F2 1	10F1 48	4268.972845(2)	9.37E-22(1)	0.0558(4)	0.07(3)	0.52(2)	0.75(1)
10	9F1 1	10F2 50	4268.909037(2)	8.94E-22(1)	0.0563(4)	0.0696(3)	0.51(2)	0.75(1)
10	9F2 2	10F1 47	4266.606303(2)	9.75E-22(1)	0.0622(4)	0.0773(4)	0.5(2)	0.76(1)
10	10E 2	10E 38	4217.773981(3)	3.3E-22(1)	0.0459(6)	0.0602(6)		0.65(2)
10	10A2 1	9A1 19	4156.887224(1)	1.493E-21(3)	0.0586(3)	0.0719(5)	0.53(2)	0.75(2)
10	10E 1	9E 39	4156.92253(2)	5.04E-22(1)	0.0578(3)	0.0742(5)	0.59(2)	0.7(2)
10	10A1 1	10A2 19	4215.966631(2)	8.52E-22(2)	0.0574(4)	0.0729(4)	0.56(2)	0.77(1)
10	10F2 2	10F1 56	4213.07271(8)	5.1E-22(8)	0.0568(8)	0.0711(9)		0.75(2)
10	10E 1	10E 37	4205.986643(4)	3.14E-22(1)	0.0536(9)	0.0637(7)		0.76(3)
10	10F2 1	10F1 54	4206.010714(5)	4.83E-22(5)	0.0571(14)	0.0635(11)		
10	10F2 1	9F1 60	4156.874962(3)	6.48E-22(3)	0.0524(4)	0.069(7)		0.92(3)
10	10F1 2	10F2 58	4217.265004(2)	4.89E-22(1)	0.059(6)	0.0749(6)		0.81(2)
10	9E 1	10E 32	4267.550174(5)	5.57E-22(4)	0.0561(11)	0.0699(8)		0.78(3)
10	10A2 1	10A1 20	4206.073073(2)	8.22E-22(1)	0.055(4)	0.0685(3)	0.5(2)	0.75(1)
10	10E 2	9E 38	4150.549498(1)	6.22E-225(4)	0.0422(1)	0.0548(2)	0.4(1)	0.67(1)
10	10A1 1	9A2 21	4152.613689(1)	1.578E-21(3)	0.0631(2)	0.0754(2)	0.43(1)	0.76(1)
10	10F1 2	9F2 58	4151.016765(1)	9.38E-22(1)	0.0602(2)	0.0758(2)	0.55(1)	0.79(1)
10	10F2 3	9F1 58	4150.058291(1)	9.3E-22(1)	0.0611(1)	0.0768(2)	0.57(1)	0.77(1)
10	10F1 1	9F2 59	4153.651498(1)	9.351E-22(5)	0.0594(1)	0.0746(2)	0.52(1)	0.73(1)
10	10F2 2	9F1 59	4154.102201(1)	9.51E-22(1)	0.06(1)	0.0738(2)	0.55(1)	0.75(1)
10	10F1 1	10F2 57	4213.600913(2)	5E-22(1)	0.0604(4)	0.0759(3)	0.63(3)	0.77(1)
11	10F1 1	11F2 52	4272.010898(3)	5.47E-22(3)	0.067(8)	0.0807(7)	0.65(3)	0.76(1)
11	10F2 2	11F1 53	4272.159158(3)	6.11E-22(3)	0.0582(5)	0.0699(5)	0.56(2)	0.74(1)
11	10F1 2	11F2 51	4271.128214(2)	6.19E-22(1)	0.0585(4)	0.0732(3)	0.58(2)	0.82(1)
11	10F2 3	11F1 52	4270.854783(2)	6.3E-22(1)	0.0587(4)	0.0724(4)	0.56(2)	0.79(1)
11	10A1 1	11A2 18	4271.57011(3)	1.05E-21(3)	0.0605(10)	0.076(10)		0.63(3)
11	10A2 1	11A1 17	4273.53687(3)	9.38E-22(3)	0.0476(7)	0.0595(8)		0.83(3)
11	11A2 1	11A1 21	4211.256385(2)	4.84E-22(1)	0.0574(5)	0.0685(4)	0.57(3)	0.71(1)
11	11F2 1	10F1 72	4155.793472(6)	1.196E-22(3)	0.0521(5)	0.0642(4)		0.71(2)
11	11F2 2	11F1 63	4211.604096(8)	2.96E-22(1)	0.0538(7)	0.0687(6)		0.66(2)
11	11F1 1	10F2 73	4155.948357(6)	1.181E-22(5)	0.053(6)	0.0628(5)		0.78(2)
11	11E 1	11E 41	4211.821883(5)	2.03E-22(1)	0.0573(9)	0.0714(6)		0.73(2)
11	11F1 2	11F2 61	4215.423844(4)	3.14E-22(1)	0.0602(9)	0.0778(10)		
11	11F1 1	11F2 59	4203.365714(18)	2.48E-22(6)	0.0474(16)	0.0629(16)		
11	11F2 3	11F1 64	4217.200666(5)	3.12E-22(2)	0.0555(12)	0.0726(13)		
11	11F2 1	11F1 61	4203.371193(10)	3.27E-22(6)	0.0557(13)	0.0654(10)		1(4)
12	11E 2	12E 38	4275.138151(4)	2.72E-22(1)	0.0437(5)	0.0557(4)		0.67(2)
12	11F1 3	12F2 56	4275.057005(3)	3.78E-22(1)	0.0553(5)	0.0689(3)		0.73(1)
12	11F1 2	12F2 57	4275.879714(3)	3.82E-22(1)	0.0576(5)	0.0706(4)		0.7(1)

12	11F2 3	12F1 55	4275.294315(3)	3.83E-22(1)	0.0568(5)	0.0719(3)		0.76(1)
12	11A2 1	12A1 20	4276.717795(3)	6.35E-22(2)	0.0561(7)	0.0657(7)		0.69(3)
12	11F2 1	12F1 57	4278.221394(3)	3.7E-22(1)	0.0521(6)	0.0653(5)		0.65(2)
12	11F1 1	12F2 58	4278.244319(3)	3.74E-22(1)	0.0544(7)	0.0653(5)		0.73(2)
12	11E 1	12E 39	4276.506827(6)	2.59E-22(3)	0.0583(10)	0.0691(9)		0.74(4)
12	12A1 1	12A2 21	4200.952244(6)	2.48E-22(1)	0.0494(8)	0.0595(7)		
12	12F2 1	12F1 65	4209.461375(9)	1.67E-22(1)	0.0601(14)	0.0732(12)		
12	12A1 2	12A2 22	4218.94833(5)	2.99E-22(2)	0.0584(13)	0.0754(16)		
12	11F2 2	12F1 56	4276.589509(4)	3.84E-22(1)	0.0579(8)	0.0717(8)		0.72(3)
12	12F2 2	12F1 67	4214.879649(8)	1.76E-22(1)	0.062(14)	0.0744(13)		
12	12A2 1	12A1 23	4216.594242(5)	3.15E-22(2)	0.0574(9)	0.0743(12)		
12	12F1 2	12F2 68	4209.853878(12)	1.66E-22(2)	0.0542(23)	0.0736(21)		
12	12A1 1	11A2 27	4149.007479(2)	2.273E-22(3)	0.0534(2)	0.0643(2)	0.53(1)	0.68(1)
12	12F1 1	11F2 79	4148.901712(4)	1.336E-22(4)	0.051(4)	0.0627(3)	0.52(2)	0.66(1)
13	12F2 1	13F1 63	4281.093222(5)	2.2E-22(1)	0.058(8)	0.0697(6)		0.68(2)
13	12F1 3	13F2 60	4279.255197(6)	2.46E-22(1)	0.0634(9)	0.0772(7)		0.88(2)
13	12A1 2	13A2 21	4279.171847(4)	3.83E-22(1)	0.0574(6)	0.0702(4)		0.8(2)
13	12A2 1	13A1 20	4279.413922(4)	3.78E-22(1)	0.0577(6)	0.0722(4)		0.75(2)
13	12F2 3	13F1 60	4279.10593(9)	1.46E-22(1)	0.0533(11)	0.0646(7)		0.82(4)
13	12A1 1	13A2 22	4282.776466(4)	3.5E-22(3)	0.0573(11)	0.0632(9)		
13	12E 1	13E 41	4282.740586(14)	1.47E-22(2)	0.0422(18)	0.0588(18)		
13	13A1 1	13A2 26	4207.816028(12)	1.44E-22(1)	0.0515(13)	0.0668(9)		
13	12E 2	13E 40	4280.239739(13)	1.46E-22(1)	0.0572(15)	0.0638(11)		
13	12F1 1	13F2 62	4282.752732(11)	2.13E-22(2)	0.0587(27)	0.0688(26)		
14	13A2 1	14A1 22	4283.915495(7)	1.95E-22(1)	0.0566(9)	0.0709(7)		0.64(3)
14	13F2 1	14F1 65	4287.153379(10)	1.23E-22(1)	0.0471(15)	0.0611(13)		
14	13A1 1	14A2 21	4285.280242(7)	2.02E-22(1)	0.0571(9)	0.0717(7)		0.67(3)
14	13F1 2	14F2 66	4285.447189(11)	1.17E-22(1)	0.0547(14)	0.067(10)		
14	13F2 3	14F1 63	4283.318251(10)	1.27E-22(1)	0.0627(16)	0.0787(14)		
14	13F2 2	14F1 64	4284.187454(11)	1.22E-22(1)	0.0558(14)	0.0698(11)		

[a]Statistical uncertainties are given in parentheses.
[b]n_1 and n_2 are temperature-dependence exponents of air- and self-broadened half-width coefficients, respectively.

Appendix D: Supplementary data of shifts along with their temperature dependences and speed dependences parameters for CH_4 broadened by itself and H_2

lml	Lower state	Upper state	Position[a] (cm^{-1})	H_2-shift[a] ($cm^{-1}atm^{-1}$)	Self-shift[a] ($cm^{-1}atm^{-1}$)	TD[b] H_2-shift[a] ($cm^{-1}atm^{-1}K^{-1}$)	TD[b] self-shift[a] ($cm^{-1}atm^{-1}K^{-1}$)	$S^{a,c}$
1	0A1 1	1A2 4	4223.906441(1)	-0.0114(3)	-0.0107(4)	0.000017(2)	0.000106(5)	0.08(1)
1	1F1 1	1F2 9	4218.416115(1)	-0.0099(3)	-0.0104(5)	0.000045(3)	0.000129(7)	0.05(1)
1	1F1 1	0F2 4	4212.980503(2)				0.000166(12)	
2	2E 1	2E 11	4218.077734(1)	-0.0102(3)		0.000045(3)	0.000228(10)	0.08(1)
2	2E 1	1E 6	4207.487244(1)	-0.0101(4)	-0.0098(4)	0.000034(4)	0.000118(5)	0.06(1)
2	2F2 1	1F1 10	4207.205927(3)	-0.0068(10)	-0.0088(11)		0.000122(9)	
2	1F1 1	2F2 15	4229.195067(1)	-0.0099(2)	-0.0091(3)	0.000016(2)	0.000088(3)	0.05(1)
2	2F2 1	2F1 14	4218.335579(1)	-0.0087(9)				
3	3F1 1	2F2 16	4201.848149(1)	-0.011(2)	-0.0121(2)	0.000035(2)	0.000097(2)	0.05(1)
3	3A2 1	2A1 6	4200.821017(1)	-0.0113(3)	-0.008(4)	0.000038(2)	0.000137(4)	0.07(1)
3	3F1 1	3F2 20	4217.55068(1)	-0.0089(2)	-0.0082(4)	0.000026(2)	0.000055(5)	0.05(1)
3	3F2 1	2F1 15	4201.40055(1)	-0.0083(3)	-0.0102(2)	0.000038(3)	0.000065(2)	0.04(1)
3	2E 1	3E 13	4234.418669(1)	-0.009(2)	-0.01(3)	0.000023(2)	0.000091(5)	0.06(0)
3	2F2 1	3F1 21	4234.351497(1)	-0.0059(3)		0.000031(2)	0.000142(7)	0.16(1)
3	3A2 1	3A1 7	4218.784496(1)	-0.0078(3)	-0.0048(6)	0.000043(2)	0.000178(7)	0.07(1)
4	3A2 1	4A1 10	4239.251865(1)	-0.0075(2)	-0.0074(3)	0.000013(1)	0.000072(4)	0.07(1)
4	3F2 1	4F1 25	4239.428865(1)	-0.0066(2)	-0.0073(4)			0.09(5)
4	3F1 1	4F2 26	4239.577837(1)	-0.012(2)	-0.0093(3)	0.000039(2)	0.00015(5)	0.04(1)
4	4E 1	3E 14	4195.649714(1)	-0.0096(1)	-0.0123(1)	0.000036(2)	0.000089(2)	0.055(4)
4	4F1 1	3F2 21	4195.970545(4)	-0.0098(1)	-0.0105(1)	0.000038(1)	0.000085(2)	0.025(4)
4	4F2 1	3F1 23	4194.757054(1)	-0.0094(2)	-0.0117(2)	0.000036(2)	0.000074(2)	0.079(4)
4	4A1 1	3A2 8	4196.395062(4)	-0.0089(1)	-0.0109(1)	0.000033(1)	0.00007(2)	0.041(4)
4	4F1 1	4F2 27	4216.993786(1)	-0.0087(2)	-0.0082(3)	0.00003(2)	0.000084(4)	0.04(1)
4	4E 1	4E 18	4217.361452(1)	-0.0094(3)	-0.0098(3)	0.000025(3)	0.000086(4)	
4	4A1 1	4A2 9	4216.474061(1)	-0.0089(2)	-0.0096(3)	0.000029(2)	0.000061(4)	0.05(1)
5	4E 1	5E 20	4244.437574(1)	-0.0089(2)	-0.0119(3)	0.000018(2)	0.000068(4)	0.09(1)
5	4F1 1	5F2 28	4244.568138(1)	-0.01(2)	-0.0091(3)	0.000021(2)	0.00011(5)	0.05(1)
5	4A1 1	5A2 11	4244.819887(1)	-0.0086(2)	-0.0091(3)	0.000014(2)	0.000097(4)	
5	5F1 2	5F2 33	4218.684057(3)	-0.0133(4)	-0.0061(9)	0.000047(3)	0.000216(14)	
5	4F2 1	5F1 30	4244.112724(1)	-0.0065(2)	-0.0089(2)		0.000033(3)	0.07(1)
5	5E 1	5E 22	4218.350008(2)	-0.009(12)		0.000099(14)		
5	5E 1	4E 19	4188.649414(1)	-0.0101(1)	-0.0128(1)	0.000036(2)	0.000093(2)	0.075(4)
5	5F1 2	4F2 28	4188.348757(5)	-0.009(1)	-0.0104(1)	0.000031(2)	0.000077(2)	0.04(4)
5	5F1 1	5F2 32	4215.628731(2)	-0.0105(2)	-0.0103(3)	0.000025(3)	0.000082(3)	
5	5F1 1	4F2 29	4190.456858(1)	-0.0106(2)	-0.0114(3)	0.000031(2)	0.000081(3)	0.04(4)
5	5F2 1	5F1 33	4216.244118(1)	-0.0087(2)	-0.0082(3)	0.000029(2)	0.000083(3)	0.04(1)
5	5F2 1	4F1 27	4189.898113(1)	-0.0035(3)		0.000044(3)	0.000189(8)	0.08(1)
6	5E 1	6E 22	4248.792264(11)		-0.0201(25)			
6	5F1 2	6F2 34	4249.132117(2)		-0.008(11)			

6	5F2 1	6F1 32	4249.439413(1)	-0.011(2)	-0.0125(2)	0.00003(2)	0.000119(2)	0.06(1)
6	5F1 2	6F2 33	4248.786427(4)	-0.013(7)			0.000151(13)	
6	5F1 1	6F2 35	4250.930668(1)	-0.0084(3)	-0.0102(3)		0.000093(2)	
6	5F1 1	6F2 34	4249.146763(1)	-0.0049(4)	-0.0062(5)		0.000138(7)	0.15(1)
6	6F2 2	5F1 34	4182.336963(1)	-0.0119(2)	-0.0122(2)	0.000039(2)	0.000105(2)	0.064(4)
6	6A2 1	5A1 10	4183.829312(5)	-0.0102(1)	-0.0117(1)	0.000041(1)	0.000093(2)	
6	6A1 1	5A2 12	4181.355176(5)	-0.0098(1)	-0.0111(2)	0.000027(2)	0.000074(2)	0.032(4)
6	6F1 1	5F2 34	4181.81703(1)	-0.008(1)	-0.0089(1)	0.000024(2)	0.00007(2)	0.039(4)
6	6F1 1	6F2 39	4218.544326(1)	-0.0109(4)	-0.0086(6)	0.00004(4)	0.000104(8)	0.05(1)
6	6F2 1	5F1 35	4184.387552(1)	-0.0098(1)	-0.0113(2)	0.000031(2)	0.000072(2)	0.028(4)
6	6E 1	5E 23	4184.546623(1)	-0.0102(2)	-0.0116(2)	0.000022(2)	0.000078(2)	0.072(5)
6	6E 1	6E 26	4214.309149(1)	-0.0085(2)	-0.0094(2)	0.000029(3)	0.000085(2)	0.03(1)
6	6A2 1	6A1 14	4215.043748(1)	-0.0077(2)	-0.0084(2)	0.000027(2)	0.000069(2)	0.068(5)
6	6A1 1	6A2 13	4219.158856(1)	-0.0116(2)	-0.0084(4)	0.000045(3)	0.000133(5)	0.05(1)
6	6F2 1	6F1 37	4214.505278(1)	-0.0093(3)	-0.0096(4)	0.000045(3)	0.000087(5)	0.05(1)
6	6F2 2	6F1 38	4217.897509(1)	-0.009(2)	-0.0094(3)	0.000037(3)	0.00007(4)	0.06(1)
7	6A1 1	7A2 14	4253.519163(1)	-0.0071(2)	-0.0084(3)	0.000014(2)	0.000051(4)	
7	7F1 2	7F2 44	4219.202731(1)	-0.012(3)	-0.0138(6)	0.000058(4)	0.000086(7)	
7	6F2 1	7F1 39	4254.59503(1)	-0.009(3)	-0.0081(6)	0.000031(3)	0.000095(7)	0.06(1)
7	6F2 2	7F1 38	4253.768243(1)	-0.0125(2)	-0.0118(3)	0.000055(2)	0.000146(4)	0.06(1)
7	6E 1	7E 25	4254.638687(1)	-0.0096(4)	-0.0132(5)	0.00003(4)	0.000078(6)	0.06(1)
7	6A2 1	7A1 13	4254.481225(1)	-0.0092(2)	-0.0143(4)	0.000031(2)	0.000047(5)	0.10(1)
7	6F1 1	7F2 37	4253.64555(1)	-0.0047(2)	-0.0053(4)			0.06(1)
7	7E 1	6E 27	4175.183036(1)	-0.0108(1)	-0.0136(2)	0.000022(2)	0.00012(2)	0.09(1)
7	7F1 1	7F2 41	4212.678024(1)	-0.0081(2)	-0.0094(2)	0.000021(3)	0.000094(2)	0.04(1)
7	7F2 2	6F1 39	4175.674689(1)	-0.0109(1)	-0.0119(2)	0.000029(2)	0.000097(2)	
7	7F1 1	6F2 41	4178.527643(1)	-0.0101(1)	-0.0119(2)	0.000017(2)	0.000089(2)	0.06(1)
7	7F1 2	6F2 40	4174.493451(1)	-0.0096(1)	-0.0104(2)		0.000089(3)	0.06(1)
7	7A2 1	6A1 15	4176.647424(1)	-0.0109(1)	-0.0126(2)	0.000024(2)	0.000088(3)	
7	7A2 1	7A1 15	4216.675194(1)	-0.0104(2)	-0.0103(3)	0.000038(2)	0.000102(3)	0.05(1)
7	7F2 1	6F1 40	4178.252417(1)	-0.0106(1)	-0.0117(2)		0.000076(3)	
7	7E 1	7E 29	4218.142548(1)	-0.0096(3)	-0.0109(5)	0.000043(4)	0.000111(8)	0.09(1)
7	7F1 2	6F2 34	4113.092352(5)	-0.0098(14)	-0.0069(6)		0.000062(7)	
7	7F2 2	7F1 45	4217.592981(1)	-0.0094(4)	-0.0089(7)		0.000064(8)	0.09(1)
7	7F1 2	6F2 35	4114.87633(3)	-0.01(9)	-0.009(6)			
7	7F2 1	7F1 43	4212.990834(1)	-0.0077(4)	-0.0151(6)			0.07(1)
8	7E 1	8E 29	4258.941223(1)	-0.0085(3)	-0.0107(2)		0.000094(3)	0.10(1)
8	8E 2	7E 30	4167.526484(1)	-0.0102(1)	-0.0139(1)	0.000015(2)	0.000089(1)	0.094(3)
8	8F2 2	7F1 47	4167.157619(1)	-0.0092(1)	-0.0102(1)	0.000017(2)	0.000087(1)	0.061(4)
8	8F1 2	7F2 45	4168.485903(1)	-0.0109(1)	-0.0134(1)	0.000025(2)	0.000081(1)	0.041(5)
8	8F2 1	7F1 48	4169.919017(1)	-0.0099(1)	-0.0118(1)	0.000018(2)	0.000082(1)	0.05(1)
8	8A1 1	8A2 15	4210.63469(1)	-0.0092(2)	-0.0119(2)		0.000082(2)	0.048(5)
8	8F1 1	8F2 47	4210.944546(1)	-0.0079(3)	-0.0107(2)	0.00003(4)	0.000091(2)	0.08(1)

8	7F1 1	8F2 44	4259.691917(1)	-0.0082(2)	-0.0112(2)	0.000019(3)	0.000075(3)	0.09(1)
8	7A2 1	8A1 15	4258.695654(1)	-0.0084(2)	-0.0102(3)	0.000024(2)	0.00008(3)	0.05(1)
8	7F2 1	8F1 43	4259.976549(1)	-0.0099(3)	-0.0131(3)	0.000026(4)	0.000081(3)	0.05(1)
8	7F1 2	8F2 43	4258.533574(1)	-0.0069(3)	-0.0086(3)		0.000057(3)	
8	7F2 2	8F1 41	4256.9843(2)	-0.0089(4)	-0.0105(3)		0.000061(4)	0.07(1)
8	7F2 1	8F1 41	4257.022338(4)	-0.0126(10)	-0.016(7)		0.000112(8)	
8	7F2 2	8F1 42	4258.831772(1)	-0.0084(3)	-0.0088(4)		0.00006(4)	0.05(1)
8	7F2 1	8F1 42	4258.869833(2)	-0.0109(8)	-0.0141(8)		0.000118(10)	
8	7F2 1	8F1 43	4259.977137(5)				0.000048(5)	
8	8E 1	8E 30	4210.053981(9)	-0.0115(10)	-0.0133(8)		0.000106(7)	
8	8E 1	8E 31	4211.351872(2)	-0.0091(6)	-0.0117(5)		0.00009(4)	0.07(1)
8	8E 2	8E 33	4219.348893(1)	-0.0104(3)	-0.0115(3)		0.000111(3)	
8	8E 1	7E 31	4172.117678(1)	-0.0094(2)	-0.0109(3)	0.000023(3)	0.000096(3)	0.06(1)
8	8F2 1	8F1 46	4215.381817(1)	-0.0074(3)	-0.009(3)		0.000092(3)	0.07(1)
8	8A1 1	7A2 16	4172.444341(1)	-0.0104(1)	-0.0123(2)	0.000019(2)	0.000091(3)	
8	8F1 1	7F2 46	4172.243915(1)	-0.0105(1)	-0.0112(2)	0.000019(2)	0.000093(3)	0.06(1)
8	8F2 2	8F1 48	4219.653706(1)	-0.0096(3)	-0.0097(2)		0.000074(3)	0.05(1)
9	8F2 1	9F1 46	4263.751122(2)	-0.0091(4)	-0.0101(3)		0.000083(3)	0.08(1)
9	8E 2	9E 30	4263.51055(7)					
9	8F1 1	9F2 46	4264.566102(1)	-0.0098(3)	-0.0118(3)		0.0001(4)	
9	8F1 2	9F2 45	4262.943221(2)	-0.0083(4)	-0.0097(3)		0.000068(3)	
9	9F1 1	9F2 50	4208.447501(2)	-0.0093(3)	-0.0115(2)		0.00009(3)	0.09(1)
9	8E 1	9E 31	4264.598911(2)	-0.0093(7)	-0.0131(6)		0.000111(7)	
9	9A1 1	9A2 19	4216.071417(1)	-0.0094(4)	-0.0116(3)		0.000084(4)	0.08(1)
9	9F2 1	9F1 51	4208.562798(2)	-0.0098(3)	-0.0119(3)		0.000075(4)	0.09(1)
9	8E 1	9E 30	4263.596388(3)	-0.0112(8)	-0.0129(6)		0.000094(7)	
9	8A1 1	9A2 17	4264.818493(1)	-0.0084(2)	-0.0104(2)		0.000097(2)	
9	8F1 1	9F2 45	4263.014328(7)	-0.0154(16)	-0.0171(10)		0.000153(12)	
9	8F2 2	9F1 45	4261.675688(2)	-0.0045(7)			0.000072(7)	
9	8E 2	9E 29	4261.690861(3)	-0.014(10)	-0.0229(10)		0.00008(11)	
9	9A1 1	8A2 17	4161.053923(1)	-0.0103(1)	-0.0134(1)	0.000029(2)	0.000084(1)	0.059(4)
9	9F1 1	8F2 54	4165.762154(1)	-0.0106(1)	-0.0132(1)	0.000018(2)	0.000083(1)	0.032(4)
9	9F2 1	8F1 52	4165.578602(1)	-0.0099(1)	-0.0114(1)	0.000016(2)	0.000083(1)	0.074(4)
9	9E 1	8E 36	4163.003536(1)	-0.0099(1)	-0.0123(1)	0.000018(2)	0.000087(2)	0.101(4)
9	9F1 2	8F2 53	4162.689677(2)	-0.0099(1)	-0.0117(1)		0.000082(2)	
9	9A2 1	8A1 18	4159.053776(1)	-0.0099(1)	-0.0107(1)		0.00008(2)	0.038(5)
9	9F2 2	8F1 51	4159.491209(1)	-0.0091(1)	-0.0092(1)		0.000084(2)	0.125(4)
9	9F1 3	8F2 52	4160.036111(1)	-0.0116(1)	-0.0137(1)	0.000021(2)	0.000082(2)	0.056(4)
9	9F1 2	9F2 51	4214.745506(2)	-0.0108(4)	-0.0119(4)		0.000088(5)	
9	9E 1	9E 35	4214.451581(2)	-0.0093(6)	-0.01(8)		0.000091(11)	0.10(1)
9	9A2 1	9A1 16	4216.902358(3)	-0.0142(10)	-0.0142(8)		0.000087(11)	
9	9E 1	8E 30	4115.990616(7)	-0.0093(14)	-0.0116(6)		0.000077(10)	
9	9F1 3	9F2 53	4217.165159(3)					

10	9F1 3	10F2 48	4266.755118(2)	-0.0143(3)	-0.016(3)	0.000044(5)	0.000127(3)	
10	9A1 1	10A2 16	4267.134602(1)	-0.0112(2)	-0.0146(2)	0.000032(4)	0.000084(2)	
10	9A2 1	10A1 17	4266.496427(1)	-0.0074(3)	-0.007(3)		0.000088(3)	
10	9F1 2	10F2 49	4267.486265(2)	-0.0093(3)	-0.0103(3)		0.000095(3)	
10	9F2 1	10F1 48	4268.972845(2)	-0.0098(3)	-0.0121(3)		0.000087(3)	
10	9F1 1	10F2 50	4268.909037(2)	-0.0097(3)	-0.012(3)		0.000084(3)	
10	10F1 2	10F2 58	4217.265004(2)	-0.0101(5)	-0.0101(6)		0.000089(9)	
10	9F2 2	10F1 47	4266.606303(2)	-0.0048(3)	-0.004(3)		0.000073(4)	
10	10F1 1	10F2 57	4213.600913(2)	-0.0096(4)	-0.0114(3)		0.000078(4)	0.09(1)
10	10E 1	10E 37	4205.986643(4)	-0.0088(9)	-0.0107(7)		0.000078(9)	
10	10F2 1	10F1 54	4206.010714(5)	-0.0071(8)	-0.0121(5)			
10	10F2 1	9F1 60	4156.874962(3)	-0.0164(4)	-0.0167(9)			
10	9E 1	10E 32	4267.550174(5)	-0.0089(10)	-0.0081(8)		0.000065(9)	
10	10A2 1	10A1 20	4206.073073(2)	-0.0093(3)	-0.0118(3)		0.000086(3)	0.05(1)
10	10E 2	9E 38	4150.549498(1)	-0.0104(1)	-0.0145(1)		0.000117(2)	0.115(4)
10	10A1 1	9A2 21	4152.613689(1)	-0.0093(1)	-0.0105(1)		0.000089(2)	0.114(4)
10	10F1 2	9F2 58	4151.016765(1)	-0.012(1)	-0.0131(1)		0.000088(2)	0.07(1)
10	10E 2	10E 38	4217.773981(3)	-0.0088(4)	-0.0123(5)		0.000123(7)	0.13(1)
10	10A2 1	9A1 19	4156.887224(1)	-0.0082(2)	-0.0096(5)	0.000056(5)	0.000101(6)	0.11(1)
10	10E 1	9E 39	4156.92253(2)	-0.0101(3)	-0.0128(5)	0.000075(5)	0.000099(6)	0.09(1)
10	10A1 1	10A2 19	4215.966631(2)	-0.0061(3)	-0.0072(5)		0.000083(6)	
10	10F2 2	10F1 56	4213.07271(8)	-0.0076(6)	-0.0107(5)		0.000075(6)	
10	10F2 3	9F1 58	4150.058291(1)	-0.0091(1)	-0.0098(1)		0.000081(2)	0.121(4)
10	10F1 1	9F2 59	4153.651498(1)	-0.01(1)	-0.0104(1)		0.000072(2)	0.034(4)
10	10F2 2	9F1 59	4154.102201(1)	-0.0107(1)	-0.0121(1)		0.00008(2)	0.074(5)
11	10F1 1	11F2 52	4272.010898(3)	-0.0086(4)	-0.0107(3)		0.00009(3)	
11	10F2 2	11F1 53	4272.159158(3)	-0.0095(4)	-0.0136(2)		0.000084(3)	
11	10F1 2	11F2 51	4271.128214(2)	-0.0124(3)	-0.0155(3)		0.000069(3)	0.07(1)
11	11E 1	11E 41	4211.821883(5)	-0.0099(8)	-0.0129(4)		0.000065(7)	
11	11F1 2	11F2 61	4215.423844(4)	-0.0106(7)	-0.0111(8)		0.000105(12)	0.14(2)
11	11F1 1	11F2 59	4203.365714(18)	-0.0108(15)				
11	11F2 2	11F1 63	4211.604096(8)	-0.0079(6)	-0.01(4)		0.000081(8)	
11	11F1 1	10F2 73	4155.948357(6)	-0.0093(5)	-0.013(4)		0.000078(8)	
11	10F2 3	11F1 52	4270.854783(2)	-0.0057(4)	-0.0077(3)		0.000049(5)	
11	11A2 1	11A1 21	4211.256385(2)	-0.0093(4)	-0.0125(3)		0.000088(4)	0.09(1)
11	10A1 1	11A2 18	4271.57011(3)	-0.0092(6)	-0.0108(7)		0.000083(9)	0.11(1)
11	11F2 3	11F1 64	4217.200666(5)	-0.0072(11)				
11	11F2 1	11F1 61	4203.371193(10)	-0.0089(12)		0.000133(20)		
11	11F2 1	10F1 72	4155.793472(6)	-0.011(4)	-0.0133(4)		0.000088(7)	
11	10A2 1	11A1 17	4273.53687(3)	-0.0164(7)	-0.0233(10)			
12	11E 2	12E 38	4275.138151(4)	-0.0086(4)	-0.0111(3)		0.000111(4)	0.13(1)
12	11F1 3	12F2 56	4275.057005(3)	-0.0045(5)	-0.0041(3)		0.000084(4)	
12	11F1 2	12F2 57	4275.879714(3)	-0.0087(5)	-0.0111(3)		0.000072(5)	

12	11F2 3	12F1 55	4275.294315(3)	-0.0146(4)	-0.0201(3)	0.000059(4)	
12	12A1 1	12A2 21	4200.952244(6)	-0.0103(7)	-0.0144(6)	0.000078(10)	
12	12F2 1	12F1 65	4209.461375(9)	-0.0091(12)	-0.0127(7)	0.000086(12)	
12	12A1 2	12A2 22	4218.94833(5)	-0.0097(8)	-0.0085(11)		0.15(2)
12	11F1 1	12F2 58	4278.244319(3)	-0.0082(5)	-0.0136(4)	0.000061(6)	0.15(1)
12	11E 1	12E 39	4276.506827(6)	-0.0098(7)	-0.0146(6)	0.000095(10)	0.13(2)
12	11A2 1	12A1 20	4276.717795(3)	-0.008(5)	-0.011(6)	0.000093(9)	
12	11F2 1	12F1 57	4278.221394(3)	-0.0085(6)	-0.0129(4)	0.000068(6)	
12	12F1 1	11F2 79	4148.901712(4)	-0.0102(3)	-0.0127(2)	0.000086(4)	0.08(1)
12	11F2 2	12F1 56	4276.589509(4)	-0.0093(6)	-0.0146(7)		
12	12F2 2	12F1 67	4214.879649(8)	-0.0098(11)	-0.0097(9)		
12	12A2 1	12A1 23	4216.594242(5)	-0.0088(8)	-0.0117(13)		
12	12F1 2	12F2 68	4209.853878(12)		-0.0174(18)		
12	12A1 1	11A2 27	4149.007479(2)	-0.0097(2)	-0.0122(1)	0.000098(2)	0.14(1)
13	12F2 1	13F1 63	4281.093222(5)	-0.0091(6)	-0.0121(3)	0.000103(7)	
13	12F1 3	13F2 60	4279.255197(6)	-0.0121(7)	-0.0118(5)	0.000132(9)	0.13(2)
13	12A1 2	13A2 21	4279.171847(4)	-0.0037(5)		0.000093(7)	
13	12A2 1	13A1 20	4279.413922(4)	-0.0159(5)	-0.0226(3)	0.00006(5)	0.11(1)
13	12F2 3	13F1 60	4279.10593(9)			0.00014(12)	
13	13A1 1	13A2 26	4207.816028(12)	-0.0085(12)	-0.0111(7)		
13	12A1 1	13A2 22	4282.776466(4)	-0.0067(7)	-0.0128(7)	0.000121(11)	0.15(2)
13	12E 1	13E 41	4282.740586(14)				
13	12E 2	13E 40	4280.239739(13)	-0.011(12)	-0.0117(7)		
13	12F1 1	13F2 62	4282.752732(11)		-0.016(14)		
14	13A2 1	14A1 22	4283.915495(7)	-0.0091(7)	-0.0119(4)	0.000079(9)	0.14(2)
14	13F2 1	14F1 65	4287.153379(10)	-0.0087(11)	-0.0134(8)	0.000109(14)	
14	13A1 1	14A2 21	4285.280242(7)	-0.0097(7)	-0.0135(4)	0.000062(9)	0.14(2)
14	13F1 2	14F2 66	4285.447189(11)	-0.0097(11)	-0.0133(6)		
14	13F2 3	14F1 63	4283.318251(10)	-0.0094(12)	-0.0115(6)		
14	13F2 2	14F1 64	4284.187454(11)	-0.0093(13)	-0.0127(9)		

[a]Statistical uncertainties are given in parentheses.

TD[b] stands for temperature dependences and S^c stands for speed-dependence parameters.

The blank spaces in all tables in appendices are appeared because the parameters were not possible to be determined correctly for those transitions.

References

[1] C. Böhringer, The Kyoto Protocol: A Review and Perspectives, Oxford Review of Economic Policy, 19 (2003) 451-466.

[2] Environmental Protection Agency, Understanding Global Warming Potentials, in, USA, 2017.

[3] E.J. Dlugokencky, L. Bruhwiler, J.W.C. White, L.K. Emmons, P.C. Novelli, S.A. Montzka, K.A. Masarie, P.M. Lang, A.M. Crotwell, J.B. Miller, L.V. Gatti, Observational constraints on recent increases in the atmospheric CH_4 burden, Geophysical Research Letters, 36 (2009).

[4] G. Tinetti, T. Encrenaz, A. Coustenis, Spectroscopy of planetary atmospheres in our Galaxy, The Astronomy and Astrophysics Review, 21 (2013) 63.

[5] B. Macintosh, J.R. Graham, T. Barman, R.J. De Rosa, Q. Konopacky, M.S. Marley, C. Marois, E.L. Nielsen, L. Pueyo, A. Rajan, J. Rameau, D. Saumon, J.J. Wang, J. Patience, M. Ammons, P. Arriaga, E. Artigau, S. Beckwith, J. Brewster, S. Bruzzone, J. Bulger, B. Burningham, A.S. Burrows, C. Chen, E. Chiang, J.K. Chilcote, R.I. Dawson, R. Dong, R. Doyon, Z.H. Draper, G. Duchêne, T.M. Esposito, D. Fabrycky, M.P. Fitzgerald, K.B. Follette, J.J. Fortney, B. Gerard, S. Goodsell, A.Z. Greenbaum, P. Hibon, S. Hinkley, T.H. Cotten, L.W. Hung, P. Ingraham, M. Johnson-Groh, P. Kalas, D. Lafreniere, J.E. Larkin, J. Lee, M. Line, D. Long, J. Maire, F. Marchis, B.C. Matthews, C.E. Max, S. Metchev, M.A. Millar-Blanchaer, T. Mittal, C.V. Morley, K.M. Morzinski, R. Murray-Clay, R. Oppenheimer, D.W. Palmer, R. Patel, M.D. Perrin, L.A. Poyneer, R.R. Rafikov, F.T. Rantakyrö, E.L. Rice, P. Rojo, A.R. Rudy, J.B. Ruffio, M.T. Ruiz, N. Sadakuni, L. Saddlemyer, M. Salama, D. Savransky, A.C. Schneider, A. Sivaramakrishnan, I. Song, R. Soummer, S. Thomas, G. Vasisht, J.K. Wallace, K. Ward-Duong, S.J. Wiktorowicz, S.G. Wolff, B. Zuckerman, Discovery and spectroscopy of the young jovian planet 51 Eri b with the Gemini Planet Imager, Science, 350 (2015) 64.

[6] H. Renyu, S. Sara, Photochemistry in Terrestrial Exoplanet Atmospheres. III. Photochemistry and Thermochemistry in Thick Atmospheres on Super Earths and Mini Neptunes, The Astrophysical Journal, 784 (2014) 63.

[7] M.R. Swain, G. Vasisht, G. Tinetti, The presence of methane in the atmosphere of an extrasolar planet, Nature, 452 (2008) 329-331.

[8] M. Hirtzig, B. Bézard, E. Lellouch, A. Coustenis, C. de Bergh, P. Drossart, A. Campargue, V. Boudon, V. Tyuterev, P. Rannou, T. Cours, S. Kassi, A. Nikitin, D. Mondelain, S. Rodriguez, S. Le Mouélic, Titan's surface and atmosphere from Cassini/VIMS data with updated methane opacity, Icarus, 226 (2013) 470-486.

[9] T.R. Geballe, S.R. Kulkarni, E.W. Charles, G.C. Sloan, The Near-Infrared Spectrum of the Brown Dwarf Gliese 229B, The Astrophysical Journal Letters, 467 (1996) L101.

[10] A. Butz, S. Guerlet, O. Hasekamp, D. Schepers, A. Galli, I. Aben, C. Frankenberg, J.M. Hartmann, H. Tran, A. Kuze, G. Keppel-Aleks, G. Toon, D. Wunch, P. Wennberg, N. Deutscher, D. Griffith, R. Macatangay, J. Messerschmidt, J. Notholt, T. Warneke, Toward accurate CO_2 and CH_4 observations from GOSAT, Geophysical Research Letters, 38 (2011).

[11] L.S. Rothman, I.E. Gordon, Y. Babikov, A. Barbe, D. Chris Benner, P.F. Bernath, M. Birk, L. Bizzocchi, V. Boudon, L.R. Brown, A. Campargue, K. Chance, E.A. Cohen, L.H. Coudert, V.M. Devi, B.J. Drouin, A. Fayt, J.M. Flaud, R.R. Gamache, J.J. Harrison, J.M. Hartmann, C. Hill, J.T. Hodges, D. Jacquemart, A. Jolly, J. Lamouroux, R.J. Le Roy, G. Li, D.A. Long, O.M. Lyulin, C.J. Mackie, S.T. Massie, S. Mikhailenko, H.S.P. Müller, O.V. Naumenko, A.V. Nikitin, J. Orphal, V. Perevalov, A. Perrin, E.R. Polovtseva, C. Richard, M.A.H. Smith, E. Starikova, K. Sung, S. Tashkun, J. Tennyson, G.C. Toon, V.G. Tyuterev, G. Wagner, The HITRAN2012 molecular spectroscopic database, Journal of Quantitative Spectroscopy and Radiative Transfer, 130 (2013) 4-50.

[12] L.R. Brown, K. Sung, D.C. Benner, V.M. Devi, V. Boudon, T. Gabard, C. Wenger, A. Campargue, O. Leshchishina, S. Kassi, D. Mondelain, L. Wang, L. Daumont, L. Régalia, M. Rey, X. Thomas, V.G. Tyuterev, O.M. Lyulin, A.V. Nikitin, H.M. Niederer, S. Albert, S. Bauerecker, M. Quack, J.J. O'Brien, I.E. Gordon, L.S. Rothman, H. Sasada, A. Coustenis, M.A.H. Smith, T. Carrington, X.G. Wang, A.W. Mantz, P.T. Spickler, Methane line parameters in the HITRAN2012 database, Journal of Quantitative Spectroscopy and Radiative Transfer, 130 (2013) 201-219.

[13] S. Albert, S. Bauerecker, V. Boudon, L.R. Brown, J.P. Champion, M. Loëte, A. Nikitin, M. Quack, Global analysis of the high resolution infrared spectrum of methane $^{12}CH_4$ in the region from 0 to 4800 cm^{-1}, Chemical Physics, 356 (2009) 131-146.

[14] L. Daumont, A.V. Nikitin, X. Thomas, L. Régalia, P. Von der Heyden, V.G. Tyuterev, M. Rey, V. Boudon, C. Wenger, M. Loëte, L.R. Brown, New assignments in the 2μm transparency window of the $^{12}CH_4$ Octad band system, Journal of Quantitative Spectroscopy and Radiative Transfer, 116 (2013) 101-109.

[15] I.M. Julianne, C. Visscher, J.J. Fortney, A.P. Showman, N.K. Lewis, C.A. Griffith, S.J. Klippenstein, M. Shabram, A.J. Friedson, M.S. Marley, R.S. Freedman, Disequilibrium Carbon, Oxygen, and Nitrogen Chemistry in the Atmospheres of HD 189733b and HD 209458b, The Astrophysical Journal, 737 (2011) 15.

[16] C.M. Sharp, A. Burrows, Atomic and Molecular Opacities for Brown Dwarf and Giant Planet Atmospheres, The Astrophysical Journal Supplement Series, 168 (2007) 140.

[17] S. David, B. Adam, H. Ivan, Theoretical Spectra and Atmospheres of Extrasolar Giant Planets, The Astrophysical Journal, 588 (2003) 1121.

[18] C. Hill, I.E. Gordon, R.V. Kochanov, L. Barrett, J.S. Wilzewski, L.S. Rothman, HITRANonline: An online interface and the flexible representation of spectroscopic data in the HITRAN database, Journal of Quantitative Spectroscopy and Radiative Transfer, 177 (2016) 4-14.

[19] P. Varanasi, Collision-broadened half-widths and shapes of methane lines, Journal of Quantitative Spectroscopy and Radiative Transfer, 11 (1971) 1711-1724.

[20] V.M. Devi, D.C. Benner, M.A.H. Smith, C.P. Rinsland, Measurements of Air-Broadening and Pressure-Shifting of Methane Lines in the 2.3-μm Region, Journal of Molecular Spectroscopy, 157 (1993) 95-111.

[21] V.M. Devi, D.C. Benner, M.A.H. Smith, C.P. Rinsland, Temperature dependence of Lorentz air-broadening and pressure-shift coefficients of $^{12}CH_4$ lines in the 2.3-μm spectral region, Journal of Quantitative Spectroscopy and Radiative Transfer, 51 (1994) 439-465.

[22] A.S. Pine, T. Gabard, Multi-spectrum fits for line mixing in the ν_3 band Q branch of methane, Journal of Molecular Spectroscopy, 217 (2003) 105-114.

[23] A. Predoi-Cross, M. Brawley-Tremblay, L.R. Brown, V.M. Devi, D.C. Benner, Multi-spectrum analysis of $^{12}CH_4$ from 4100 to 4635cm^{-1}: II. Air-broadening coefficients (widths and shifts), Journal of Molecular Spectroscopy, 236 201-215.

[24] A. Predoi-Cross, L.R. Brown, V.M. Devi, M. Brawley-Tremblay, D.C. Benner, Multi-spectrum analysis of $^{12}CH_4$ from 4100 to 4635cm^{-1}: 1. Self-broadening coefficients (widths and shifts), Journal of Molecular Spectroscopy, 232 (2005) 231-246.

[25] A. Predoi-Cross, A.V. Unni, H. Heung, V. Malathy Devi, D. Chris Benner, L.R. Brown, Line mixing effects in the $\nu_2+\nu_3$ band of methane, Journal of Molecular Spectroscopy, 246 (2007) 65-76.

[26] D. Chris Benner, V. Malathy Devi, M.A.H. Smith, C.P. Rinsland, Air-, N_2-, and O_2-broadening and shift coefficients in the ν_3 spectral region of $^{12}CH_4$, Journal of Quantitative Spectroscopy and Radiative Transfer, 50 (1993) 65-89.

[27] V.M. Devi, B. Fridovich, D.G.S. Snyder, G.D. Jones, P.P. Das, Tunable diode laser measurements of intensities and Lorentz broadening coefficients of lines in the ν_2 band of $^{12}CH_4$, Journal of Quantitative Spectroscopy and Radiative Transfer, 29 (1983) 45-47.

[28] V.M. Devi, C.P. Rinsland, M.A.H. Smith, D.C. Benner, Measurements of $^{12}CH_4$ ν_4 band halfwidths using a tunable diode laser system and a Fourier transform spectrometer, Appl. Opt., 24 (1985) 2788-2791.

[29] V. Malathy Devi, B. Fridovich, G.D. Jones, D.G.S. Snyder, Strengths and lorentz broadening coefficients for spectral lines in the ν_3 and $\nu_2 + \nu_4$ bands of $^{12}CH_4$ and $^{13}CH_4$, Journal of Molecular Spectroscopy, 97 (1983) 333-342.

[30] C.P. Rinsland, V.M. Devi, M.A.H. Smith, D.C. Benner, Measurements of air-broadened and nitrogen-broadened Lorentz width coefficients and pressure shift coefficients in the ν_4 and ν_2 bands of $^{12}CH_4$, Appl. Opt., 27 (1988) 631-651.

[31] M.A.H. Smith, D.C. Benner, A. Predoi-Cross, V.M. Devi, Multi-spectrum analysis of $^{12}CH_4$ in the ν_4 band: I, Journal of Quantitative Spectroscopy and Radiative Transfer, 110 (2009) 639-653.

[32] M.A.H. Smith, D.C. Benner, A. Predoi-Cross, V. Malathy Devi, A multi-spectrum analysis of the ν_4 band of $^{13}CH_4$: Widths, shifts, and line mixing coefficients, Journal of Quantitative Spectroscopy and Radiative Transfer, 112 (2011) 952-968.

[33] M.A.H. Smith, D.C. Benner, A. Predoi-Cross, V. Malathy Devi, Air- and self-broadened half widths, pressure-induced shifts, and line mixing in the ν_2 band of $^{12}CH_4$, Journal of Quantitative Spectroscopy and Radiative Transfer, 133 (2014) 217-234.

[34] M.A.H. Smith, C.P. Rinsland, V.M. Devi, D.C. Benner, Temperature dependence of broadening and shifts of methane lines in the ν_4 band, Spectrochimica Acta Part A: Molecular Spectroscopy, 48 (1992) 1257-1272.

[35] V.M. Devi, D.C. Benner, M.A.H. Smith, A.W. Mantz, K. Sung, T.J. Crawford, A. Predoi-Cross, Self- and air-broadened line shape parameters in the $\nu_2+\nu_3$ band of $^{12}CH_4$: 4500–4630 cm^{-1}, Journal of Quantitative Spectroscopy and Radiative Transfer, 152 (2015) 149-165.

[36] R. Hashemi, A. Predoi-Cross, A.V. Nikitin, V.G. Tyuterev, K. Sung, M.A.H. Smith, V. Malathy Devi, Spectroscopic line parameters of $^{12}CH_4$ for atmospheric composition retrievals in the 4300–4500 cm^{-1} region, Journal of Quantitative Spectroscopy and Radiative Transfer, 186 (2017) 106-117.

[37] P. Varanasi, S. Chudamani, The temperature dependence of lineshifts, linewidths and line intensities of methane at low temperatures, Journal of Quantitative Spectroscopy and Radiative Transfer, 43 (1990) 1-11.

[38] J.S. Margolis, Hydrogen broadening and collision-induced line shifts of methane at 4200 cm^{-1}, Journal of Quantitative Spectroscopy and Radiative Transfer, 49 (1993) 71-79.

[39] J.S. Margolis, Measurement of hydrogen-broadened methane lines in the ν_4 band at 296 and 200 K, Journal of Quantitative Spectroscopy and Radiative Transfer, 50 (1993) 431-441.

[40] J.S. Margolis, Hydrogen and helium broadening and pressure induced line shifts of $^{13}CH_4$ in the ν_4 band, Journal of Quantitative Spectroscopy and Radiative Transfer, 55 (1996) 823-836.

[41] J.M. Hollas, Modern Spectroscopy, 4th ed., John Wiley & Sons Ltd, Sussex, UK, 2004.

[42] P.F. Bernath, Spectra of atoms and molecules, 2nd ed., Oxford University Press, New York, 2005.

[43] F. Rohart, H. Mäder, H.W. Nicolaisen, Speed dependence of rotational relaxation induced by foreign gas collisions: Studies on CH_3F by millimeter wave coherent transients, The Journal of Chemical Physics, 101 (1994) 6475-6486.

[44] P.R. Berman, Speed-dependent collisional width and shift parameters in spectral profiles, Journal of Quantitative Spectroscopy and Radiative Transfer, 12 (1972) 1331-1342.

[45] F. Rohart, Mäder, H., Nicolaisen, H. W.,, Speed dependence of rotational relaxation induced by foreign gas collisions: Studies on CH_3F by millimeter wave coherent transients, in: J. Chem. Phys., 1994, pp. 6457-6486.

[46] B. Gentry, Strow, L.L.,, Line mixing in a N_2-broadened CO_2 Q branch observed with a tunable diode laser, J. Chem. Phys., 86 (1987) 5722-5730.

[47] A. Lévy, Lacome, N., Chackerian Jr. C., Collisional Line Mixing: Spectroscopy of the Earth's Atmosphere and Interstellar Medium, (1992) 261-337.

[48] L.R. Brown, D. Chris Benner, V. Malathy Devi, M.A.H. Smith, R.A. Toth, Line mixing in self- and foreign-broadened water vapor at 6μm, Journal of Molecular Structure, 742 (2005) 111-122.

[49] D.C. Benner, C.P. Rinsland, V.M. Devi, M.A.H. Smith, D. Atkins, A multi-spectrum nonlinear least squares fitting technique, Journal of Quantitative Spectroscopy and Radiative Transfer, 53 (1995) 705-721.

[50] B.C. Smith, Fundamentals of Fourier Transform Infrared Spectroscopy, 2nd ed., CRC Press, Taylor and Francis Group, New York, 2011.

[51] P. Connes, Astronomical Fourier Spectroscopy, Annual Review of Astronomy and Astrophysics, 8 (1970) 209-230.

[52] K. Sung, A.W. Mantz, M.A.H. Smith, L.R. Brown, T.J. Crawford, V.M. Devi, D.C. Benner, Cryogenic absorption cells operating inside a Bruker IFS-125HR: First results for $^{13}CH_4$ at 7μm, Journal of Molecular Spectroscopy, 262 (2010) 122-134.

[53] G.L. Carr, M. Hanfland, G.P. Williams, Midinfrared beamline at the National Synchrotron Light Source port U2B, Review of Scientific Instruments, 66 (1995) 1643-1645.

[54] L.M. Miller, R.J. Smith, Synchrotrons versus globars, point-detectors versus focal plane arrays: Selecting the best source and detector for specific infrared microspectroscopy and imaging applications, Vibrational Spectroscopy, 38 (2005) 237-240.

[55] A. Rogalski, Infrared detectors: status and trends, Progress in Quantum Electronics, 27 (2003) 59-210.

[56] A. Rogalski, Infrared detectors: an overview, Infrared Physics & Technology, 43 (2002) 187-210.

[57] D.R. Lide, Handbook of Chemistry and Physics, 79th ed., CRC, LLC, USA, 1998.

[58] A.W. Mantz, K. Sung, L.R. Brown, T.J. Crawford, M.A.H. Smith, V. Malathy Devi, D. Chris Benner, A cryogenic Herriott cell vacuum-coupled to a Bruker IFS-125HR, Journal of Molecular Spectroscopy, 304 (2014) 12-24.

[59] L. Mertz, Auxiliary computation for Fourier spectrometry, Infrared Physics, 7 (1967) 17-23.

[60] L. MERTZ, Transformations in Optics, John Wiley & Sons, Inc, New York 1965.

[61] K. Levenberg, A method for the solution of certain non-linear problems in least squares, Quarterly of applied mathematics, 2 (1944) 164-168.

[62] D. Marquardt, An Algorithm for Least-Squares Estimation of Nonlinear Parameters, Journal of the Society for Industrial and Applied Mathematics, 11 (1963) 431-441.

[63] N. Jacquinet-Husson, R. Armante, N.A. Scott, A. Chédin, L. Crépeau, C. Boutammine, A. Bouhdaoui, C. Crevoisier, V. Capelle, C. Boonne, N. Poulet-Crovisier, A. Barbe, D. Chris Benner, V. Boudon, L.R. Brown, J. Buldyreva, A. Campargue, L.H. Coudert, V.M. Devi, M.J. Down, B.J. Drouin, A. Fayt, C. Fittschen, J.M. Flaud, R.R. Gamache, J.J. Harrison, C. Hill, Ø. Hodnebrog, S.M. Hu, D. Jacquemart, A. Jolly, E. Jiménez, N.N. Lavrentieva, A.W. Liu, L. Lodi, O.M. Lyulin, S.T. Massie, S. Mikhailenko, H.S.P. Müller, O.V. Naumenko, A. Nikitin, C.J. Nielsen, J. Orphal, V.I. Perevalov, A. Perrin, E. Polovtseva, A. Predoi-Cross, M. Rotger, A.A. Ruth, S.S. Yu, K. Sung, S.A. Tashkun, J. Tennyson, V.G. Tyuterev, J. Vander Auwera, B.A. Voronin, A. Makie, The 2015 edition of the GEISA spectroscopic database, Journal of Molecular Spectroscopy, 327 (2016) 31-72.

[64] M.A.H. Smith, D. Chris Benner, A. Predoi-Cross, V. Malathy Devi, Multi-spectrum analysis of $^{12}CH_4$ in the ν_4 spectral region: II. Self-broadened half widths, pressure-induced

shifts, temperature dependences and line mixing, Journal of Quantitative Spectroscopy and Radiative Transfer, 111 (2010) 1152-1166.

[65] V.P. Kochanov, On parameterization of spectral line profiles including the speed-dependence in the case of gas mixtures, Journal of Quantitative Spectroscopy and Radiative Transfer, 189 (2017) 18-23.

[66] M. Ghysels, L. Gomez, J. Cousin, H. Tran, N. Amarouche, A. Engel, I. Levin, G. Durry, Temperature dependences of air-broadening, air-narrowing and line-mixing coefficients of the methane ν_3 R(6) manifold lines—Application to in-situ measurements of atmospheric methane, Journal of Quantitative Spectroscopy and Radiative Transfer, 133 (2014) 206-216.

[67] V.M. Devi, D.C. Benner, K. Sung, T.J. Crawford, S. Yu, L.R. Brown, M.A.H. Smith, A.W. Mantz, V. Boudon, S. Ismail, Self- and air-broadened line shapes in the $2\nu_3$ P and R branches of $^{12}CH_4$, Journal of Molecular Spectroscopy, 315 (2015) 114-136.

[68] H. Tran, P.M. Flaud, T. Gabard, F. Hase, T. von Clarmann, C. Camy-Peyret, S. Payan, J.M. Hartmann, Model, software and database for line-mixing effects in the ν_3 and ν_4 bands of CH_4 and tests using laboratory and planetary measurements—I: N_2 (and air) broadenings and the earth atmosphere, Journal of Quantitative Spectroscopy and Radiative Transfer, 101 (2006) 284-305.

[69] H. Tran, J.M. Hartmann, G. Toon, L.R. Brown, C. Frankenberg, T. Warneke, P. Spietz, F. Hase, The $2\nu_3$ band of CH_4 revisited with line mixing: Consequences for spectroscopy and atmospheric retrievals at 1.67μm, Journal of Quantitative Spectroscopy and Radiative Transfer, 111 (2010) 1344-1356.

[70] T. Gabard, V. Boudon, Line broadening coefficient calculations for methane perturbed by nitrogen, Journal of Quantitative Spectroscopy and Radiative Transfer, 111 (2010) 1328-1343.

[71] V.G.N.A. Tyuterev, Rey M, Tashkun S, Private communication, in, 2015.

[72] A.V. Nikitin, M. Rey, V.G. Tyuterev, Accurate line intensities of methane from first-principles calculations, Journal of Quantitative Spectroscopy and Radiative Transfer, 200 (2017) 90-99.

[73] A.V. Nikitin, M. Rey, V.G. Tyuterev, First fully ab initio potential energy surface of methane with a spectroscopic accuracy, The Journal of Chemical Physics, 145 (2016) 114309.

[74] V.G. Tyuterev, V.I. Perevalvo, Generalized contact transformations of a hamiltonian with a quasi-degenerate zero-order approximation. Application to accidental vibration-rotation resonances in molecules, Chemical Physics Letters, 74 (1980) 494-502.

[75] V. Tyuterev, S. Tashkun, M. Rey, R. Kochanov, A. Nikitin, T. Delahaye, Accurate Spectroscopic Models for Methane Polyads Derived from a Potential Energy Surface Using High-Order Contact Transformations, The Journal of Physical Chemistry A, 117 (2013) 13779-13805.